The University of Nottingham

UNITED KINGDOM · CHINA · MALAYSIA

Porous scaffolds and soft hydrogel scaffolds for soft tissue engineering

Yang Yang, MSc.

Bioengineering Group, Division of Materials, Mechanics and Structures

Faculty of Engineering

Thesis submitted to the University of Nottingham for the degree of

Doctor of Philosophy, June 2017

Abstract

Three dimensional (3-D) porous scaffolds are valuable in tissue engineering as they can provide the micro-environment for cell adhesion, proliferation, migration and induce tissue regeneration. Collagen is regarded as the most valuable biomaterial in tissue engineering as it is the most important and abundant structural protein in the human body.

This thesis consists of three parts. Part one describes investigation of porous scaffolds fabricated from gelatin-chitosan; part two concerns a study of porous scaffolds developed based on recombinant human collagen-polypeptide (RHC); part three investigates soft hydrogels scaffolds based on recombinant collagen-polypeptide.

Firstly, porous gelatin-chitosan scaffolds were developed in order to refine and understand fabrication methods, as well as to improve characterization techniques for highly porous scaffolds. Gelatin/chitosan (Gel/Chi) porous scaffolds were fabricated using a freeze-drying method and cross-linked by proanthocyanidin (PA) or glutaraldehyde (GA). Porous micro-structures, swelling in aqueous media, *in vitro* degradation and mechanical strength were characterized in this study. Cytocompatibility of the fabricated porous scaffolds was investigated by seeding

3T3 fibroblasts into the porous structures, and the cellular metabolic activity, proliferation, distribution, and morphology were investigated.

Secondly, Recombinant Human Collagen-polypeptide (RHC) and RHC-chitosan (RHC-CHI) porous scaffolds were fabricated by a freeze-drying method and cross-linked with 1-ethyl-3-(3-dimethyl aminopropyl) carbodiimide (EDC). Porous structures, cross-linking mechanisms, cross-linking degree, swelling ratio, *in vitro* degradation and mechanical properties were investigated. Cytocompatibility of the porous scaffolds was investigated using 3T3 fibroblasts as before.

Finally, a series of RHC based soft hydrogel scaffolds were fabricated through cross-linker induced polymerization, and these hydrogels were studied to determine their feasibility as potential biomaterials. Changes in cell morphology and proliferation in response to hydrogel composition were also investigated.

Scanning electron microscopy and micro computed tomography (micro-CT) indicated that highly porous structures had been obtained in freeze-dried gelatin and collagen based porous scaffolds. Fourier transform infrared spectroscopy determined that cross-linking had occurred through covalent bonding between the biopolymer molecules. The degree of cross-linking was determined using high performance liquid chromatography, and the results confirmed that the biopolymers in the porous scaffolds were efficiently cross-linked. *In vitro* degradation tests

indicated that the porous scaffolds showed acceptable biostability. The mechanical tests showed that mechanical stiffness of the porous scaffolds could be tailored to their end-use application by either adjusting the biopolymer or cross-linker concentration and their mechanical strengths were found to be comparable to biological soft tissues. Cytocompatibility tests using Alamar Blue and DNA assays confirmed that gelatin and RHC based porous scaffolds had no toxicity to fibroblasts and could support cell proliferation, while fluorescence microscopy and cell morphology showed the adhesion, migration and proliferation of seeded cells in porous scaffolds. Quantitative reverse transcription-polymerase chain reaction further showed a high expression of extracellular matrix associated protein (β-integrin, collagen I and collagen III) genes as tissue regeneration progressed.

Results from soft hydrogel scaffold characterization found that the gelation time could be optimized by adjusting the RHC fraction, biopolymer concentration, or reaction temperature. Acceptable mechanical properties and biostability were verified in mechanical and *in vitro* degradation tests, and as with the porous scaffolds, mechanical strengths could be tuned by modifying either RHC fraction or total polymer concentration. Cytotoxicity tests showed that the fabricated soft hydrogels had no toxicity to fibroblasts and cytocompatibility tests indicated that they promoted adhesion and proliferation. The DNA assay and cell morphology study also confirmed that cellular activities were affected by both mechanical

properties and polymer composition, however RHC fraction in these hydrogel scaffolds was the major factor influencing cellular activity.

In conclusion, the results of this study show that gelatin and RHC based porous scaffolds as well as homogeneous soft hydrogel scaffolds will be highly applicable in current and future applications in tissue engineering.

Project highlights:

1. Developed repeatable, consistent methods to fabricate 3-D porous and soft hydrogel scaffolds with tunable mechanical properties and acceptable cytocompatibility.

2. Studied the behaviours of fibroblasts as they respond to scaffolds.

3. Confirmed that cell adhesion and proliferation can be affected by RHC molecules.

4. Confirmed the β-intergin, collagen I and collagen III gene expression levels of related proteins from molecular aspect.

Acknowledgements

I would like to take this opportunity to thank Dr. Nicola Everitt and Dr. Alastair Campbell Ritchie for guiding and supporting me throughout my PhD studies. Also, I would like to thank the technical staff and lecturers who supported my work, Julie Thompson, Keith Dinsdale, Tom Buss and Dr. Colin Scotchford. This work would not have been completed without your kind help, and finally, I would like to thank my beloved parents, and this thesis is dedicated to both of you.

List of publications

‘**Comparison of glutaraldehyde and procyanidin cross-linked scaffolds for soft tissue engineering**’ Yang Yang, Alastair Campbell Ritchie, Nicola M. Everitt, Materials Science and Engineering: C, Volume 80, 1 November 2017, Pages 263-273.

‘**Perfusion culture of cell seeded porous scaffolds**’ Yang Yang, Ana Luisa Encerrado, Nicola M. Everitt, Alastair Campbell Ritchie, The 4th international conference on biotechnology and bioengineering (ICBB2015), December 11-13, 2015, Singapore.

‘**3-D recombinant type III collagen-polypeptide porous scaffolds for soft tissue engineering**’ Yang Yang, Alastair Campbell Ritchie, Nicola M. Everitt (Pending submission).

‘**Soft hydrogel scaffolds fabricated from recombinant type III collagen-polypeptide**’ Yang Yang, Alastair Campbell Ritchie, Nicola M. Everitt (Pending submission).

Table of contents

Abbreviations

3-D	Three-dimensional
bFGF	Basic fibroblast growth factor
Ca^{2+}	Calcium ion
CAD	Computer-aided design
cDNA	Complementary DNA
CHI	Chitosan
DMEM	Dulbecco’s Modified Eagle Medium
ECM	Extracellular matrix
EDC	1-ethyl-3-(3-dimethyl aminopropyl) carbodiimide
ELISA	Enzyme linked immunosorbent assay
ESEM	Environmental scanning electron microscope
FT-IR	Fourier transform infrared spectroscopy
GA	Glutaraldehyde
GAG	Glucosaminoglycan
HBSS	Hank's Balanced Salt Solution
HMDS	hexamethyldisilazane
Micro-CT	X-ray micro-computed tomography
MIP	Porosimetry
MSC	Mesenchymal stem cells
MTT	3-(4,5-dimethylthiazol-2-yl)-2,5-diphenyltetrazolium bromide
NHS	N-hydroxysuccinimide
PA	Procyanidin
PBS	Phosphate buffer saline
PLGA	Poly(DL-lactic-co-glycolic acid)
PGA	Poly(glycolic acid)
PLLA	Poly(L-lactic acid)
PTFE	Polytetrafluoroethylene
qRT-PCR	Quantitative reverse transcription-polymerase chain reaction
RHC	Recombinant human collagen-polypeptide
RNA	Ribonucleic acid
SEM	Scanning electron microscope
XTT	2,3-Bis-(2-Methoxy-4-Nitro-5-Sulfophenyl)-2H-Tetrazolium-5-Carboxanilide

Chapter 1 Introduction

1.1 Project background

Tissue engineering can be defined as using methods of cell biology, engineering and material science to design and construct functional, living components that can be used for repairing or regenerating dysfunctional tissue [1, 2]. Currently, tissue engineering covers the replacement and repair of partial or whole tissues including skin, bone, cartilage, blood vessels and nerve [3].

Collagen is widely used as a constituent material of scaffolds in tissue engineering as it is the main structural protein of the extracellular matrix (ECM) in most soft and hard tissues in the human body, and it plays an important role in maintaining biological function as well as structural integrity of extracellular matrix. To date, collagen and collagen based biomaterials have principally been derived from animal tissues; the concerns of using these collagens in medical applications are purity, quality, and most important of all, xenogeneous collagen carries the risk of transmission of pathogens such as prions and immunological reactions [4]. It is therefore necessary to find alternatives to replace animal derived collagen with collagen from a safer source. Recombinant collagens offer one solution due to their non-animal source and purity. With developments in genetic engineering, it becomes possible to produce human collagen from host cells such as bacteria, yeast, plant and insect cells as well as from genetically modified mammalian cells [5].

The collagen produced in such systems is highly pure and chemically defined, with no risks of prion or virus contamination. In addition, recombinant collagen can be engineered to obtain specific conformation and composition for a specific application through genetic modification [6].

1.2 Project objectives

The aim of this project was to investigate the properties and performance of porous and soft hydrogel scaffolds based on type III recombinant collagen-polypeptide (RHC), and to evaluate their performance as potential biomaterials for applications in general soft tissue engineering.

The specific objectives set for this project are therefore:

- To assemble and cross-link porous 3-D scaffolds with tunable mechanical stiffness from gelatin-chitosan blends, recombinant type III collagen-polypeptide (RHC), and RHC-chitosan blends and characterize their properties;

- To construct recombinant type III human collagen-polypeptide based soft hydrogel scaffolds with tunable mechanical properties and investigate their properties;

- To investigate and understand the cellular behavioural response to the mechanical and biochemical environment provided by the scaffolds, and to demonstrate the feasibility of applications of RHC based scaffolds in biomedical science.

1.3 Structure of the thesis

Chapter 1 covers the general introduction of the project;

Chapter 2 reviews the literature on both animal tissue derived collagen and recombinant human collagen, and their associated biomaterials in tissue engineering applications. The advantages and disadvantages of these collagen based materials are discussed;

Chapter 3 describes the fabricating and characterization methods of the gelatin based, RHC based 3-D porous scaffolds as well as soft hydrogels;

Chapter 4 presents the results which determined from each type of samples;

Chapter 5 discusses and evaluates their feasibilities as biomaterials in soft tissue engineering as well as investigates interaction between cellular activities and properties of the porous scaffolds;

Chapter 6 and 7 present the summaries and conclusions of the entire project;

Chapter 8 presents the recommendations for future research.

Chapter 2 Literature review

2.1 General tissue engineering

The concept of tissue engineering is to use appropriate scaffolds to host the seeded cells and generate a cell-material complex to replace or improve dysfunctional biological tissues [3]. Currently, tissue engineering covers the replacement and repair of partial or whole tissues including skin, bone, cartilage, blood vessels, nerves and oculus [7]. Tissue regeneration in tissue engineering is usually associated with cell seeding in a scaffold followed by proliferation, and once the cells have built up a new functional tissue, it can be implanted into the body. There are a number of sources of cells: primary cells are mature cells from a specific tissue type, while stem cells have the ability to differentiate into certain lineages if provided with specific culture conditions and stimuli [8]. Acellular scaffolds have also been used *in vivo* [9, 10]. A general concept of the tissue engineering is shown in Figure 2-1.

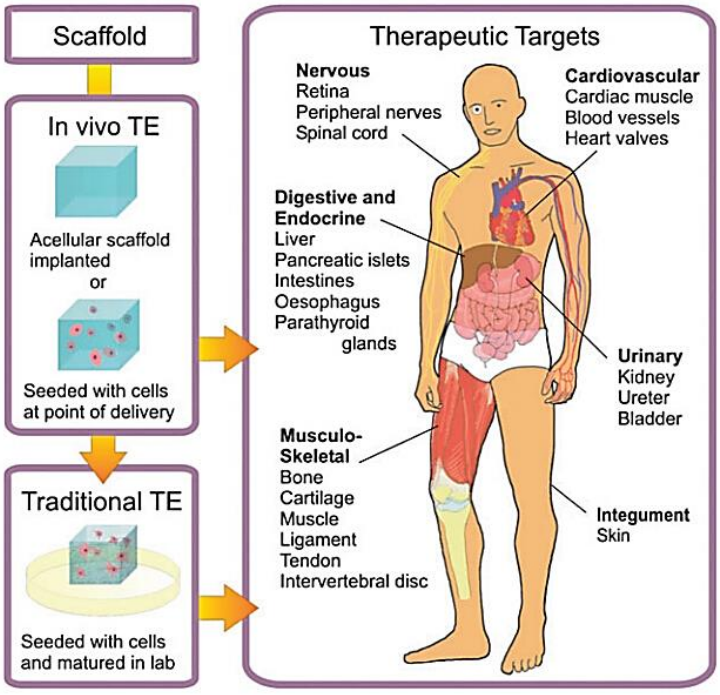

Figure 2-1. Scaffold and its targeted applications in tissue engineering [3].

2.2 Collagen

2.2.1 Collagen in human body

Collagen is the most abundant structural protein of most hard and soft tissues in human body and it plays a dominate role in maintaining structural integrity and biological function [11]. Collagen types I, II and III are the most common fibril forming collagens found in the human body, and their basic triple helix structure is comprised by Gly-X-Y repeats [12], the triple-helix structure as well as forming of fibrils are presented in Figure 2-2. The majority of the collagen found in the tissues is type I while type III collagen is found in association with collagen type I in limited quantities (about 10%) in most tissues. Proportions of Type III collagen are higher in the skin, ligaments, and blood vessels [13]. Specifically, in healthy human skin, it was found that collagen fibrils are composed of both collagen I and III with collagen III comprising around 20% of the total [14, 15]. Type I and III collagen have similar molecular structures: type I collagen contains two α1(I) polypeptide chains and one α2(I) polypeptide chain while type III collagen is composed of three α1(III) polypeptide chains [16].

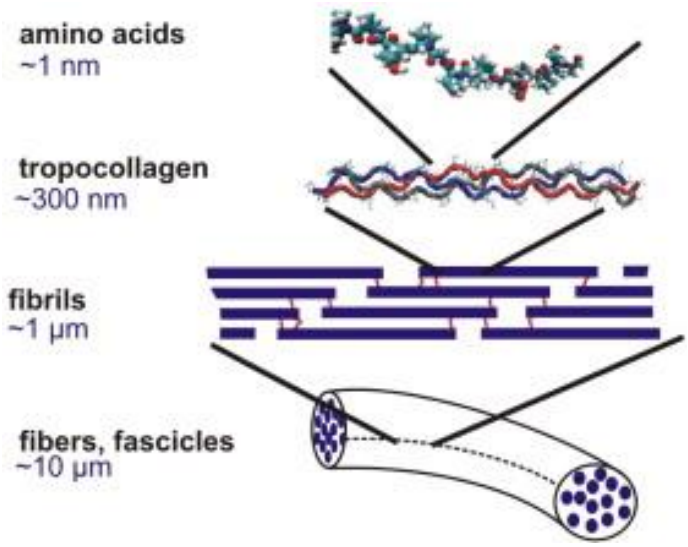

Figure 2-2. Schematic view of basic structure of collagen and collagen formed fibrils [17].

Collagens are also known to be key components in wound healing and tissue regeneration. Type I and III collagens are known to associate with skin wound healing progress and it has been found that wound granulation tissue expresses 30-40% type III collagen [18]. Increased synthesis of type III collagen is found at early stages of wound healing while the fraction of type I collagen increases in the late phase [19-21]. Both collagen types play important roles in soft tissue regeneration as well as wound healing.

2.2.2 Risks of using collagens derived from animal source

To date, most of collagens used as biomaterials in tissue engineering are derived from animal tissues, and they mainly contain type I collagen. However, since more than 27 different types of collagens have been found in biological tissues [22, 23], collagen I extracted from animal tissues could easily become contaminated by other types of collagen. Another problem with xenogeneic collagens is that the ratio of

different types of collagen and their degree of cross-linking may vary with the age and physiological condition of the donor. These variations may result in inconsistent chemical and physical properties [4].

One of the main concerns with using collagen derived from animal tissues is that such products have the potential to transfer animal pathogens, especially prion proteins [24, 25]. Prions can cause transmissible spongiform encephalopathy (scrapie and bovine spongiform encephalopathy - BSE) are the most difficult of contaminating agents to detect and remove from animal tissues [4, 24].

Animal tissue derived collagens have the potential to cause immune and allergic reactions. It has been reported that a number of patients experienced hypersensitivity reactions to implanted biomaterials containing animal sourced collagens (e.g. porcine and bovine collagen) [26-29]. The use of a bovine collagen based microfibrillar collagen hemostat (Aitene®) was found to induce necrotizing granulomatous inflammation [30]. Similarly, patients experienced local inflammatory reactions with elevated levels of antibodies against bovine collagen after treating with Zyderm®, a bovine collagen based injectable gel [31, 32]. Hence a safe collagen source free of animal components may reduce post-implantation reactions.

2.2.3 Gelatin

Gelatin is partially hydrolyzed collagen and it shares a homology with collagen[33]. As discussed in section 2.2.1, collagen is composed of three peptide chains which intertwine with each other to form a specific three-helix structure while gelatin is composed of a single alpha peptide chain which comes from the breakdown of the collagen triple-helix (Figure 2-3). Since the amino acid composition of gelatin is similar to collagen, it has similar cytocompatibility[34]. As a biologically derived water-soluble biodegradable polymer, gelatin has the advantages of easy degradation and a lack of antigenicity because of the absence of aromatic radicals [35]. It has been frequently used as a biopolymer to fabricate scaffolds and wound dressings in tissue engineering [36-38].

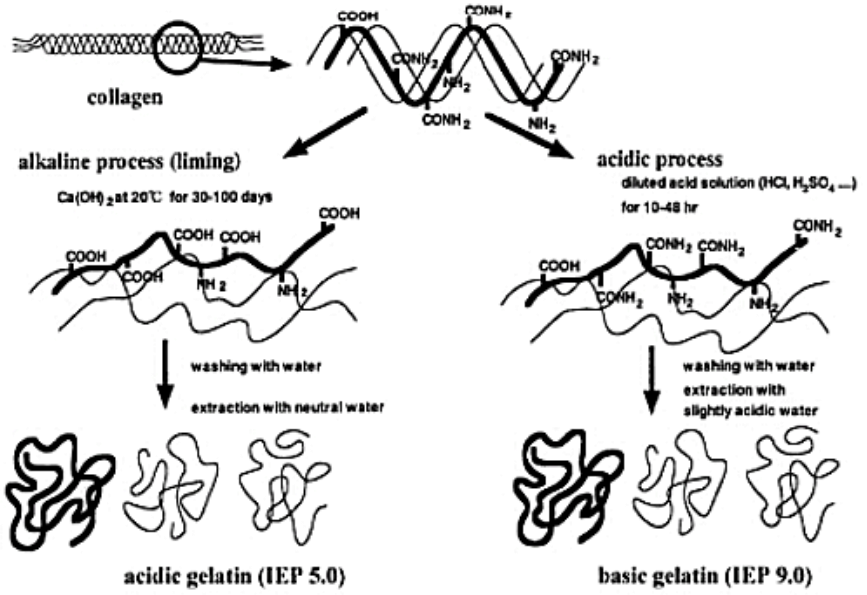

Figure 2-3. Acid and alkaline process to obtain gelatin from collagens [39].

2.3 Recombinant human collagen

Risks such as transmission of infectious agents and inflammatory reactions are some of the concerns when using animal derived collagens as discussed in section 2.2.2. In contrast to collagen extracted from animal tissues, recombinant human collagen or collagen-polypeptide is made by recombinant technology (molecular biology and transgenic engineering) where micro-organisms produce recombinant collagen with the same amino acid sequence as human tissue derived collagen [5, 40].

2.3.1 Source of RHC

With the development of genetic engineering, various types of recombinant collagens or collagen polypeptides are produced from host cells such as mammalian cells [41, 42], insect cells [43-45], yeasts [46-50] and bacteria [51]; similarly, recombinant collagens can be also produced from animal transgenic systems including mouse milk [52, 53], silk worm [54], and transgenic plants - for example, tobacco plants and tobacco plant cells in culture have been used to produce collagens [55-57]. The manufacture and purification process to harvest recombinant human collagen from yeast, plants and bacterial systems doesn't involve any animal derived components, which allows the final product to be considered to be free of animal sources. The process of collection and purification of recombinant collagen is summarized and shown in Figure 2-4.

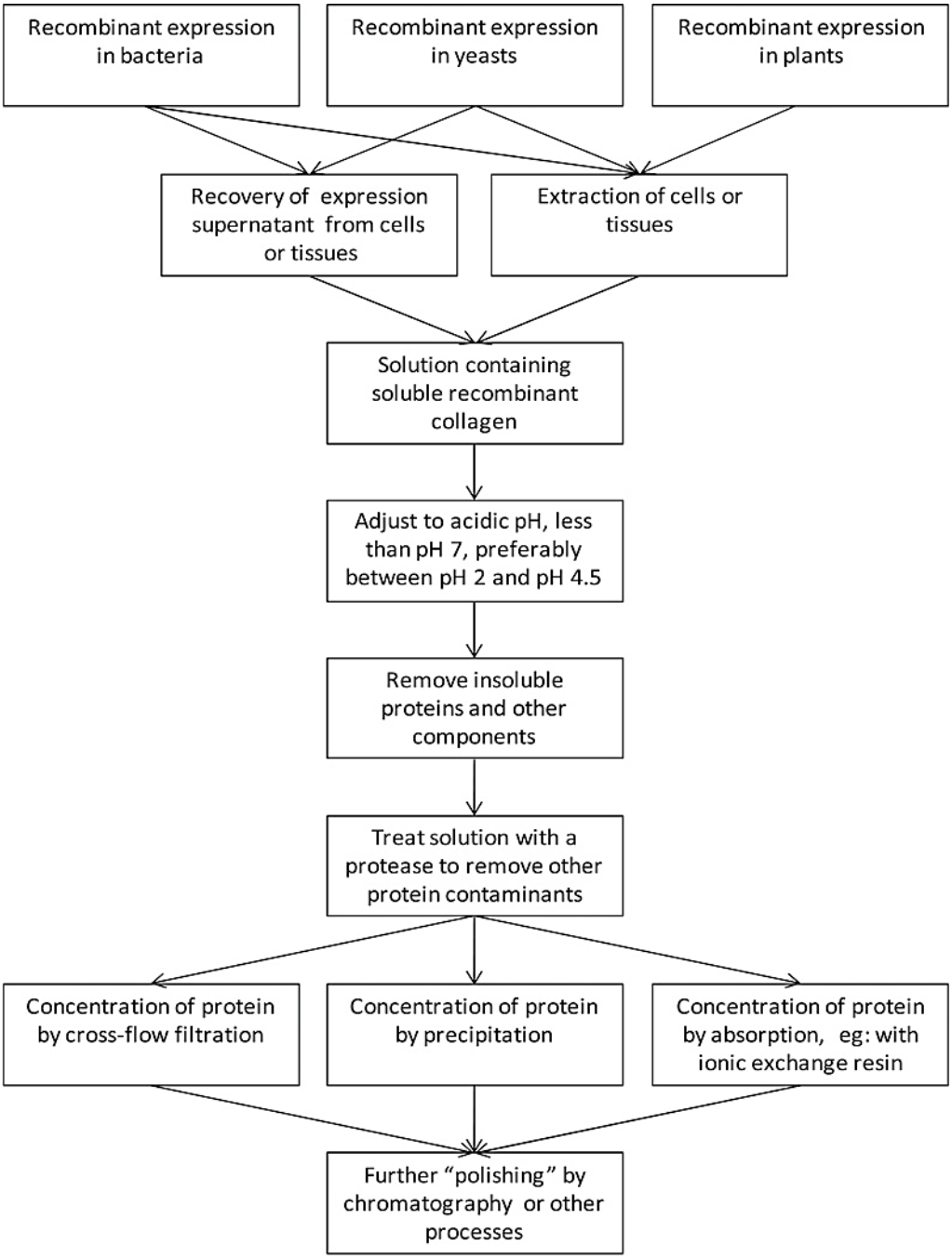

Figure 2-4. Flow chart of the fabrication and purification of the recombinant human collagen. Cited from Peng *et al.* [51].

The recombinant type III collagen-polypeptides used in this study are harvested from yeasts (Pichia pastoris). Briefly, the codon-optimized recombinant human collagen-polypeptide monomeric gene (GenBank Access Number: EF376007) was designed and synthesized based on the mRNA sequence of human type III collagen

(part of the sequence and its corresponding amino groups are provided in Appendix A). Then the RHC expression vector (pPIC9KG6) that contains genes fragments was transformed into Pichia pastoris. Subsequently a high-level expression strain was selected from the transformants for high cell-density fermentation (Patent Cooperation Treaty: PCT/CN2016/102430 and 102435)[58]. The secreted RHC-polypeptides were further purified by gel filtration chromatography and demonstrated by comparing to the type III collagen (Sigma) in protein structure as characterized by amino acid analyses, infrared spectra, ultraviolet-visible spectroscopy (UV) and nuclear magnetic resonance [48].

2.3.2 Recombinant human collagens vs animal derived collagens

Distinct from collagens extracted from animal tissues, the polypeptide chains of recombinant human collagen are based on highly defined genes, and these polypeptide chains are then specifically expressed in the host cells. The recombinant collagens produced by the transgenic yeast cells are uniform, predictable and there are no concerns regarding purity [59]. Besides the expression, as described in section 2.3.1, the recombinant human collagens are processed in a chemically defined source where all components involved in harvesting the collagen are free of animal components and consistent purification procedures can be applied to reduce variability in harvest media composition with no risk of introducing animal pathogens. According to Olsen *et al.* [5], Pichia pastoris has been commercially used to express recombinant human collagen types I, II and III,

and all these collagens show much more homogeneous composition than animal derived collagens. A more detailed comparison between animal-derived collagens and recombinant human collagens is given in Table 2-1.

Table 2-1. Comparison of animal derived collagen with recombinant collagen. Adapted and edited from [4].

Parameter	Animal-derived collagen	Recombinant collagen
Source	Collagen extracted from numerous animal carcasses and tissues [60]	Produced in defined and genetically equivalent expression systems [47, 50]
Safety	Risk of contamination with prions and virus [61]	No risk of prion and animal virus contamination and fully characterized, defined source material [59]
Predictability	Batch-to-batch variability high with mixture of type I and type III chains	Consistent and reproducible leading to predictable performance
Structure	Derived from multimeric type I and type III collagen with degree of crosslinking dependent on animal age and tissue; homogeneous gelatin difficult to purify [62]	Derived from mostly monomeric collagen or fragment of a single chain from which predefined, homogeneous, recombinant gelatin can be derived [63]
Customizability	Limited	Collagens of specific conformation and composition can be designed and engineered to enhance or remove certain characteristics for the application of interest [6, 48, 64, 65]

2.3.3 Interaction between collagen and cells

Collagens are used as biomaterials in tissue engineering applications due to their advance cytocompatibility and biological recognition as well as they are the structural proteins in ECM. A schematic diagram shown in Figure 2-5 illustrates the interaction between various ECM structural proteins (including collagens) and single cell to induce tissue formation and regeneration in human body. Specifically, collagens provide receptor-binding ligands which are known to be powerful regulators [12], and interactions between cell and ligand can further trigger several signaling pathway to regulate the cellular activities such as adhesion, proliferation and migration [66, 67]. For instance, cells utilize the trans-membrane receptors to interact with the ligand binding sites presenting on the ECM, where the most common receptor is the collagen-binding integrin [68]. The interactions between collagen and integrin have been found to not only link ECM signals to intracellular events, but are also associate with the actin cytoskeleton which regulates the cellular morphology and motility [69, 70]. Generally, integrins are composed of two subunits named alpha and beta, where the alpha subunit recognizes the ligands and the beta subunit sets cellular event in motions. Meanwhile, the integrin subunits presenting at cell surface are found influenced by the cell type and cell cycle [71]. It is also noticed that the variety of ligands available in collagen molecules can be recognized by integrins with specific alpha and beta subunits. For example, α2β1 integrin has been found to bind specifically to fibrous collagens [72, 73].

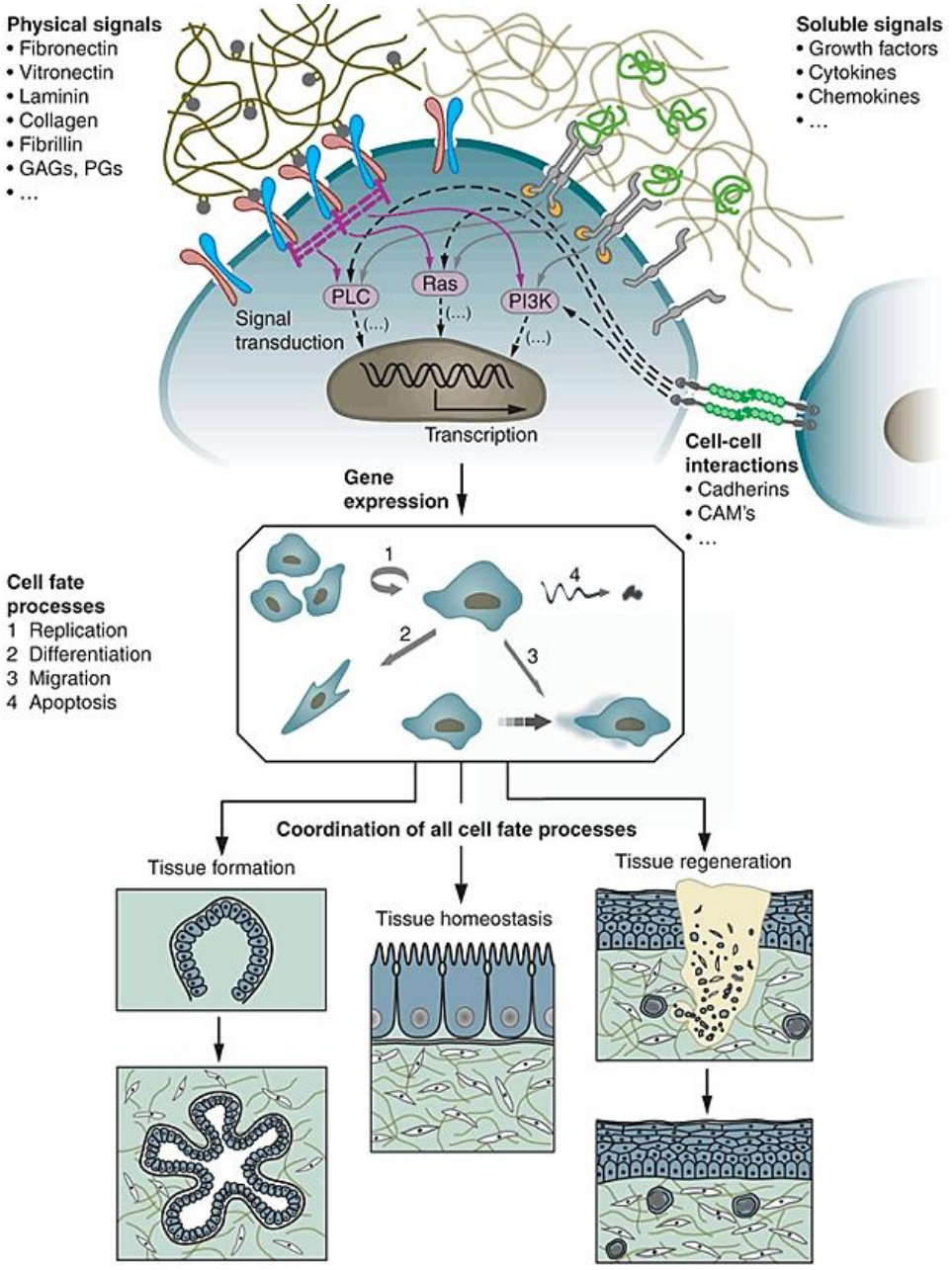

Figure 2-5. The schematic diagram of interaction between proteins (including collagens) and single cell to induce tissue formation and regeneration. Cited from Lutolf *et al*. [74].

2.4 Chitin and Chitosan

Chitosan is a natural biopolymer produced as the deacetylated derivative of chitin, where chitin is commonly found in shells of marine crustaceans and cell walls of fungi and considered as the second most abundant natural polymer after cellulose [75]. The structure of chitin is known consist of 2-acetamido-2-deoxy-β-D-glucose through a β (1→4) linkage as shown in Figure 2-6, while the structure of chitosan is composed of both N-glucosamine and N-acetyl glucosamine (Figure 2-6) [76].

2.4.1 Source of chitosan

Since chitosan is the deacetylated form of chitin, harvesting chitin is the first step to produce chitosan [75]. Chitin is the primary structural biopolymer in arthropods and fungi and has a similar function to cellulose in plants. It is present in crustaceans and the cell walls of fungi and yeast as well as the exoskeletons of insects. Sources of chitin are listed in Table 2-2 below. Chitin production is associated with the food processing industry, where large quantities of chitin can be easily obtained from the shells of crabs, shrimp or other sea crustaceans as the by-products from the canning industry [77]. The processing of these shells requires removal of proteins and calcium carbonate which are also present in the shells of crustaceans [78].

Alkalis are usually used to deacetylate the chitin into chitosan. Typically, the deacetylation of chitin is carried out in 40 - 50% NaOH solution, and the

temperature is set to 100 - 160 ℃ and the process takes 1-3 hours. This treatment can produce 70 - 95% deacetylated chitosan. 50 - 70% N-deacetylation is normally classified as a low degree of deacetylation of chitosan, 70 - 85% is medium and 85 - 95% is high deacetylation chitosan [79]. The schematic of the chemical reaction is shown in Figure 2-6. Studies also found that the degree of deacetylation can be influenced significantly by either increasing the alkaline concentration or process temperature [80]. An alternative to alkaline solutions is chitin deacetylase [81], but it has been observed that because the enzyme deacetylates the surface of the chitin due to the large enzyme molecules, penetration into the bulk of the material is poor [82].

Table 2-2. Source of the raw chitin. Taken from [76].

Sea animals	**Insects**	**Microorganisms**
Crustaceans	Scorpions	Green algae
Coelenterata	Brachiopods	Yeast (β-Type)
Annelida	Cockroaches	Fungi (cell walls)
Mollusca	Spiders	Mycelia penicillium
Lobster	Beetles	Brown algae
Shrimp	Ants	Chytridiaceae
Prawn		Ascomydes
Krill		Blastocladiaceae
Crab		Spores

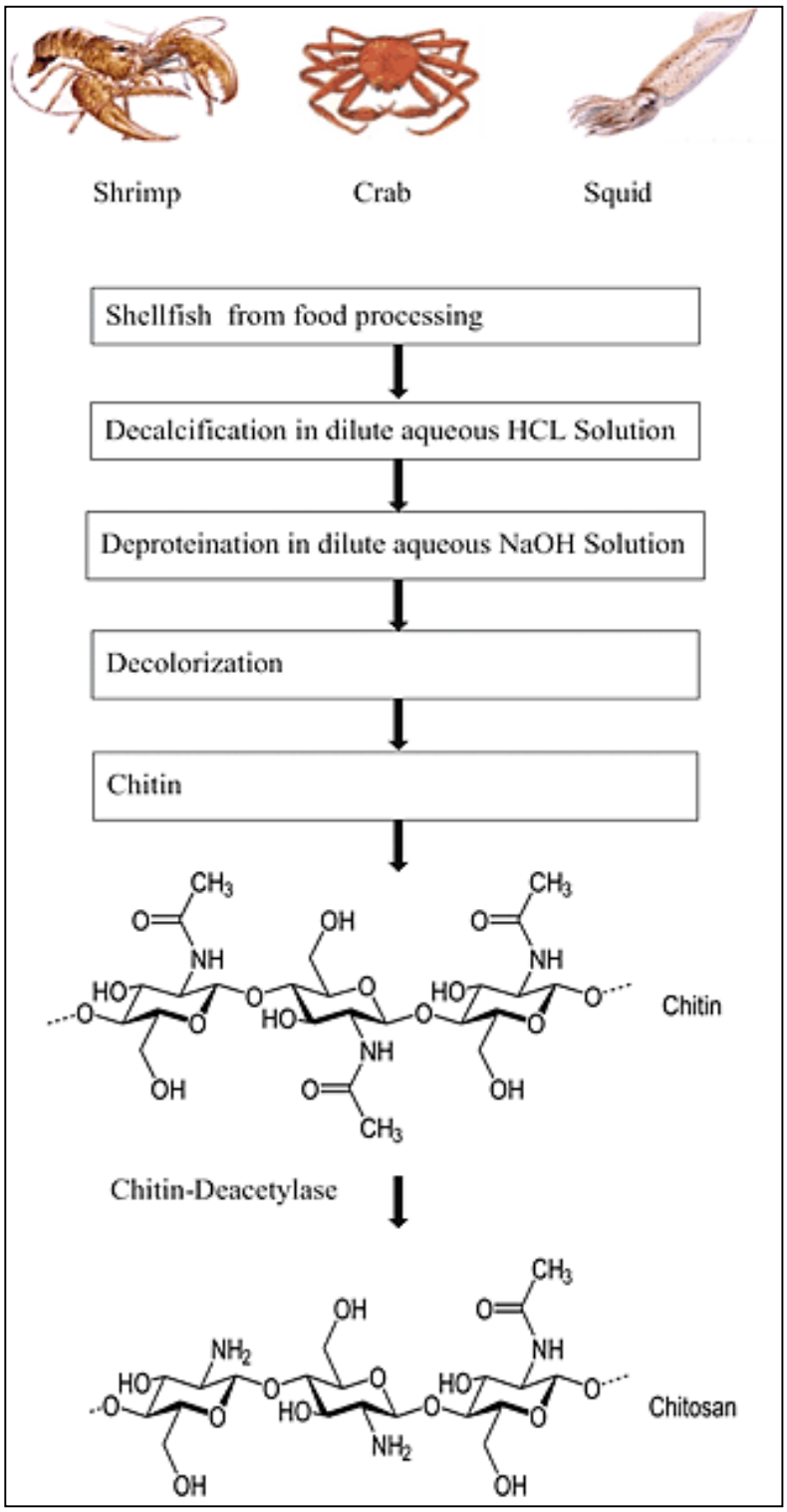

Figure 2-6. Processing of the chitosan and structures of chitin and chitosan. Cited from [83].

2.5 Cross-linking strategy in collagen based materials

Improving the mechanical strength of collagen based biomaterials without compromising their cytocompatibility is the fundamental concern in selecting cross-linking agents. Collagen molecules can be chemically modified through linking the carboxylic acid and amino groups presenting on the polypeptide chains to form covalent bonds to improve biostability [84]. Synthetic chemicals such as glutaraldehyde (GA) and 1-ethyl-3-(3-dimethyl aminopropyl) carbodiimide (EDC) are two of the most frequently used cross-linking agents in tissue engineering. EDC is an efficient cross-linker which activates the carboxylic groups and subsequently forms amides between the carboxylic and amino groups. The schematic cross-linking reaction mechanisms of collagen and collagen-chitosan are shown in Figure 2-7, which shows collagen cross-linking with and without N-hydroxysuccinimide (NHS). It has been found that the mechanical properties of the porous collagen scaffolds and collagen hydrogels can be significantly improved by cross-linking with EDC and no cytotoxic issues have been observed. The mechanical properties of these biomaterials can be further tuned by varying the concentration of EDC used [85-87]. For instance, Liu *et al.* [88] used EDC as the cross-linking reagent to cross-link collagen hydrogels. They found that the mechanical properties of the fabricated hydrogels were significantly affected by the amount of EDC added; the elongation at break varied from 20 to 60% as the molar equivalent ratio of EDC to collagen was changed. Powell *et al.* [89] used EDC with varied concentrations (0, 1, 5, 10, 50 mM) to cross-link porous collagen scaffolds

fabricated by freeze-drying. They noticed that degradation by collagenase was significantly reduced with increasing EDC concentration, and ultimate tensile strength of the collagen sponges increased proportionally with EDC concentration up to 10 mM. Cell viability tests indicated that EDC had no toxicity to seeded fibroblasts and histological samples showed a continuous basal cell layer in all samples. EDC is considered to be low in toxicity as it is not incorporated into the cross-linked product, hence no cytotoxins are released during degradation [90]. In contrast to EDC, glutaraldehyde reacts with the available free amine groups of the collagen to form a Schiff base [91]. Although GA can produce a high degree of cross-linking, it has been reported that unreacted GA can cause local inflammation and calcification. Even at concentrations of 3.0 ppm cross-linked collagen materials showed cytotoxicity after host implantation due to biodegradation of the collagen matrix [92-95]. Gelatin and collagen scaffolds have also been cross-linked using ultraviolet radiation (UV) without compromising biological functionality, and seeded cells proliferated well in porous structures [96].

Responding to concerns over the toxicity induced by synthetic cross-linkers, naturally derived collagen cross-linkers with significantly lower toxicity have become popular. Genipin, derived from Gardenia jasminoides is an excellent collagen cross-linker with high cross-linking efficiency and low toxicity. Sung *et al.* [97] used genipin to cross-link collagen based scaffolds and treated scaffolds were subjected to various tests including characterization of their mechanical properties,

stability and cytocompatibility. It was found that genipin significantly improved the mechanical properties while stability and cytocompatibility of genipin treated scaffolds was significantly higher than GA treated controls. Proanthocyanidin (PA) is another natural polymer which is normally derived from seeds of fruits and vegetables. It stabilizes collagen and gelatin through hydrogen bonding, covalent linkage, and ionic and hydrophobic bonding [98-100]. Choi *et al.* [101] used procyanidin to cross-link collagen hydrogel scaffolds, and human periodontal ligament cells were seeded on both treated and untreated hydrogels. They found that cells cultured on PA treated hydrogel scaffolds had significantly higher proliferation rates compared to untreated scaffolds. Kim *et al.* [102] used PA to cross-link gelatin/chitosan films, and found that PA treated films exhibited a lower biodegradation rate, and cell adhesion was improved by PA treatment compared to untreated controls.

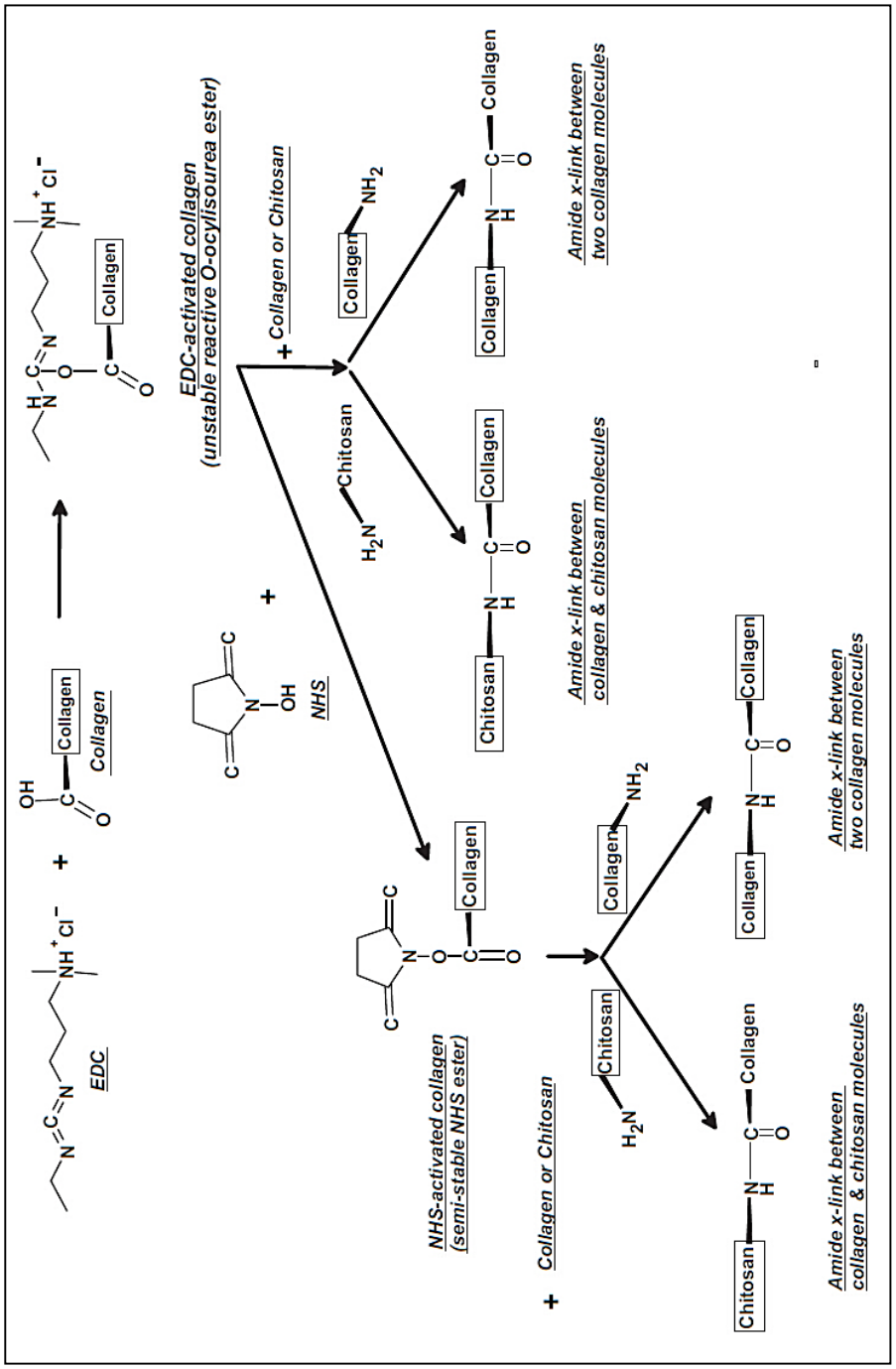

Figure 2-7. Cross-linking reaction mechanisms of collagen and collagen/chitosan by presenting EDC or EDC/NHS. Cited from Rafat *et al.* [85].

2.6 Tissue engineering scaffolds

2.6.1 Collagen in tissue engineering

2.6.1.1 Collagen as biomaterials in soft tissue engineering and wound healing

Collagen has been widely used in tissue engineering applications due to its biological function and biodegradability. Collagen based biomaterials usually undergo enzymatic degradation within the body via collagenases and completed degradation time ranges from days to weeks depending on the degree of cross-linking [103] Recombinant human collagen shows similar degradation behaviour compared to animal collagen under enzymatic treatment [104]. Collagen and collagen-based materials have been fabricated into a variety of forms including films, sheets, tubes, porous sponges, foams, nanofibrous matrices, powders, fleeces, injectable viscous solutions and dispersions [105], and their mechanical and biological behaviours have been extensively investigated for tissue engineering applications. Collagen has been regarded as the ideal material for scaffolds in soft tissue regeneration (e.g. skin replacement, blood vessels, ligaments, etc.) [106].

2.6.1.2 Collagen scaffolds in skin tissue engineering

Numbers of studies have been conducted to investigate collagen based biomaterials for skin tissue engineering. Porous collagen scaffolds fabricated by Ma *et al.* [107] was firstly cross-linked by EDC to eliminate the issue of rapid degradation, they

then seeded fibroblasts onto the porous collagen scaffold to induce dermal regeneration. Flourescent images of cell seeded scaffolds showed that fibroblasts distributed evenly in the collagen scaffold with their normal shuttle-like morphology. Histological results showed that after 21 days implantation, fibroblasts had migrated through the interior of the scaffold as well as populating the peripheral regions of the scaffold. A collagen nanofibrous matrix was developed to study its effects on human keratinocytes and applications in skin tissue engineering by Rho *et al.* [108] using electrospinning from 8% collagen solution. The ultimate tensile strength of the fabricated collagen matrix was 11.4 and 7.4 MPa in dried and hydrated status, respectively, and cytocompatibility tests showed that the matrix promoted human keratinocyte adhesion, migration and proliferation. Results from open wound healing tests in rats showed that the collagen based matrix accelerated early stage wound healing compared to a control group, and they suggested that collagen matrix may be suitable as a wound dressing or a scaffold for skin tissue engineering. Recently, collagen derived from fish has been used to fabricate scaffolds for skin tissue engineering: Cao *et al.* [109] used freeze-drying to produce highly porous scaffolds incorporating bFGF-loaded poly(DL-lactic-co-glycolic acid) (PLGA) microspheres. The fibroblasts were then seeded, and the results obtained from cell proliferation and *in vivo* evaluation showed these scaffolds supported proliferation of seeded fibroblasts and enhanced regeneration of the skin tissue.

Besides porous scaffolds, collagen based hydrogels have also been fabricated and investigated for skin tissue engineering [110]. Hu *et al.* [111] studied the mechanical properties and cytocompatibility of a collagen based hydrogel as a scaffold for constructing tissue-engineered skin. Results from *in vitro* cell culture indicated that compressed collagen gels induced seeded dermal fibroblasts to gradually develop into a stratified epidermal layer. Braziulis *et al.* [112] demonstrated that a type I collagen hydrogel can be safely and conveniently handled by the surgeon, and showed that hydrogel scaffolds as skin substitutes have the ability to reconstitute full thickness skin defects in an animal model.

2.6.1.3 Collagen scaffolds for vascular, tendon and ligament repair

A collagen gel mixed with mesenchymal stem cells (MSCs) was produced by Awad *et al.* [113] and this cell-collagen composite was introduced into full thickness, full length, and central defects created in the patellar tendons of the animal models. After implantation, the group found that the surgically implanted cell-collagen conposite improved the biomechanical properties of tendon repair tissues signficantly. In another study, Juncosa-Melvin *et al.* [114] firstly fabricated porous collagen sponges, which they then encapsulated with mesenchymal stem cells (MSCs) in collagen gel. The mixed collagen gel was then injected into the porous scaffold, and the constructs were implanted in bilateral full-thickness defects. Histological results showed that the scaffolds had induced the formation of collagen

and fibronectin, and cellular alignment was found to be comparable to an undamaged tendon. Collagen based scaffolds have also been investigated for vascular tissue. Boccafoschi *et al.* [115] fabricated a type I collagen film from neutralized acid-soluble solutions, and the film was subjected to cytocompatibility and platelet adhesion tests. Their results indicated that the neutralized collagen film did not enhance blood coagulation although slight amounts of platelet adhesion and aggregation were recorded. Cell culture showed that the film promoted the adhesion and proliferation of both smooth muscle and endothelial cells. Collagen based scaffolds have also been used to assist ligament repair. A collagen hydrogel incorporating platelets has been investigated by Murray *et al.* [116]. Hydrogels were used to fill wound sites created in both extra- and intra-articular ligaments of animal models. The results indicated that the collagen hydrogel filled wound increased the expression of various proteins and growth factors, and they concluded that their collagen hydrogel was suitable for ligament repair.

2.6.1.4 Collagen as coating material in tissue engineering

ECM derived collagens are ligands to the integrins of cells, and cell adhesion to a substrate is highly dependent on the interactions between integrins and ligands [117]. Collagens are often used as bioactive molecules to modify the surface of biomaterials to improve cell adhesion [118, 119].

Collagen has been shown to improve the biological function of materials in tissue engineering. Chen *et al.* [120] coated collagen onto the fibril structures of a knitted silk matrix which was used as a ligament scaffold implanted in rabbit medial collateral ligament defect models. The results showed that, compared to uncoated matrix, collagen coated matrix had better mechanical properties, and host cells deposited more collagen, with more collagen fibril formation. The fibrils formed had a larger diameter and an improved healing interface between scaffold and ligament. Silicone is usually considered to lack cytocompatibility due to its surface characteristics, and protein adsorption as well as cell adhesion on silicone materials is relatively low. Hauser *et al.* [121] used type I collagen to coat a plasma pre-treated silicone surface, and *in vitro* cell culture using calcein-AM stain revealed that the collagen coating increased adhesion of 3T3 fibroblasts as well as cell viability. Olivero *et al.* [122] immobilized type IV collagen, fibronectin and laminin respectively on material surfaces onto which they seeded rabbit lens epithelial cells. They discovered that surfaces coated with type IV collagen promoted adhesion of seeded cells at optimized concentrations compared to laminin and fibronectin, and laminin was found to enhance cell migration. Similarly, Cooke *et al.* [123] used the functional domains of ECM proteins (type I and type IV collagen, fibronectin and laminin) instead of the whole protein molecules to enhance cell adhesion on glass. Surfaces coated with motifs from both types of collagen had significantly increased cell attachments compared to untreated glass, with type IV collagen giving the highest numbers of attached cells.

2.6.2 Chitosan in tissue engineering

2.6.2.1 Chitosan as biomaterials

Chitosan is composed of N-acetyl-β-Glucosamine, and it has a similar structure to glycosaminoglycans (GAGs), the main ground substance component of ECM [124]. The cationic nature of chitosan promotes retention and concentration of negatively charged molecules such as cytokines, growth factors and nucleic acids which are essential to cell proliferation and differentiation [125]. The biodegradability of chitosan is another key to its suitability for tissue engineering applications. Chitosan is known to be degraded by chitosanase, lysozyme and papain *in vitro* [126], while *in vivo* degradation of chitosan is primarily due to lysozyme and takes place through the hydrolysis of acetylated residuals in the chitosan [105]. The degradation rate of chitosan is found to be inversely proportional to the degree of acetylation of the polymer [127]. Due to its cytocompatibility, biodegradability, non-toxicity, wound healing support, and bacteriostatic effects, chitosan has been processed into various forms such as fibres, sponges, membranes and hydrogels to mimic the original tissues or tissue-biomaterial interfaces [128-134].

2.6.2.2 Chitosan in soft tissue engineering and wound dressing

Studies have found chitosan and its based materials had the abilities to promote the cell infiltration, increase ECM deposition as well as maintain the homeostasis [135, 136]. Previous studies had shown chitosan based materials induced the formation

of the collagen fibers during wound healings [137, 138], and Kojima *et al.* [139] had also found type I and III collagen were largely synthesized in chitosan based materials during wound healing. Ueno *et al.* [140] have suggested that the production of ECM and ECM-related collagen was not directly induced by chitosan but may be due to the increased synthesis of ECM-related growth factors. Meanwhile, in joint connective tissue, significant increasing on collagen productions was found in cells seeded chitosan scaffolds [141]. Similarly, Funakoshi *et al.* [142] discovered the collagen production increased dramatically in a fibroblasts seeded chitosan scaffold. What's more, both *in vivo* and *in vitro* studies showed that human mesenchymal stem cells cultured in chitosan scaffolds had an increased collagen synthetize [143, 144].

2.6.2.3 Chitosan based porous scaffolds

Scaffolds used for wound healing and soft tissue regeneration usually require high porosity to facilitate nutrient and metabolite transport, cell proliferation and migration, and vascularization during tissue regeneration [145, 146]. Porous scaffolds can also provide appropriate mechanical properties to support the regeneration of epithelial and soft tissues, and controlled porosity in chitosan scaffolds has been found to promote angiogenesis [124, 147]. A chitosan based porous scaffold cross linked with glutaraldehyde (GA) has been fabricated by Ma *et al.* [148]. The porous structures of the scaffold supported infiltration and proliferation of human fibroblasts *in vitro*. Similarly, Ko *et al.* [147] investigated a

bilayer porous chitosan scaffold fabricated with varied pore sizes using ice as a porogen. The large open surface pores and interconnected bulky pores beneath the scaffold surface were found to facilitate human dermal fibroblast penetration into the inner part of the scaffold, and homogeneous new tissue formation was observed *in vivo.*

2.6.2.4 Chitosan based hydrogel

Chitosan and chitosan based materials have also been fabricated into hydrogel substrates which have been mainly used as scaffolds, drug delivery systems and biomolecule carriers [149, 150]. A chitosan hydrogel produced by Wu *et al.* [151] showed significant cytocompatibility as 3T3 fibroblasts were found to have successfully migrated into the hydrogel. Insulin and bovine serum albumin were pre-mixed into the hydrogel and the release of these two proteins was also assessed, and it was found the release rate of the proteins was controllable. Obara *et al.* [152] fabricated chitosan hydrogels incorporating fibroblast growth factor through UV light cross-linking. Full thickness skin defects in diabetic mice were replaced by the hydrogel. Histology showed the formation of both advanced granulation tissue and capillaries as well as epithelialization in wound tissue that indicated that growth factor-loaded chitosan hydrogels were a promising wound healing biomaterial. Crompton *et al.* [153] seeded foetal mouse cortical cells into a thermally responsive 3-D chitosan hydrogel, and poly-D-lysine was added to the hydrogel system to improve cell adhesion. Neurite outgrowth within the chitosan hydrogel was

observed and cell numbers increased.

2.6.3 Collagen/chitosan based tissue engineering scaffolds

Although collagen scaffolds have excellent biological function for tissue engineering, they have crucial limitations due to poor mechanical properties and rapid degradation *in vivo* and *in vitro*. Approaches including chemical cross-linking of collagen and blends of collagen and other biopolymers have been tried to improve their mechanical properties and reduce degradation rates [154, 155].

2.6.3.1 Cross-linking collagen with chitosan

Another approach to improve mechanical properties and biostability of collagen based biomaterials is to blend collagen with synthetic or natural polymers. Natural polymers such as chitosan, silk fibroin, alginate and hyaluronic acid have been used. Chitosan is one of the most used natural polymers to its non-immunogenic and biodegradable characteristics [156]. As noted in section 2.6.2.1, Chitosan has a similar molecular structure to glycosaminoglycans (GAGs) which confers desirable biological functions in tissue engineering [124].

Collagen/chitosan porous scaffold

Scaffolds based on collagen/chitosan blends have been investigated in soft tissue engineering. Han *et al.* [157] seeded epidermal cells on an asymmetric porous collagen/chitosan scaffold with varying pore sizes on either side to mimic human

dermal tissue. After three weeks in culture, the composite skin substitute had a histological structure similar to that of normal skin tissue, confirming that this porous collagen/chitosan scaffold was suitable for skin tissue engineering. Mart ńez *et al.* [158] have tailored the mechanical properties of scaffolds with a tensile modulus between 5.5 and 24 kPa. They also found that cross-linked collagen/chitosan scaffolds undergo much slower degradation compared to uncross-linked scaffolds: At day 14 of collagenase digestion, 40% mass loss was found in crosslinked scaffolds while 80-100% mass loss was observed in uncross-linked scaffolds.

Gingras *et al.* [159] used a porous collagen/chitosan scaffold to investigate whether tissue engineered dermal tissue could promote nerve regeneration. They began by fabricating porous collagen/chitosan through freeze-drying, then keratinocytes and fibroblasts were seeded into the reconstructed dermis and cultured for 7 days before transplantation onto the back of nude mice. The results showed that nerve growth was first detected 60 days after grafting and became abundant from 90 days. They concluded that their porous collagen/chitosan skin sponge had the ability to induce nerve growth.

Collagen/chitosan hydrogel scaffold

Hydrogels can be defined as 3-D networks composed of cross-linked hydrophilic molecules which contains large amounts of water [160]. Hydrophilic hydrogels

were introduced by Wichterle and Lim for biological application in the 1960s [161]. Because of their unique water absorption and retention and biomimetic properties, hydrogels have been widely used in drug delivery, wound healing, tissue engineering and other biomedical applications [162].

To date, various collagen/chitosan hydrogels have been investigated in soft tissue engineering. Deng *et al.* [163] designed collagen based hydrogel scaffold as a potential treatment biomaterial for cardiovascular disease, where they improved the hydrogel's mechanical properties by adding chitosan to the hydrogel blend. They found that introducing chitosan improved the stability of the hydrogel and *in vitro* culture results showed that endothelial cells formed more vascular-like structures compared to collagen-only hydrogels. They also found that collagen/chitosan hydrogels induced expression of vascular endothelial-cadherin which indicated greater maturation of endothelial cells. Similarly, McBane *et al.* [164] fabricated two kinds of hydrogels, one was pure collagen and the other contained collagen/chitosan at a ratio of 10:1. Adding chitosan to collagen improved the mechanical properties of the hydrogel significantly (the elastic modulus increased from 0.4 to 0.7 kPa). Testing *in vivo* resulted in increased expression of vascular cell adhesion protein in collagen-chitosan compared to pure collagen hydrogels, and collagenase degradation was slower, finally they concluded that collagen/chitosan hydrogel is suitable for use as pro-angiogenic ectopic islet transplant site. Fiejdasz *et al.* [165] investigated using genipin to cross-link

injectable collagen and collagen/chitosan hydrogels. Mechanical tests showed that chitosan increased the mechanical properties of the collagen hydrogel, and properties could be further modulated by adjusting the genipin concentration. Genipin cross-linked collagen/chitosan hydrogels also showed promising cytocompatibility in their cytotoxicity studies.

.

Besides porous scaffolds and hydrogels, collagen/chitosan film scaffolds have also been developed. Shanmugasundaram *et al.* [166] fabricated a collagen/chitosan based thin film scaffold onto which human epidermoid carcinoma cells were seeded to test its biocompatibility, the results proved the fabricated scaffold could be utilized as a substrate. Chitosan is regarded as a reliable copolymer which can be combined with collagen to improve mechanical properties.

2.7 Applications of RHC based biomaterials in soft tissue engineering

At the time of writing, few studies have reported the use of recombinant collagen as biomaterials in tissue engineering application and wound healing, where recombinant collagen based biomaterials have been used as films, porous scaffolds and hydrogels [88, 167-169].

2.7.1 RHC based porous scaffolds

In the same way as collagen derived from animal sources, recombinant human collagen can be fabricated into highly porous scaffolds and applied to a variety of applications in soft tissue engineering. Hu *et al.* [170] used freeze-drying method to fabricate recombinant human collagen based scaffold with porosity more than 90%. Fibroblasts were then seeded into the porous scaffold. And they found the recombinant human collagen significantly enhanced the cells adhesion, and proliferation (compared to the fibroin scaffolds control), and they suggested recombinant collagen was a good candidate for skin tissue engineering. Jia *et al.* [171] combined freeze-drying and cross-linking method together to fabricate a porous scaffold which contains recombinant human collagen and nano-hydroxyapatite at ratio of 1:1. Their mechanical test showed the porous scaffold had Young's modulus of 36.7 MPa which was comparable to Relive® Artificial Bone, a commercial product with a compressive modulus measured at 27.7 MPa [172].

They also seeded rabbit chondrocytes on the composite scaffold and cultured for 21 days and the results confirmed recombinant human collagen/nono-hydroxyapatite porous scaffold was capable of encouraging both cell adhesion and GAG synthesis. In skin tissue engineering, Wang *et al.* [173] applied recombinant collagen to rat skin trauma and found that synthesis of collagen was enhanced and wound healing was accelerated through epidermal. In addition, recombinant human collagen has also shown its potential in hard tissue engineering such as used in bone regeneration. It has been reported from Zhu *et al.* [174] that they fabricated a complex which based on phosphorylated recombinant collagen, and results from calcium uptake test showed the complex had great bioavailability, and mouse model of osteoporosis indicated the fabricated complex was superior for treating osteoporosis than gluconate-calcium and $CaCl_2$.

2.7.2 RHC based hydrogel scaffolds

Merrett *et al.* [175] used recombinant human collagen I and III to produce transparent hydrogels as human corneal substitutes where solutions of recombinant human collagens were cross-linked with 1-ethyl-3-(3-dimethyl aminopropyl) carbodiimide (EDC). The mechanical test on both hydrogels indicated adequate tensile strength had been achieved where type III recombinant human collagen hydrogel is found mechanically superior. The cytocompatibility test showed both collagen based hydrogels supports *in vitro* epithelium and nerve over-growth. Results from twelve months implantation showed regeneration of the corneal cells

on recombinant human collagen corneal substitute where the hydrogels remain their optical clarity and stable integration. Recently, Zhao *et al.* [176] investigated the biodegradation and cytocompatibility of microbial transglutaminase cross-linked recombinant collagen, where they found by changing the amount of enzyme in cross-linking could produce hydrogels with different mechanical properties as well as collagenase degradation rate. They had also noticed the hydrogel formed by ratio of enzyme to collagen at 40 U/g had the best cytocompatibility results from the *in vivo* test, and they suggested the hydrogel can be used as an injectable soft tissue filling biomaterial.

2.8 Scaffolds for soft tissue engineering

Scaffolds act as the ECM to provide an ideal environment for the replacement of defective tissue where treatment and tissue regeneration required. Two main categories of biomaterial (biopolymers) based scaffolds are currently involved in this field, synthetic and natural biopolymers [177-179].

2.8.1 Design concepts of collagen based scaffolds

To mimic the native biological environment and support the regeneration of new tissues, the ideal biomaterial scaffold should have the following features: sufficient porosity and suitable pore size as ideal microstructure, adequate mechanical properties, excellent cytocompatibility, specific shape of contact surface with potential chemical composition, controlled degradation rate, less steps during manufacture as well as material resources budget concern [124, 178-180].

2.8.1.1 Suitable pore size, porosity and interconnectivity

In order to mimic the ECM and promote the cell growth and migration, scaffolds with appropriate pore size, high porosity and great interconnectivity are demanded. All these three key elements benefit the tissue regeneration as an idea pore size with high porosity provide a large surface area to the scaffold volume that supports cell attachments to the pore structures [149]; sufficient interconnectivity (usually more than 80%) in microstructure of porous scaffold facilitates the nutrient transportation,

waste exchange as well as oxygen diffusion, it also allow the migration of the proliferated cells and assist the neovascularization [145, 181, 182]. For instance, it has been reported that the optimal culturing pore size for vascular from epithelial is 5 μm [183], the proliferation of the fibroblasts is found between 80 to 250 μm [184], and 20 to 125 μm of the pore size benefits the regeneration of the adult mammalian skin[185]. In addition, not only the cell proliferation activity, but also the ECM production such as expression of ECM collagen is also found affected by the pore size of the fabricated biomaterials [186]. The features of such porous structures with the desired pore size and porosity are found highly depended on the fabrication methods and discussed in section 2.8.2 [178, 187].

2.8.1.2 Adequate mechanical properties

Generally speaking, tissue engineering scaffold should have sufficient mechanical strength to maintain its structural integrity during the tissue regeneration and its mechanical properties should match the original healthy tissue or organ to support and transfer the loads generated from both the micro-environment and daily activities [177, 179]. It's important to determine the mechanical properties of the fabricated scaffolds in soft tissue engineering that scaffolds should have adequate mechanical strength can support the maintenance of the microstructures that provide sufficient space for cell ingrowth, nutrient transportation [188], and also support the loading *in vivo* as implants [189]. What's more, porous scaffolds and hydrogels which own different mechanical strengths have also been found influence

the cell activities as stiffness of the substrates are known to regulate the cellular behaviors such as spreading, migration and proliferation [190, 191]. Specifically, Haugh *et al.* [192] fabricated porous collagen based scaffold with tunable stiffness, they found that the cell proliferation rate was increased as increasing the mechanical strengths of the scaffolds. Meanwhile, Liu *et al.* [193] seeded fibroblasts on the surface of hydrogels with varied stiffness where they found the cell spreading and proliferation were substrate stiffness dependent. The encapsulation of the neural stem cells in hydrogel studied by Banerjee *et al.* [194] showed that, as increasing the mechanical strengths of the hydrogel system, the proliferation activities of the encapsulated cells reduced. And they also found neuronal marker β-tubulin III had the highest expression within the softest hydrogels.

2.8.1.3 Acceptable cytocompatibility

One of the concerns in designing of the functional soft tissue engineering scaffolds is their cytocompatibility. Biocompatible scaffolds means the biomaterials should show no harmful to the cells and host as no toxic products are involved during their applications [149, 195]. Meanwhile, as *in vitro* culturing are required in some of the soft tissue engineering, the biocompatible scaffolds should have the ability to enhance the proliferation of the seeded cells and induce the regeneration of the ECM [177, 180].

To date, both synthetic biodegradable polymers and natural derived materials are involved in soft tissue engineering [196]. Synthetic polymers such as poly(glycolic acid) (PGA), poly(L-lactic acid) (PLLA) and PLGA are widely used as biomaterials in producing the tissue engineering scaffolds. Such polymers are considered biocompatible and their degradation rates were found tunable to match the regeneration of the new tissue [180, 197]. On the other hand, it has been reported that some of the synthetic polymers are general low in bioactivity and their degradation process might produce acidic byproducts that lower the local pH which might cause tissue necrosis [198]. Differ from some of the synthetic polymers, biological materials such as gelatin, collagen and chitosan are biocompatible to the cells and host tissues or organs, meanwhile, those materials are also found had the abilities that provide cell adhesion and growth (as discussed in Chapter 2.6.1 and 2.6.3). What's more, they are biodegradable in body and such degradation can be synchronized with the tissue regeneration.

Natural biomaterials based porous scaffolds and hydrogels usually are weak in their mechanical strengths as compared to synthetic polymers, which is why cross-linkers are frequently applied to improve their mechanical properties. For instance, collagen based porous scaffolds and hydrogels are usually cross-linked by chemical cross-linker such as EDC [86, 199] and glutaraldehyde [200], where glutaraldehyde is also frequently applied to cross-link the chitosan based porous scaffolds and hydrogels [201, 202]. However glutaraldehyde are found cause local

incompatibility, inflammation or calcification that limits cell ingrowth and cytotoxicity (even at concentrations as low as 3.0 ppm) after being released into the host as a result of cross-linked polymer degradation [203] and [94]. So cross-linkers with high efficiency but low in toxicity are required. For example, natural cross-linking reagents such as genipin is used to cross-link the collagen, chitosan or collagen-chitosan based scaffolds due to its low toxicity [154, 204], where procyanidin as another natural cross-linker is also found has the ability to cross-link the collagen derived biomaterials to improve their biostability, and the treated scaffolds show excellent cytocompatibility to the cells and tissues [102, 205].

2.8.1.4 Cell adhesion ability

A suitable surface property of the scaffold should assist the cell adhesion to the scaffold and induce proliferation *in vitro* or *in vivo*. Synthetic polymers based scaffolds can be easily fabricated, however, most of synthetic polymers have been found only function as empty scaffolds for seeded cells that do not promote cell-material interactions [206-208]. To improve the cells adhesion to the scaffolds, maintain cellular morphologies and promote proliferation activities, surfaces of synthetic polymer based porous scaffolds, hydrogels as well as films are commonly modified by adding or immobilizing bioactive polymers, such as Arg-Gly-Asp (RGD) sequence contained peptides [209, 210], growth factors [211, 212] or ECM derived collagens etc. [122, 213]. Besides that, growth factors had also been introduced into the wound dressings to accelerate the healing progress [214, 215].

2.8.1.5 Controllable degradation rate

As biomimetic scaffolds join into the tissue repair and regeneration progress, a balance between ECM synthesis and biodegradation in scaffold is desired, and it means the rate of neo tissue formation should be same as the degradation progress on biomaterials [105, 216]. The degradation of collagen materials *in vivo* is mainly through enzymatic activities , and their degradation time is found ranged from 2 to 24 weeks which is dependent to the cross-linking degree [103]. The chitosan based biomaterials show varied degradation rates and it has been found the rate is highly dependent to the deacetylation degree. The degradation behaviours of the collagen and chitosan based biomaterials are mentioned in sections 2.6.

2.8.2 Methods to fabricate 3-D porous scaffolds and hydrogel scaffolds

To date, various techniques have been developed to fabricate three dimensional porous scaffolds for the soft tissue engineering applications. The method for fabricate the porous scaffolds usually include electro-spinning, solvent casting, phase separation, gas foaming and solid freeform fabrication, where gelation of the hydrogels are achieved through covalent, ionic bonds or physical interactions between the polymer chains. And each method is known to have its own advantages and disadvantages [180].

2.8.2.1 Electrospinning

Electrospinning is a technique that uses an electric field to draw microfibers from a charged polymer solution, and it allows to produce fibers with varied diameters and morphologies by manipulating various process parameters such as polymer concentrations, voltage and temperature [217-219]. It has been reported a variety of natural polymers (e.g. collagen) as well as synthetic polymers had been fabricated into nonwoven fabrics by electrospinning, where excellent cell attachments, proliferations were reported [220-222]. On contrary, the toxic organic solvents (e.g. chloroform and methanol) are usually required in electrospinning process that known as the disadvantage of this technique, and other drawbacks such as low rigidity of the formed scaffolds as well as less control of pore sizes and shapes might become the limitations of the electrospinning method in certain applications [177, 180, 223].

2.8.2.2 Porogen leaching

This method uses porogens to create porous structures. Usually, the polymer solution together with porogens are added into a mold to form a stable construction, then the porogens are leached away using certain solvent or water to produce a porous scaffold [224]. The main advantage of this technique is the controllable of both pore size and porosity by tuning the porogens size and its concentration [225, 226]. However, the porous structures fabricated through this technique had been found poor in interconnectivity [226].

2.8.2.3 Freeze-drying

Freeze-drying has been frequently used to create porous 3-D scaffolds. The freeze-drying usually uses a cooling procedure to produce thermodynamic instability within the samples and leading to a phase separation. The porous structures are then obtained by sublimation under vacuum condition that remove the solvent and ice crystals [178]. The porosity, pore size as well as porous structures have been found largely dependent to the fabrication conditions such as cooling rate, freezing temperature, concentration of polymer solution as well as the concentration of the used solvent [180, 227, 228]. For instance, Davidenko *et al.* [229] noticed that by altering the freezing conditions could produce desirable pore size and pore orientations, and they had produced a porous collagen scaffold with complex pore orientations by introducing multiple temperature gradients to the freezing conditions. Ma *et al.* [148] used freeze-drying method prepared the porous collagen-chitosan scaffold and their scaffold showed ability to host the seeded fibroblasts and promoted the cells proliferation. Meanwhile, O'Brien *et al.* [230] studied the effect on pore size of the porous scaffold to the cells adhesion, they produced a series of porous scaffolds with varied pore size by tuning the samples freezing temperature to fulfil the requested structures. Other than natural biopolymers, synthetic polymers such as PLGA and PLLA had also been involved to fabricate porous scaffolds for tissue engineering successfully [178, 231].

2.8.2.4 Gas foaming

Gas can be used as porogen instead of solid particles in the fabrication of porous scaffolds [232]. To form porous structures, solid compressed polymer discs are treated with high pressure CO_2 in a closed chamber firstly for 2 to 3 days, and then the pressure is rapidly dropped to atmosphere level [233]. It has been reported that this technique could produce scaffold with porosity up to 93% [180]. Although this method does not require any organic solvent and chemistry, but the scaffold formation usually requires high temperature which may damage the bioactive polymer molecules [233]. Furthermore, it is difficult to control the pore sizes and pore connectivity within the solid scaffolds.

2.8.2.5 Solid freeform fabrication

Solid freeform fabrication is a novel technology supported by the computer aided design, and it allows production of objects with unique materials and geometries such as predefined porous structures [234]. A typically application of using solid freeform fabrication is inkjet printing, the jet head ejects the binder onto a polymer powder surface to form the layer or viscous biopolymer which is in accordance with the CAD cross-sectional data [188], where commercial inkjet printer has been report to produce the cell encapsulated scaffold [235, 236].

2.8.2.6 Hydrogel forming

Polymers that form hydrogels can be divided into two categories, one is synthetic polymer based hydrogels and another is natural derived biopolymers such as collagen, fibrin, and alginate. Different from solid porous scaffolds, natural biopolymer based soft nonporous hydrogels are formed through a variety of gelation mechanisms where polymer chains are cross-linked via ionic, physical or chemical interactions [237], and commonly used cross-linking methods in hydrogel formations are listed in Figure 2-8. Natural forming hydrogels are usually formed via ionic and physical cross-linking. Alginate known as a linear polysaccharide copolymer of (1–4)-linked b-dmannuronicacid (M) and a-l-guluronicacid (G) monomers that its hydrogel has been used in soft tissue engineering applications including drug delivery and cell encapsulation [238]. The forming of alginate hydrogel is initiated by Ca^{2+} interact with monomers to form ionic bridges between different polymer chains [239]. Differ from ionic interactions, the collagen, gelatin or chitosan based hydrogels are usually formed through covalent cross-linking. 1-ethyl-3-(3-dimethyl aminopropyl) carbodiimide (EDC) known as an amide-type cross-linker that is widely used in cross-linking collagen based materials mainly through linking the carboxylic acid and amino groups presenting on the chains to form covalent bonds[84]. Ahn *et al.* [104] had fabricated porcine and collagen hydrogels for corneal implants by using EDC cross-linker, and they found the mechanical strengths of the obtained hydrogels could be modulated by varying the content of EDC, and the cytocompatibility test indicated their EDC cross-linked

hydrogels are biocompatible and infiltration of the proliferated cells were found within the hydrogels from *in vivo* implantation tests.

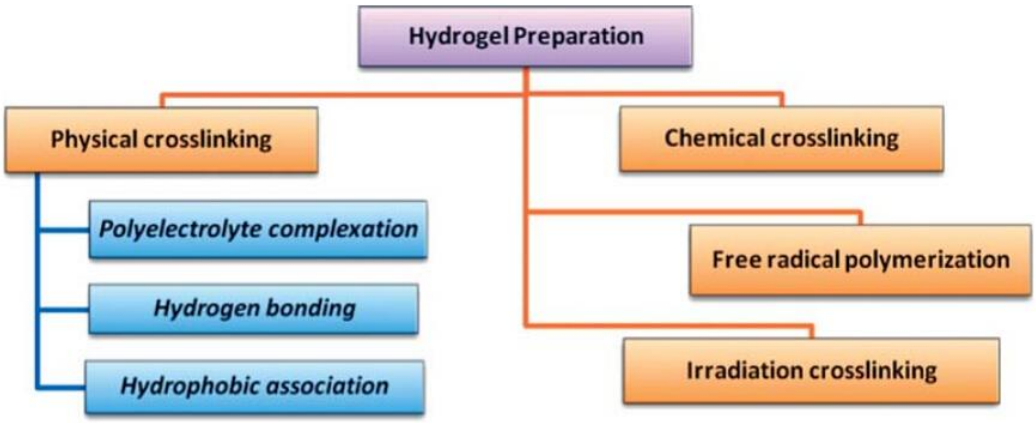

Figure 2-8. Schematic diagram listing the most used methods of hydrogel formations [149].

Chapter 3 Materials and methods

Gelatin and RHC based 3-D porous scaffolds were constructed from freeze-drying method and a series of RHC based soft hydrogel scaffolds were also developed through covalent bonding. Morphologies, swelling ratio, gelation time, *in vitro* biodegradation, mechanical properties including compression modulus and elastic modulus were evaluated. Cytotoxicity tests were carried out by using Alamar Blue assay where metabolic activities of cells were evaluated. Importantly, the proliferation and morphologies of seeded 3T3 fibroblasts were assessed at defined culture time using DNA assay, fluorescent stain, SEM as well as optical microscopy. The gene expressions of the ECM associated proteins were quantified by the quantitative reverse transcription-polymerase chain reaction (qRT-PCR) technique. Finally, results were discussed by comparing to the literature to confirm the phenomena and findings discovered in current study.

3.1 Fabrication methods

Gelatin based porous scaffolds

Gelatin powder with a molecular weight range of 13,000-44,000 Da (JiangShan Chemical Co., Ltd. China) and chitosan powder with deacetylation degree > 90.0% (Shanghai Lanji Technology Development Co., Ltd) were dissolved in 0.5 M ethanoic acid at weight ratio of 1:1 and stirred for 1 h to prepare homogeneously mixed 1.5% (w/v) GEL-CHI solutions. The mixtures were poured into the moulds and frozen at -20 ℃ then lyophilized in the freeze-drier (Eyela. Fdu-1200. Japan) at -45 ℃ for 48 h to obtain cylindrical porous scaffolds with a 13 mm diameter and 6 mm thickness. Grape seed extracted procyanidin (PA) powder (Jianfeng Natural Product R&D Co., Ltd, China) and glutaraldehyde solution (Sigma Aldrich) were prepared in 50% (v/v) ethanol separately to prepare PA and GA cross-liking solutions at concentrations of 0.1%, 0.5% and 1.0% by weight. The cross-linked scaffolds were then named as PA 0.1 to 1.0 and GA 0.1 to 1.0 that referred to the type of cross-linker and its concentration respectively, the names of the fabricated porous scaffolds are listed in Table 3-1 and images of typical scaffolds are shown in Figure 3-1. The prepared scaffolds were then fully immersed into the cross-linking solutions for 48 h at room temperature. The cross-linked scaffolds were dried over filter paper and stored at 4 ℃.

Table 3-1. Type of fabricated porous GEL-CHI scaffolds

Type of scaffolds	Glutaraldehyde (w/v)	Procyanidin (w/v)
Uncross-linked	Not added	Not added
PA 0.1		0.1%
PA 0.5		0.5%
PA1.0		1.0%
GA 0.1	0.1%	Not added
GA 0.5	0.5%	
GA 1.0	1.0%	

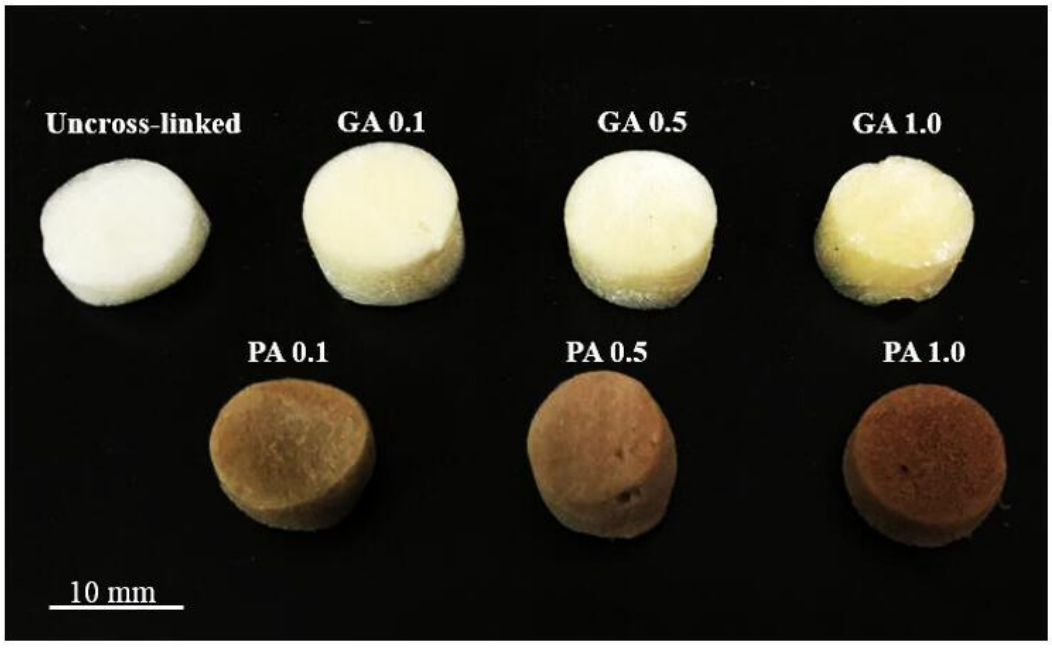

Figure 3-1. Fabricated gelatin-chitosan porous scaffolds

RHC based porous scaffolds

To prepare 1.5% w/v RHC-CHI (50:50) solution, 750 mg RHC (Bioengineering lab of Nanjing University of Science and Technology, Jiangsu, China,) and 750 mg chitosan powder (deacetylation degree > 90.0%, Shanghai Lanji Technology Development Co., Ltd) were weighed and poured into 0.2 mol/L acetic acid solution then stirred by a magnetic stirrer for 1 h to fully dissolve the powders. 100 mL final solutions were used to immediately cast. The prepared RHC and RHC-CHI solutions were poured into Polytetrafluoroethylene (PTFE) molds and frozen in the freezer at -20 ℃ overnight. After that, the frozen samples were lyophilized in a freeze-drier (Eyela. Fdu-1200. Japan) at 45 ℃ for 48 h to obtain cylindrical porous scaffolds with 13 mm diameter and 5 mm thickness. The freeze-dried samples were then carefully taken out from the molds with the tweezers. A modified cross-linking method according to a previous study by Damink *et al.* [240] was used to cross-link the porous scaffolds in this study. Briefly, different amounts of EDC (50, 75 and 100 mg) were dissolved in 75% ethanol respectively to prepare 10 mL cross-linking solutions at final EDC concentration of 0.5, 0.75 and 1.0% (w/v). The porous scaffolds were then fully immersed in 10 ml cross-linking solution with varied EDC concentrations for 24 h at 37 ℃ followed by washing in 10 ml distilled water 3 times and freeze-dried for further use. The cross-linked RHC-CHI scaffolds were named RHC-CHI-50, 75 and 100 according to the amount of EDC that prepared the cross-linking solutions. Meanwhile, pure RHC scaffolds with RHC concentration of 1.5, 2.0 and 3.0% (w/v) were fabricated with the same method. The names and

compositions of the fabricated RHC and RHC-CHI scaffolds are listed in Table 3-2, and images of typical scaffolds are shown in Figure 3-2.

Table 3-2. Types of fabricated RHC and RHC based porous scaffolds

Porous scaffolds	**Biopolymers concentration (w/v)**	**RHC:CHI ratio**	**Cross-linker: EDC (mg)**
RHC-1.5	1.5%	/	50
RHC-2.0	2.0%	/	50
RHC-3.0	3.0%	/	50
RHC-CHI-50	1.5%	50:50	50
RHC-CHI-75	1.5%	50:50	75
RHC-CHI-100	1.5%	50:50	100

Figure 3-2. Fabricated RHC and RHC-CHI porous scaffolds

RHC based hydrogel scaffolds

RHC (Bioengineering lab of Nanjing University of Science and Technology, Jiangsu, China) and chitosan (Shanghai Aladdin Biochemical Technology Co., Ltd.) at 3 different ratios (80:20, 50:50 and 20:80) were fully dissolved in universal tubes to prepare 1.5% w/v RHC-CHI hydrogel solutions respectively. The mixture was filtered through a 0.22 μm filter and collected in a sterilized universal tube. Then 50 mg EDC was added into each 10 ml RHC-CHI mixture and stirred for 1 min. 300 μL final solution was then transferred into each well of a 48-well plate. The plate was placed into the 37 ℃ incubator for 2 h to achieve full gelation. Hydrogels of 2.0% and 3.0% w/v were prepared in the same manner. The name of fabricated hydrogels corresponding to the biopolymer concentration and RHC to chitosan ratio are listed in the Table 3-3 and the fabricated series hydrogel scaffolds are shown in Figure 3-3.

Table 3-3. Types of fabricated hydrogels

Hydrogel	**Biopolymers concentration (w/v)**	**RHC:CHI ratio**
A	1.5%	80:20
B	1.5%	50:50
C	1.5%	20:80
2A	2.0%	80:20
3A	3.0%	80:20

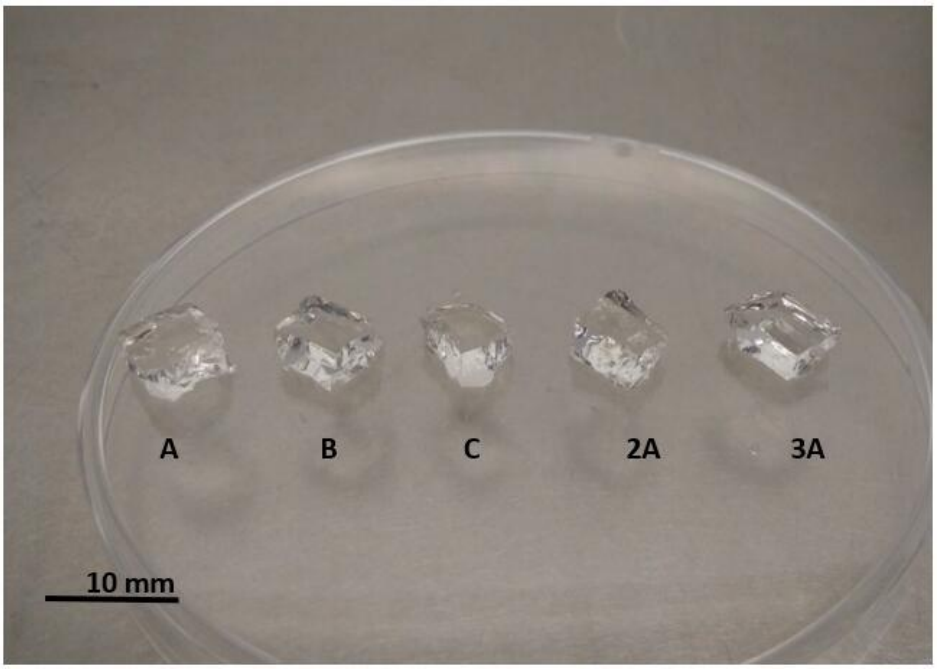

Figure 3-3. Picture showing the fabricated hydrogels placed on petri-dish

3.2 Morphology analysis

Porous scaffolds

To examine the morphology of the porous scaffolds, samples were sectioned using a microtome and then sputter-coated with platinum before imaging using a scanning electron microscope (Philips XL30, Netherlands) at an accelerating voltage of 10 kV, the working distance was set to 15 mm and images with different magnifications were recorded. In addition, the internal structures of the porous gelatin-chitosan scaffolds were also characterised using X-ray micro-computed tomography (Micro-CT; XRADIA XRM-500), where the scaffold was cut into small cube ($2 \times 2 \times 2 = 8\,mm^3$) and scanned at an exposure of 2 seconds/slice with resolution of 3.034 μm/pixel. The obtained cross-section two-dimensional (2D) images were reconstructed into 3-D image through Image J. Mercury intrusion porosimetry (MIP; Micromeritics Autopore IV, United States) was used to determine the average pore sizes and porosities of the porous scaffolds.

Hydrogel scaffolds

The morphology of the hydrogel were examined using scanning electron microscopy (SEM). Flat hydrogel samples were carefully placed in the petri-dish and frozen in liquid nitrogen, the frozen samples were then lyophilized in freeze-drier (Eyela. Fdu-1200. Japan) at -45℃ for 24 h under vacuum. After vacuum drying, the dried samples were attached to the metal holder using conductive tape and sputter-coated with platinum for 90 s. The coated surfaces were imaged by a scanning electron microscope (Philips XL30, Netherlands) at an accelerating

voltage of 10 kV, the working distance was set to 15 mm. Images with different magnifications were recorded. In addition, the surface morphology of the wet hydrogel was analyzed by using the Philips XL 30 FEG ESEM in wet mode with an accelerating voltage of 10 kV.

3.3 Fourier transform infrared spectroscopy (FT-IR) and cross-linking degree

FT-IR spectra of the RHC and RHC-CHI samples were obtained from a Fourier transform infrared spectrophotometer (Bruker-EQUINOX55, Germany). Part of a dry scaffold was peeled off by tweezers and placed onto the testing stage directly where spectra were recorded under absorbance mode at 2 cm^{-1} interval in the wavelength range of 400 to 4000 cm^{-1}. Reference spectra were collected before each test.

The cross-linking degree (efficiency) of the EDC cross-linked RHC-CHI and RHC scaffolds were determined as sum of detected uncross-linked RHC concentrations from both solutions of cross-linking and washing process to the total RHC in fabricated scaffolds. After cross-linking finished, 1 ml cross-linking solution was then taken out and tested by high performance liquid chromatography (HPLC, AGILENT 1260 INFINITY) to confirm the RHC concentration in the solution. 1 ml used distilled water from wash process was taken out and tested by HPLC to

confirm the RHC concentration, and this procedure was repeated in the second and third wash. Finally, the detected RHC were summed and converted to the weight of RHC powder, the cross-linking degree was then defined as the ratio of detected RHC to the total RHC in porous scaffolds. The determination of the standard curve of RHC concentration that used to calculate the RHC content in tested solution is provided below.

A series of known concentration of RHC solutions (as listed in Table 3-4) were tested by HPLC to generate the standard curve of RHC concentration. Triplicate samples of each RHC concentration were tested and averaged results were used to determine the standard curve. The expression of RHC concentration in solution was determined as: $Y=9718.5X-78.4$ and $R^2=0.9995$, where Y is the area of the detected peak wave of RHC in solution and X is the concentration (mg/mL) of RHC in solution (Figure 3-4).

Table 3-4. RHC concentrations used to generate standard curve

RHC solution	**RHC concentration** (mg/mL)	**Retention time** (min)	**Peak area**	**Averaged peak area**
A-1	0.0980	11.048	890.66	888.72
A-2		11.051	889.06	
A-3		11.054	886.43	
B-1	0.3036	11.053	2907.98	2908.36
B-2		11.056	2910.12	
B-3		11.056	2906.98	
C-1	0.5162	11.058	4940.67	4939.67
C-2		11.059	4942.64	
C-3		11.060	4935.70	
D-1	0.6968	11.059	6594.24	6594.49
D-2		11.061	6597.40	
D-3		11.056	6591.83	
E-1	0.8708	11.055	8343.12	8321.65
E-2		11.054	8315.43	
E-3		11.055	8306.40	
F-1	1.0096	11.051	9845.57	9842.82
F-2		11.048	9841.77	
F-3		11.048	9841.11	

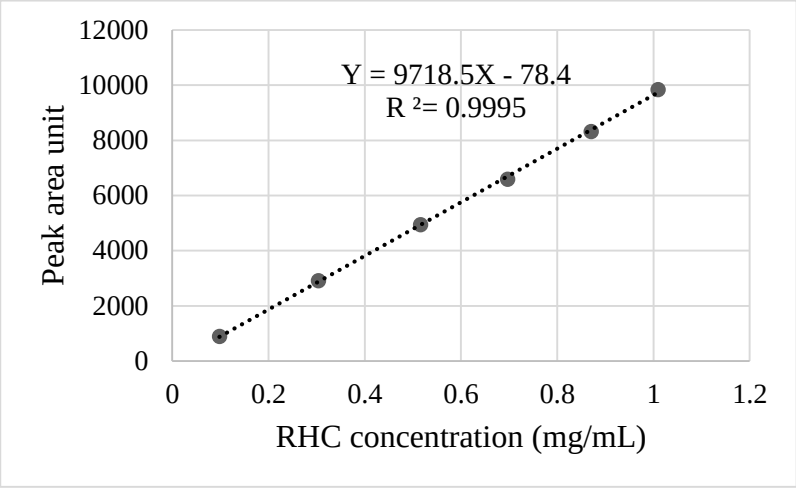

Figure 3-4. RHC standard curve.

3.4 Gelation time of hydrogels

To investigate the gelation time, 700 μL each type of hydrogel solution was put into 1.5 mL vials and incubated at three different temperatures (4 ℃, 24 ℃ and 37 ℃) respectively. The status of the hydrogel solutions were checked every minute by tilting the vials and disturbing of the pipette to observe the gel formation, once hydrogel solution stopped moving and sticky gels were observed when disturbing by the pipette, the time was recorded.

3.5 Swelling ability

Swelling of the porous scaffolds was determined by measuring the change in mass of scaffolds between dry and wet status. To establish dry weight, vacuum dried scaffolds were weighed then fully immersed in PBS for 24 h. Scaffolds were then

removed from the solution, and any drops of PBS were removed with filter paper before the wet scaffolds were weighed. The swelling ratio (SR) of the scaffolds were calculated from the expression: $SR=(W_w-W_d)/W_d$ where W_d and W_w refers to the dry and wet weight of the scaffolds respectively.

3.6 *In vitro* degradation

Porous scaffolds

Biodegradation degree of fabricated gelatin-chitosan scaffolds were determined by examining the concentration of dissolved gelatin. Each sample was incubated in 1 ml PBS containing 100 µg collagenase type I (Sigma Aldrich) at 37 ℃ for 12 h. The PBS solution was then centrifuged and 20 µL supernatant was transferred into a 96 well-plate followed by adding 200 µL bicinchoninic acid (BCA) assay (Thermo working reagent). The concentrations of degraded gelation were then determined by the ultraviolet spectroscopy (Tecan Infinite 200 Pro) where light absorption of the solution was measured at 562 nm and compared with the values obtained from solutions with defined gelatin concentrations. The biodegradation degree was then defined as the ratio of detected gelatin to the gelatin in each scaffold.

To determine the biodegradation rate of the RHC and RHC-CHI scaffolds, each scaffold was immersed into 3 mL PBS and kept in an incubator at 37 ℃. To ensure continuous biodegradation, PBS was changed every 2 days. At each defined time point (Day 3, 7, 10, 14, 21 and 28), scaffolds were taken out and rinsed 3 times with

distilled water. After that, the scaffolds were frozen in freezer overnight and freeze-dried to measure the mass. The degradation rate was calculated as: (Wo-Wt)/Wo× 100%, where Wo is the initial weight of the dry scaffold, while Wt is the weight of degraded scaffold at specific time point.

Hydrogel scaffolds

RHC based hydrogel scaffolds (5mm × 5mm × 5mm) were firstly pre-conditioned in PBS for 24 h before weighing. To avoid dryness from the environment, each hydrogel cube was quickly placed into the 1.5 mL vials and weighed. After measuring the masses, the hydrogels were carefully transferred into a 10 ml universal tube where 3 ml PBS was added and kept at 37 ℃ in an incubator for biodegradation. PBS was refreshed every 2 days to ensure the continuous of degradation. At defined time points (Day 1, 3, 7, 10, 14, 21 and 28), the hydrogel scaffolds were taken out and gently rinsed 3 times with distilled water then blotted dry with filter paper to remove extra water and weighed immediately. The degradation rate was calculated as: (Wo-Wt)/Wo× 100, where Wo is the initial weight of the hydrogel while Wt is the degraded weight at selected time point.

3.7 Static mechanical testing

3.7.1 Compression test on gelatin based and RHC based porous scaffolds

To determine the mechanical properties of all fabricated porous scaffolds, compression and stress-relaxation tests were performed using a universal testing

machine (Instron 5969) in uniaxial compression mode. The samples (cylindrical porous scaffolds with a 13 mm diameter and 6 mm thickness) were compressed up to 70% strain at a constant cross-head loading speed of 2 mm/min (method applied and modified based on ASTM F2150-13 and D1261-16). The compressive modulus was obtained from the slope of initial linear (0 to 10% strain) of the stress- strain curves and compressive stresses at 70% strain were recorded. For repetitive compression tests, the interval between the 1st and 2nd compression on each sample was set to 5 min. After the second compression, scaffolds were freeze-dried for SEM. In stress relaxation tests on gelatin based porous scaffolds, each sample was compressed up to 30% of its initial thickness and this displacement was maintained while the stresses were recorded over 600 s. The stress relaxation was calculated as: $(1-\sigma_{final}/\sigma_{max})\times 100\%$ where σ_{max} is the compressive stress at 30% deformation and σ_{final} is the final recorded stress of the test. All samples in the static mechanical tests were previously hydrated in PBS solution for 24 h and three samples were tested for each type of scaffold.

3.7.2 Tensile test on porous scaffolds

The tensile properties of the scaffolds were determined using a universal testing machine (Instron 5969) in uniaxial tensile mode, and a 50 N load cell with speed of 2 mm/min was used in the test (method applied and modified based on ASTM F2150-13 and D1623-17). The maximum tensile strengths of the RHC and RHC-CHI scaffolds were recorded at the break point and the elastic moduli were obtained

from the gradient at the initial linear region of the stress-strain curve. Samples were cut into 13 mm x 5 mm rectangular strips with thickness of 3 mm and the gauge length was set to 5 mm. Samples were pre-hydrated in PBS for 24 h prior to testing.

3.7.3 Compression test on RHC based hydrogels

The stiffness of the hydrogels were determined at defined time points (Day 1, 3 and 5) by using universal testing machine (Instron 5969) under compressive mode. The fresh prepared hydrogel solutions was first poured into the glass petri-dish, then the petri dish was transferred into the 37 ℃ incubator where gelation took place to form fully gelled hydrogel with thickness of 5 mm. The glass petri-dish and hydrogel was then sterilized under UV light for 40 min. After sterilization, 20 mL PBS was then poured into the petri dish to fully cover the hydrogel and the petri-dish was placed back into the incubator for 24 h before the test in order to achieve their equilibrium status. A flat aluminum punch at diameter of 12 mm was used to compress the hydrogel, crosshead speed was set to 1 mm/min (method applied and modified based on ASTM F2150-13 and D1261-16). The compressive modulus was obtained from slope of the linear region between 5% and 10% of the strain. Hydrogel scaffolds formed from different RHC to CHI ratios (80:20, 50:50 and 20:80), different biopolymer concentrations (1.5%, 2.0% and 3.0%) as well as different amount of cross-linker (EDC 50, 75 and 100 mg) were tested in this study. Five random compression points were selected at each type of hydrogel and all tests were carried out under room temperature.

3.8 Cytocompatibility analysis

3.8.1 Cell culture

NIH-3T3 mouse fibroblasts (European Collection of Cell Cultures) were used in cytocompatibility analysis and complete Dulbecco's Modified Eagle Medium (DMEM) with 10% foetal calf serum, 2% HEPES buffer, 2% penicillin/ streptomycin, 1% L-glutamine, 1% non-essential amino acids (Gibco Invitrogen) was used as cell culture medium throughout the tests.

3.8.2 Sample sterilization

Dry porous scaffolds were immersed in 70% ethanol and stirred on a magnetic stirrer for half hour to remove any bubble trapped in the porous structures. After that, the scaffolds and ethanol solution were transferred into 50 ml sterile universal tubes and kept for another 3 h at room temperature for sterilization. At the end of sterilization, scaffolds were taken out from the universal tubes and washed with sterile distilled water 3 times before transferring into sterilized universal tubes. The universal tubes were then filled with PBS and stored in -20 ℃ for further use.

Hydrogel solution was first filtered through a 0.22 μm filter, and cast in the 48-well plate. After incubating in 37 ℃ incubator overnight to obtain fully gelled hydrogels, the hydrogel samples were further neutralized by washing with PBS solution 3 times. The plate was then transferred into the hood for sterilization under the UV

light for one hour. After sterilization, 300 μL warm PBS containing 4% chloroform was used to fill each well in order to maintain sterility. The plate was then stored in a 4 ℃ fridge until further use.

3.8.3 Cytotoxicity elution test

UV sterilized porous scaffolds were incubated in 37 ℃ culture medium for 24 h with a surface area/medium volume ratio of 3 cm^2/mL, where hydrogel samples were cut into 1 cm^3 cube and each sample incubated in 2 ml fresh medium (medium extraction method applied according to ISO 10993-12 of larger items with thickness > 1.0 mm) for 24 h before removing for test. Fresh medium was used as control. Meanwhile, 3T3 cells were seeded at a density of 40 x 10^3 cells/cm^2 in each well of a 48 well-plates and incubated for 24 h until fully confluent. Then the culture medium was replaced with extracted test eluents and incubated for another 24 h. Cells cultured in complete DMEM were used as control. The extraction medium was removed and cells were washed with PBS 3 times and incubated in Alamar Blue solution (1:10 Alamar Blue: Hank's Balanced Salt Solution) for 80 min along with 3 blank wells. 100 μL aliquots were transferred to a 96-well plate in triplicate, the fluorescence were measured at the excitation wavelength at 530 nm and emission at 590 nm in FLx800 plate reader (BioTek Instruments Inc.). In the current study, according to the ISO 10993-5, cellular viability which reduce to less than 70% of the control group, the sample is then considered has cytotoxic potential.

3.8.4 Cell seeding & culturing in porous scaffolds and hydrogel scaffolds

The sterilized porous scaffolds were pre-conditioned in cell culture medium overnight before seeding. 3T3 cells at number of 150k were seeded on top of each porous scaffold while 30K were seeded onto each hydrogel scaffolds. The seeded scaffolds were then immersed in culture medium (1 mL/well) and maintained at 37 ℃ in 5% CO_2 humidified incubator and the medium was changed every 2 days. The time points of the culturing were set to day 1, 3, 7, 10 and 14. Similar to the porous scaffolds, 30k 3T3 fibroblasts were seeded onto each hydrogel sample and the culture medium was changed every 2 days.

3.8.5 Cell metabolic activities (Alamar Blue assay)

The metabolisms of cells in seeded scaffolds were determined using Alamar Blue assay at defined time points (day 1, 3, 7. 10 and 14 were selected for RHC and RHC-CHI porous scaffolds, 12h after initial seeding was selected for RHC based hydrogels). Culture mediums were firstly removed from each well and scaffolds were washed 3 times with warm PBS at approximately 37 ℃. 1 mL of Alamar Blue assay (Bio-Rad) (1:10 Alamar Blue: Hank's Balanced Salt Solution (Invitrogen)) was added into each well to fully cover the scaffold and 3 wells were filled as blanks. The plate was transferred into incubator to incubate at 37 ℃, 5% CO_2 for 80 min. After that, the plate was wrapped with aluminium foil to avoid direct exposed to light and placed on a plate shaker to shake 10 min at 150 rpm. 100 μL extraction from each sample was transferred into a 96-well plate in triplicate including 3

blanks. The florescence were measured at the excitation wavelength at 530 nm and emission at 590 nm in FLx800 plate reader (BioTek Instruments Inc.). The readings from blank were subtracted from results. Triplicates of each sample were tested and experiments were repeated twice.

3.8.6 Cell proliferation (Hoechst DNA assay)

Porous scaffolds

Cell proliferation was determined by quantifying the total DNA content at each time point. To lyse cell, porous scaffolds were washed with PBS twice before adding 1 mL sterile distilled water into the well. The well plate was then stored at -20 ℃ to freeze the samples. After frozen, plate was taken out from the freezer and thawed in 37 ℃ incubator, samples were freeze-thawed 3 times. Aliquots of 100 μL test sample from each well were transferred into a 96 well-plate, 100 μL Hoechst stain (Hoechst DNA assay 33258, Sigma-Aldrich, UK) was also added to each well. The well-plate was then placed on plate shaker for 10 min at 300 rpm before reading on FLX-800 plate reader using fluorescence excitation at 360 nm, emission 460 nm. The results were calculated from the pre-determined standard curve of series of known DNA concentrations. The procedures that used to determine the DNA standard curve are described as following.

DNA standard curve preparation

- **Hoechst DNA assay**

The calf thymus DNA solution was reconstituted with 1 mL of 0.01 M NaCl solution firstly, then diluted the reconstituted DNA solution with 50 mL 0.01 NaCl solution to prepare a stock solution of 20 μg/mL.

- **DNA standard curve**

DNA concentrations were prepared as listed in Table 3-5 and vortexed prior to use. Aliquots 100 μL of each DNA standard solution into a 96-well plate along with 100 μL of Hoechst stain, gently mixed on a plate shaker at 300 rpm and then read on a plate reader with 360 nm excitation and 460 nm emission. The standard curve was then plotted from the results.

Table 3-5. DNA concentrations used to make the DNA standard curve

Concentration (μg.mL^{-1})	**DNA stock** (μL)	**TNE buffer** (μL)
10	500	500
6	300	700
5	250	750
4	200	800
3	150	850
2	100	900
1	50	950
0.5	25	975
0.25	12.5	987.5
0.125	6.25	993.8

RHC based hydrogel scaffolds

Cells grew on hydrogel surface were firstly washed with warm PBS 3 times and 200 μL fresh prepared trypsin was added into each well to detach the cells. The plates were then incubated at 37 ℃ for 5 min to fully detach the cells from the hydrogel. To confirm the detachment of the cells from hydrogel, plates with hydrogels were examined by optical microscopy. In order to obtain cell-medium suspension, 300 μL warm medium was poured into each well and gently stirred by using the 1 ml pipette. The suspensions were then transferred into 1.5 mL vials and centrifuged at 1200 rpm for 5 min to obtain pellets. Supernatants were aspirated from the vials and pellets were re-suspended with 1 ml sterile distilled water. The vials were freeze-thawed 3 times to fully lyse the cells. The thawed test samples were then mixed on vortex for 60 s. The final DNA concentrations were calculated from a predetermined DNA standard curve that obtained from a series of known DNA concentrations (method refers to determination of the DNA concentration from porous scaffolds).

3.8.7 Fluorescent images

The proliferation and distribution of cells in porous scaffolds were examined at defined time points (day 3, 7, 14 for gelatin-chitosan porous scaffolds, day 7 and 14 for RHC based porous scaffolds). When each time point was reached, the designated scaffolds were taken out from the wells and washed with PBS 3 times and then stained in calcein AM solution (Live/Dead^{TM}, Invitrogen) for cell

proliferation study. To investigate the cells growth at the internal part of scaffolds, the stained scaffolds were cut into half horizontally and observed by the fluorescent microscopy (DMLB, Leica) at an excitation wavelength of 495 nm and emission of 530 nm.

3.8.8 Cell morphology study

Cell morphology in seeded porous scaffolds

For cell morphology study, at end of culture period (Day 14), porous scaffolds were washed in PBS and fixed in 3% glutaraldehyde in 0.1 M cacodylate buffer for 30 min. Then the fixative was replaced with 7% sucrose solution and the scaffolds were stored at 4℃ for overnight. Scaffolds were then washed 3 × 5 min in 0.1 M cacodylate buffer before post-fixing in 1% osmium. Scaffolds were gradually dehydrated through a series of ethanol gradients from 20% to 100% at 5 min each and finally dried in hexamethyldisilazane (HMDS) before being sputter-coated with platinum for 90 s and viewed by scanning electron microscopy. The working distance was set to 15 mm for cell morphology study.

Cell morphology on seeded hydrogel scaffolds

Due to the transparence of the hydrogels, cells which seeded on hydrogel scaffolds were monitored by optical microscopy. At defined culturing time points, plate which carried cell seeded hydrogels was taken out from the incubator and placed onto the stage of the optical microscope (Nikon Eclipse TS 100), the x40

magnification of the objective lens was used. The brightness was adjusted to optimized condition and digital photos were recorded using a digital camera. After recording, the plate was either sprayed with ethanol and returned into the incubator or put into hood for DNA content test.

3.9 Quantitative reverse transcription-polymerase chain reaction (qRT-PCR)

NIH 3T3 seeded RHC and RHC-CHI scaffolds (3-D) were used for qRT-PCR where cells cultured in 35 mm culture dishes were used as control. At selected time points, fibroblast seeded scaffolds were taken out from culturing medium and washed three times in warm PBS. The scaffolds were then grinded with liquid nitrogen and immersed in Trizol® for 5 min to fully lysed cells (cells cultured in 35 mm culture dishes were treated with Trizol® directly) and supernatants were then collected by centrifugation at 12×10^3 rpm for 5 min. 0.5 mL chloroform was then added into the vials and shaken vigorously for 15 s then left to stand at room temperature for another 3 min. The suspensions were further centrifuged at 12×10^3 rpm for 15 min at 4°C. After centrifugation, the transparent aqueous phase which contained RNA was isolated from the mixture and carefully transferred into a new vial, after that 0.5 ml isopropanol was added into the vial. The vial was then gently shaken and left to stand at room temperature for 10 min before centrifuging at 12×10^3 rpm at

4°C. The supernatant was discarded and RNA pellet washed three times by 1 ml 75% ethanol and further centrifuged at 7.5×10^3 rpm for 5 min at 4°C. The supernatant was then discarded and pellet left to air dry for 15 min. The dried pellet was resuspended in 20 μL Rnase-free water. The RNA concentration and purity in each sample was measured using ELISA reader (Infinite M200 PRO) at wave length of 260 and 280 nm. The absorbance ratio of 260 to 280 nm in each sample should between 1.8 and 2.0 to indicate a purity of the RNA samples. The primers used for RT-PCR are shown below:

β-actin: forward 5'-GGCTGTATTCCCCTCCATCG-3'

reverse 5'-CCAGTTGGTAACAATGCCATGT-3'

Integrin α: forward 5'-TGTCTGGCGTATAATGTTGGC-3'

reverse 5'-CTTGTGGGTTAGTAAGCTGCT-3'

Collagen I: forward 5'-GGTGAGCCTGGTCAAACGG-3'

reserve 5'-ACTGTGTCCTTTCACGCCTTT-3'

Collagen III: forward 5'-CTGTAACATGGAAACTGGGGAAA-3'

reserve 5'-CCATAGCTGAACTGAAAACCACC-3'

Reverse transcription works are summarized in the following steps. First, template RNA were diluted to the final concentration of 300 ng/μL with RNase-free water. The reverse transcription system were listed below at 20 μL. Reverse transcription was conducted by incubation at 50°C for 50 min and terminated the reaction by heating at 85°C for 5 min (procedure referred to manual of Applied Biosystems).

RNaseOFF Ribonuclease Inhibitor (40U/μL)	0.5 μL
Oligo(dT) (10μM)	1 μL
5×Reaction Buffer	4 μL
10 mM dNTP MIX	1 μL
Total RNA	2 μL
Nuclease-free water	10.5 μL
OneScript^{TM} Plus RTase (200 U/μL)(Abm)	1 μL
Total	20 μL

The polymerase chain reaction which is used to amplify the cDNA was set to 10 μL reaction system and the reagents used were listed below.

EvaGreen 2× qPCR MasterMix(Abm)	5 μL
Template cDNA	3 μL
PCR Forward Primer (10 μM)	1 μL
PCR Reverse Primer (10 μM)	1 μL
Total	10 μL

The real-time PCR was performed in a Real-Time PCR System (StepOne Plus, Applied Biosystems) with SYBR Green PCRMasterMix (Applied Biosystems) under the conditions of 15 s at 95 ℃, 60 s at 60 ℃, and the fluorescence intensity

was recorded for 40 cycles. The melting curve was performed at 95°C for 15 s, 60°C 1min and 95°C 15s.

3.10 Statistical analysis

The data are presented as mean ± standard deviation (SD), and at least 5 samples were measured for each group of tests throughout the study. Statistical analysis was carried out using Graphpad Prism 6.0 and statistical significance was assessed using One-way ANOVA (analysis of variance) with Tukey test by the software. Significance was indicated with *P<0.05, **P<0.01 and ***P<0.001, where P>0.05 was considered as not statistically significant.

Chapter 4 Results

4.1 Morphology and pore property of the porous scaffolds

Gelatin based porous scaffolds

Typical macro and SEM images of the fabricated porous gelatin-chitosan scaffolds are shown in Figure 4-1. It shows that cross-sections of uncross-linked scaffold (Figure 4-1 B) and all cross-linked scaffolds (Figure 4-1 C to H) shared similar internal morphologies as no significant changing in pore structures were observed. The internal morphology of the porous scaffolds was also investigated using Micro-CT, as shown in Figure 4-2, the reconstructed 3-D image indicates a homogenous interconnected pore distribution had been reached in porous scaffolds fabricated from freeze-drying method. The determined average pore sizes as well as porosities are shown in Figure 4-3. It shows that fabricated uncross-linked scaffold has pore size of 44 μm and porosity around 93%; meanwhile. Pore size and porosity of PA and GA cross-linked scaffolds show no significant differences as compared to uncross-linked scaffold.

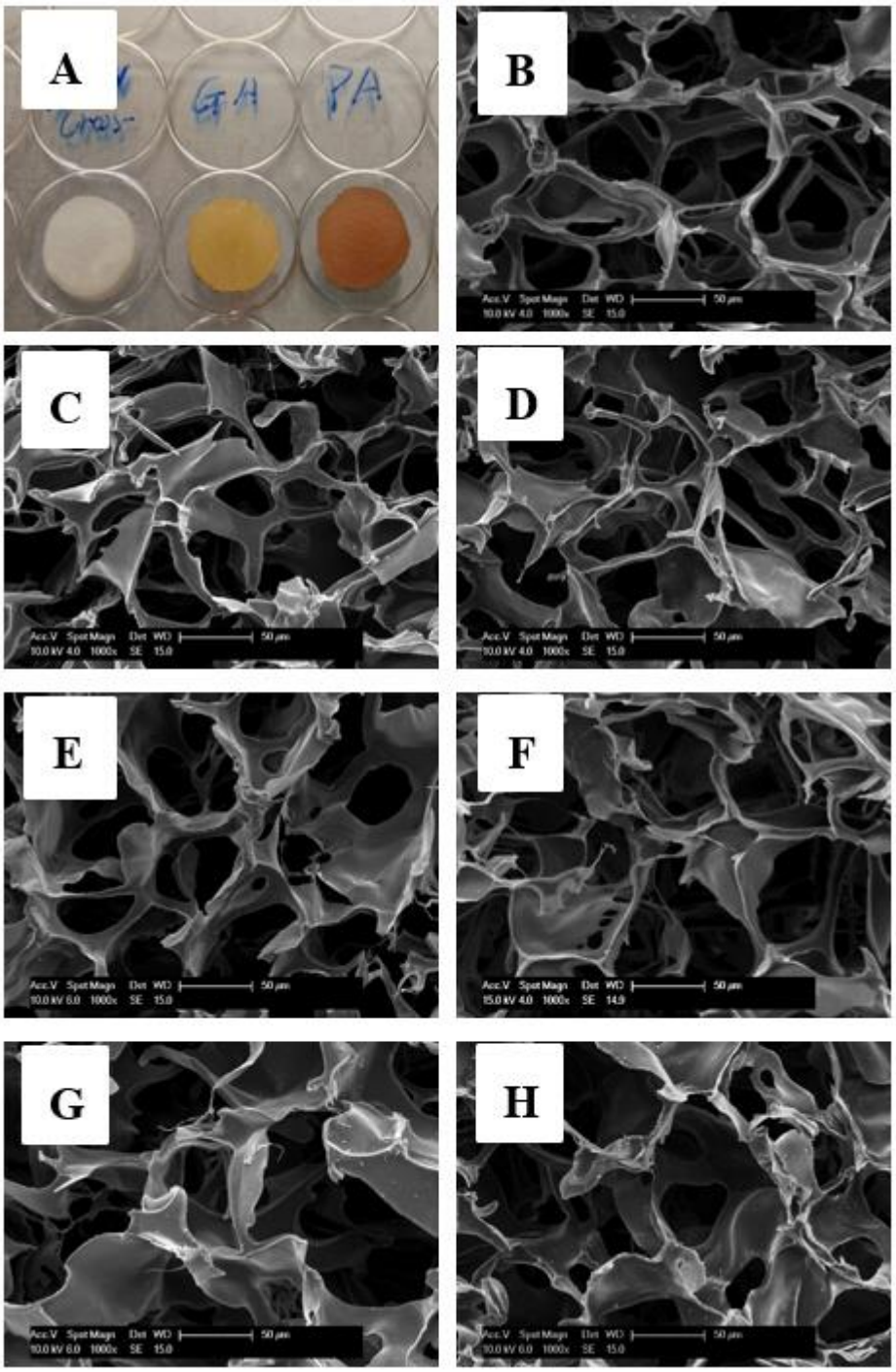

Figure 4-1. (A) Fabricated porous gelatin-chitosan scaffolds; (B) SEM image of cross-section of uncross-linked scaffold, scale bar = 50 µm; (C-E) SEM images of cross-section of PA 0.1, 0.5 and 1.0 scaffold, scale bar = 50 µm; (F-H) SEM images of cross-section of GA 0.1, 0.5 and 1.0 scaffold, scale bar = 50 µm

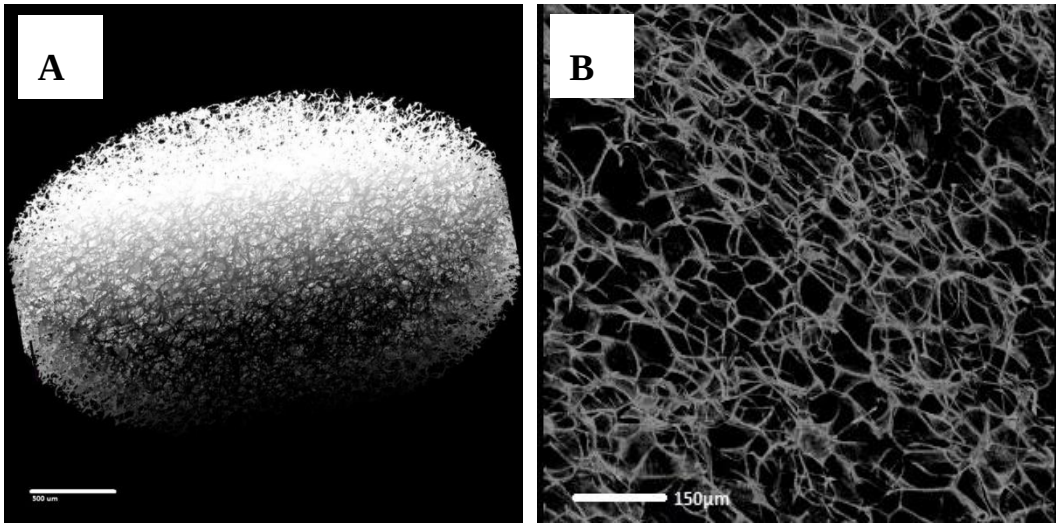

Figure 4-2. Reconstructed 3-D view of the uncross-linked scaffold, white colour represented solid part of scaffold, (A) Scale bar = 500 µm. (B) scale bar = 150 µm

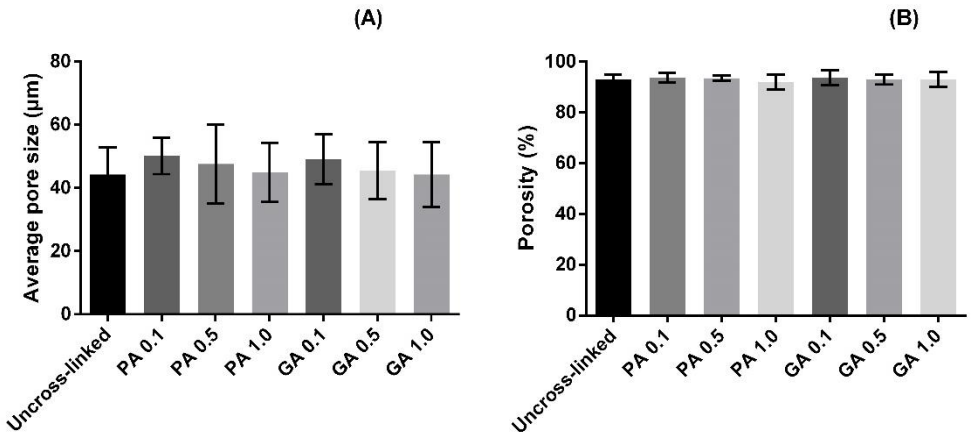

Figure 4-3. (A) Average pore size of uncross-linked and PA, GA cross-linked porous scaffolds; (B) Porosity of the uncross-linked and PA, GA cross-linked porous scaffolds. Bars represent mean ± SD and significance is indicated with *P<0.05, **P<0.01 and ***P<0.001.

RHC based porous scaffolds

The cross-section images of the porous RHC scaffolds fabricated from different RHC concentrations were investigated by SEM and shown in Figure 4-4, the obtained pore size as well as porosity are summarized in Table 4-1. The interconnected and porous structures could be found in all fabricated scaffolds. It also found that the pore shapes and pore wall thicknesses were varied with RHC concentration that used to fabricate the porous scaffolds. At low RHC concentration (1.5% w/v), the pores were formed with thin sheet-like structures, while RHC concentration increased, the thicker pore wall structures became more clearly observed (see in Figure 4-4). In Table 4-1, it shows that the pore sizes of the cross-linked RHC scaffolds were in between 111 μm and 131 μm and the porosities of the cross-linked RHC scaffolds remain constant as they are found ranged from 90% to 93%. As shown in Figure 4-4 A-B; C-D; E-F, there were no significant differences on pore size and porous morphology discovered between its cross-linked and uncross-linked scaffolds.

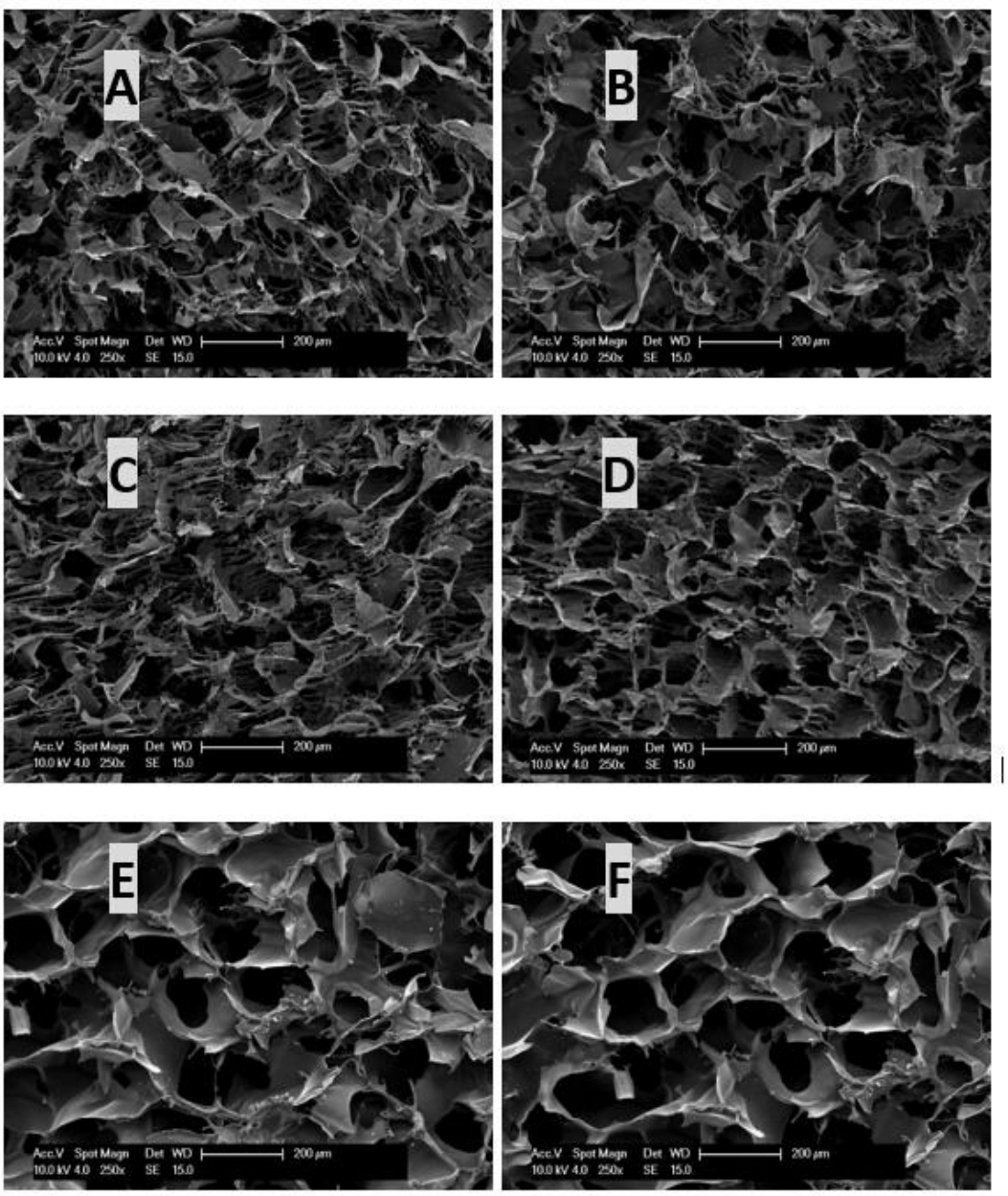

Figure 4-4. SEM image of cross-section of uncross-linked RHC-1.5 porous scaffold (A); cross-linked RHC-1.5 porous scaffold (B); uncross-linked RHC-2.0 porous scaffold (C); cross-linked RHC-2.0 porous scaffold (D); uncross-linked RHC-3.0 porous scaffold (E); cross-linked RHC-3.0 porous scaffold (F). Scale bar = 200 µm in all images.

Table 4-1. Pore sizes and porosities of the RHC porous scaffolds

RHC scaffolds	Pore size (μm)	Porosity
RHC-1.5	111±20	93%
RHC-2.0	128±19	91%
RHC-3.0	131±10	90%

The cross-section images of the fabricated RHC-CHI (50:50) scaffolds which cross-linked with varied amount of EDC as well as images of uncross-linked scaffold were shown in Figure 4-5 where pore size and porosity were summarized in Table 4-2. From the images, it shows that all scaffolds had interconnected porous structures. The homogenous pore structures were also found presented in all cross-sections. There was no significant difference observed on pore shapes and structures among tested samples. Table 4-2 shows that the pore size of the uncross-linked scaffold was slightly smaller compared to 50 mg EDC cross-linked scaffold (RHC-CHI-50) (see Figure 4-5 A-B; C-D), where the average pore size of uncross-lined scaffold was 129 μm and 50 mg EDC scaffold was around 176 μm. It also shows the RHC-CHI-100 scaffold had slightly smaller pore size (136 μm) compared to RHC-CHI-75 scaffold (159 μm) (Figure 4-5 E-F; G-H). Moreover, no significant differences on pore shapes as well as wall thickness were observed among three cross-linked scaffolds Figure 4-5 C, E, G. The porosities of the cross-linked scaffolds were determined between 91% and 92% which had no significant difference compared to uncross-linked scaffold (porosity of 91%)

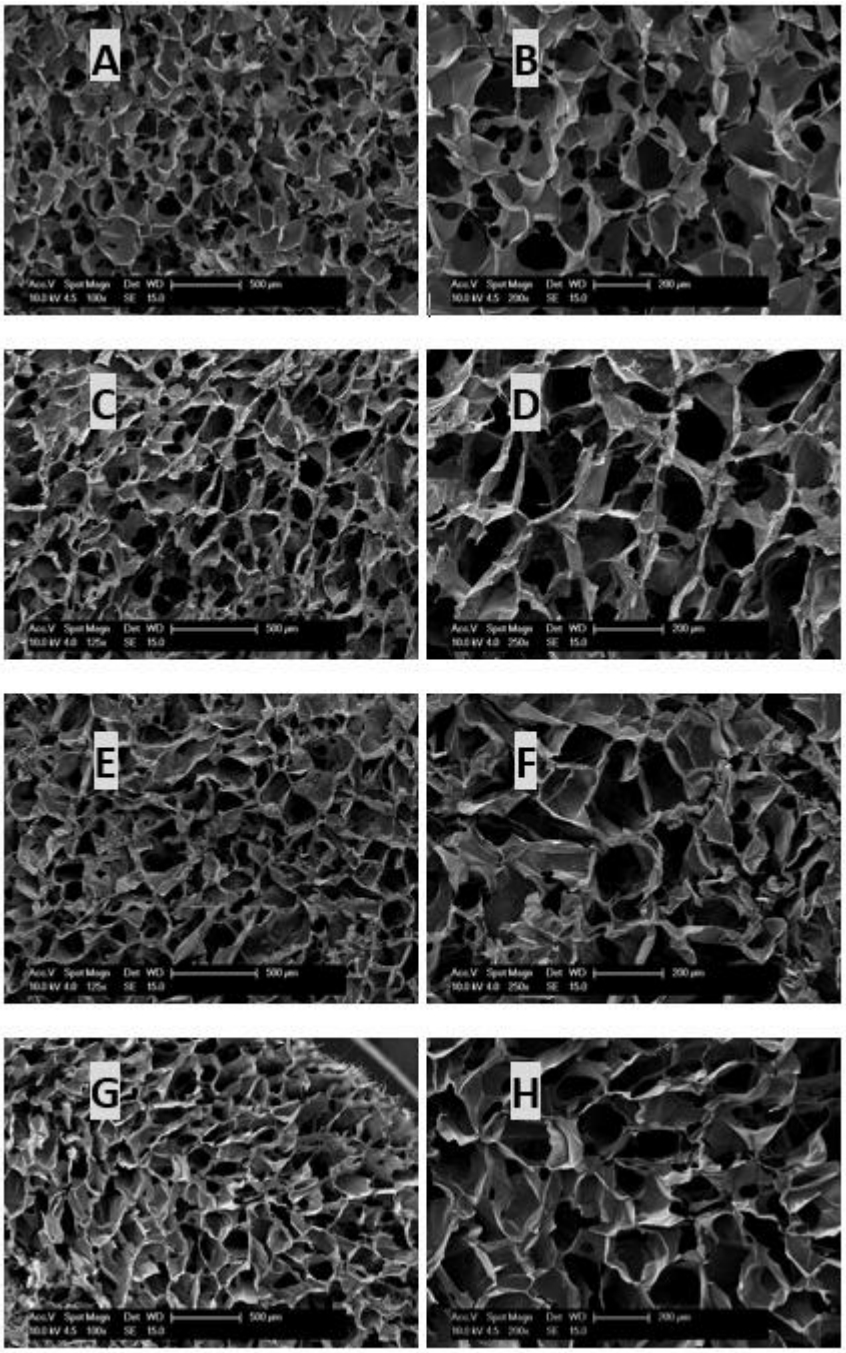

Figure 4-5. SEM images magnification at ×100(left) and ×200(right) of cross-section of uncross-linked RHC-CHI porous scaffold (A-B); RHC-CHI-50 porous scaffold (C-D); RHC-CHI-75 porous scaffold (E-F); RHC-CHI-100 porous scaffold (G-H)

Table 4-2. Pore sizes and porosities of the RHC-CHI scaffolds

RHC:CHI scaffolds	Pore size (μm)	Porosity
Uncross-linked RHC-CHI	129±18	91%
RHC-CHI-50	176±19	92%
RHC-CHI-75	159±22	92%
RHC-CHI-100	136±21	91%

Hydrogel morphology

Figure 4-6 shows the SEM images of hydrogel surfaces after freeze-drying. The texture of hydrogel surfaces were found varying by increasing the chitosan fraction from 80:20 (hydrogel A) to 50:50 (hydrogel B) in RHC hydrogel system while further increase of the chitosan fraction to 20:80 (hydrogel C) showed a less smooth texture on freeze-dried hydrogel surface. Comparing images of 3, 4 an 5, it can also be seen that the morphology of initial fabricating concentrations of 2.0% and 3.0% w/v hydrogel (80:20) showed slightly different texture compared to 1.5% hydrogel. In addition, the ESEM images indicated the fabricated hydrogel scaffolds at their hydrated status had flat surfaces and no significant differences were found among three type of hydrogels.

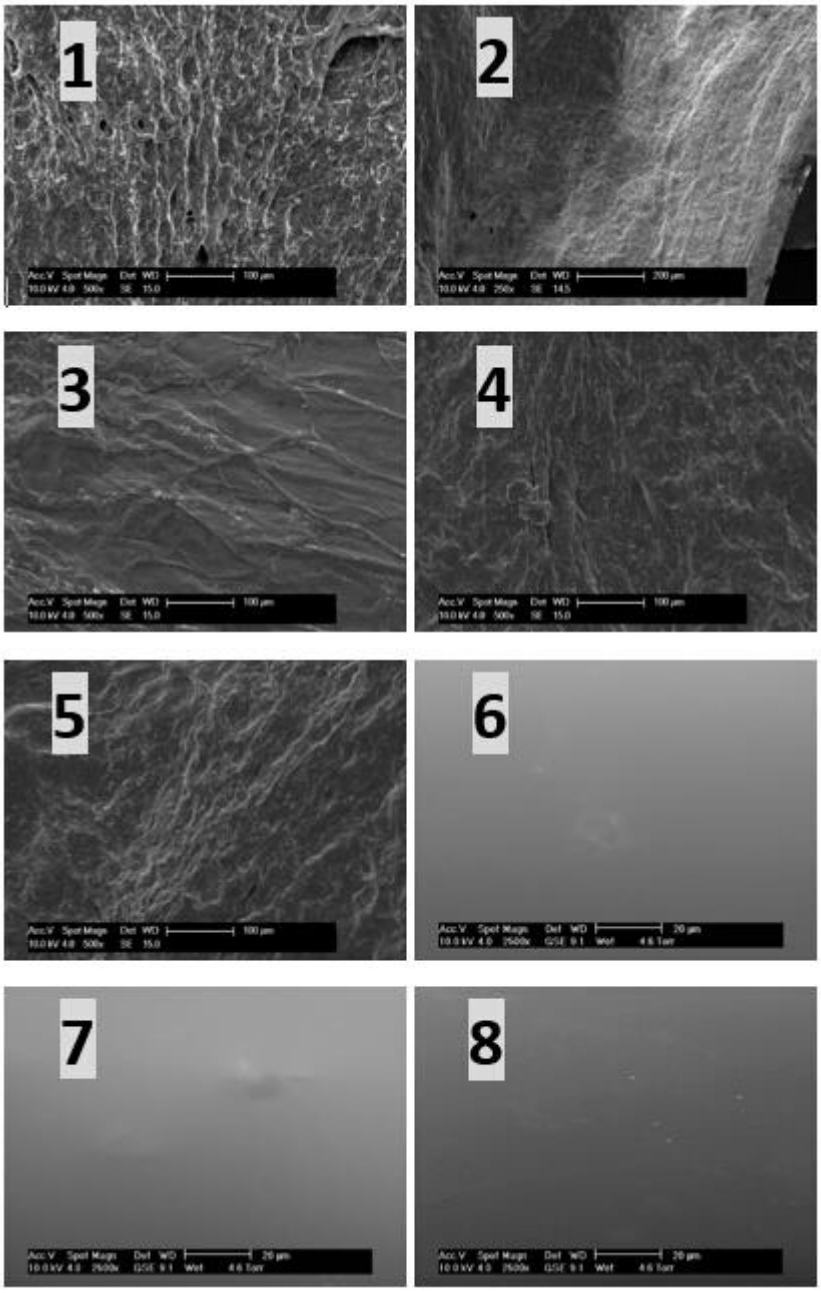

Figure 4-6. SEM images of freeze-dried hydrogels (1)A, (2)B, (3)C, (4)2A, (5)3A; ESEM images of hydrogel surface of (6)A, (7)B and (8)C. Scale bar in SEM images 100 μm, scale bar in ESEM images 20 μm.

4.2 Fourier transform infrared spectroscopy (FT-IR)

The changes of the RHC structures after cross-linking were analysed by FT-IR and absorbance results are shown in Figure 4-7 and wavenumber of amide groups are summarized in Table 4-3. In the uncross-linked RHC spectrum, typical collagen bands can be noticed (Figure 4-7 A). Specifically, Amide I was found at 1625 cm^{-1} which correspond to stretching vibrations of *ν*C=O and *ν*N-H. Amide II at 1540 cm^{-1} and corresponds to *δ*N-H deformation vibrations and *ν*C-N stretching vibrations. Amide A was found at 3291 cm^{-1} correspond to the *ν*O-H and *ν*N-H vibrations, and *ν*N-H corresponding to Amide B was found at 3079 cm^{-1}. After cross-linking with 50 mg EDC, the wavenumber of all cross-linked RHC samples showed no difference compare to the uncross-linked RHC sample (Figure 4-7 A). The intensity of Amide II were found decreased after cross-linking while there were no differences can be found among three cross-linked scaffolds that used different amount of EDC. Meanwhile, there were no other changes on intensity as well as positions of bands can be found among all cross-linked RHC samples as the EDC content increased (Figure 4-7 B). Comparing the spectra, no significant difference on wavenumber of the cross-linked and uncross-linked RHC scaffolds were found, which may suggest the secondary structure of the RHC was not affected by the cross-linking.

The FT-IR spectrum of RHC-CHI porous scaffolds are shown in Figure 4-8 and wavenumbers of amide groups are summarized in Table 4-4. For the uncross-linked

RHC-CHI sample, the typical Amide A band shown at 3272 cm^{-1} which corresponds to *v*O-H and *v*N-H vibrations. Amide B was found at 2930 cm^{-1}. Amide I was found at 1633 cm^{-1} which correspond to stretching vibrations of *v*C=O and *v*N-H. Amide II at 1531 cm^{-1} and corresponds to *δ*N-H deformation vibrations and *v*C-N stretching vibrations (Figure 4-8 A). As cross-linked by 50 mg EDC, the wavenumber of Amide A and B showed no movement while the intensity on Amide A increased. On the contrary, the intensity of Amide I and II decreased significantly compared to the spectrum of uncross-linked RHC-CHI. Meanwhile, it also noticed that the wavenumber of both Amide I and II moved to higher wavenumbers (Amide I 1640 cm^{-1}, Amide II 1556 cm^{-1}) compared to uncross-linked sample. Figure 4-8 B shows the spectra of EDC cross-linked RHC-CHI samples that wavenumber of Amide II shifted slightly to the lower frequency. The intensity of the Amide A band was found increased with increasing concentration of cross-linker so that the spectrum of 100 mg EDC cross-linked RHC-CHI sample (RHC-CHI-100) shows the highest intensity on Amide A band. Similarly, the intensity of Amide I and II were also found to increase as the EDC concentration increased. Specifically, a significant higher intensity on Amide I and Amide A was found in 75 and 100 mg EDC cross-linked RHC-CHI samples as comparing to 50 mg EDC cross-linked RHC-CHI sample.

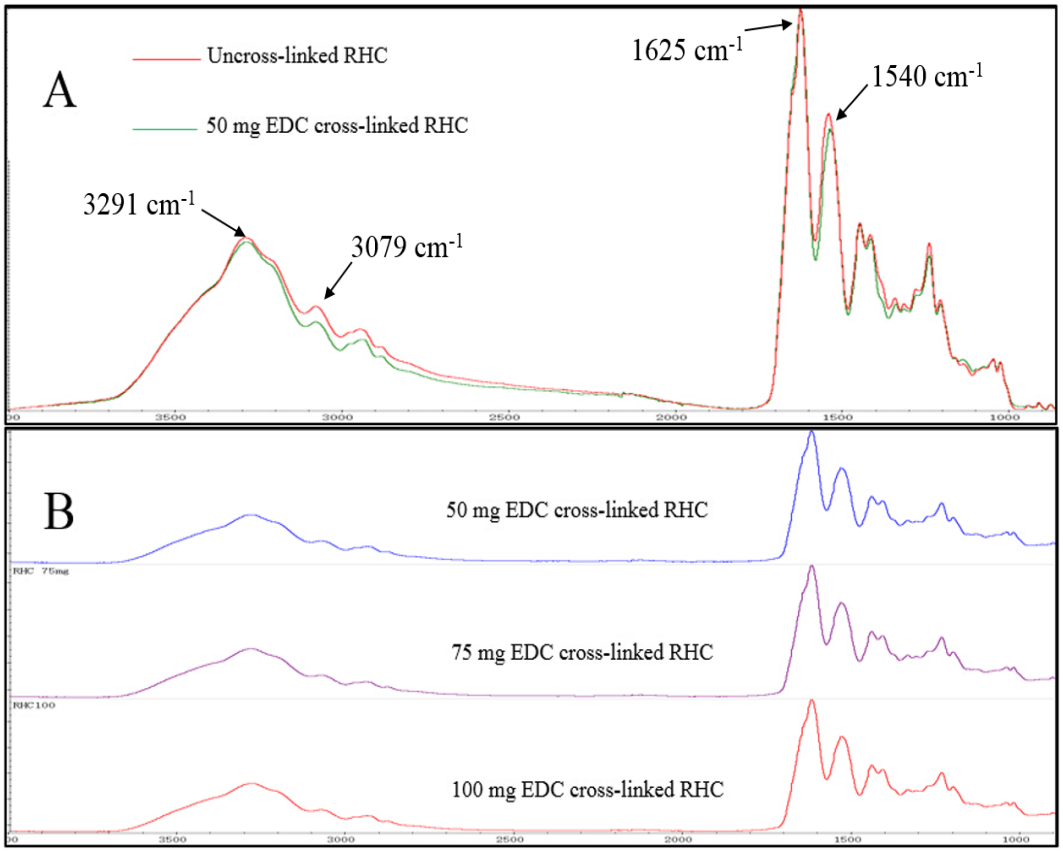

Figure 4-7. FT-IR spectra of (A) pure uncross-linked RHC and 50 mg EDC cross-linked RHC scaffold; (B) 50, 75 and 100 mg EDC cross-linked RHC scaffold

Table 4-3. FT-IR spectra characteristics of uncross-linked and cross-linked RHC scaffolds

Band assignment & region / **Sample**	*ν*O-H& *ν*N-H (Amide A)	*ν*N-H (Amide B)	*ν*C=O & *ν*N-H (Amide I)	*δ*N-H& *ν*C-N (Amide II)
Uncross-linked RHC	3291 cm^{-1}	3079 cm^{-1}	1625 cm^{-1}	1540 cm^{-1}
50 mg EDC cross-linked RHC	3291cm^{-1}	3079 cm^{-1}	1625 cm^{-1}	1540 cm^{-1}
75 mg EDC cross-linked RHC	3291cm^{-1}	3079 cm^{-1}	1625 cm^{-1}	1540 cm^{-1}
100 mg EDC cross-linked RHC	3291 cm^{-1}	3079 cm^{-1}	1625cm^{-1}	1540 cm^{-1}

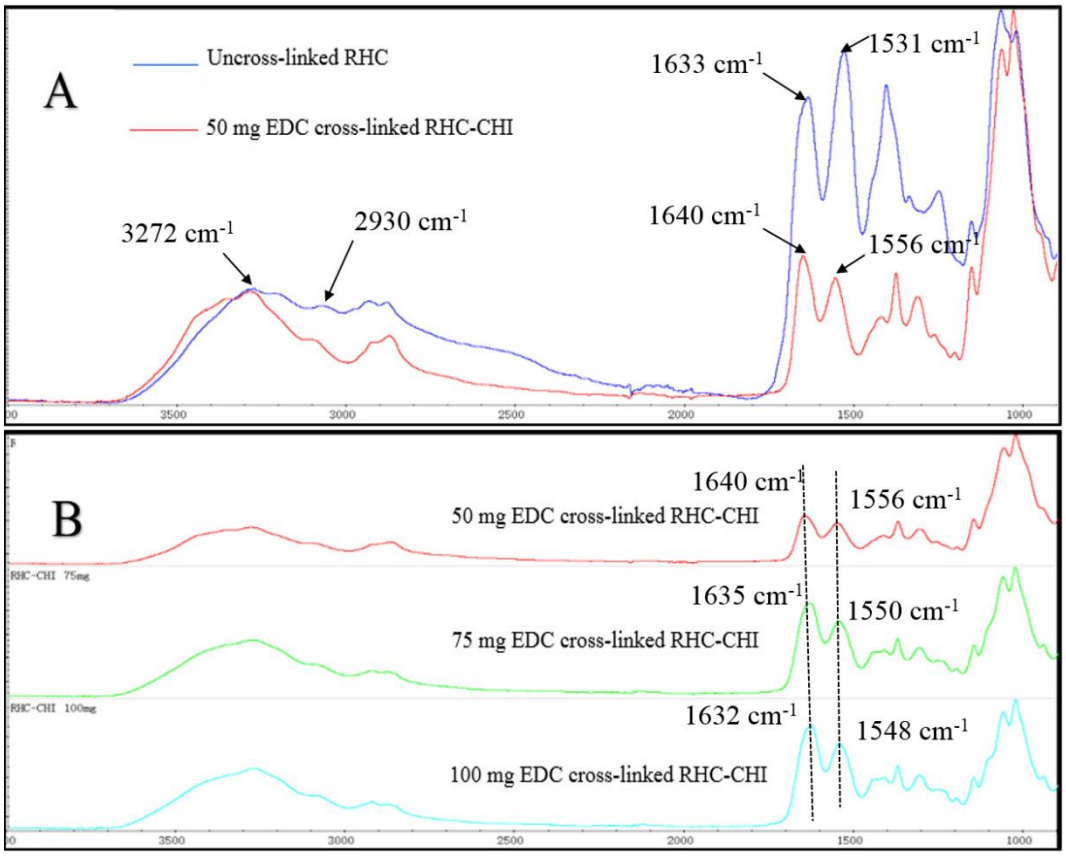

Figure 4-8. FT-IR spectra of (A) uncross-linked RHC-CHI and 50 mg EDC cross-linked RHC-CHI scaffold (RHC-CHI-50); (B) 50, 75 and 100 mg EDC cross-linked RHC-CHI scaffolds (RHC-CHI-50, RHC-CHI-75 and RHC-CHI-100).

Table 4-4. FT-IR spectra characteristics of uncross-linked and cross-linked RHC-CHI scaffolds

Band assignment & region / **Sample**	*ν*O-H & *ν*N-H (Amide A)	*ν*N-H (Amide B)	*ν*C=O & *ν*N-H (Amide I)	*δ*N-H &*ν*C-N (Amide II)
Uncross-linked RHC-CHI	3272 cm^{-1}	2930 cm^{-1}	1633 cm^{-1}	1531 cm^{-1}
50 mg EDC cross-linked RHC-CHI	3272 cm^{-1}	2930 cm^{-1}	1640 cm^{-1}	1556 cm^{-1}
75 mg EDC cross-linked RHC-CHI	3272 cm^{-1}	2930 cm^{-1}	1635 cm^{-1}	1550 cm^{-1}
100mg EDC cross-linked RHC-CHI	3272 cm^{-1}	2930 cm^{-1}	1632 cm^{-1}	1548 cm^{-1}

4.3 Cross-linking degree

To determine the cross-linking degree of the porous scaffolds, the amount of uncross-linked RHC which was present in the processing solutions (solution from cross-linking and distilled water washing process) were firstly detected by HPLC, and compared with the RHC standard solution. These data are shown in Figure 4-9. It shows the RHC peak in RHC standard solution was detected at retention time around 11 min, and no obvious RHC peaks could be found in all EDC cross-linked porous scaffolds. It is suggested that the peaks shown at around 17 min of the retention time for the RCH-CHI samples are a contribution from the uncross-linked chitosan molecules (Figure 4-9 F, G and H). The crosslinking degree of the fabricated scaffolds were then calculated from determined uncross-linked RHC to the total RHC powder used in fabricating of porous scaffolds. Cross-linking degree of RHC scaffolds fabricated with varied amounts of EDC were shown in Figure 4-10. No significant differences of the cross-linking degree were discovered among 50, 75 and 100 mg EDC cross-linked RHC-1.5 scaffolds as all of the determined cross-linking degree were higher than 96%. Meanwhile, the crosslinking degree at around 95% from RHC-2.0 and RHC-3.0 scaffold that cross-linked with 50 mg EDC were also determined. No significant difference on cross-linking degrees was found in these five types of RHC scaffolds.

The cross-linking degree on RHC-CHI scaffold shown in Figure 4-11 were the sum of detected RHC from cross-linking and washing procedures. The cross-linking degree of RHC-CHI-50 scaffold was 95% which shows no significant difference compared to scaffolds that cross-linked by 75 and 100 mg EDC.

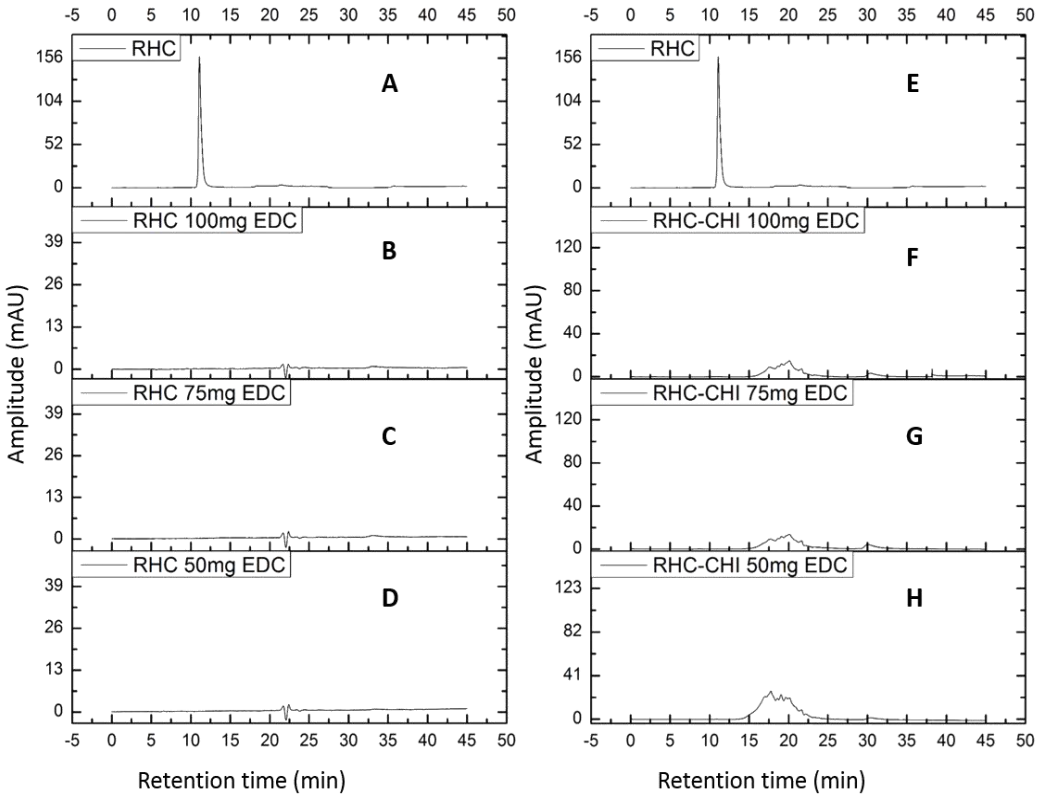

Figure 4-9. RHC present in cross-linking and washing solution detected by HPLC. (A, E) RHC solution; (B, F) RHC detected from RHC and RHC-CHI scaffold cross-linked with 100 mg EDC; (C, G) RHC detected from RHC and RHC-CHI scaffold cross-linked with 75 mg EDC; (D, H) RHC detected from RHC and RHC-CHI scaffold cross-linked with 50 mg EDC.

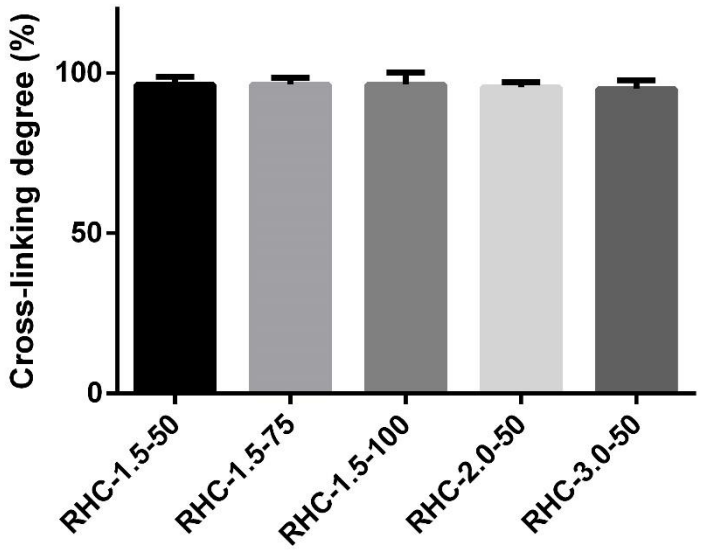

Figure 4-10. Cross-linking degree of RHC-1.5, 2.0 and 3.0 porous scaffolds cross-linked by 50, 75 and 100 mg EDC. Bars represent mean ± SD.

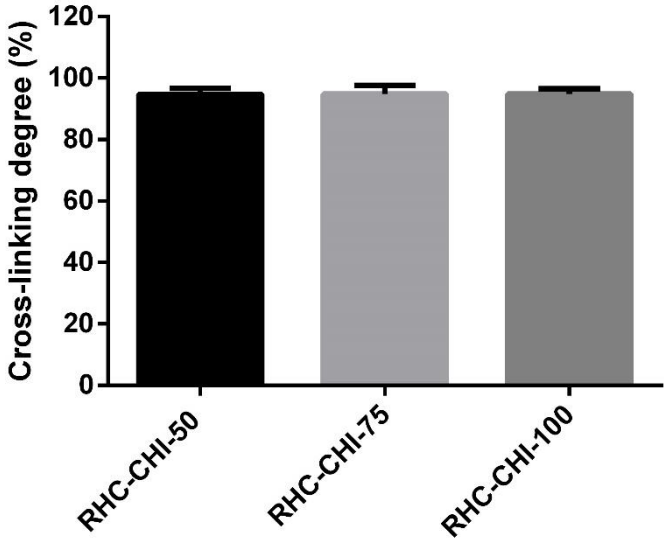

Figure 4-11. Cross-linking degree of RHC-CHI scaffolds cross-linked by 50, 75 and 100 mg EDC. Bars represent mean ± SD.

4.4 Gelation time

Gelation times of the hydrogels at different temperatures are given in Table 4-5. In general, for each type of hydrogel, the gelation times reduced as the temperature increased. For instance, at 4 ℃ the gelation of hydrogel A occurred at 30-35 min while it became gelled at 15 min at 24 ℃, and by further increasing the temperature to 37 ℃, the gelation time shortened to 5-7 min. Another finding was that the gelation times reduced with increasing biopolymer content. It was observed that hydrogel A had general longer gelation times compared to hydrogel 2A and 3A which concentration was 1.33 and 2.0-fold of hydrogel A corresponding to the selected temperatures. What's more, it also shows the gelation time increased with increasing chitosan content in hydrogel where hydrogel C took the longest time to gel under each selected temperature compared to hydrogel with other formulas.

Table 4-5. Gelation times of each type of hydrogel at different temperatures.

Hydrogel	**Biopolymers concentration (w/v)**	**RHC:CHI ratio**	**Gelation time (min)**		
			4 ℃	**24 ℃**	**37 ℃**
A	1.5%	80:20	30-35	15	5-7
B	1.5%	50:50	55	30	12-15
C	1.5%	20:80	70	40	25
2A	2.0%	80:20	13-15	5	2-3
3A	3.0%	80:20	8-10	3-4	1-2

4.5 Swelling ability

Gelatin based scaffolds

Figure 4-12 shows that the uncross-linked gelatin-chitosan scaffold could bind at least 37-fold of PBS which was significantly higher compared to all of cross-linked scaffolds (P<0.001). No significant differences on swellings were observed among different levels of PA cross-linked scaffolds. Of the scaffolds treated with GA, the scaffold with 1.0% GA by weight had a significantly lower swelling ability than the 0.5% GA scaffold, while no significant difference was seen between 0.1% GA and 0.5% GA.

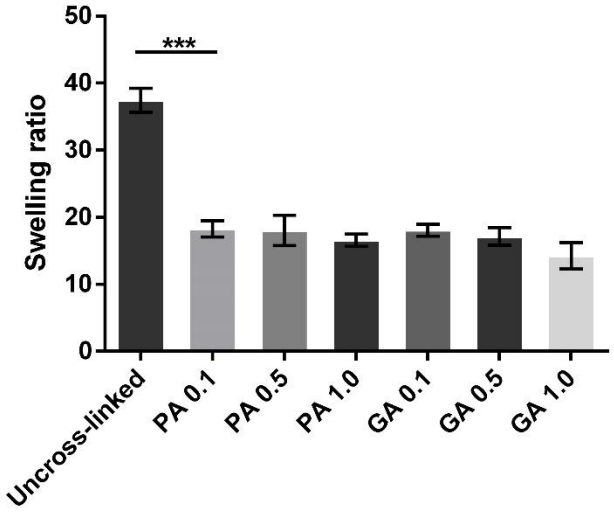

Figure 4-12. Swelling ratio of fabricated scaffolds with different amounts of cross-linking concentrations. Bars represent mean ± SD and significance is indicated with ***P<0.001.

RHC based porous scaffolds

The swelling ratios of the RHC-1.5, RHC-2.0 and RHC-3.0 scaffold were determined by measuring the increasing in mass of porous scaffolds after

submerging in PBS for 24 h and results are shown in Figure 4-13. It shows that the swelling capabilities were proportional to the increase of RHC concentration in scaffolds. RHC-1.5 and RHC-2.0 scaffold could bind about 34 and 36-fold of PBS respectively. RHC-3.0 scaffold had the highest swelling ability that could bind nearly 40-fold of PBS which was statistically significant compared to RHC-1.5 ($P<0.05$).

The swelling ratio of RHC-CHI-50, 75 and 100 scaffolds are shown in Figure 4-14. It shows that the amount of absorbed water decreased with increasing EDC content during fabrication. The highest swelling ratio was achieved in the RHC-CHI-50 scaffold that could bind at least 88-fold of the PBS. Meanwhile, RHC-CHI-100 scaffold had the lowest water binding ability that only 34-fold of PBS was absorbed, which was significant lower compared to scaffold RHC-CHI-50 and 75 ($P<0.001$).

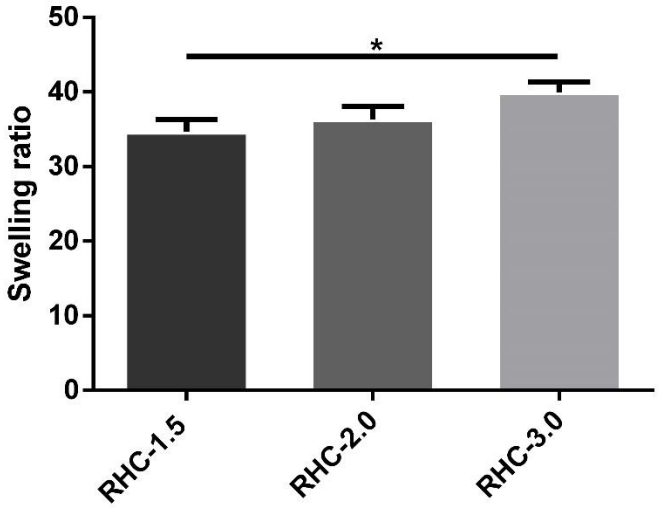

Figure 4-13. Swelling ratios of the RHC-1.5, 2.0 and 3.0 porous scaffolds. Bars represent mean ± SD and significance is indicated with *$P<0.05$.

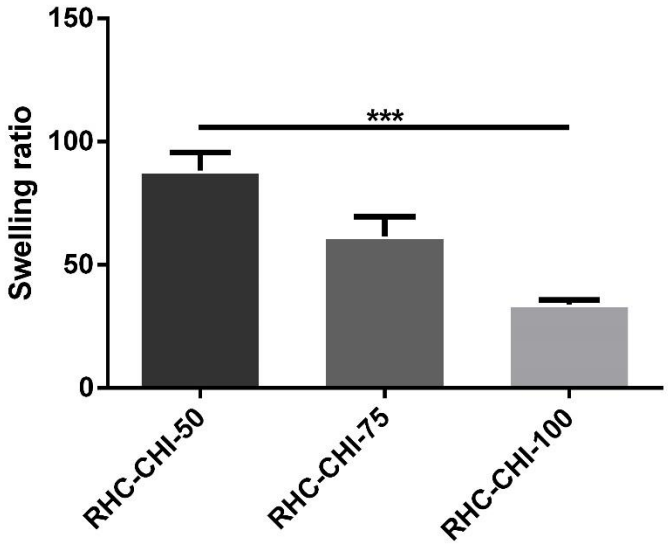

Figure 4-14. Swelling ratios of the RHC-CHI-50, 75 and 100 porous scaffolds. Bars represent mean ± SD and significance is indicated with ***P<0.001.

4.6 *In vitro* degradation

Gelatin based porous scaffolds

The enzymatic biodegradation on each type of scaffolds are shown in Figure 4-15. It shows that around 70% gelatin degraded from uncross-linked scaffold after incubating in collagenase solution for 12 h, whilst much less gelatin was lost in all the cross-linked scaffolds. Specifically, PA 0.1 scaffold only lost 28% gelatin which was significantly lower than uncross-linked scaffold ($P<0.001$). By increasing the PA concentration, only 16% gelatin were digested from PA 1.0 scaffolds, which was significantly lower compared to PA 0.1 scaffold ($P<0.01$). Meanwhile, GA cross-linked scaffolds also show great ability to resist the enzymatic degradation, the degradation rates were found in between 7% to 10%, and the degradation of GA 0.1 was much lower than PA 0.1 ($P<0.001$). Meanwhile, no significant difference was observed among GA groups ($P>0.05$).

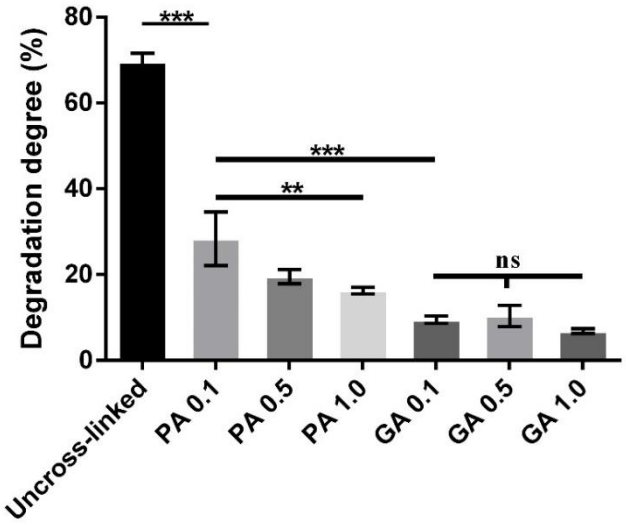

Figure 4-15. The degradation degree of uncross-linked and cross-linked collagen/chitosan scaffolds. Bars represent mean ± SD, significance is indicated with **P<0.01, ***P<0.001 and not significant is indicated with ns.

RHC based porous scaffolds

To determine the degradation degree of the RHC and RHC-CHI based porous scaffolds, at each time point, the scaffolds were firstly taken out from PBS solution and vacuum dried 12 h before measuring the mass loss, then compared to their original weight before degradation. The degradation degrees of the RHC scaffolds are shown in Figure 4-16. It shows that the degradation degree of each type of RHC scaffolds increased gradually along with the degradation date, and all three type of porous scaffolds had similar degradation rate throughout the entire degradation test as no significant difference was found at each individual time point ($P>0.05$).

The biodegradation degrees of the RHC-CHI-50, 75 and 100 scaffolds at each time point were shown in Figure 4-17. Again, degradation increased steadily with degradation time. Generally, the degree of biodegradation decreased as the EDC fabrication content increased. At Day 3, significant differences on mass loss were found among three types of scaffolds ($P<0.05$), 8% and 4% of the mass loss were determined on RHC-CHI-50 and 75 scaffolds respectively where RHC-CHI-100 scaffolds had the lowest mass loss at 2%. All scaffolds had an increasing mass loss from 7 to 14 days. Similarly, Significant differences were also observed at day 21 as degradation degree of RHC-CHI-50 show much higher compared to RHC-CHI-100 ($P<0.001$). After 28 days, the RHC-CHI-100 scaffolds showed the lowest mass loss, which was significant lower than RHC-CHI-75 and RHC-CHI-50 ($P<0.01$).

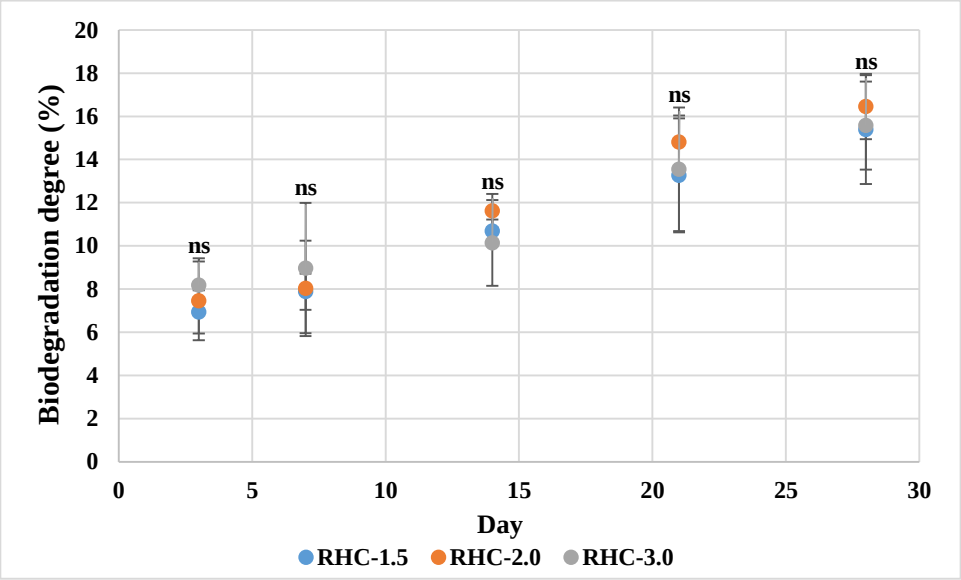

Figure 4-16. Biodegradation degrees of the RHC porous scaffolds at day 3, 7, 14, 21 and 28. Values represent mean ± SD. Not significant is indicated with ns.

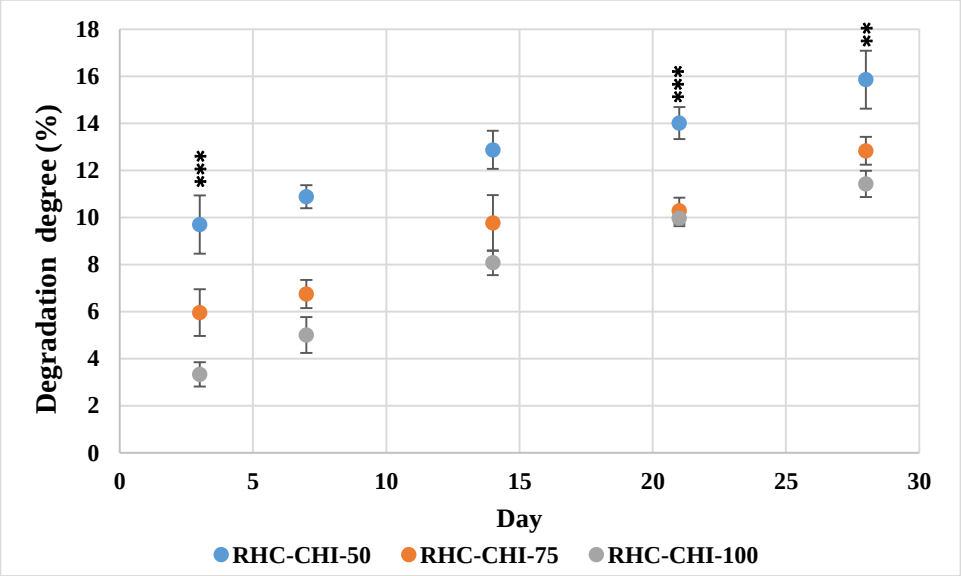

Figure 4-17. Biodegradation degrees of the RHC-CHI porous scaffolds at day 3, 7, 14, 21 and 28. Values represent mean ± SD, significance is indicated with **P<0.01 and ***P<0.001.

RHC based hydrogel scaffolds

The degradation degree of the fabricated hydrogels were determined by weight loss. Fully hydrated hydrogels were soaked in PBS for a designated period before removing and measuring the masses. The percentages of mass loss of the degraded hydrogel samples are presented in Figure 4-18. In general, at day 3 around 20% weight loss had been founded among all samples (P>0.05). The degradation degree of the sample A and B gradually increased along with the time, whereas hydrogel C showed accelerated its degradation from day 14 compared to other two hydrogels (P<0.01). As a result, at day 28, hydrogel C had been founded had the largest weight loss which was nearly 90% of its initial mass, but, hydrogel A and B showed significantly slower degradation degrees compared to hydrogel C (P<0.01), which was 65.3% and 59.8% respectively.

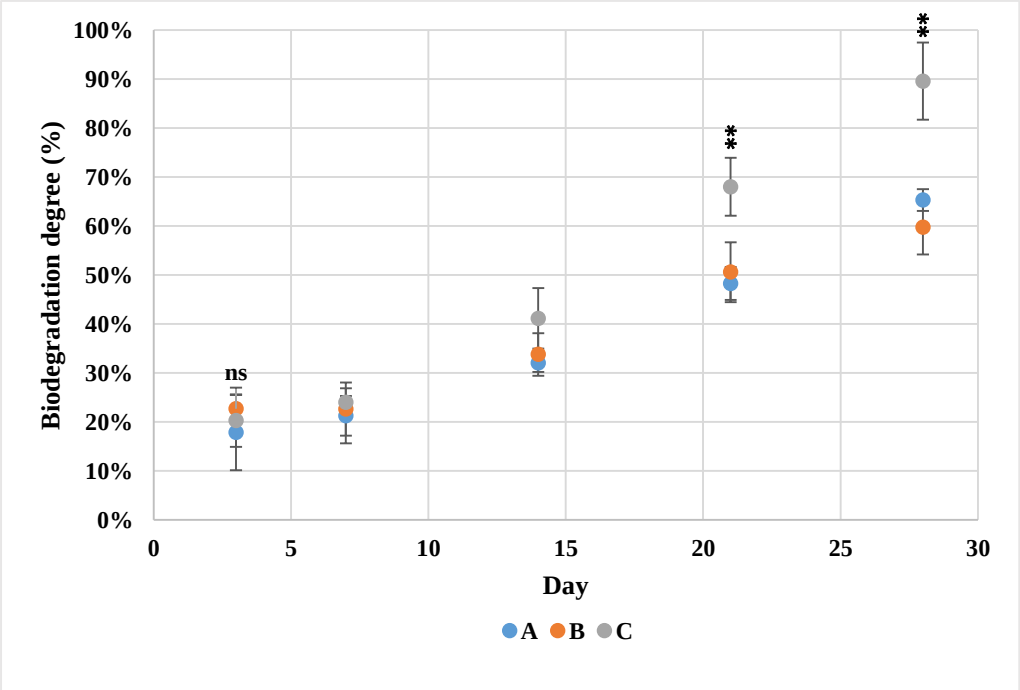

Figure 4-18. Biodegradation degrees of hydrogel A, B and C at different time points, values represent the mean ± SD, significance is indicated with **P<0.01, and not significant is indicated with ns.

4.7 Mechanical properties of porous scaffolds

Gelatin based porous scaffolds

The stress-strain curves, compressive modulus and compressive strength were determined from compression tests with a constant strain rate (2 mm/min) onto the scaffolds. The compression stress-strain curves in Figure 4-19 A shows that cross-linked scaffolds (PA 0.1 and GA 0.1) have a higher stiffness than untreated scaffolds. The stress-strain curves also indicate that the compressive stiffness increased with increasing cross-linker concentration. Compressive stresses to produce 70% strain and compressive modulus obtained at the initial slope of the curves are shown in Figure 4-20. In Figure 4-20 A, it shows that at a defined deformation (70% strain), PA 0.1 cross-linked scaffolds had much higher compressive strength compared to uncross-linked samples ($P<0.01$), where the increase in stiffness was dependent on the cross-linkers' concentration as PA 1.0 shows significantly higher compressive strength compared to PA 0.1 ($P<0.01$). GA was also found to have a stronger influence on scaffold strength than PA, the stress in GA 0.1 was found significantly higher compared to PA 0.1 ($P<0.001$) and GA 1.0 was found significant higher compared to GA 0.1 ($P<0.001$). Meanwhile, Figure 4-19 B shows that compressive modulus of scaffolds were significantly influenced by the all PA and GA ($P<0.001$), and it also shows that the modulus were increased with increasing of cross-linker concentration in both groups as PA 1.0 was found much higher than PA 0.1($P<0.001$) and GA 1.0 was significantly higher than GA 0.1 ($P<0.001$). Meanwhile, GA 0.5 was also found significantly higher than PA 0.5 ($P<0.01$).

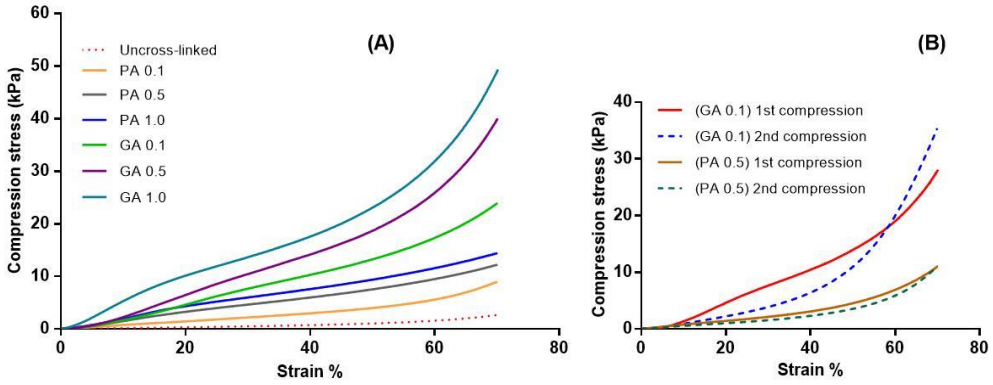

Figure 4-19. (A) Representative stress-strain curves of different scaffolds (uncross-linked, PA 0.1 to PA 1.0 and GA 0.1 to GA 1.0 cross-linked) up to 70% strain. (B) Stress-strain curves of repetitive compression test on PA 0.5 and GA 0.1 scaffolds

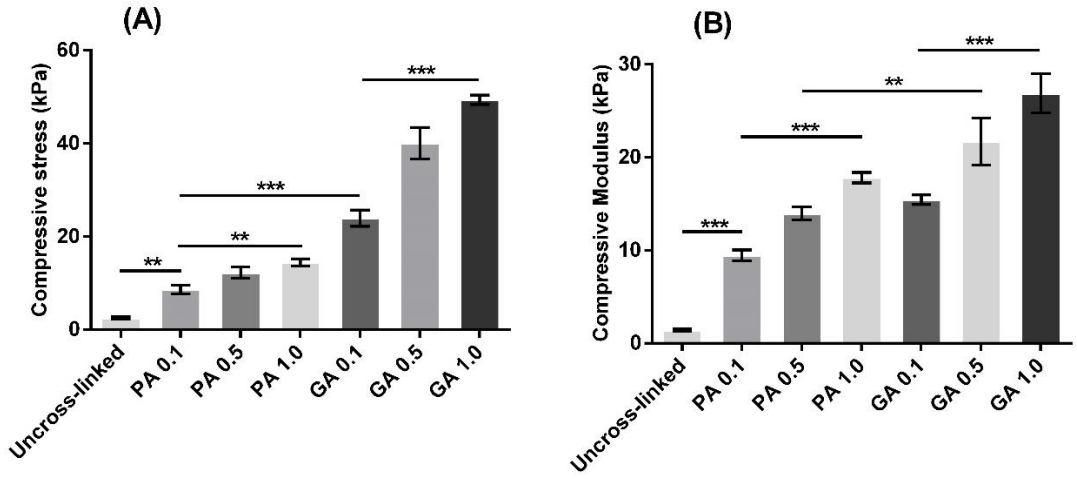

Figure 4-20. (A) Compressive strength at 70% strain of uncross-linked, PA and GA cross-linked scaffolds. (B)Compressive modulus of uncross-linked, PA and GA cross-linked scaffolds. Bars represent mean ± SD and significance is indicated with **P<0.01 and ***P<0.001.

In addition, the stress-strain curves of repeated compression tests on GA 0.1 and PA 0.5 are shown in Figure 4-19 B. There was little difference between the first and second compression of PA 0.5 cross-linked scaffolds, while there were significant differences observed for scaffolds cross-linked with GA. When the scaffold's

internal morphology was imaged using SEM, the structure of PA 0.5 cross-linked scaffolds had slight changes in pore shape and size, but little damage to the scaffold itself was seen (Figure 4-21 A). Fractured structures were discovered in GA 0.1 treated scaffold (Figure 4-21 B). The crushed structures in GA 0.1 scaffolds were perpendicular to the direction of loading, and the porous structures were seen to be denser, with evidence of buckling of interconnecting struts.

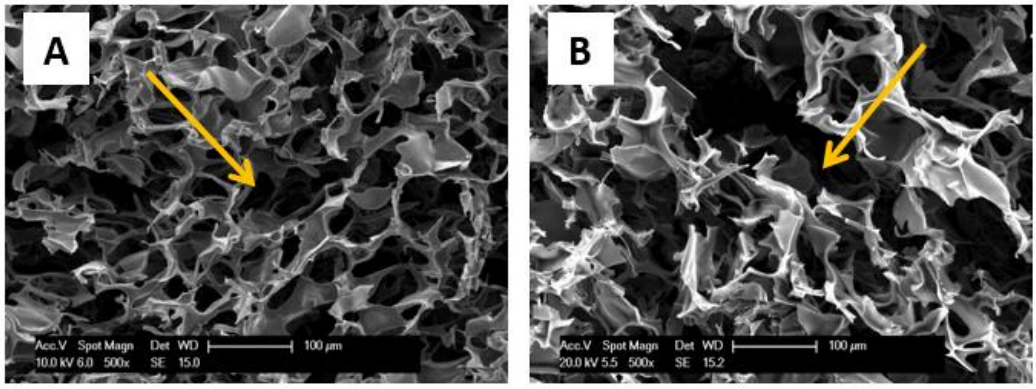

Figure 4-21. (A) Cross-section view of PA 0.5 cross-linked scaffold after compressive tests, arrow indicating direction of load to porous structures; (B) GA 0.1 cross-linked scaffold after compressive tests, arrow indicating direction of load to porous structures.

For the stress relaxation test, samples were compressed under a constant speed (2 mm/min) until strain of 30% was reached and this static strain was maintained for another 600 s to record the variations of stress at constant strain. The results on different samples are shown in Figure 4-22 A. The curves indicate that the relaxation behaviours of all cross-linker treated samples were similar where stress decreased rapidly in the first 60 s, then decreased gradually until the end of each

test. Compression stresses of uncross-linked and PA treated scaffolds were close to equilibrium at end of the tests, while stresses in GA treated scaffolds were still decreasing. However taking the stress relaxation from the maximum stress to the stress at 600 seconds, Figure. 4-22 B shows that PA cross-linked scaffolds had more relaxation compared to GA groups at same concentration as well as uncross-linked scaffolds. The compression stress of PA 0.5 scaffold at 30% strain was 4.52 kPa and decreased to 2.39 kPa at end of test where compression stress of uncross-linked scaffold decreased from 0.55 kPa to 0.37 kPa. It also shows the stress relaxation increased with the PA concentration: PA 1.0 samples had the highest stress relaxation, of nearly 53% which was significantly higher than PA 0.1 ($P<0.01$). Meanwhile, no significant differences in stress relaxation were observed between GA groups ($P>0.05$).

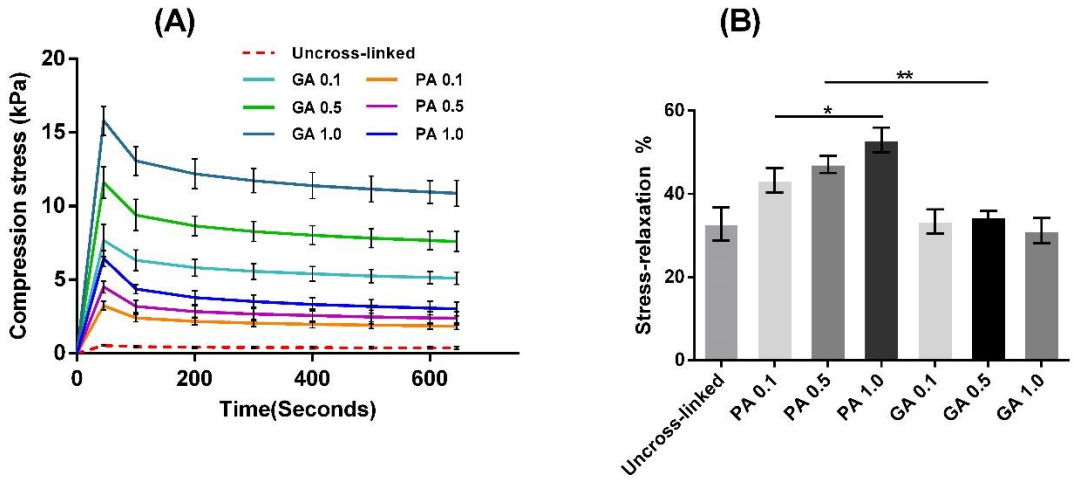

Figure 4-22. (A) Stress-relaxation curves of uncross-linked, PA and GA cross-linked scaffolds. (B) Stress-relaxation of uncross-linked, PA and GA cross-linked scaffolds, bars represent mean ± SD and significance is indicated with *P<0.05 and **P<0.01.

Porous RHC scaffolds

The compression stress-strain curves of cross-linked RHC-1.5, 2.0 and 3.0 porous scaffold are shown in Figure 4-23. It shows that the compressive stress needed to reach a particular strain increased as the RHC concentration increased. Figure 4-24 brings together all the data and shows that the compressive strength obtained from RHC-3.0 scaffold reached 0.42 kPa, which was 1.6-fold of RHC-1.5 scaffold ($P<0.01$) and 1.3-fold of RHC-2.0 scaffold ($P<0.05$). Meanwhile, the compressive moduli (obtained as the slope at the linear region of the stress-strain curves in the first 10% strain) are shown in Figure 4-25. Similar to the trend in compressive strength compressive modulus were proportional to the RHC concentrations, the compressive modulus of RHC-3.0 scaffolds at 0.54 kPa was significantly higher than the RHC-1.5 scaffold ($P<0.001$) and RHC-2.0 ($P<0.01$).

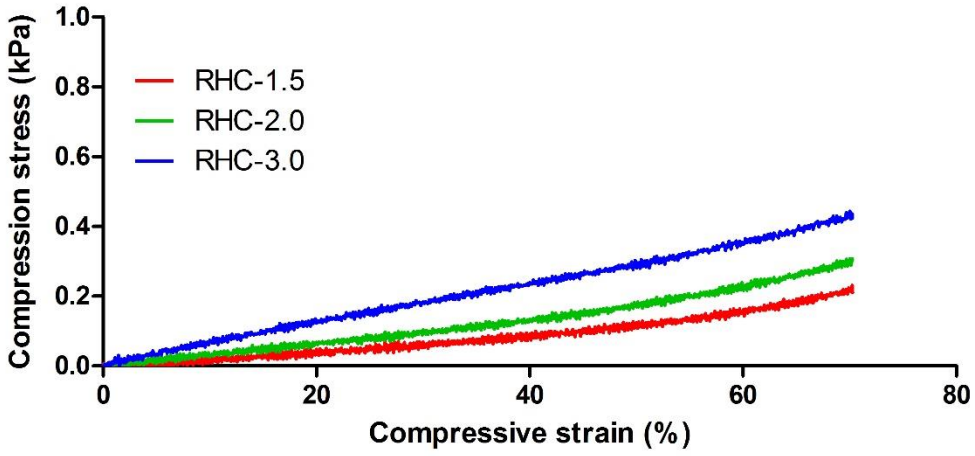

Figure 4-23. Representative compression stress-strain curves up to 70% strain of RHC-1.5, 2.0 and 3.0 porous scaffold.

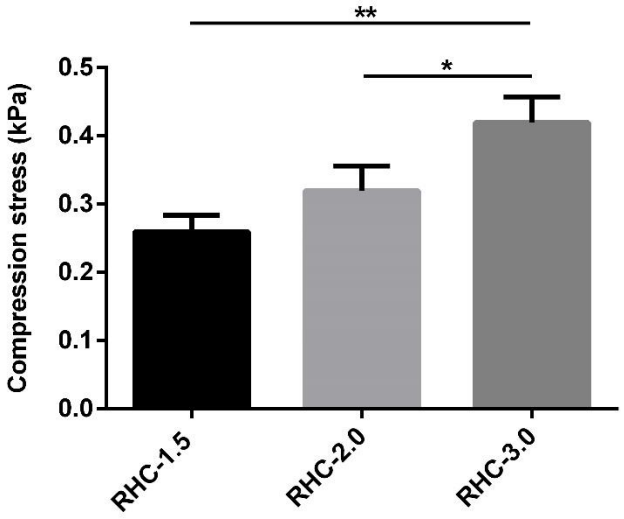

Figure 4-24. Compression stress at 70% strain of RHC porous scaffolds. Bars represent mean ± SD and significance is indicated with *P<0.05 and **P<0.01.

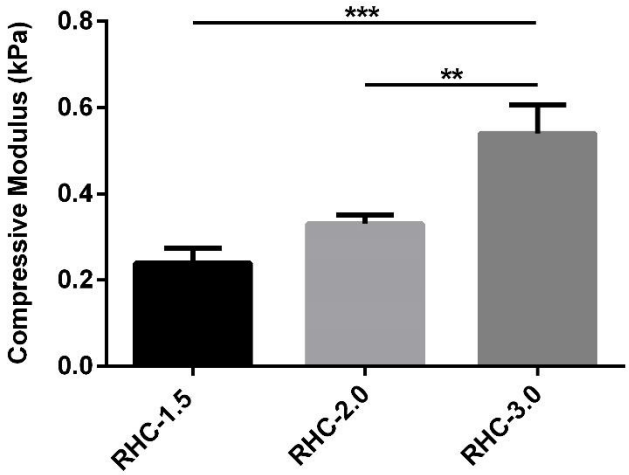

Figure 4-25. Compressive modulus of RHC porous scaffolds. Bars represent mean ± SD and significance is indicated with **P<0.01 and ***P<0.001.

RHC scaffolds were also subjected to tensile testing. Tensile stress-elongation curved determined from porous RHC-1.5, 2.0 and 3.0 scaffold are shown in Figure 4-26, and it shows the RHC-3.0 porous scaffold had the largest elongation

at break strength among all three pure RHC porous scaffolds. Ultimate tensile strengths (as defined as the stress at fracture) are shown in Figure 4-27. It shows that tensile stress increased as the RHC concentration increased and tensile stress of RHC-3.0 was significant higher compared to RHC-1.5 ($P<0.001$). The elastic modulus obtained from linear part of the stress-strain curves are expressed in Figure 4-28. The RHC-1.5 had the lowest elastic modulus (5.1 kPa) among three RHC scaffolds, the RHC-3.0 had the highest modulus (12.2 kPa) which was significantly higher ($P<0.001$) than RHC-1.5.

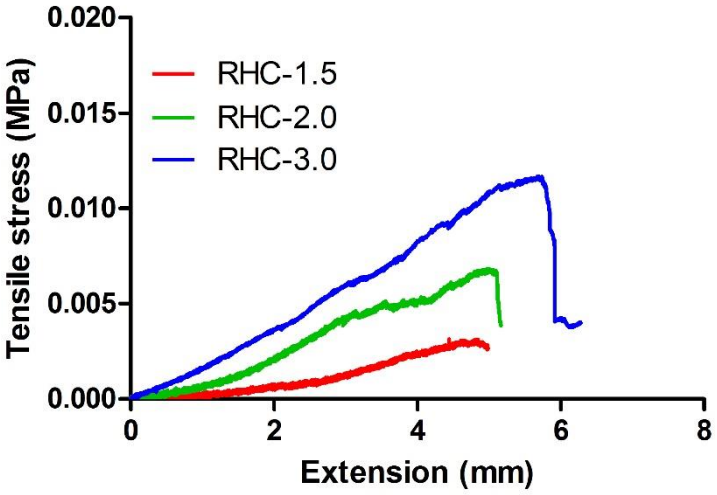

Figure 4-26. Representative tensile elongation curves of RHC-1.5, 2.0 and 3.0 porous scaffold

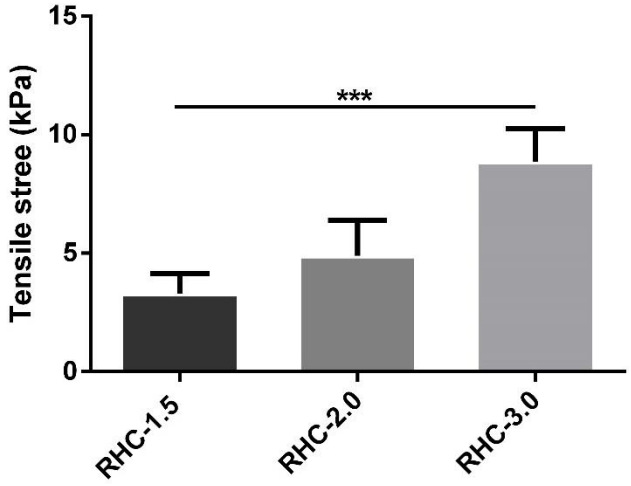

Figure 4-27. Tensile stress at break point of RHC-1.5, 2.0 and 3.0 porous scaffolds. Bars represent mean ± SD and significance is indicated with ***P<0.001.

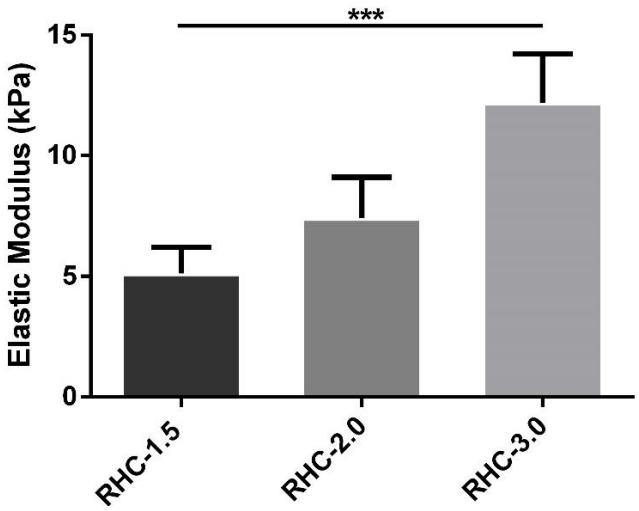

Figure 4-28. Elastic Modulus of RHC-1.5, 2.0 and 3.0 porous scaffolds. Bars represent mean ± SD and significance is indicated with ***P<0.001.

RHC-1.5 scaffolds that cross-linked with different amount of EDC were subjected to the compression test, the compression stresses at 70% strain were presented in Figure 4-29. No significant difference was observed in compressive strength from EDC 50, 75 and 100 mg cross-linked scaffolds as the mean compression stress to

reach 70% compression from these three types of scaffolds were all about 0.26 kPa. The compression moduli of the tested scaffolds were presented in Figure 4-30, where no significant difference was found and the modulus from each types of scaffold were close to 0.24 kPa (P>0.05).

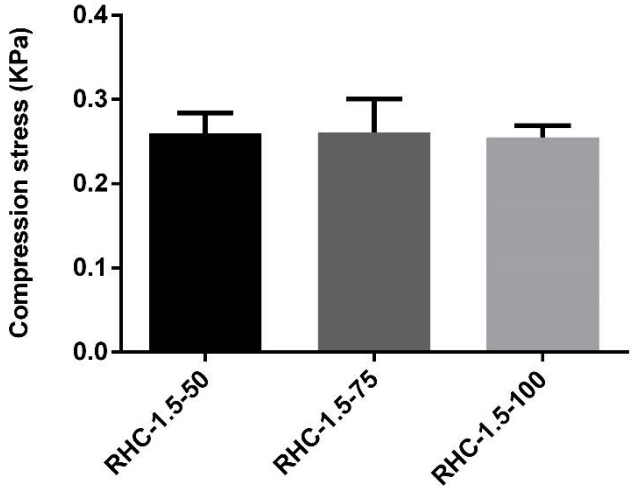

Figure 4-29. Compression stress at 70% strain of 50, 75 and 100 mg EDC cross-linked RHC-1.5 porous scaffolds.

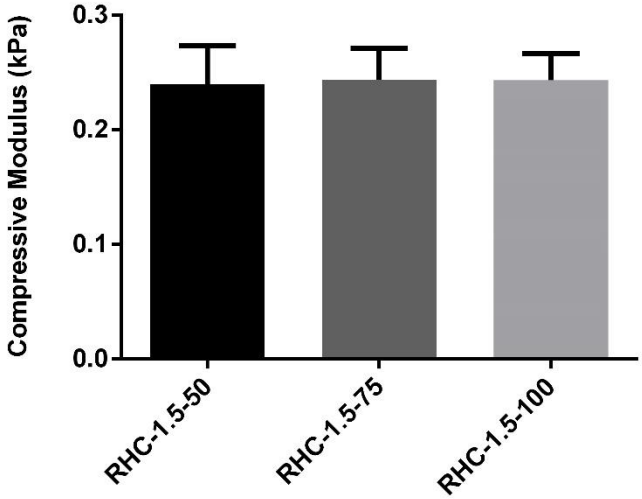

Figure 4-30. Compressive Modulus of 50, 75 and 100 mg EDC cross-linked RHC-1.5 porous scaffolds.

Porous RHC-CHI scaffolds

Figure 4-31 presents the compression stress-strain curves of tested RHC-CHI-50, 75 and 100 porous scaffold. Compression stress at 70% strain of RHC-CHI scaffolds which cross-linked with different amount of EDC (50, 75 and 100 mg) are shown in Figure 4-32. It shows the obtained stresses were proportional to the amount of EDC that was used in cross-linking process. Scaffold which cross-linked with 100 mg EDC had the highest compressive stress at 0.83 kPa which was significantly higher than that 50 mg EDC cross-linked scaffold ($P<0.001$). Compressive modulus that obtained from the linear region of the stress-strain curves were shown in Figure 4-33. Similar to trend found in compression stress, the moduli increased as amount of EDC that was used in cross-linking increased and statistically significant differences were found between RHC-1.5 and 3.0 ($P<0.001$) .

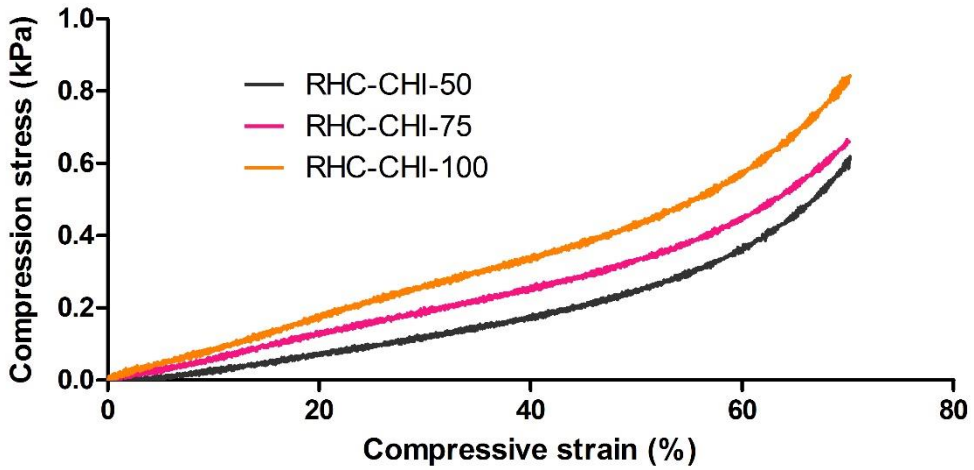

Figure 4-31. Representative compression stress-strain curves up to 70% strain of RHC-CHI-50, 75 and 100 porous scaffold

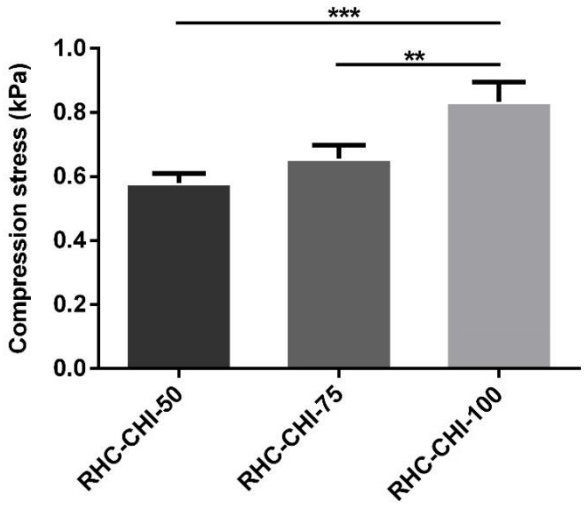

Figure 4-32. Compression stress at 70% strain of RHC-CHI-50, 75 and 100 porous scaffolds. Bars represent mean ± SD and significance is indicated with **P<0.01 and ***P<0.001.

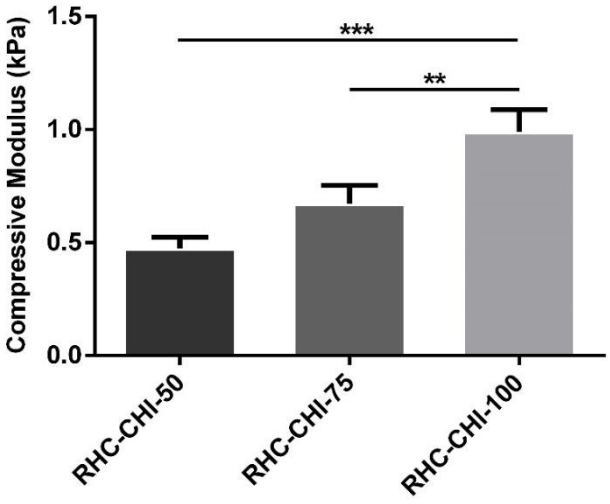

Figure 4-33. Compressive Modulus of RHC-CHI-50, 75 and 100 porous scaffolds. Bars represent mean ± SD and significance is indicated with **P<0.01 and ***P<0.001.

Figure 4-34 presents the tensile stress-strain curves of the RHC-CHI-50, 75 and 100 porous scaffold. The ultimate tensile strength of three types of RHC-CHI scaffolds are shown in Figure 4-35. It shows that the recorded tensile stresses at break point increased as the amount of EDC that was used in scaffold fabrication increased. The scaffold fabricated with 100 mg EDC had the highest ultimate tensile strength at 50 kPa which was significantly higher than RHC-CHI-50 ($P<0.01$). The elastic moduli of the tested scaffolds are shown in Figure 4-36. It shows the elastic moduli tended to increase as the EDC content that was used in cross-linking increased, Specifically, tensile modulus of scaffold RHC-CHI-100 reached to 70 kPa that was significantly higher than the RHC-CHI-50 ($P<0.01$) and RHC-CHI-75 ($P<0.05$).

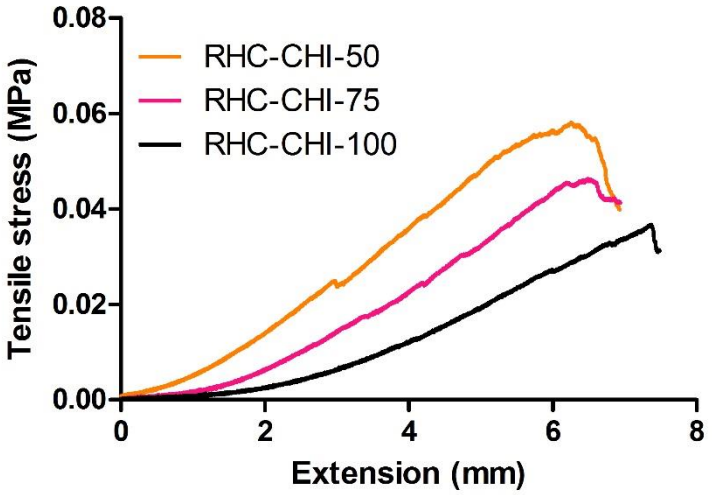

Figure 4-34. Representative tensile stress-strain curves of RHC-CHI-50, 75 and 100 porous scaffold

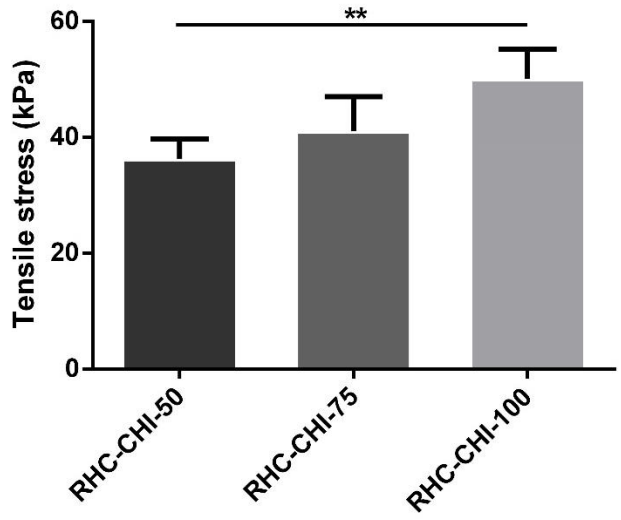

Figure 4-35. Tensile stress at break point of RHC-CHI-50, 75 and 100 porous scaffolds. Bars represent mean ± SD and significance is indicated with **P<0.01.

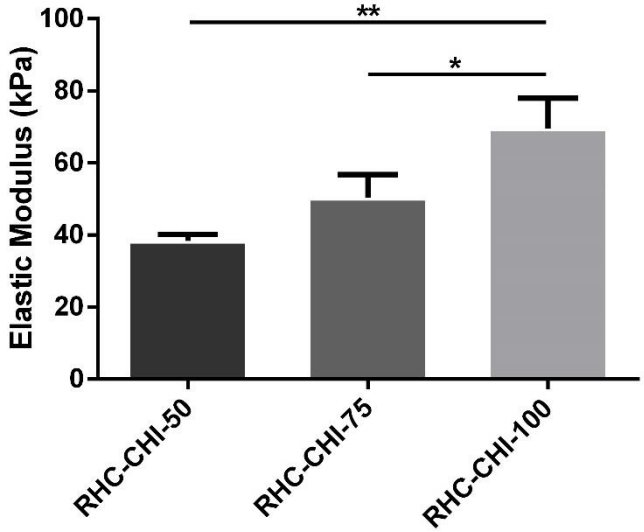

Figure 4-36. Elastic Modulus of RHC-CHI-50, 75 and 100 porous scaffolds. Bars represent mean ± SD and significance is indicated with *P<0.05 and **P<0.01.

A summary of all the compressive strengths at 70% strain of porous scaffolds with different RHC to CHI ratios are presented in Figure 4-37. It shows that the stresses

were increased as increasing the chitosan fraction in scaffold. Scaffold RHC:CHI (80:20) has the lowest compressive stress (0.4 kPa), stress of scaffold RHC:CHI (67:33) increased to 0.5 kPa but lower than scaffold RHC:CHI (50:50) which was 0.6 kPa. The compressive stress on scaffold RHC:CHI (20:80) reached to 1.2 kPa, which was significantly higher than RHC:CHI (50:50) ($P<0.001$). The compressive moduli obtained from linear region of the stress-strain curves are shown in Figure 4-38. Compressive modulus were found increased as increasing of chitosan ratio. Scaffold RHC:CHI (20:80) owns the highest modulus (1.54 kPa) that was nearly twice the value of scaffold RHC:CHI (50:50) and more than 4-fold of scaffold RHC:CHI (67:33) ($P<0.001$).

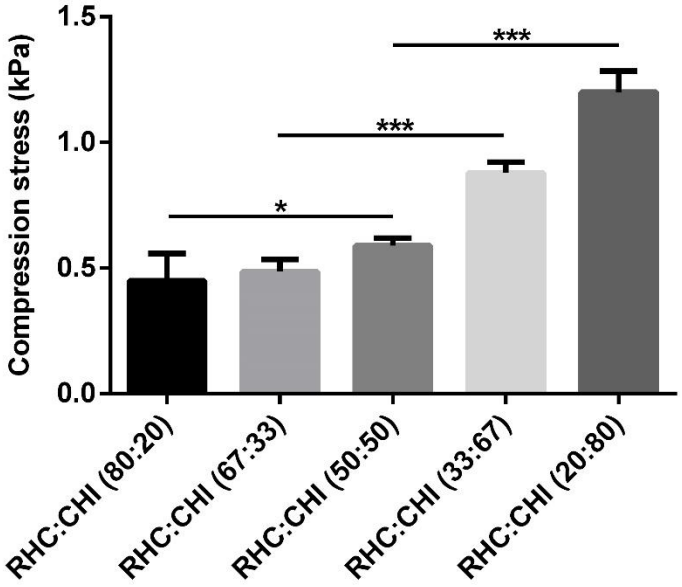

Figure 4-37. Compression stress at 70% strain of RHC-CHI porous scaffolds with different RHC to chitosan ratios. Bars represent mean ± SD and significance is indicated with *$P<0.05$ and ***$P<0.001$.

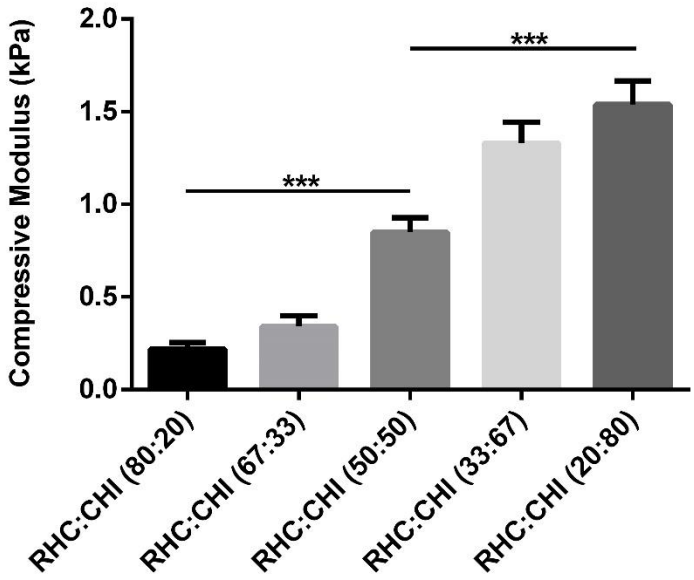

Figure 4-38. Compressive Modulus of RHC-CHI porous scaffolds with different RHC to chitosan ratios. Bars represent mean ± SD and significance is indicated with ***P<0.001.

Ultimate tensile stress of different scaffolds are shown in Figure 4-39. The same trends are shown as with compressive strength. Scaffold RHC:CHI (80:20) had the lowest stress of 13.48 kPa, and the stress increased as increasing the RHC fraction in porous scaffolds where RHC:CHI (20:80) had the highest tensile stress among all ($P<0.05$). The elastic moduli of the scaffolds are shown in Figure 4-40. The results show that the obtained elastic modulus values from each type of samples were highly dependent on the RHC to CHI ratio. Scaffolds with higher content of chitosan showed higher elastic modulus, where elastic modulus of scaffold RHC:CHI (20:80) reached to 196 kPa, which was 6.5 times of elastic modulus on scaffold RHC:CHI (67:33) and 13 times of RHC:CHI (80:20).

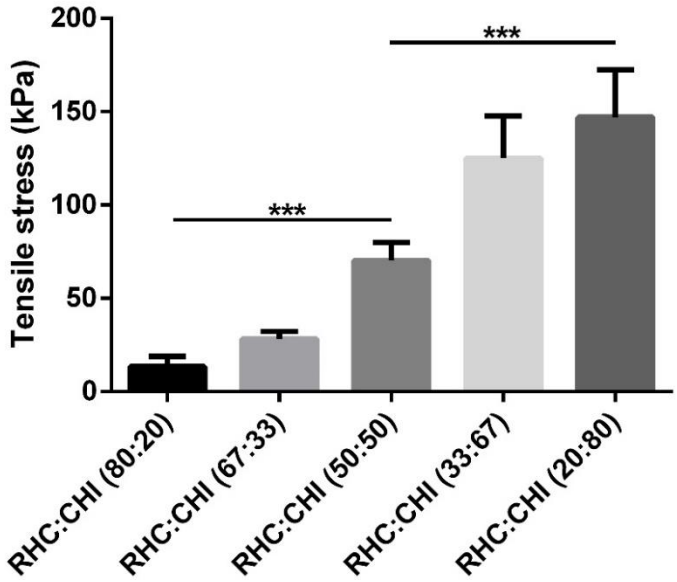

Figure 4-39. Tensile stress at break point of RHC-CHI porous scaffolds with different RHC to chitosan ratios. Bars represent mean ± SD and significance is indicated with ***P<0.001.

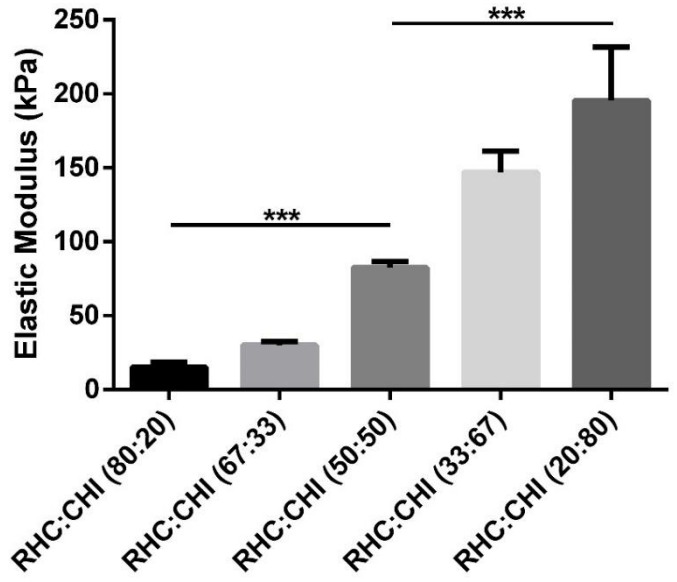

Figure 4-40. Elastic Modulus of RHC-CHI porous scaffolds with different RHC to chitosan ratios. Bars represent mean ± SD and significance is indicated with ***P<0.001.

RHC based hydrogel scaffolds

The mechanical property of the fabricated hydrogels were investigated by compression testing. The determined compressive modulus of hydrogels with different RHC fractions at different degradation times are shown in Figure 4-41. At day 1, the compressive modulus of hydrogel A was 3.46 kPa, by increasing the chitosan/RHC ratio to 50:50, the compressive modulus reached 12.33 kPa (hydrogel B) which was significantly higher than hydrogel A ($P<0.001$), but decreased to 2.01 kPa (hydrogel C) as chitosan content further increased. The compressive modulus of all hydrogels decreased gradually as degradation time increased (up to 5 days). Hydrogel A decreased to 2.82 kPa at day 3 and further decreased to 2.07 kPa, hydrogel B dropped to 9.68 kPa at day 3 and further decreased to 8.28 kPa on day 5. Modulus of 1.54 and 1.24 kPa were found on hydrogel C on day 3 and day 5, respectively.

Hydrogel scaffolds fabricated from different biopolymer concentrations were also subjected to the compression test, and the obtained modulus are shown in Figure 4-42. It can be observed that the compressive modulus increased as increasing the biopolymer concentration in solution. Modulus of hydrogel 2A was 3-fold of hydrogel A, and the hydrogel 3A had significant higher compressive modulus that reached to 29 kPa ($P<0.001$), which was 2.7 and 8.5- fold of compressive modulus found in hydrogel 2A and A, respectively.

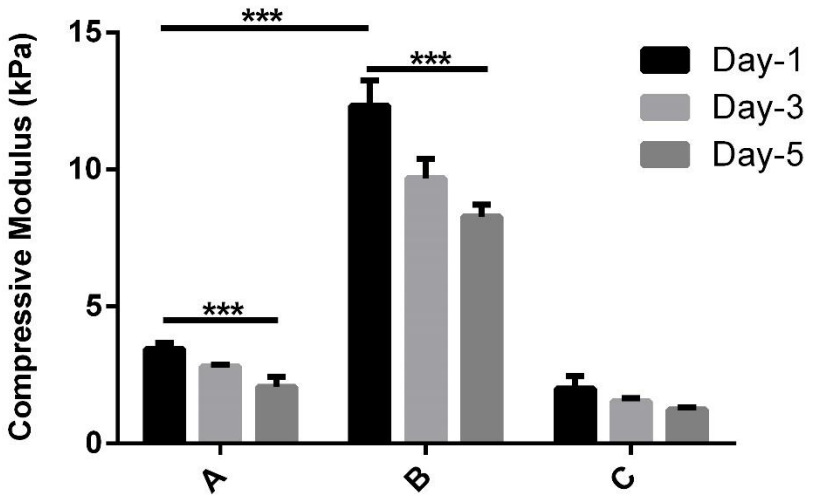

Figure 4-41. Compressive modulus of hydrogel A, B and C at different degradation dates. Bars represent mean ± SD and significance is indicated with ***P<0.001.

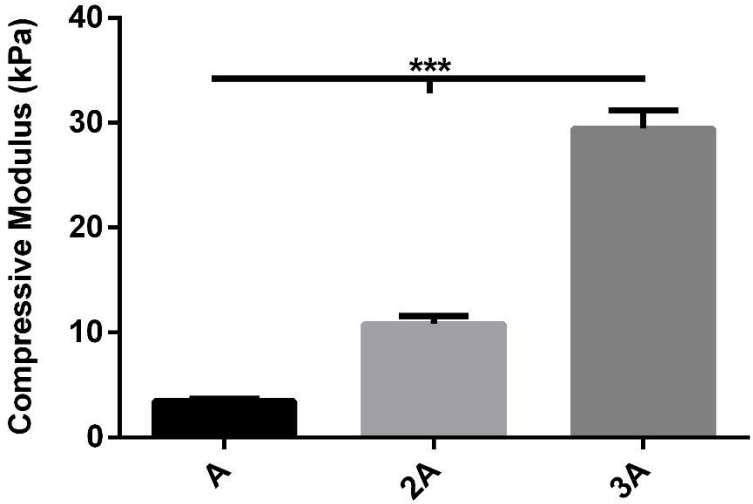

Figure 4-42. Compressive modulus of hydrogel A, 2A and 3A. Bars represent mean ± SD and significance is indicated with ***P<0.001.

4.8 Cytocompatibility analysis

4.8.1 Cytotoxicity test

Gelatin based porous scaffolds

The cytotoxicity test results were carried out by determining the metabolic activity of 3T3 cells that were cultured in extractions from different scaffolds where viability below 70% of the control group is considered has cytotoxic potential. Figure 4-43 shows cells cultured in extractions from all PA groups show similar metabolic level compared to the control. In contrast, metabolic levels of cells cultured in extractions from GA treated samples gradually decreased as the increasing of GA concentration. Specifically, metabolic level in GA 1.0 group was significantly lower compared to GA 0.1 ($P<0.01$).

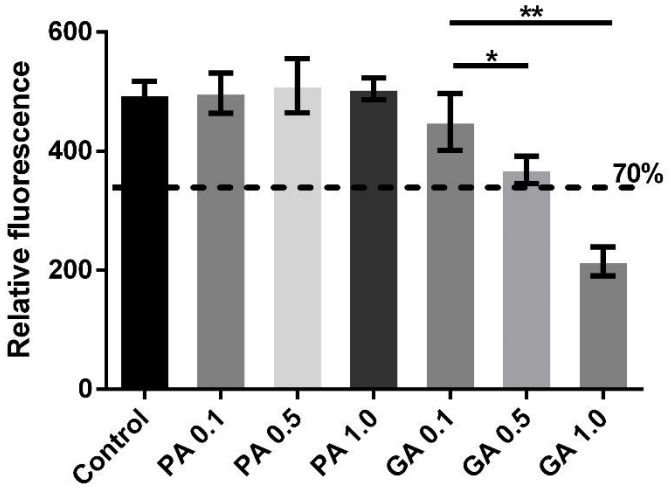

Figure 4-43. Cytotoxicity tests of fabricated scaffolds by using Alamar Blue assay. Bars represent mean ± SD and significance is indicated with *P<0.05 and **P<0.01.

RHC based porous scaffolds

The cytotoxicity of the fabricated porous scaffolds with varied RHC concentrations were examined by medium extraction test where the metabolisms level of the 3T3 fibroblasts were evaluated by using Alamar Blue assay. As shown in Figure 4-44, no potential toxicity were found from the tested samples as cell viabilities obtained from tested samples were higher than 70% of the control. Meanwhile, no significant differences were founded among all samples ($P>0.05$).

The cytotoxicity of porous RHC-CHI scaffolds that cross-linked with different amount of EDC were determined by using Alamar Blue assay and shown in Figure 4-45. It can be noticed that all tested samples show no cytotoxicity to the cells as all fluorescent results from tested samples were higher than 70% viability that determined from the control. Meanwhile, there was no significant difference among 50, 75 and 100 mg EDC cross-linked scaffolds ($P>0.05$).

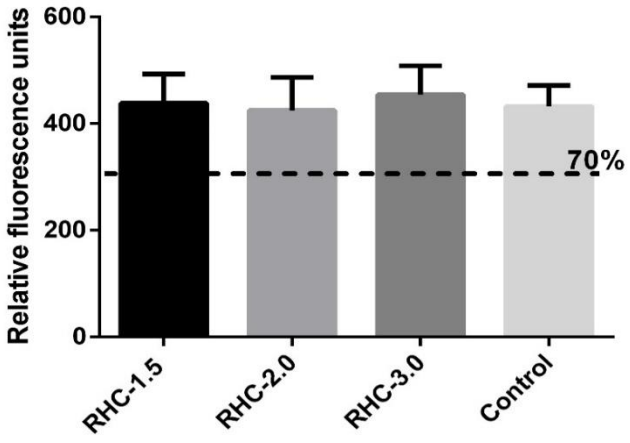

Figure 4-44. Cytotoxicity of fabricated RHC porous scaffolds determined by assessing the cellular metabolic activity levels, fresh medium used as control. Bars represent mean ± SD.

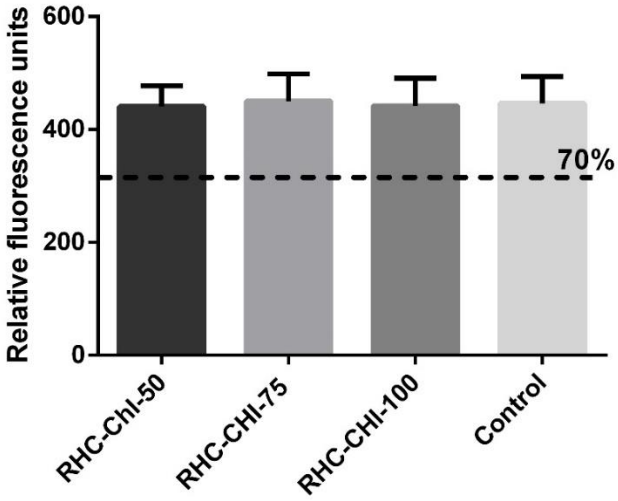

Figure 4-45. Cytotoxicity test of fabricated RHC-CHI porous scaffolds determined by assessing the cellular metabolic activity levels, fresh medium used as control. Bars represent mean ± SD.

RHC based hydrogel scaffolds

Elution test was also used to assess the cytotoxicity of the hydrogel scaffolds where Alamar Blue assay was used to assess the metabolic activity of the cells and the results are shown in Figure 4-46. The results indicated that all fabricated hydrogels had no potential cytotoxicity to the cells as cell viabilities obtained from tested samples were higher than 70% of the control.

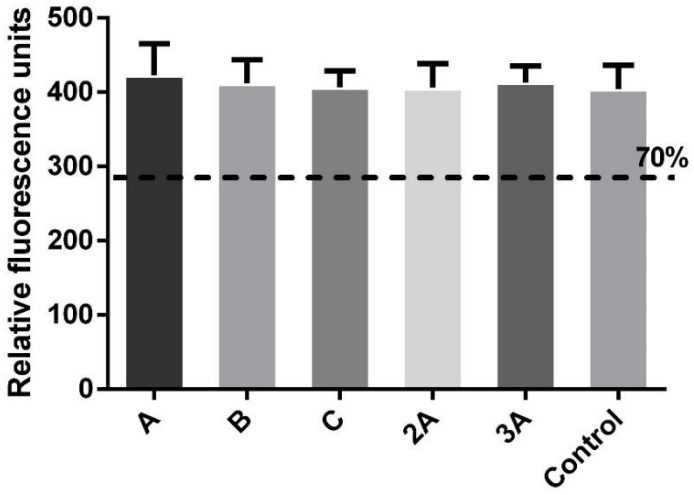

Figure 4-46. Cytotoxicity test of fabricated hydrogel scaffolds by using Alamar Blue assay. Bars represent mean ± SD.

4.8.2 Cell metabolic activities (Alamar Blue assay)

RHC based porous scaffolds

Alamar Blue assay was used to evaluate the cell viabilities by determining their metabolic levels in the seeded scaffolds. At defined time point, scaffolds were taken out and washed with PBS before incubation in Alamar Blue assay. The metabolic levels of the 3T3 cells seeded RHC-1.5, 2.0 and 3.0 scaffolds were determined by incubating the scaffolds in Alamar Blue assay for 80 min at defined culturing time

points. The determined relative fluorescent raw data from seeded scaffolds was normalised to the DNA concentration obtained from each sample and shown in Figure 4-47. At each selected culture time, it shows that there were no significant differences of normalised fluorescent results among RHC-1.0, 2.0 and 3.0 scaffolds ($P>0.05$). Meanwhile, normalised cell metabolic activities determined from each sample at day 3 were found significantly higher compared to individual result obtained at day 1 and 7.

The normalised metabolic activities of the cells seeded RHC-CHI scaffolds at specific culture time are presented in Figure 4-48. It shows that the metabolic activities in each scaffold increased significantly from day 1 to day 3 ($P<0.01$). From day 7 to 14, the metabolic activities obtained from each type of sample remained constant as no significant differences were found ($P>0.05$). Additionally, there were no significant differences can be found among three type of scaffold at each individual selected point ($P>0.05$).

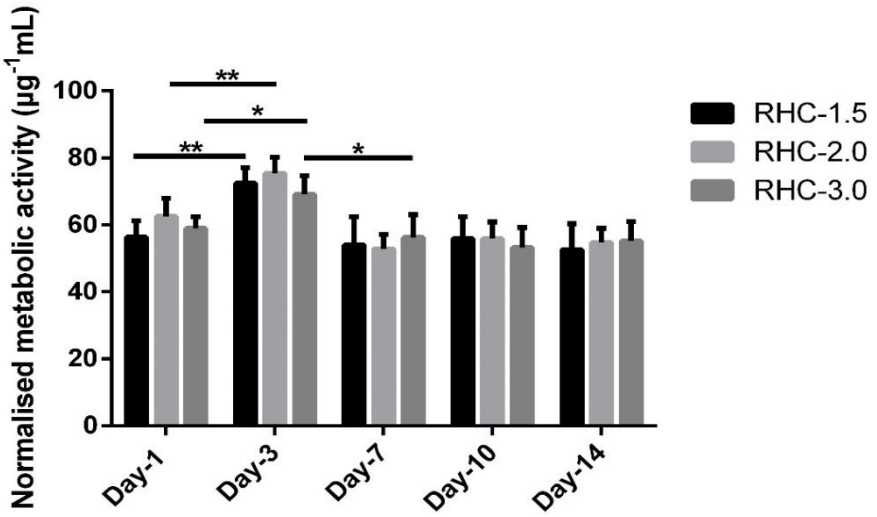

Figure 4-47. Normalised cell metabolic activities in seeded RHC-1.5, 2.0 and 3.0 porous scaffolds at culture day 1, 3, 7, 10 and 14. Bars represent mean ± SD and significance is indicated with *P<0.05 and **P<0.01.

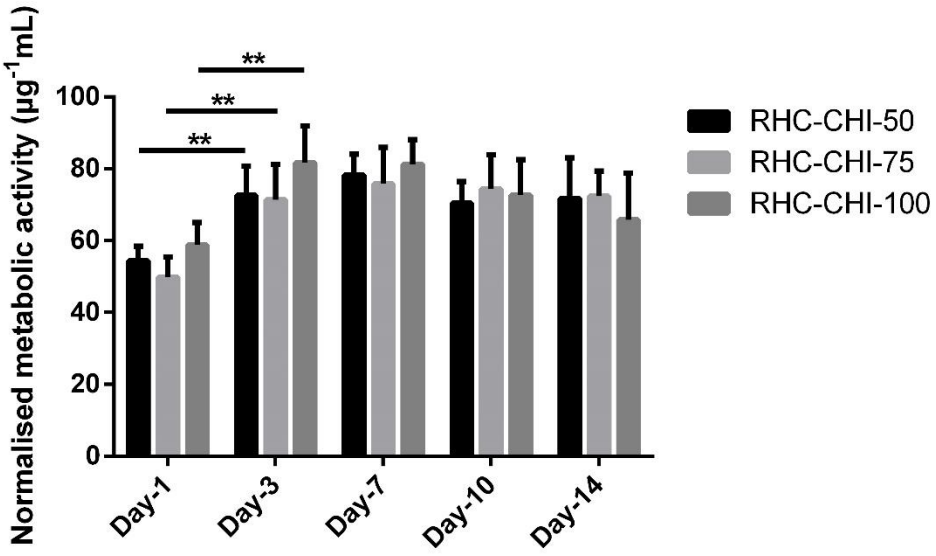

Figure 4-48. Normalised cell metabolic activities in seeded RHC-CHI-50, 75 and 100 porous scaffolds at culture day 1, 3, 7, 10 and 14. Bars represent mean ± SD and significance is indicated with **P<0.01.

RHC based hydrogel scaffolds

The viabilities of attached fibroblasts were studied by determining their metabolic activities at early stage (6 h) after seeding. The result is shown in Figure 4-49, and it illustrates the cell metabolic activities were increased as increasing the RHC fraction in hydrogel scaffolds. Metabolic activity of fibroblasts on hydrogel A was found significant higher than hydrogel B and C ($P<0.001$) while there were no significant differences of determined fibroblasts metabolic levels among hydrogel A, 2A and 3A ($P>0.05$).

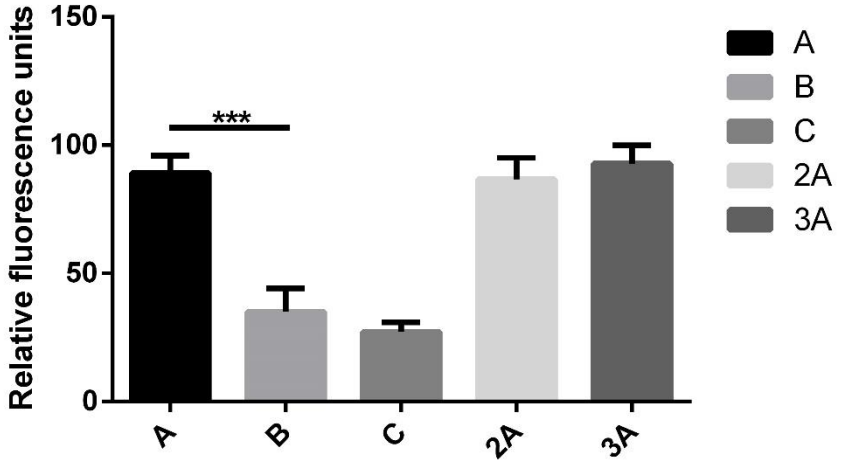

Figure 4-49. Cell metabolic activities measured at 6th h after initial seeding. Values represent mean ± SD and significance is indicated with ***P<0.001.

4.8.3 Cell proliferation

Gelatin base porous scaffolds

To evaluate the fibroblasts proliferation rate in seeded scaffolds, DNA contents were determined by using Hoechst DNA assay at defined time points (culturing day 1, 3, 7, 10 and 14) and shown in Figure 4-50. It shows that the proliferation was increased significantly along with the *in vitro* culture time on uncross-linked and PA 0.5 scaffold, while the proliferation of fibroblasts on GA 0.1 scaffold was only found from day 1 to day 3. Meanwhile, at each selected time point from day 3 till day 14, the DNA concentration of PA 0.5 scaffold was significant higher compared to both uncross-linked and GA scaffold, specifically, at day 14, the DNA concentration determined from PA 0.5 scaffold were found significant higher than uncross-linked ($P<0.01$) and GA cross-linked scaffold ($P<0.001$), respectively.

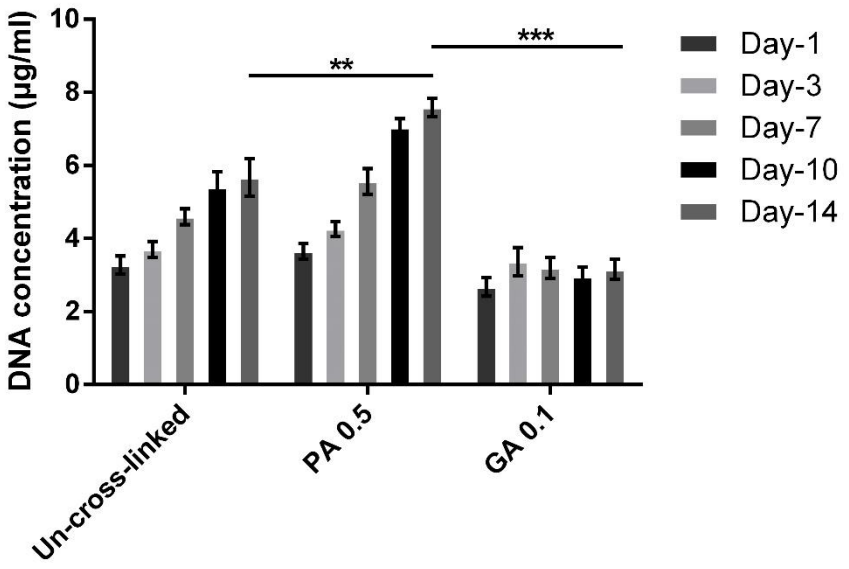

Figure 4-50. Fibroblasts proliferation measured using Hoechst DNA assay as determination on DNA concentration of un-cross-linked, PA 0.5 and GA 0.1 scaffold at different culturing time points. Bars represent mean ± SD and significance is indicated with **P<0.01 and ***P<0.001.

RHC based porous scaffolds

The calculated DNA concentration in RHC-1.5, 2.0 and 3.0 scaffolds at each selected culture time points are shown in Figure 4-51. In general, the DNA concentration was proportional to the RHC concentrations at all selected time points. Significant differences on DNA concentrations were found at culturing day 1, 3 and 7 between RHC-1.5 and 3.0 scaffold ($P<0.05$). No significant difference was found between RHC-1.5 and 2.0 scaffolds throughout the entire culture period. Meanwhile, the DNA concentration determined from RHC-1.5 was found slightly lower than RHC-3.0 at day 10 and 14.

The DNA concentrations of 3T3 cell seeded RHC-CHI scaffolds are shown in Figure 4-52. Similarly to the RHC scaffolds, it shows that the DNA concentrations gradually increased along with the culturing time in all three type of scaffolds throughout the test. Meanwhile, it also could be found at each time point, the DNA concentration was proportional to the amount of EDC that used to cross-link the RHC-CHI scaffolds as 100 mg EDC cross-linked scaffold had generally higher DNA concentration compared to the other two scaffolds. Significant differences on DNA concentrations between 50 and 100 mg scaffolds were observed at culturing day 7, 10 and 14. Specifically, at day 14, the DNA concentration determined in RHC-CHI-100 scaffold reached to 7.5 μg/ml which was significantly higher ($P<0.001$) compared to RHC-CHI-50 scaffold (5.4 μg/ml). Meanwhile, there was no significant difference found between RHC-CHI-50 and 75 scaffolds in the entire

culture period (P>0.05). Significant difference between RHC-CHI-75 and 100 was only found at day 14 (P<0.01).

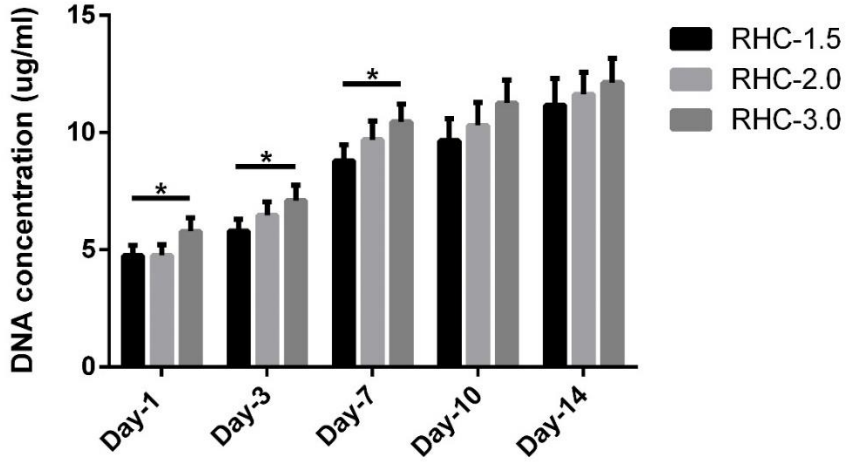

Figure 4-51. DNA concentrations measured using Hoechst DNA assay in RHC-1.5, 2.0 and 3.0 porous scaffolds at culture day 1, 3, 7, 10 and 14. Bars represent mean ± SD and significance is indicated with *P<0.05.

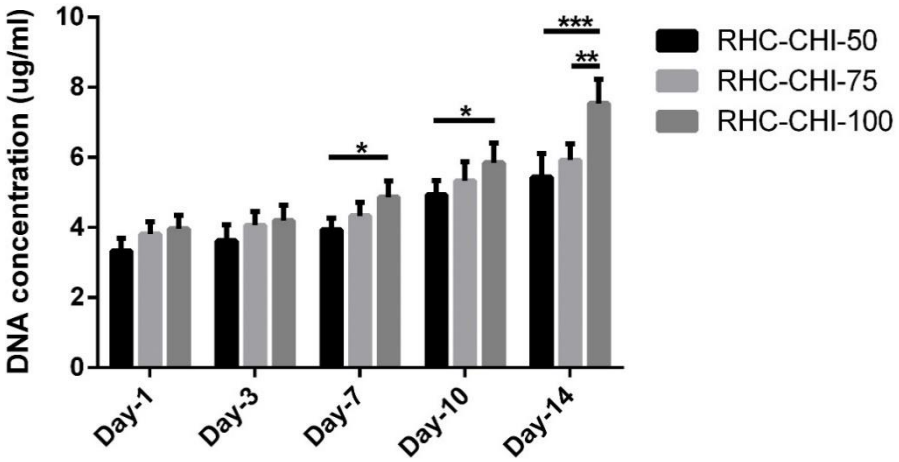

Figure 4-52. DNA concentrations measured using Hoechst DNA assay in RHC-CHI-50, 75 and 100 porous scaffolds at culture day 1, 3, 7, 10 and 14. Bars represent mean ± SD and significance is indicated with *P<0.05, **P<0.01 and ***P<0.001.

RHC based hydrogel scaffolds

The DNA content results determined from hydrogel A, B and C are shown in Figure 4-53. It can be seen that the DNA concentration increased with increased culturing time on hydrogel A, B and C. It also shows DNA content was proportional to the RHC fraction as hydrogel A had the highest DNA content among all three hydrogels at each time point compared to hydrogel C ($P<0.01$). At day 5, the DNA concentration of hydrogel A was 1.6 and 3.1-fold of DNA concentration found in hydrogel B and C respectively ($P<0.001$). Another finding is that hydrogel C showed a relatively slow proliferation rate compared to hydrogel A and B as a slightly increasing on DNA content along with the culture period, specifically, it was found DNA concentration of day 3 and 5 were 1.54 and 1.64 μg/m, which shows no significant increasing ($P>0.05$). The results of DNA content in each hydrogel was in accordance with the findings obtained in optical microscopy images (Figure 4-61) i.e. hydrogel A has the highest proliferation rate among all hydrogels scaffolds.

The DNA concentration results of fibroblasts that proliferated on hydrogels with different biopolymer concentrations are shown in Figure 4-54. Generally, the DNA concentrations from all samples increased along with the culture time, where an acceleration increasing could be noticed from day 3 to 5 as DNA concentration found from each type of hydrogel on day 5 was at least 2-fold of day 3 ($P<0.001$). Meanwhile, at each time point, the DNA concentrations were found to increase slightly as the biopolymer concentration increased. At day 3, a significant higher

DNA concentration was found on hydrogel 3A (2.91 µg/ml) that was 1.2-fold of DNA content found on hydrogel A (2.43 µg/ml) ($P<0.05$). There were no significant differences could be found between hydrogel 2A and 3A at day 5 while both hydrogels showed slightly higher DNA concentration compared to hydrogel A ($P<0.05$).

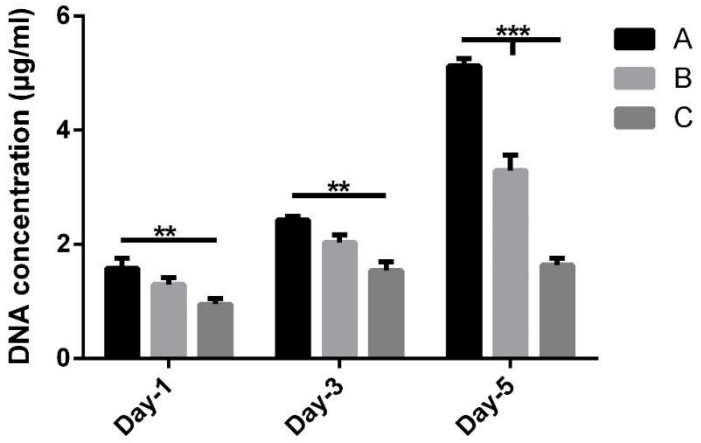

Figure 4-53. DNA concentrations of cell seeded hydrogel A, B and C at culture day 1, 3 and 5 determined by Hoechst DNA assay. Bars represent mean ± SD and significance is indicated with **P<0.01 and ***P<0.001.

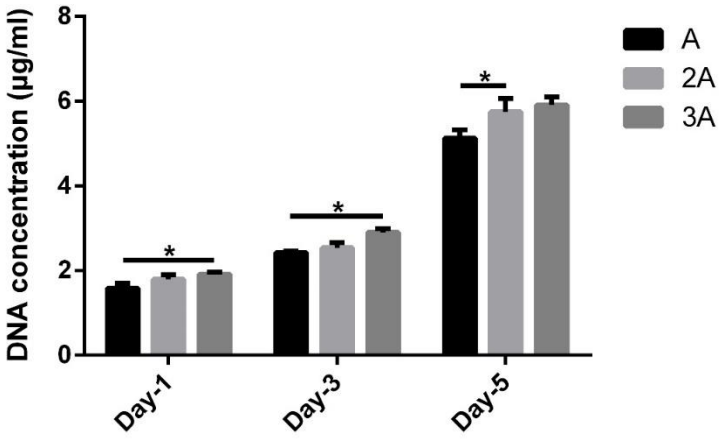

Figure 4-54. DNA concentrations of hydrogel A, 2A and 3A at culture day 1, 3 and 5 determined by Hoechst DNA assay. Bars represent mean ± SD and significance is indicated with *P<0.05.

4.8.4 Fluorescent images of proliferated cells

Gelatin based porous scaffolds

To investigate the proliferation status of 3T3 cells in different scaffolds, fluorescent images were taken at defined time points (day 3, 7 and 14) from the best performing groups in the cytotoxicity tests (Control, PA 0.5 and GA 0.1). Typical images are shown in Figure 4-55. At day 3, the number of live cells in both uncross-linked and PA 0.5 scaffold were higher than GA 0.1 scaffold (Figure 4-55 A1, B1 and C1). At day 7, it shows the PA 0.5 cross-linked scaffold had the highest cell density, and lower numbers of cells with inhomogeneous distribution were found in GA 0.1 cross-linked scaffold (Figure 4-55 A2, B2 and C2). By day 14 cells became confluent on most available porous structures of the control and the PA 0.5 cross-linked scaffold (Figure 4-55 A3, B3). It was found that the poorest cell proliferation was seen on the GA 0.1 scaffold at selected time points (Figure 4-55 C1-C3).

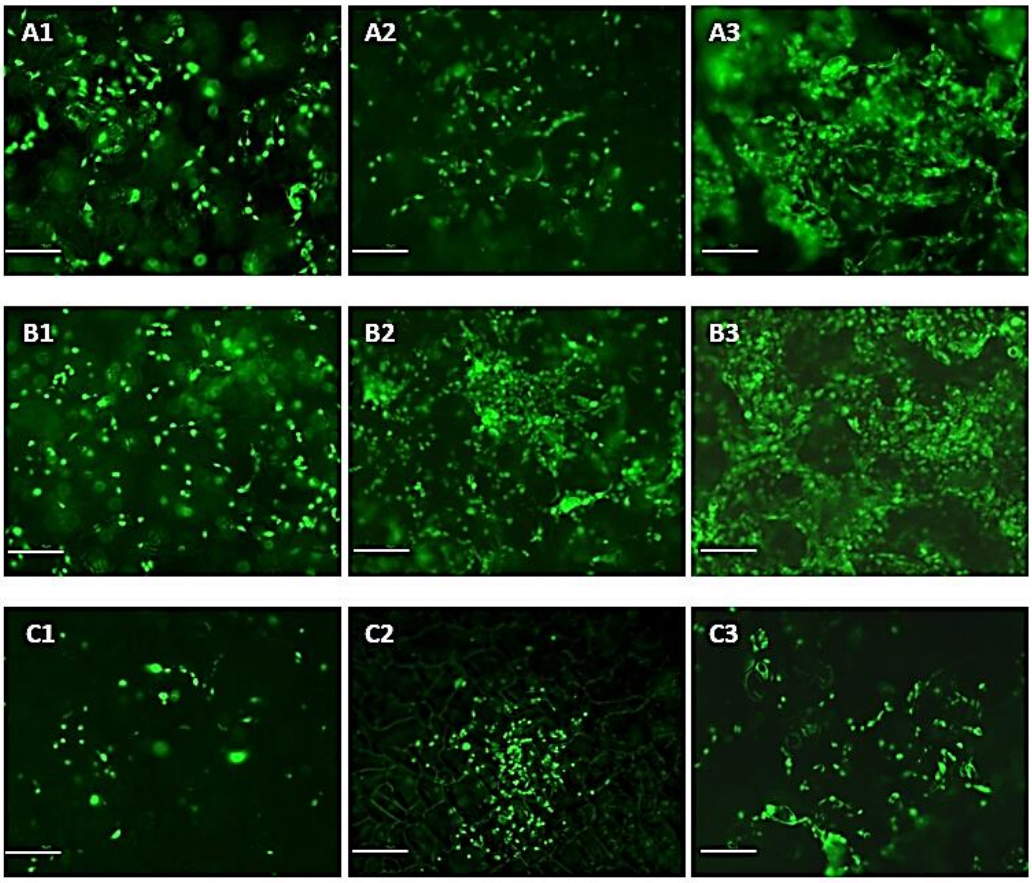

Figure 4-55. Fluorescent images of proliferated 3T3 cells presenting in different scaffolds at three defined culturing time points, bar equals to 50 μm. (A1-A3) indicated 3T3 cells in uncross-linked scaffold at culturing day 3, 7 and 14. (B1-B3) indicated 3T3 cells in PA 0.5 cross-linked scaffold at culturing day 3, 7 and 14. (C1-C3) indicated 3T3 cells in GA 0.1 cross-linked scaffold at culturing day 3, 7 and 14.

RHC based porous scaffolds

To investigate the proliferation status of 3T3 cells in different scaffolds, fluorescent images were taken at defined time points (day 7 and 14) and are shown in Figure 4-56. At day 7, the numbers of live cells presented in RHC-1.5, 2.0 and 3.0 scaffold were uniform, and the distributions of the cells in each scaffold were homogenous (Figure 4-56 A, C and E). At culturing day 14, the higher density of

the cells grew in each scaffold was noticed as comparing to day 7. Meanwhile, it observed that porous structures of all three types of RHC scaffolds were mostly covered by the proliferated 3T3 fibroblast where cells were also homogenously distributed (Figure 4-56 B, D, F).

The fluorescent images of 3T3 fibroblasts seeded RHC-CHI scaffolds were taken at culturing day 7 and 14, as shown in Figure 4-57. At culturing day 7, RHC-CHI-75 and 100 scaffold showed higher cell density compared to RHC-CHI-50 scaffold, and the fibroblasts in these two scaffolds were found well-distributed in the porous structures (Figure 4-57 A, C, E). On day 14, it can be seen 3T3 fibroblasts were homogenously distributed in the porous structures of all three types of scaffolds and the cell densities were significantly increased as compared to day 7 (Figure 4-57 B, D, F). It also observed that the RHC-CHI-100 scaffold had the highest cell density among all three samples where similar cell densities were found in scaffold RHC-CHI-50 and 75 (Figure 4-57 D, F).

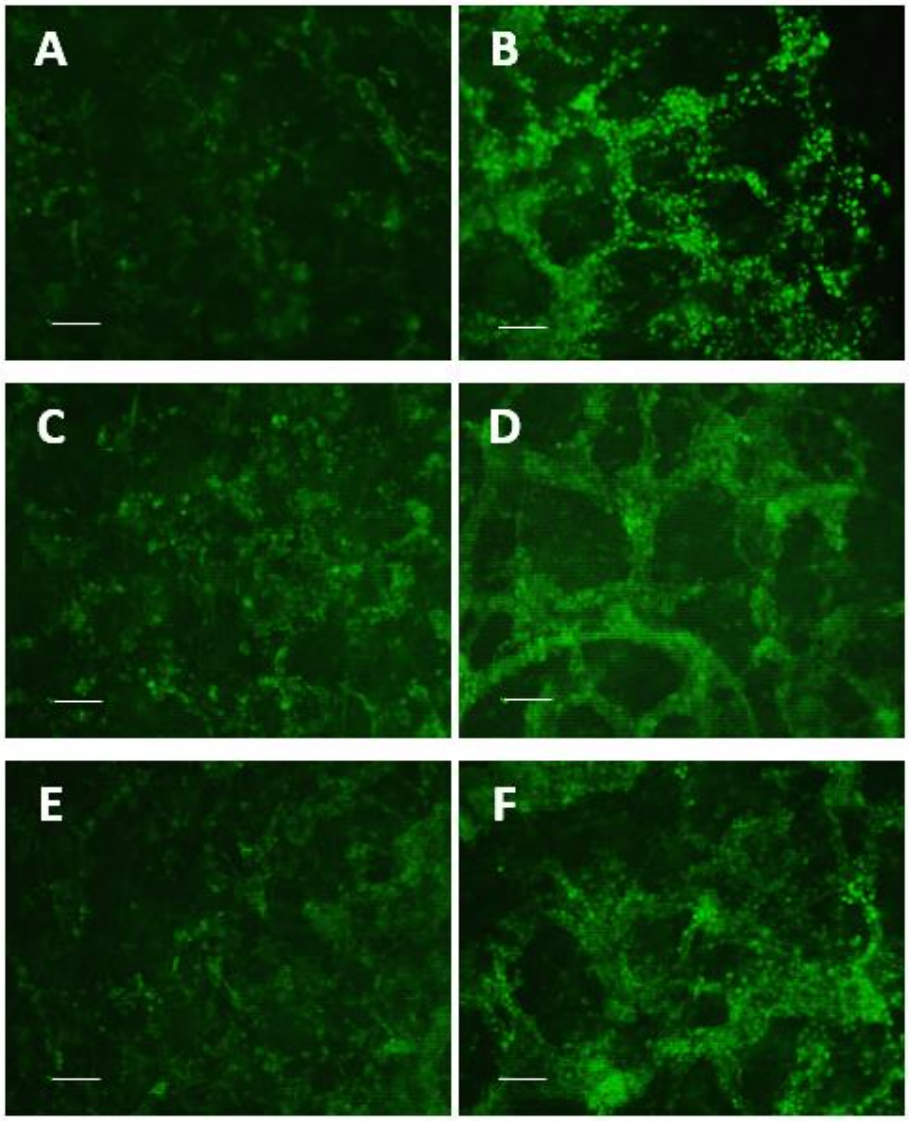

Figure 4-56. Fluorescent images of proliferated 3T3 fibroblasts in RHC porous scaffolds. (A-B) show the proliferated cells in RHC-1.5 scaffold at culture day 7 and 14; (C-D) proliferated cells in RHC-2.0 scaffold at culture day 7 and 14; (E-F) proliferated cells in RHC-3.0 scaffold at culture day 7 and 14. Scale bar = 50 μm.

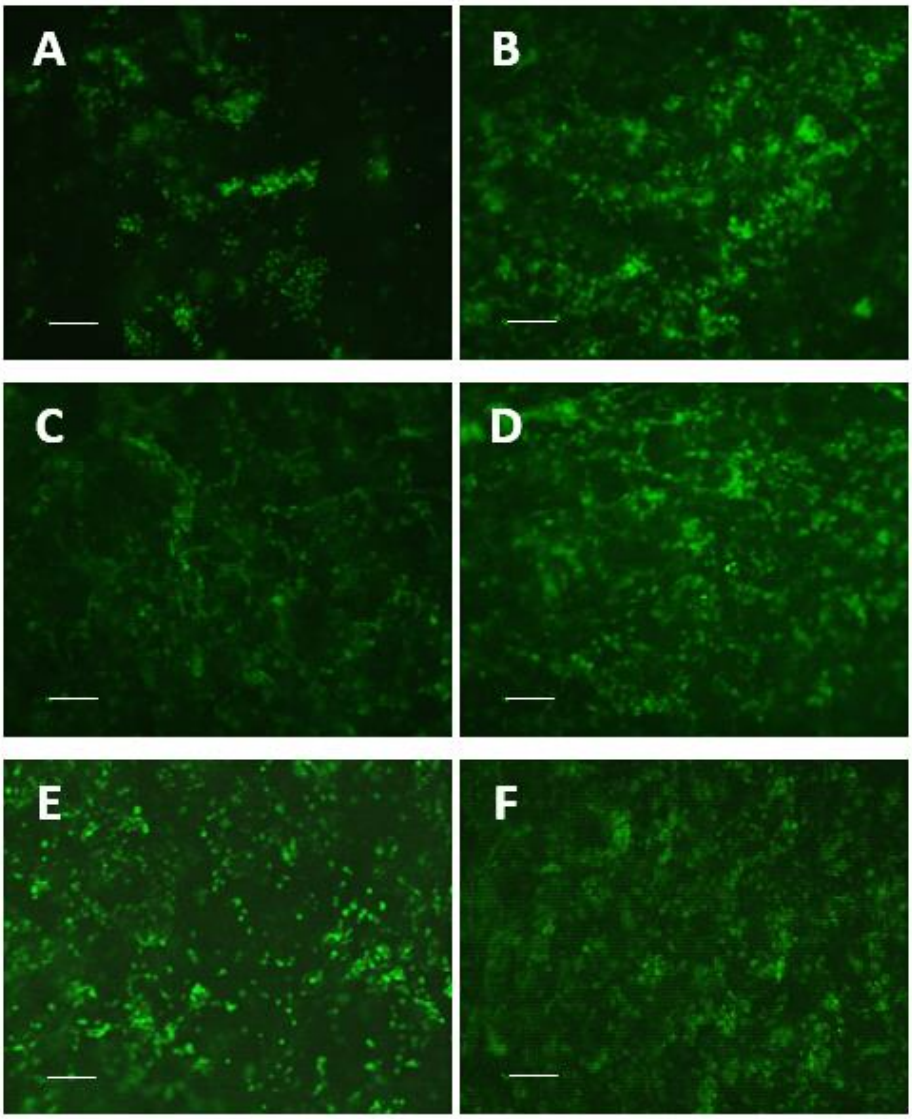

Figure 4-57. Fluorescent images of proliferated 3T3 fibroblasts in RHC-CHI porous scaffolds. (A-B) show the proliferated cells in RHC-CHI-50 scaffold at culture day 7 and 14; (C-D) proliferated cells in RHC-CHI-75 scaffold at culture day 7 and 14; (E-F) proliferated cells in RHC-CHI-100 scaffold at culture day 7 and 14. Scale bar = 50 μm.

4.8.5 Cell morphology

Gelatin based scaffolds

The morphology of 3T3 cells growing on uncross-linked, PA and GA cross-linked scaffold at day 14 were investigated by SEM and are shown in Figure 4-58. At day 14, the pore structures of PA 0.5 cross-linked scaffold were largely covered by well-connected 3T3 cells with spindle shaped morphology (Figure 4-58 A1). The cells growing in internal part of scaffold were also investigated where the proliferated cells were found attached to the wall structures of the pores and started to link to one other via lamellipodia (Figure 4-58 A2). As shown in Figure 4-58 B1 and B2, the connected 3T3 cells formed flat sheet-like structures on the surface of uncross-linked scaffolds, and fewer cells were observed in the inner part of scaffold compared to PA cross-linked sample. In contrast to the PA scaffold and uncross-linked scaffold, GA 0.1 scaffold had lower number of cells presenting on the porous structures as well as internal part of the scaffold as shown in Figure 4-58 C1 and C2.

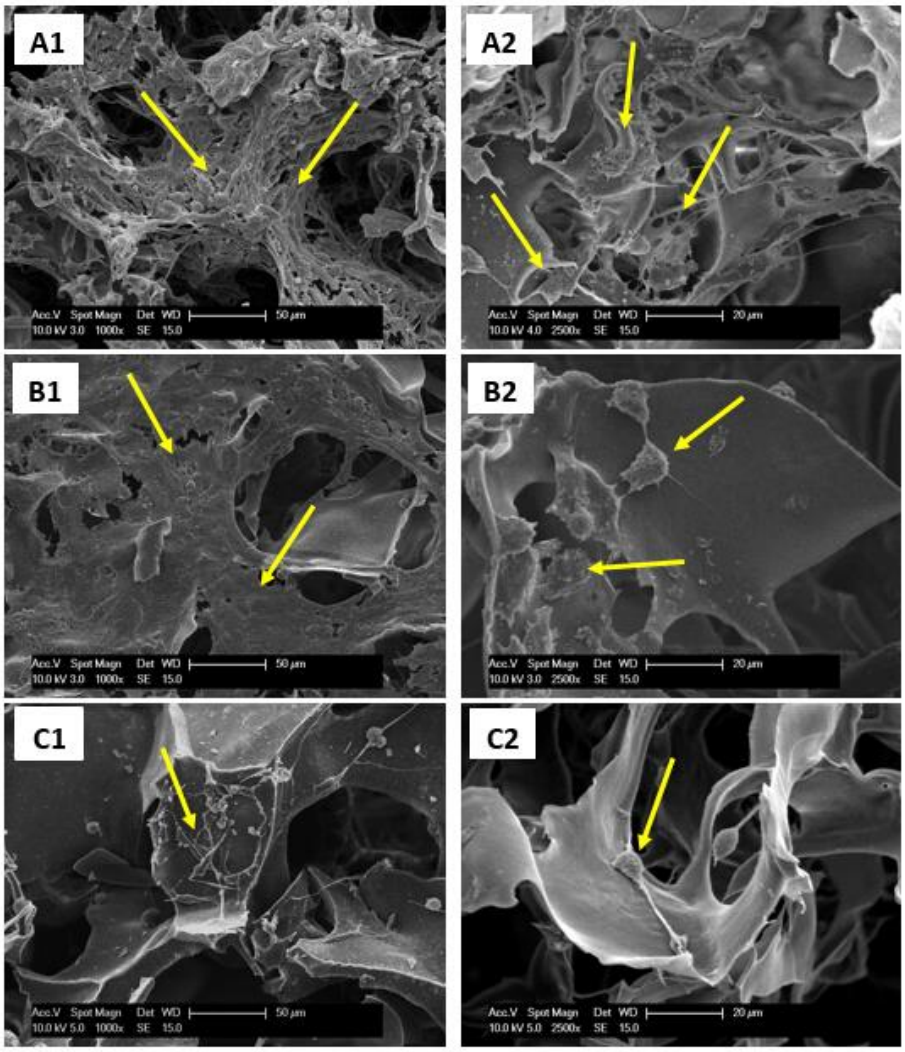

Figure 4-58. SEM images of proliferated 3T3 cells on scaffolds (arrows indicating cells). (A1) Cells grow on porous structures of PA 0.5 scaffold, (A2) Cells grow in inner PA 0.5 scaffold; (B1) Cells grow on porous structures of uncross-linked scaffolds, (B2) Cells grow in inner uncross-linked scaffold; (C1) Cells grow on porous structures of GA 0.1 cross-linked scaffolds, (C2) Cells grow in inner GA 0.1 cross-linked scaffold.

RHC based porous scaffolds

At culture day 14, the morphology of 3T3 cells growing in RHC-1.5, 2.0 and 3.0 scaffolds were investigated by SEM and images are shown in Figure 4-59. It can be observed that the wall structures of pores were covered with 3T3 cells in all three types of scaffolds, as shown in images of lower magnification (Figure 4-59 A, C, and E). In images of higher magnification (Figure 4-59 B, D and F), it can be seen that the proliferated cells were well connected and firmly attached to the wall structures of the scaffolds. Meanwhile, no significant difference of the cell morphology and density could be observed among these three RHC scaffolds.

The SEM images of 3T3 cells grow in RHC-CHI-50, 75 and 100 scaffolds at culture day 14 are shown in Figure 4-60. In images of lower magnification, cells grew in RHC-CHI-50 and 75 scaffold formed flat structures which firmly covered around 50% wall structures within the scaffolds. Meanwhile, fibroblasts in RHC-CHI-100 scaffold covered a slightly larger area (as shown in Figure 4-60 A, C and E) compared to the other two scaffolds. In images of higher magnification (Figure 4-60 B, D and F), fibroblasts showed well-connected structures and firmly attached to the wall of porous structures in all three seeded porous scaffolds. What's more, no significant difference on cell morphology such as shape and orientation could be observed among all these three type of scaffolds at day 14.

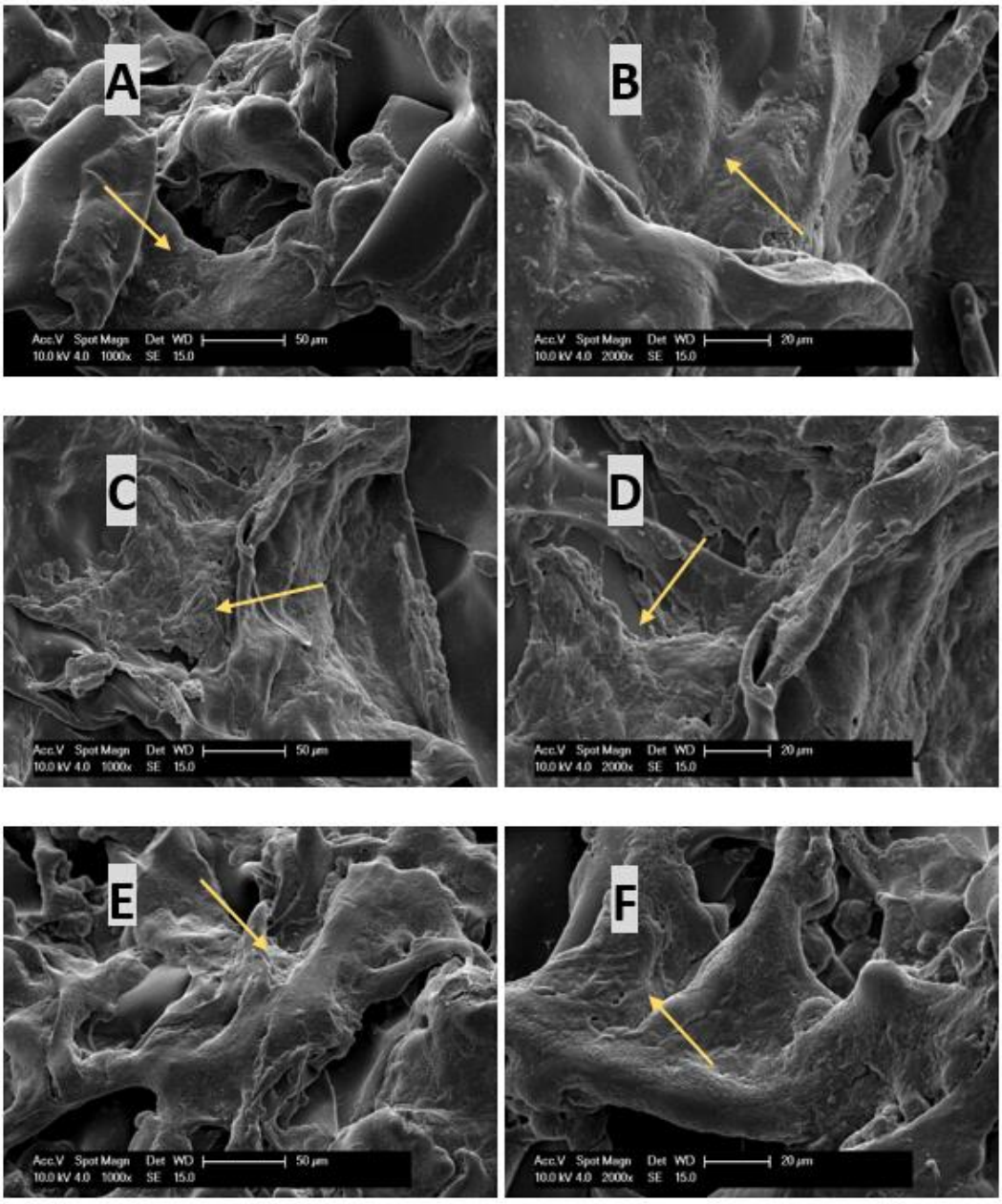

Figure 4-59. SEM images of proliferated 3T3 cells grew in RHC porous scaffolds (arrows indicating cells) at cell culture day 14. Cells grown on porous structures of RHC-1.5 scaffold with lower (A) and higher (B) magnification; cells grown on porous structures of RHC-2.0 scaffold with lower (C) and higher (D) magnification; cells grown on porous structures of RHC-3.0 scaffold with lower (E) and higher (F) magnification. Scale bar (left) = 50 μm, scale bar (right) =20 μm.

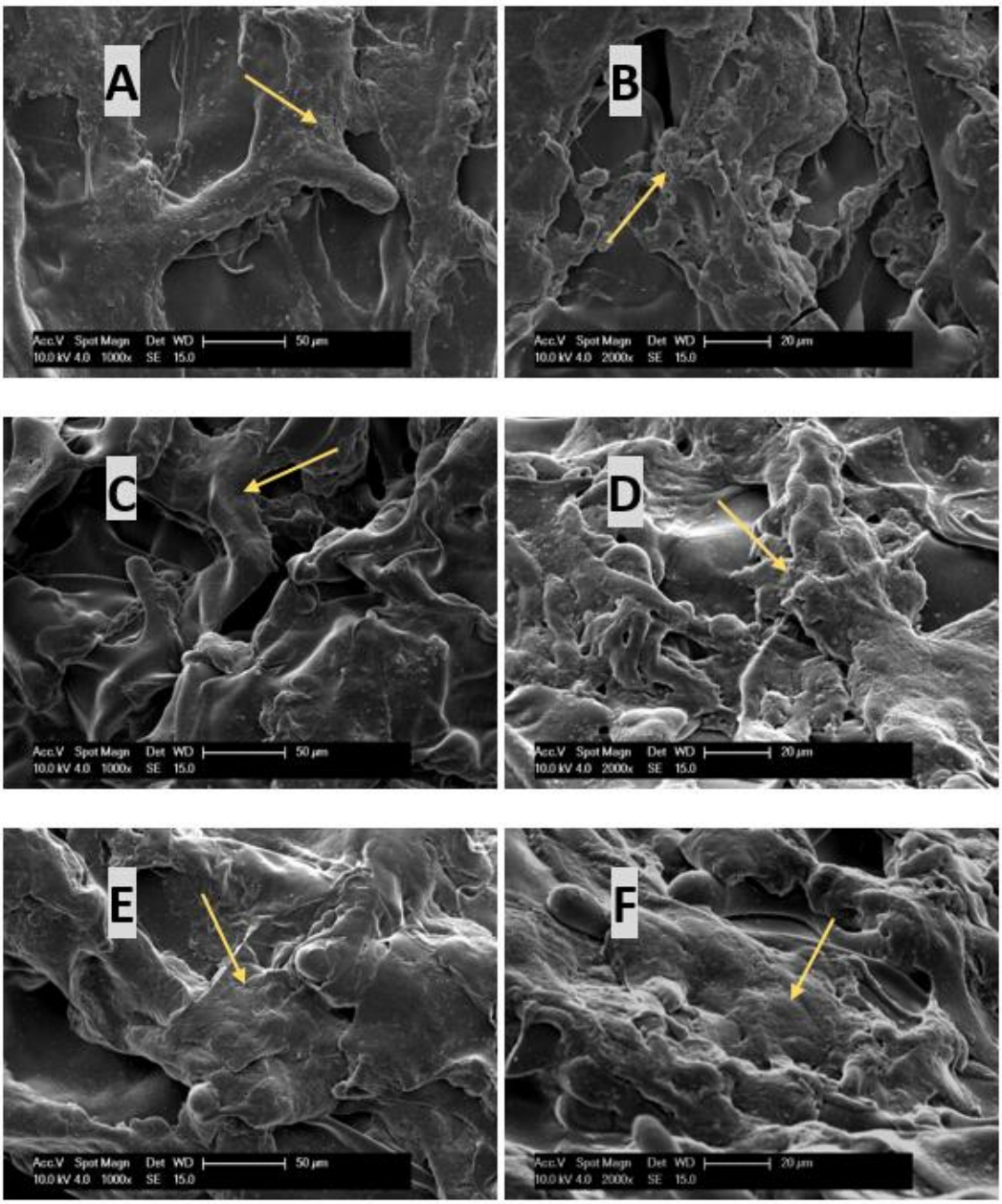

Figure 4-60. SEM images of proliferated 3T3 cells grew in RHC-CHI porous scaffolds (arrows indicating cells) at cell culture day 14. Cells grown on porous structures of RHC-CHI-50 scaffold with lower (A) and higher (B) magnification; cells grown on porous structures of RHC-CHI-75 scaffold with lower (C) and higher (D) magnification; cells grown on porous structures of RHC-CHI-100 scaffold with lower (E) and higher (F) magnification. Scale bar (left) = 50 μm, scale bar (right) =20 μm.

RHC based hydrogels

The images of fibroblasts grew on seeded hydrogels (A, B and C) were taken at different intervals (day 1, 3 and 5) and shown in Figure 4-61. Generally, from the images, it can be seen that fibroblasts proliferated the most in hydrogel A among these three types of hydrogels throughout the test. At culturing day 1, a large spread fibroblasts with uniformity were presenting on hydrogel A, where hydrogel B had less spread cells. Meanwhile, the morphology of fibroblasts on hydrogel C showed round or nearly spherical shape and no elongations could be observed. At culturing day 3, it can be observed that the number of fibroblasts proliferated on hydrogel A was significantly higher than hydrogel B and C, where fibroblasts with elongated shapes could be observed on hydrogel B and C. What's more, the shapes of cells on hydrogel B showed a greater spread area compared to cells on hydrogel C. The fibroblasts became fully confluent on day 5 on hydrogel A i.e. they formed continuous monolayer. Whereas fibroblasts presented on hydrogel B were nearly confluent, the proliferated fibroblasts on hydrogel C became more elongated at their morphologies and more cell to cell linkages could be noticed.

Figure 4-62 shows the fibroblasts that grew on hydrogels with different concentrations. Generally, the number of cells displayed an accelerated proliferation rate from day 1 to 5 on all hydrogels. It can be seen that, cell density of the 2.0% and 3.0% hydrogel were slightly higher compared to 1.5% hydrogel while there were no significant differences on the cell morphology could be observed among three different hydrogels. At day 3, all fibroblasts had elongated

polygonal shapes with increased spread area on three hydrogels where around 85% surface area of all three type of hydrogels were covered by proliferated cells and similar cell densities were also noticed. At day 5, the fully confluent cells were observed on all seeded hydrogels and fibroblasts were found squeezed on the substrates, cells with decreased spread area were also recorded. In addition, the cytoplasmic protrusions between cells and towards the substrate which could be observed at day 1 and 3 were limited due to over confluence.

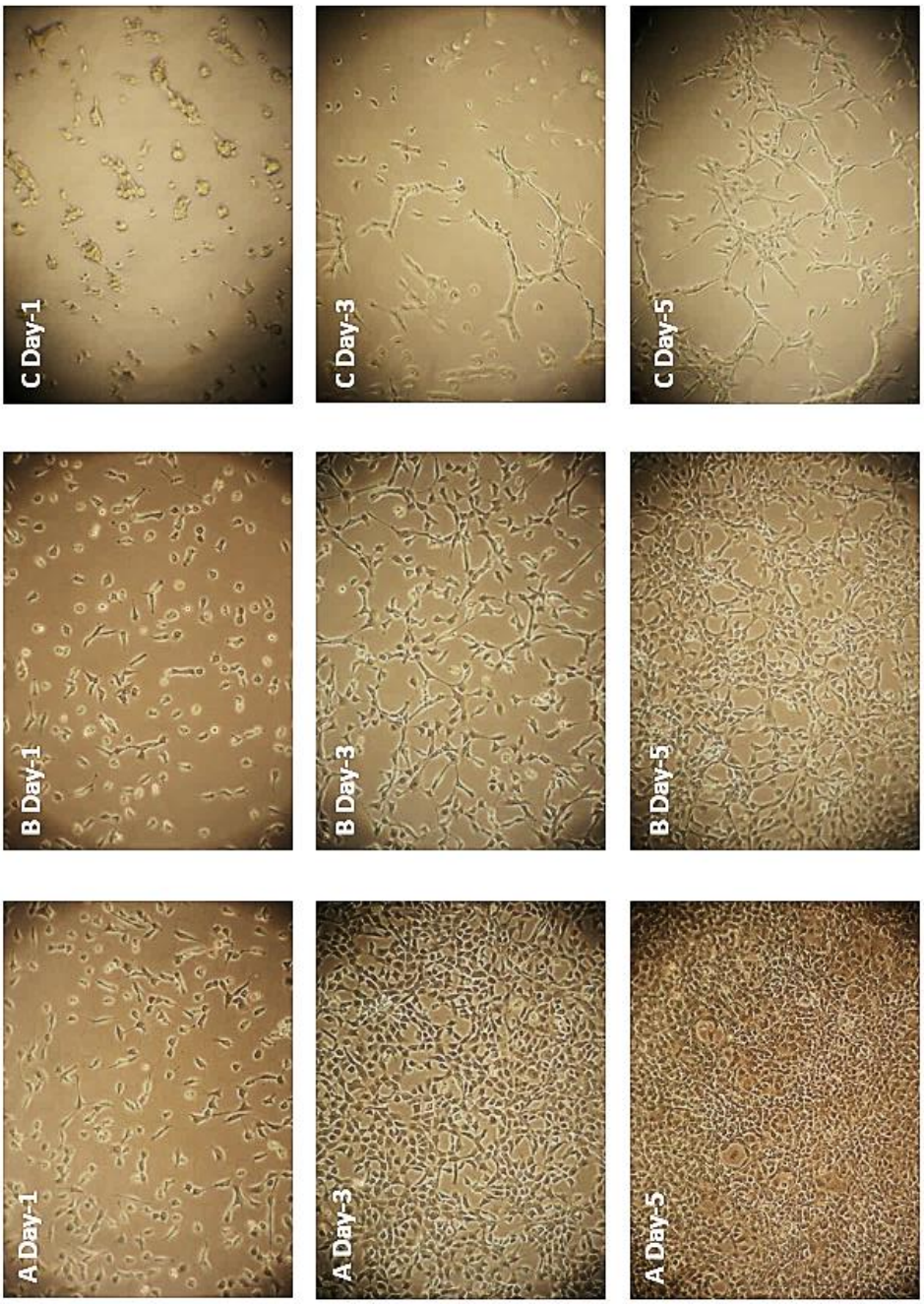

Figure 4-61. Light microscopy images (x40) of 3T3 fibroblasts on hydrogel A, B and C at culture day 1, 3 and 5

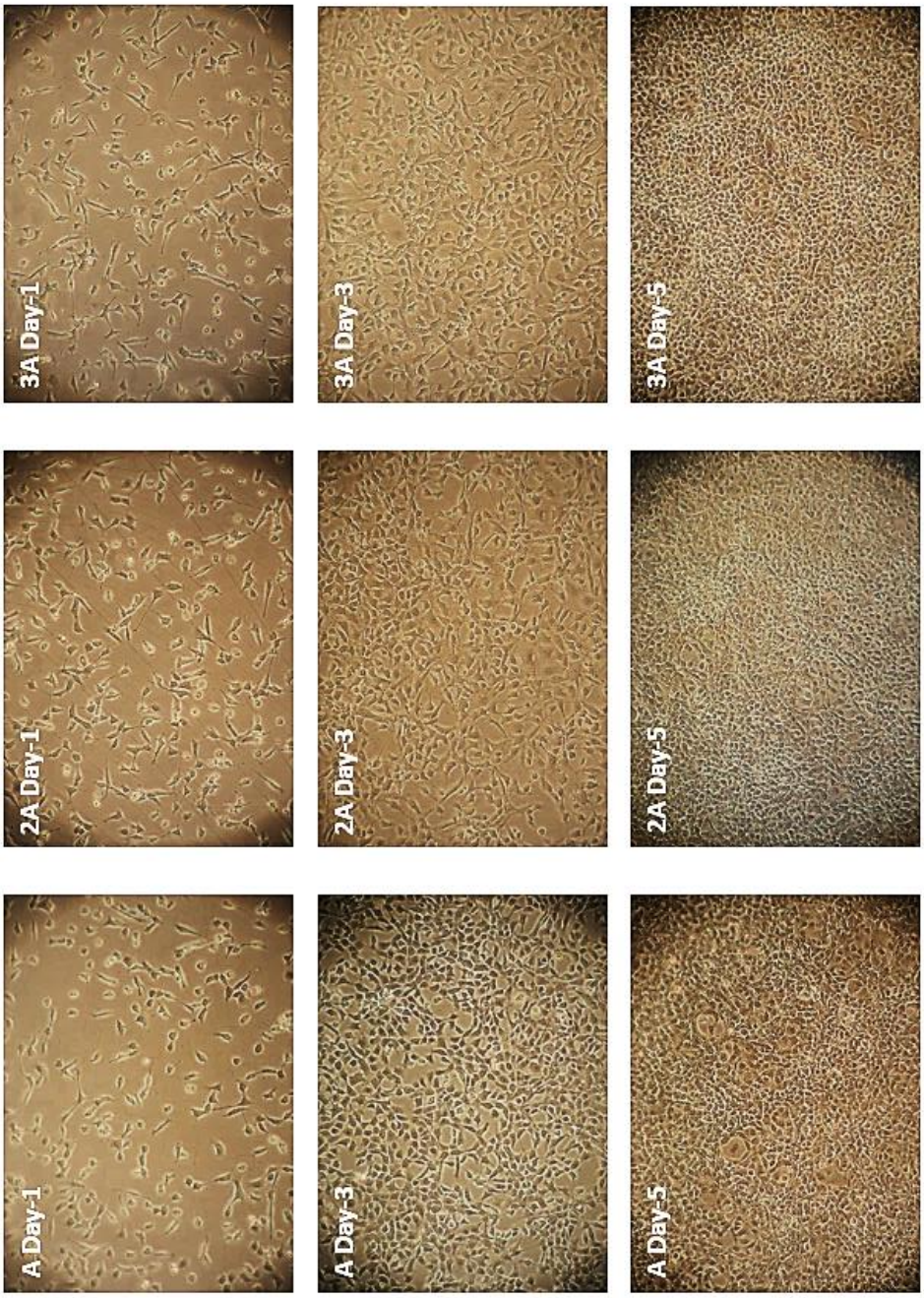

Figure 4-62. Light microscopy images (x40) of 3T3 fibroblasts on hydrogel A, 2A and 3A at culture day 1, 3 and 5

Additionally, an ESEM image of the hydrogel A seeded with fibroblasts at culture day 3 is shown in Figure 4-63. Proliferated cells that were firmly attached on the flat surface of the hydrogel can be observed from the middle to the bottom of the image, whereas a cell-free area (black circle) is shown as contrast in the upper part of the image. Connected fibroblasts which increased their spread area and showed polygonal shape which were well contacted to each other and formed a continuous monolayer are labelled in red circle.

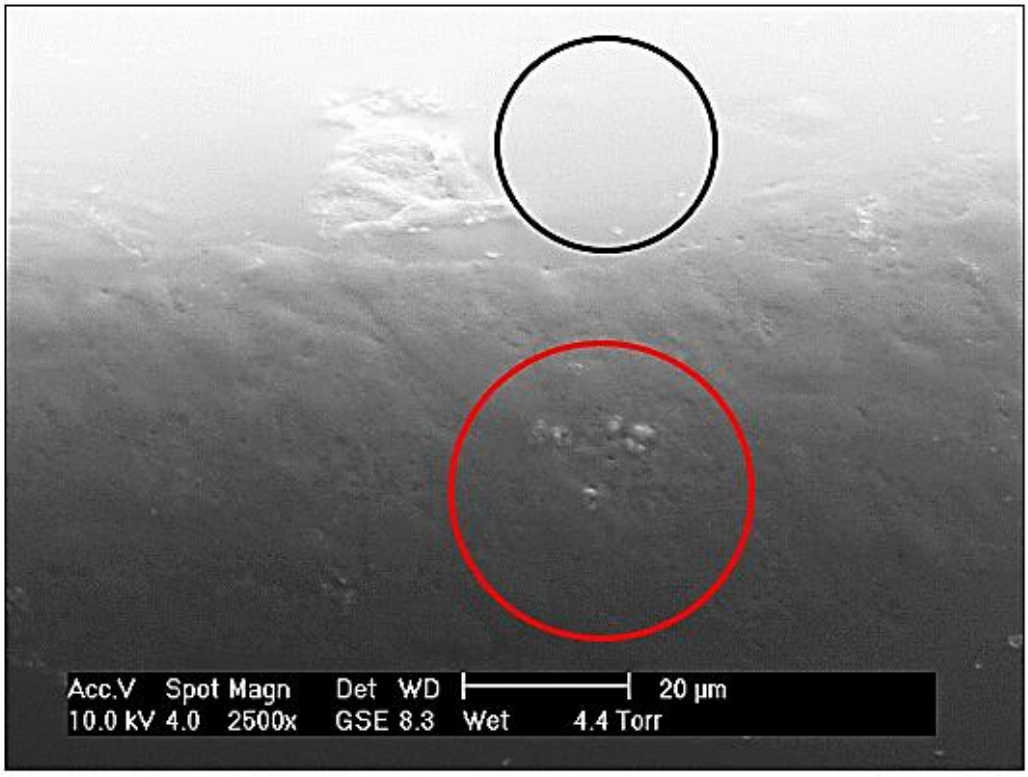

Figure 4-63. ESEM image of 3T3 fibroblasts growing on hydrogel A at day 3

4.9 qRT-PCR

qRT-PCR were used in this study to determine the expressions of extracellular matrix associated protein gene, and the primers (β-actin, Integrin, Collagen I and Collagen III) melt curves as well as amplification plots are presented in Figure 4-64. Specific single characteristic peak was found in melt curve of each selected primer, and indicated that specific and reasonable designed primers had been achieved. Meanwhile, the amplification plots showed that the Ct values (threshold cycle values) which indicate the efficiency of the amplification and further ensured the accuracy and reliability of the amplification results in qRT-PCR.

The expression levels of integrin, collagen I and III in RHC and RHC-CHI scaffolds at different time points were shown in Figure 4-65. It can be found the expression of integrin in both RHC and RHC-CHI scaffold increased throughout the cell culture period, where the highest expression was found 80-fold higher than the control from RHC scaffold at culture day 7, a slight reducing of the integrin transcription was also noticed at day 14 compared to day 7 (Figure 4-65 A). The expression of the type I collagen in both scaffolds were found increased along with the culture time (Figure 4-65 B). Generally, the mRNA expression levels of type III collagen from both scaffolds were relatively low at day 1 and 3, while at day 7 the expression level on RHC scaffold was 0.54 where RHC-CHI was 1.96 (Figure 4-65 C). Meanwhile, by comparing expression levels of type III collagen

with RHC scaffold, RHC-CHI scaffolds had higher expression level at day 7 while lower mRNA expression was found at day 14.

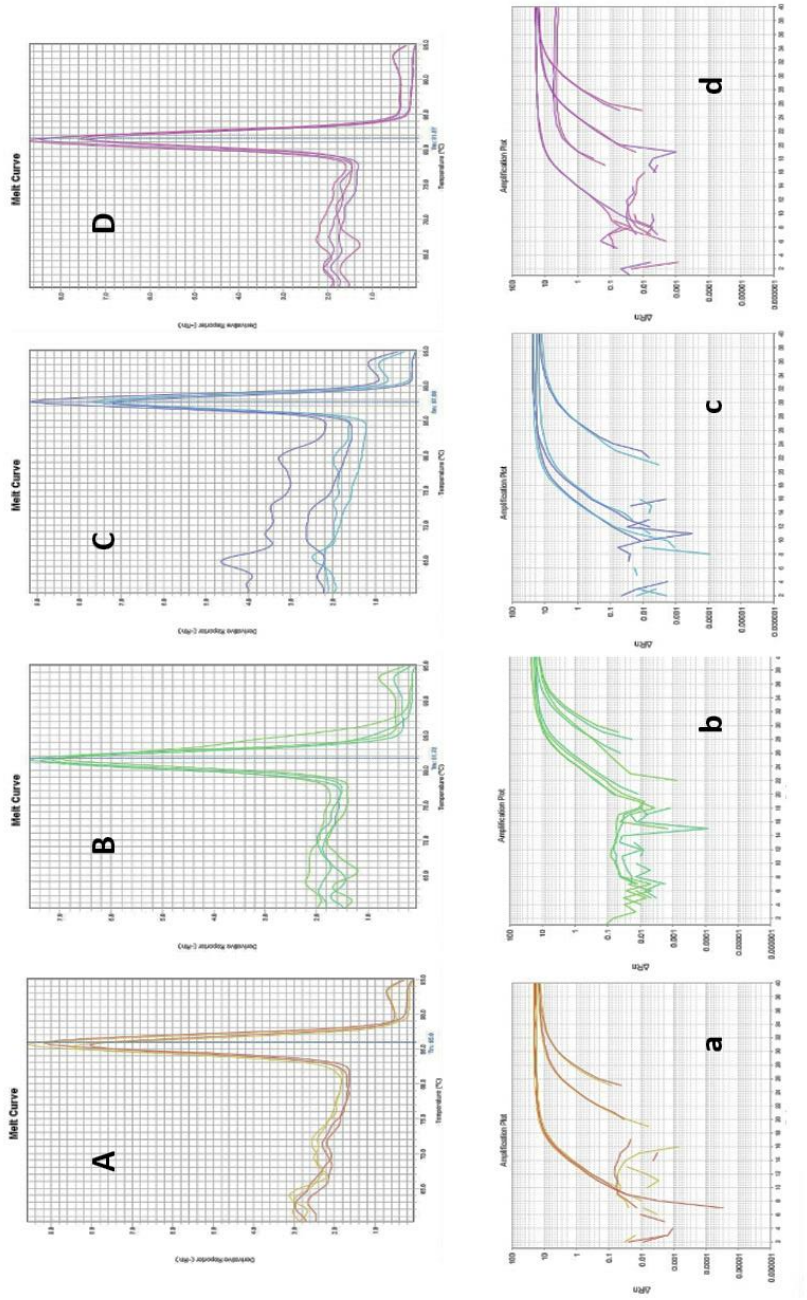

Figure 4-64. Melt curves of primer, (A) β-actin, (B) Integrin, (C) Collagen I and (D) Collagen III; amplification plots of primer, (a) β-actin, (b) Integrin, (b) Collagen I and (d) Collagen III

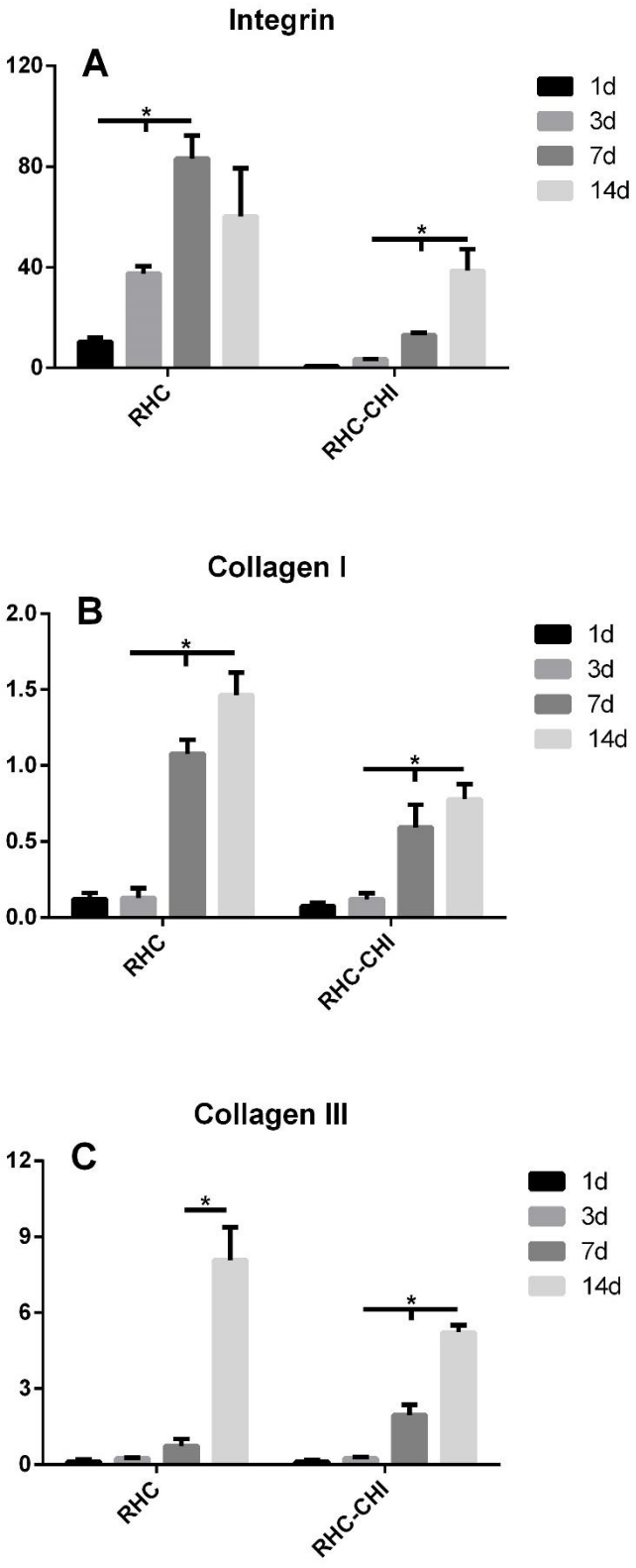

Figure 4-65. (A) Integrin, (B) collagen I and (C) collagen III mRNA expression levels by fibroblasts from RHC and RHC-CHI scaffold at different culturing time points.

Chapter 5 Discussion

This chapter provides the interpretation of the characterization results of 3-D gelatin based and RHC based porous scaffolds as well as RHC based hydrogels. There are seven sections are included in this chapter. Section 5.1 discusses the characterization of the fabricated porous scaffold including the suitability of pore morphology and porosity, section 5.2 covers the FT-IR characterization and cross-linking degree of the porous scaffolds. Section 5.3 and 5.4 discuss the gelation mechanism and swelling ability of the scaffolds where 5.5 analyse the *in vitro* degradation of the porous scaffolds. The evaluation of mechanical properties including compression and tensile tests on various porous scaffolds and RHC based hydrogels are discussed in section 5.6. Section 5.7 contain the discussion and comparison of cytotoxicity assessment, metabolic activities as well as proliferation activities in seeded scaffolds where cell distribution and morphology are also discussed.

5.1 Morphology of the porous structure

Porosity, pore size as well as internal structures together play important roles in design of porous scaffolds in soft tissue engineering as such factors can directly influence the swelling abilities, mechanical properties where optimized porous structures can benefit the cell proliferation, migration, nutrients transportation as well as oxygen diffusion.

Gelatin based scaffolds

Images from SEM and micro-CT (Figure 4-1 and 4-2) indicated that well-formed porous structures with interconnected pores were found in fabricated GEL-CHI scaffolds, and mercury intrusion porosimetry investigation showed that a porosity of 93% had been achieved where previous study had shown scaffolds with similar pore size (30 - 40 μm) to gelatin based scaffolds that support penetration and proliferation of seeded cells [241]. The SEM images as well as pore sizes and porosities determined by MIP (Figure 4-3) indicated that, PA and GA used as cross-linkers did not significantly influenced the internal porous structures of the pre-fabricated uncross-linked scaffold since similar pore sizes and porosities were obtained in PA and GA treated scaffolds. Similar to our finding, previous studies also noticed that, GA as an efficient cross-linker had little effect on porous morphology of a collagen/chitosan scaffold as no significant difference was found after treating with GA solution [242].

RHC based porous scaffolds

Differ from porous microstructures that generated from size defined porogens or 3-D printing, pore size and porosity of scaffolds that fabricated from freeze-drying method were highly depended on the fabrication parameters such as freezing temperature, freezing rate, mixture concentration and solvent that used to dissolve the material [187, 229]. In this study, the fabricated pure RHC scaffolds had pore sizes in the region of 111-131 μm, and it had been found that the pore size of the RHC scaffolds were slightly varied with RHC concentrations. Similar to the current finding, Perez-Puyana *et al.* [243] used 1%, 2% and 5% (w/v) type I collagen solutions to fabricate porous scaffolds, and they found the pore size increased gradually (range from 75 to 92 μm) as a function of collagen concentration from 1% to 5%, which correspond to the RHC concentrations (1.5%, 2% and 3.0%) that been used to fabricate porous RHC scaffolds in this study. Similar phenomenon had also been found in type I collagen fabricated scaffolds that solution with higher collagen concentration led to larger pore size after freeze-drying [244, 245], and it suggested the increase of collagen will raise the freezing temperature of the slurry where Searles *et al.* [246] confirmed ice crystal size was proportional to the freezing temperature. Meanwhile, pore sizes of the fabricated RHC-CHI scaffolds that cross-linked with different amount of EDC were determined ranging from 136 to 176 μm where the uncross-linked RHC-CHI scaffold had the average pore size of 129 μm. In this study, it also discovered that the pore size of cross-linked RHC-CHI porous scaffolds decreased slightly as increasing the EDC concentration during fabrication where RHC-CHI-100 porous scaffold has the smallest pore size among all three

cross-linked RHC-CHI scaffolds (Table 4-2). It is suggested that the increasing of the EDC concentration results an increasing on mechanical properties of the RHC-CHI porous scaffolds, therefore, scaffold had higher stiffness can prevent the pore structure expansions caused by crystallization during the second freeze-drying as the procedure mentioned in chapter 3. The pore size determined from gelatin-chitosan as well as RHC based porous scaffolds were in the range of parameters that recommended by previous studies where pore size of 30 - 40 μm was found able to support the cell migration and 90 - 360 μm was found favored by fibroblasts penetration. [189].

The fabricated RHC and RHC-CHI scaffolds showed similar morphologies of interconnected microstructures (see Figure 4-4 and 5), and such morphologies were also found in PA cross-linked porous scaffolds as described previously. The porosities of the RHC-CHI scaffolds were found between 91% and 92%, and the fabricated pure RHC scaffolds were between 90% and 93%. Specifically, porosity of the RHC scaffolds were found dependent on RHC concentrations and wall structures of the pores in RHC-3.0 scaffold were thicker compared to RHC-1.5 scaffold (Figure 4-4). The scaffolds with high porosity were preferred in tissue engineering since sufficient interconnected porous structures facilitate the nutrients transportation and cell ingrowth, and it has been suggested that scaffold with porosity above 90% was preferred in cell seeded tissue engineering [247]. By comparing the porous structure of the PA cross-linked GEL-CHI porous scaffolds

and RHC based porous scaffolds, it can be noticed that the selected freeze-drying technique can be considered as a reliable fabrication method to produce scaffolds with homogenous pore distribution and desired pore size which benefit for their applications.

RHC based hydrogel

The SEM images present in Figure 4-6 shows that freeze-dried hydrogel B showed different surface texture morphology compared to hydrogel A and C, where less smooth surface were observed. Such differences might largely attributed by the variations in the amount of crystallized water during lyophilisation where hydrogel with higher structural integrity and mechanical properties might have higher resistance to the water crystallisation during sample preparation. Previous studies carried out by Reis *et al.* [248] and Chiu *et al.* [249] had found similar morphology on their collagen-chitosan hydrogel surfaces where chitosan to collagen ratio was set to 1:1. Similarly, Deng *et al.* [163] also noticed in their research that by adding chitosan into the pure collagen hydrogel system produced a much denser material with greater surface structure. In current study, hydrogel surfaces were also imaged by using an environmental scanning electron microscopy (ESEM) to investigate the hydrogel at its hydrated condition and all hydrogels were found to have flat surfaces with no apparent differences (Figure 4-6). These results indicated the variation on RHC to chitosan ratios did not affect the surface structures of hydrated hydrogel

scaffolds. The fibroblasts that grew on hydrogel were also investigated with ESEM and will be discussed in latter section.

5.2 FT-IR and Cross-linking degree

The molecular structure of uncross-linked RHC and EDC cross-linked RHC were analysed by FT-IR. Figure 4-7 A shows that all typical wavenumber of collagen bands retained their positions after cross-linked with 50 mg EDC, this is in agreement with the results found by Sionkowska [250], as they suggested the EDC cross-linking process did not affect the secondary structure of the RHC. Meanwhile, the intensity of Amide II band decreased greatly after cross-linking with 50 mg EDC, Wang *et al.* [251] explained these phenomenon, since the -NH_2 band in collagen was stronger than N-H and amidation had no effect on the C=O band, the decreased on intensity of Amide II was caused by free -NH2 groups changing into -NH groups during the formation of iso-peptide. The intensity of Amide A also shows a decrease in the 50 mg EDC cross-linked RHC where previous study suggested that the decreasing intensity was associated with the formation of the covalent bond where less NH_2 free groups were available due to cross-linking [252]. The spectrums of the RHC samples that were cross-linked with 50, 75 and 100 mg EDC are shown in Figure 4-8 B. It can be seen that there were no movements of the wavenumber or variations in intensity among spectrums of cross-linked RHC samples, which indicated that increasing the cross-linker concentration did not cause any changing in the secondary structure and further confirmed the RHC

samples were fully cross-linked with the selected EDC concentrations. This finding is in agreement with the results found in cross-linking degree assessment where minimal amount of RHC were detected in elution of cross-linked RHC scaffolds and there were no significant differences on quantification of the determined cross-linked degrees among 50, 75 and 100 mg EDC cross-linked RHC scaffolds as shown in Figure 4-8 B. All these discoveries proved that there were no differences in between 50, 75 and 100 mg EDC treated RHC-1.5 scaffolds and further confirm that RHC-1.5 scaffold can be fully cross-linked with 50 mg EDC and by further increasing the EDC concentration had no other effects on the scaffolds. The results from the compression tests (Figure 4-29 and 30) that had been done on RHC-1.5 scaffolds (cross-linked by 50, 75 and 100 mg EDC) further confirms this finding.

By comparing the uncross-linked RHC-CHI sample and 50 mg EDC cross-linked sample, it was found the intensity on Amide B, Amide I as well as Amide II decreased significantly. What's more, the Amide I and II band were found moved to the higher wavenumbers after cross-linked with 50 mg EDC (Figure 4-8 A). Wang *et al.* [251] found in their study that the intensity of Amide II decreased greatly as the $-NH_2$ changed to N-H groups in cross-linked collagen molecules where the intensity of the N-H band was much weaker compared to $-NH_2$ band. The movement of the Amide I and II toward the higher wavenumbers were in agreement with the results found in a study by Staroszczy *et al.* [253] where fish gelatin and chitosan were cross-linked with EDC, and the movements of the Amide bands were

suggested as the formation of new N-H bonds. The spectrums in Figure 4-8 B shows the intensity of the Amide A increased as increasing the EDC content. The increasing of the intensity on Amide A may contributed by the formation of iso-peptide bonds between amine groups of RHC or chitosan and active carboxylic groups from RHC. Similar result was also find in FT-IR study by Staroszczyk *et al.* [253] as mentioned previously. These findings are also in agreement with previous study where Kuijpers *et al.* [254] indicated the increased intensity on Amide A reflected an increased number of bounded -NH groups, as iso-peptide bonds formed by EDC between amine groups of gelatin or chitosan and activated carboxylic acid groups of glutamic or aspartic acid residue of gelatin. The increasing on intensity of Amide I and II were also found in the spectrums of the cross-linked RHC-CHI samples, where the intensity was increased with the increasing of the EDC concentration. The increasing on intensity of Amide A is in agreement with the result found by previous study where they mentioned in their research that the intensity of Amide I band of collagen increased with the increasing of cross-linking associated with the increasing in C=O stretching and N-H bending in the newly formed covalent bonds [252]. The increasing of intensity on Amide II found in this study that can be explained as the formation of new N-H bonds, where the N-H bending and C-N stretching vibrations of the amide groups increased in intensity [253]. This finding on the spectrum changings can further confirm that, by increasing the EDC content in the cross-linking process on RHC-CHI scaffolds, resulted the formation of new iso-peptides that occurred between RHC and chitosan

or within RHC molecules. The hypothesis of the increasing on mechanical properties that found in different amount of EDC cross-linked RHC-CHI scaffolds can be given as there were unreacted amino and carboxylic terminus might available in both RHC and chitosan molecules since chitosan was introduced as the second polymer that brought in lots amino groups, and by increasing the concentration of cross-linker, the activated free carboxylic groups reacted with amino groups and formed new iso-peptides which increased the biostability as well as the mechanical properties of the RHC-CHI scaffolds. The above finding indicate the increasing on numbers of covalent bonds between RHC and chitosan as well as within RHC molecules are directly influenced by adding the extra EDC to the two biopolymers, and the differences on degradation rate as well as mechanical stiffness found among 50, 75 and 100 mg EDC treated RHC-CHI scaffolds were further proved the increased of EDC had improved the stabilities of the scaffolds. On contrary, result obtained from cross-linking degree test among 50, 75 and 100 mg EDC cross-linked RHC-CHI showed different trends as no up-regulated relationship was found between the amount of EDC used and detected RHC concentrations. As shown in Figure 4-10 and 11, all HPLC detections indicated that by increasing the EDC from 50 mg up to 100 mg did not affect the cross-linking degree. And there was no significant difference can be found among 50, 75 and 100 mg EDC cross-linked RHC-CHI scaffolds where the minimal presence of RHC was detected by HPLC that indicated RHC molecules were cross-linked with either chitosan or RHC itself and well locked in the porous scaffolds. The possible explanation of the finding on

cross-linking degree may refer to all selected amount of EDC (50, 75 and 100 mg) are sufficient to cross-link RHC with chitosan or RHC via amino groups from either RHC or chitosan reacted to the carboxylic terminus of RHC that secured the majority of the RHC molecules within the scaffolds.

5.3 Gelation time

It had been found in previous studies that increasing chitosan content in collagen based hydrogel resulted in slowing down the gelation process [255, 256]. Similarly, in current study, the results indicated the gelation times were varied with hydrogel composition and thermal depended (Table 4-5). This is in agreement with Deng *et al.* [163] who used EDC to cross-link porcine collagen (1.0% w/v) and chitosan (1.5% w/v) at 37ºC, their results showed that onset of the gelation time was increased by the increasing of chitosan fraction in collagen-chitosan solution where gelation time of pure collagen and collagen/chitosan ratio of 1:1 ranged from 3 to 5 min approximately. It should be noticed that they used a rheometer to assess the occurring of gelation by observing at what time a sudden increase in viscosity occurred and such method was also involved in other studies [257, 258]. Meanwhile, Yang *et al.* [259] studied the relationship between collagen gelation time and gelation temperature and revealed that, increasing the gelation temperature sped up the gelation process which was in consistent with the trend found in current study. An historical study has also shown that collagen precipitation was accelerated by

increasing the collagen concentration as well as by increasing the gelation temperature [260].

5.4 Swelling

The swelling ratio is one of the important parameters in design of tissue engineering scaffolds as it influences the mechanical and structural stability after implantation or *in vitro* culturing. Cross-linking is considered to be a primary factor decreasing the swelling ability (water absorption) and retention of scaffolds, and the results of this study are in accordance with similar results where gelatin and chitosan have been investigated [261, 262]. In this study, we also found the swelling ability of untreated gelatin based porous scaffolds was approximately double that of PA 0.1 and GA 0.1 scaffolds (Figure 4-12). This suggests that cross-linking treatment not only reduces the number of hydrophilic groups on the bio-polymers (chitosan and gelatin) which have the ability to bind water but also decreases the flexibility of the polymer chains [263]. A further effect is a reduction in the space between the chains. As a result, the capability of water absorption gradually decreases as the concentration of cross-linker increases.

The swelling ratios of the pure RHC scaffolds were found increased gradually as the RHC content increased (Figure 4-13), whereas swelling ratio of RHC-CHI scaffolds decreased with increased EDC content during cross-linking (Figure 4-14).

It is known that water binding ability is mainly depend on the hydrophilic group of the materials and the maintenance of 3-D structure of the scaffolds. Since the collagen is considered hydrophilic biopolymer, the differences from the swelling ratios of pure RHC scaffolds could be explained as scaffold with higher RHC concentration had higher stiffness that helped scaffold to maintain its microstructural stability under hydration condition. The cross-linking is also known to reduce the swelling ability by reducing number of hydrophilic groups (amino or carboxylic groups) of material [242, 264]. Similarly, in EDC treated RHC-CHI samples, 100 mg EDC cross-linked scaffold showed the lowest swelling ratio while 50 mg EDC treated RHC-CHI scaffold was the highest, and such trend is also recorded in gelatin based porous scaffolds as PA and GA cross-linked scaffolds show lower swelling abilities compared to un-treated scaffolds. Another finding on RHC-CHI scaffolds is they had higher swelling ability compared to pure RHC scaffolds, where swelling ratio of 50mg EDC cross-linked RHC-CHI scaffold was at least 2-fold of RHC-1.5 scaffold. A possible explanation can be given is that adding chitosan increased the stiffness of the scaffold that more PBS can be retained with the microstructures that similar result was found in previous study as collagen/chitosan (1:1) scaffold could bind twice of the PBS compared to pure collagen scaffold [154]. What's more, it has been found that the swelling ratio could be influenced by porosity and pore size. A previous study of fabricated 3-D scaffold from silk fibroin had noticed that the swelling ratio decreased gradually as decreasing in pore size where significant decreasing of swelling had been found

associated with decreasing of porosity [265]. This could be another possible reason which could explain the variation of swelling ratios that found among EDC treated RHC-CHI scaffolds since slight differences on pore size had been found among fabricated scaffolds.

5.5 *In vitro* degradation

A predictable synchronization between regenerated ECM and degradation of the scaffold is desired as the scaffold will be totally replaced by the new tissue eventually. To reduce the degradation rate might also improve the mechanical and structural stability of the fast degradable scaffolds as implanted *in vivo*. In this case, it is important to determine the degradation rate of the materials once used in making the scaffolds.

Gelatin based porous scaffolds

Results from collagenase degradation test indicated both PA and GA improved the biostability of the scaffolds, and also showed that the resistance to the collagenase degradation is increased as the PA concentration increased. Similarly, a previous study found that PA cross-linked elastin scaffolds own great resistance to enzymatic degradation as no more than 20% of elastin was lost, and suggested the interactions between PA and hydrophobic amino acids of elastin might be formed which blocked the acting sites of enzymes and protected elastin from degradation [205]. What's more, Zhai et al [266] also found that after enzymatic degradation, the weight loss

of PA cross-linked collagenous matrix was 7% to 15% while uncross-linked matrix dissolved completely.

RHC based porous scaffolds

In this study, the results of degradation rate from fabricated scaffolds are considered that directly related to using EDC as cross-linker. As shown in Figure 4-16, at each time point the degradation rates of the three types of pure RHC scaffolds were close to each other and there were no significant differences could be found throughout the degradation period. The degradation rates of 3 days were found between 7% and 8%, where at the degradation day 28, it found the mass loss of the three samples were between 15 % and 16%. Since no significant differences on degradation rates had been found in three pure RHC scaffolds, this finding is in agreement with the cross-linking degree that found in three cross-linked RHC scaffolds, as well as FT-IR results shown in Figure 4-7 B. Thus, it further indicated the EDC was an efficient cross-liker to RHC scaffolds and the selected amount of EDC in current study was sufficient for fully cross-linking. Meanwhile, the results show the degradation rates are reduced by the increasing of EDC content in RHC-CHI scaffolds cross-linking processing. This finding is also in agreement with the FT-IR results as discussed in previous section where spectrums showed additional covalent bonds were formed by increasing the EDC content. Yahyouche *et al.* [267] used EDC to cross-link the porous collagen matrix that found by increasing the EDC concentration (10, 33 and 50 mM) could improve cross-linking degree and

made the scaffold more resistant to the biodegradation as scaffolds degraded by collagenase. Meanwhile, by comparing the degradation rates (Figure 4-16 and 17), it shows 75 and 100 mg EDC cross-linked RHC-CHI scaffolds had lower degradation rates compared to all pure RHC scaffolds throughout the degradation period. Similar phenomenon had been reported from previous study that Lin *et al.* [268] indicated the presenting of chitosan could significantly improve the biostability of collagen-hyaluronan scaffolds under EDC treatment as they suggested the amine bonds that formed between collagen and chitosan had enhanced the biostability of the scaffolds. And Tan *et al.* [269] also found the integrity increased with proportion of the chitosan in collagen-chitosan composed three dimensional matrixes.

RHC based hydrogel scaffolds

Determining the degradation degree of fabricated hydrogels can predict the changes on hydrogel integrity, mechanical property as well as stability during *in vitro* or *in vivo* applications. Biopolymer based hydrogels are usually considered as fast degraded biomaterials and rapid degradation might lead to a sudden loss of mechanical properties and further induce a failure during application. In this manner, ideal degradation rate of the applied hydrogel should be controllable to prevent the mechanical failure as well as maintain the structural integrity. A previous study had proved that the addition of chitosan in collagen hydrogel system could enhance the stability where collagenase was used to degrade the collagen and collagen-chitosan hydrogel *in vitro* [163]. They found the collagen-chitosan hydrogel at 1:1 had a

significantly lower degradation rate compared to collagen-chitosan hydrogel with collagen to chitosan ratio at 20:1 as well as pure collagen hydrogel. In current study, no significant differences on degradation rate were found at the first two time points (day 3 and 7) among the three types of RHC-CHI hydrogels (Figure 4-18), but degradation rate on hydrogel C with collagen-chitosan ratio of 20:80 increased significantly from day 14. It has been found that, the additional chitosan present in hydrogel C (RHC to chitosan ratio at 20:80) brought extra amino groups which was not cross-linked or partially cross-linked to RHC but locked in the gelled networks, and such cross-linked collagen-chitosan networks might also sequestered by the molecules of extra chitosan. As a result, both mechanical property and structural integrity of hydrogel C (RHC to chitosan ratio at 20:80) were lower compared to hydrogel A (RHC to chitosan ratio at 80:20) and B (RHC to chitosan ratio at 50:50) which has a larger number of valid bonds between RHC and chitosan. Finally, it led to the accelerated breakdown after the swelling in PBS.

5.6 Mechanical properties

Scaffolds as implantation that replace the faulty tissue would encounter stresses such as compression and tension in native environment. The designed scaffolds should have enough tolerances to keep their structural stability that provide a stable environment as culturing *in vitro* or implanting *in vivo*. Meanwhile, in designing the tissue engineering scaffold, the fabricated scaffolds should have sufficient

mechanical properties that are close to the healthy native tissue. What's more, the stiffness of the scaffolds could also influence the other performances such as swelling and degradation that both are considered as important parameters that directly influence the biostability. Thus, scaffolds with suitable mechanical properties that close to native tissue are highly demanded. Natural derived biomaterials such as collagen and gelatin are generally low in mechanical strengths, and have relatively fast degradation rate as exposed to the biophysical environments, to overcome these drawbacks, the most commonly used method is to cross-link the biomaterials to increase their stiffness. In this study, PA was selected to cross-linked GEL-CHI porous scaffolds and EDC was used to cross-link the RHC based porous scaffolds as well as RHC based hydrogels in order to increase their stiffness. Tensile test, compression test are two of common mechanical tests that used to evaluate the mechanical properties of the porous biomaterials where several parameters such as tensile stress, compression stress, compressive modulus as well as elastic modulus are determined. Since it has been found that the mechanical properties of the biomaterials show significant differences between dry and hydrated status [251], in this study, all scaffolds were pre-hydrated in PBS solution and tested under fully hydrated mode in order to mimic the biological environment.

Gelatin based porous scaffolds

The compression stress and compressive modulus of the GEL-CHI porous scaffolds measured in this study (Figure 4-20) indicates that cross-linking with PA and GA significantly increased the mechanical properties of the original scaffolds, and the

increasing on stiffness is proportional to the concentration of used cross-linker. Similarly, previous study has also found that PA as a natural cross-linker that can improve the mechanical properties of the collagenous based matrix where they found ultimate tensile strength of PA cross-linked collagen matrix was significantly higher than uncross-linked and GA cross-linked matrix [266].

Significant recoverability of native soft tissue (e.g. skin and muscle) are required to overcome the deformations (stretching or compression) caused by motions. In this case, the fabricated scaffolds need to fulfil the feature of recoverability in their applications. Repeated compressions were applied to investigate the recoverability of the cross-linked scaffolds in this study and distinguishing results were found. The stress-strain curves (Figure 4-19 B) between 1st and 2nd compression on GA scaffold were significantly different from each other while PA scaffold shows excellent repeatability. Figure 4-21 shows that crushed porous walls with condensed wall structures were observed on GA scaffold after deformation but less impact was found on PA treated scaffold. It is hypothesized that the large number of fractures occurred during deformation on GA treated scaffold because GA increased the brittleness nature of the materials during cross-linking. Similar behaviours had been noted in previous studies on GA cross-linked scaffolds [270, 271], and a possible explanation is that as GA forms C=N bonds between GA and chitosan or collagen during cross-linking these present a barrier to the rotation of the associated chains and therefore reduce the chain flexibility [272].

The ability of relaxation under loading is directly linked to viscoelastic properties of the samples (as it is for most soft tissues) [273]. Figure 4-22 A shows similar stress relaxation behaviours of all the scaffolds where stress decreased progressively. It has been described that within 600 seconds the stress reached to equilibrium on a chitosan-modified poly (L-lactide-co-ε-caprolactone) (PLCL) scaffold, as well as in bovine articular cartilage [274]. Similar stress relaxation results have been found on mammal soft tissue that a compression test had been done on skeletal muscle where 49% and 60% stress relaxation were found as 30% strain of compression was applied [275]. Meanwhile, fabricated scaffolds with nearly 90% of relaxation on stress was found in tensile relaxation test of a GEL-CHI blend scaffold [276]. The percentage of stress relaxation on maximum stress of PA groups were higher compared to GA groups that shown in Figure 4-22 B, which indicated a large number of chain movements occurred in the PA cross-linked scaffolds under stress to structural deformation compared to GA scaffolds, and further confirmed PA cross-linked scaffolds own higher flexibility.

RHC based porous scaffolds

The increasing collagen concentration (density) in porous pure RHC scaffold fabrication was expected to improve the mechanical properties, where previous studies have discovered that the compressive and elastic modulus increased proportionally to the increasing of collagen concentration that used in the fabrication of porous scaffolds [245]. Specifically, it had been found within 4-fold

of increasing in collagen concentration in fabricated porous scaffold lead to 56 and 30-fold of increasing in compressive and tensile modulus, respectively [277] and such findings are in agreement with the results found in mechanical test from current study. As see in section 4.7, it shows that the compression modulus as well as elastic modulus increased gradually as the RHC concentration increasing. What's more, previous studies had also found the mechanical properties of the fabricated scaffolds could be modulated by controlling the parameters such as pore size, porosity and polymer concentrations. Harley *et al.* [278] had fabricated a series of porous collagen-glycosaminoglycan (GAG) scaffolds with different pore sizes through freeze-drying process where compressive modulus of the scaffolds were found between 0.176 to 0.23 kPa; meanwhile, the averaged elastic modulus was found around 2.0 kPa where it shows both compressive and elastic modulus were close to the range of mechanical strengths of RHC scaffolds that obtained in this study.

By introducing chitosan into the RHC scaffolds in current study, it successfully been shown that the RHC-CHI scaffolds exhibited higher mechanical strengths compared to the RHC scaffolds fabricated in the same concentration (results of mechanical test of the fabricated porous scaffolds summarised in Table 5-1). The compressive stress at 70% compression strain of the RHC-CHI-50 reached to 2-fold of the RHC-1.5 scaffold and its compressive modulus was also found around twice of RHC-1.5 scaffold. Additionally, it has been found both tensile stress and

elastic modulus of the RHC-CHI scaffolds were much higher compared to pure RHC scaffolds. The tensile stress of RHC-CHI scaffolds reached to 50 kPa which was significantly higher compared to all RHC scaffolds. The results of compression and tensile tests showed that the mechanical strengths of the RHC-CHI scaffolds were largely influenced by the amount of EDC that used in cross-linking. Specifically, the compressive modulus as well as tensile modulus were proportional to the increasing of amount EDC used in cross-linking the RHC-CHI scaffolds. Interestingly, mechanical test on PA cross-linked gelatin-chitosan scaffolds show much higher modulus compared to RHC based porous scaffolds (see in Table 5-1), a possible explanation of such phenomenon is that the pore size of the gelatin based porous scaffold is much smaller compared to all RHC based porous scaffolds, where previous studies had emphasised the porous structures could largely influence the mechanical properties of the 3-D porous scaffolds, specifically, scaffolds with smaller pore size were found owning larger mechanical strengths [278, 279].

Table 5-1. The comparison table of tested porous scaffolds

Samples	Compression Stress(kPa)	Compression Modulus(kPa)	Tensile Stress(kPa)	Elastic Modulus(kPa)
PA 0.1	8.60 ±0.94	9.46 ±0.57	/	/
PA 0.5	12.27 ±1.20	13.97 ±0.71	/	/
PA 1.0	14.43 ±0.82	17.83 ±0.56	/	/
RHC-1.5	0.26 ±0.02	0.24 ±0.03	3.28 ±0.85	5.12 ±1.09
RHC-2.0	0.32 ±0.04	0.33 ±0.02	4.89 ±1.51	7.40 ±1.70
RHC-3.0	0.42 ±0.04	0.54 ±0.07	8.37 ±1.38	12.20 ±2.02
RHC-CHI-50	0.58 ±0.03	0.47 ±0.05	36.30 ±3.41	38.38 ±1.84
RHC-CHI-75	0.66 ±0.04	0.67 ±0.08	41.04 ±5.91	50.26 ±6.52
RHC-CHI-100	0.83 ±0.06	0.99 ±0.10	50.00 ±5.11	69.59 ±8.35

Additional, mechanical test had also been done on RHC-CHI scaffolds fabricated with different RHC to chitosan proportions (80:20, 66:33, 50:50, 33:66 and 20:80). As results shown in the Figure 4-37 and 38, the stiffness were improved by increasing the chitosan ratio in scaffolds. Both compressive strength at 70% strain and compressive modulus increased significantly as the chitosan content increased; meanwhile, similar trend had been found in the tensile stress and tensile modulus that higher chitosan ratio in scaffold showed higher tensile stress and elastic modulus. The ultimate tensile stress and tensile modulus at break point was achieved by RHC-CHI (20:80) scaffold where near 145 and 200 kPa were recorded (Figure 4-39 and 40). Raftery *et al.* [280] found that, the incorporation of chitosan into bovine-derived collagen scaffolds and chemically cross-linked with EDC had caused significant increasing in compressive modulus from 0.92 kPa to 1.09 kPa and 1.23 kPa for the collagen-chitosan at ratios of 75:25 and 50:50 respectively. On the contrary, Wang *et al.* [251] found out by adding chitosan into collagen slurry would provide many more amino groups than required for EDC cross-linking that led to the decreasing on relative cross-linking degree and further influenced mechanical strength.

The mechanical property of the tissue engineering scaffold should closely match the healthy native tissue that provide enough mechanical support for the implantation as well as tissue regeneration. Mechanical tests on current study show that our porous scaffolds are comparable to some of the native tissue (such as skin,

brain tissue etc.) which modulus were determined from previous studies. The *in vitro* mechanical tests on different native skin discovered that the modulus were varied significantly to the locations where a range between 5 kPa and 140 MPa were summarized in previous review [281], and it also illustrated the available methods that characterize the mechanical properties of the skin including tensile, indentation, suction and torsion test. The very soft connective tissue such as adipose tissue which composed of adipocytes, fibroblasts, collagenous ECM and blood vessels had also been intensely investigated in tissue engineering [282]. It has been found the modulus of adipose tissue that determined from tensile test had the range from 0.3 to 24 kPa for the breast samples [283], and in the range of 0.3 to 3.0 kPa on abdominal fat [284], which is within the range of elastic modulus that found in both RHC and RHC-CHI scaffolds. Meanwhile, unconfined compression test that done on brain tissue showed that the compressive modulus was around 3.16 kPa [285], and elastic modulus of the selected human brain tissue were found around 66.7 kPa [286, 287], which is also considered close to mechanical strengths of the fabricated scaffolds. In addition, scaffolds with similar mechanical strengths to the RHC and RHC-CHI scaffolds had also been obtained in other studies. A study by Raftery *et al.* [280] discovered the porous collagen scaffolds fabricated from fish collagen and bovine collagen had the compressive modulus of 0.13 and 0.93 kPa, by incorporating the collagen scaffolds with chitosan, the modulus increased to 0.56 and 1.23 kPa respectively, and it suggested the fabricated scaffolds suitable for soft tissue regeneration such as skin and muscle tissue engineering. What's more,

Keogh *et al.* [288] reported EDC cross-linked porous collagen-glycosaminoglycan scaffolds that prompted the proliferation of the osteoblasts owned compressive modulus of 1.17 kPa, which was close to the compressive modulus of fabricated RHC based porous scaffolds in this study.

Biological soft tissues are known owning viscoelastic mechanical properties, and when collagen-rich soft tissue subjected to the tensile test, the obtained tensile stress-strain curve presents its viscoelastic mechanical behavior that normally composed by three regions, known as the toe region, linear region and failure region [289]. A typical tensile stress-strain curve illustrates the viscoelastic property of the soft human biological tissue is shown in Figure 5-1. A toe region which also known as non-linear stress-strain region can be seen in the curve, and the slope in this region is increased with increasing the loading which correspond to the straightening of the collagen fibrils, and the collagen fibrils are found originally present at crimped structures. In the linear region, strain is directly related to the stress where collagen fibers tend to line up with the load direction, and by further increasing the load, collagen fibers become stretched. The failure region represents the disruption of fibril structures that shows a sudden drop of the stress. The ultimate tensile stress-strain curves which determined in current study (shown in Figure 4-26 and 34) show similarity to the typical collagen-rich soft tissue mentioned on below (Figure 5-1), where three distinct regions are identifiable in the obtained curves of both RHC and RHC-CHI porous scaffolds. Under tensile conditions, the toe region of the tensile curve might refer to the straightening of the

pore walls (struts) to accompany with the applied load, while in linear region, the wall structures become stretched (elongated) and alignment of the struts is in the direction of the loadings[290]. Finally, further stretching of the pore wall structures (struts) results the disruption. Thus, the mechanical behaviors of the RHC and RHC-CHI porous scaffolds suggested they are mechanically similar to the biological soft tissues (e.g. skin, blood vessels, tendons, ligaments, etc.) [273, 275].

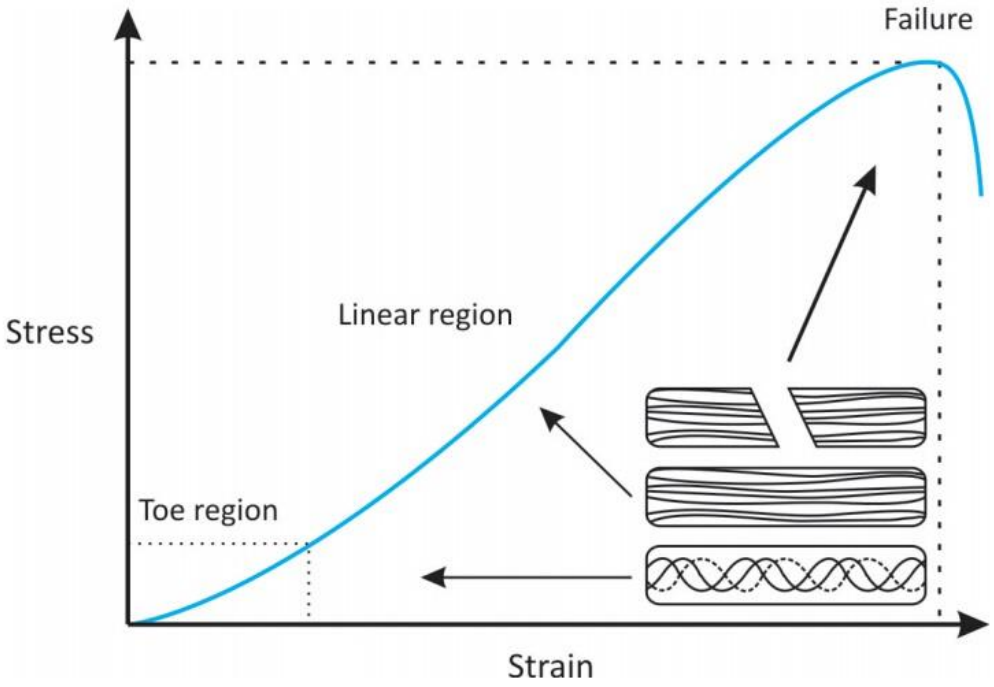

Figure 5-1. Schematic diagram of a typical tensile stress-strain curve of human soft biological tissue which demonstrates the toe region, linear region and failure region which associated collagen fibers morphology. Image edited and adapted from[291].

RHC based hydrogels

The stiffness of the fabricated hydrogels were determined using compression test, and the compressive modulus were obtained from the slope of the initial linear

region of the strain-stress curves. Previous studies had shown that introducing chitosan into collagen hydrogel could significantly enhance the mechanical properties of the hydrogels due to the formation of covalent bondings [85, 164, 269], and mechanical test results obtained by Deng *et al.* [163] clearly indicated that the stiffness of the collagen-chitosan hydrogel increased gradually with the increase of chitosan fraction in the blend where EDC was used as cross-linker. In current study, it was found the compressive modulus of the hydrogels were not continuously increased with the increasing of chitosan fraction in collagen hydrogels (Figure 4-41). Similar to this finding, Lin *et al.* [292] discovered that the tensile strength of a series of biomaterials which composed of chitosan-collagen-hyaluronan increased by addition of 10% chitosan while decreased by further increasing the chitosan fraction up to 20% of the mixture. Wang *et al.* [251] studies on an EDC cross-linked collagen-chitosan film suggested that adding chitosan to the blend actually provided extra amino groups than were required for cross-linking, as a result, the decreasing on mechanical properties occurred. Similar to the mechanical property findings in this study, Reis *et al.* [248] studied a collagen-chitosan hydrogel system and found that the hydrogel with chitosan-collagen ratio at 1:3 had lower mechanical property in terms of storage modulus as compared to hydrogel with chitosan-collagen ratio of 1:1, while by further increasing the chitosan-collagen ratio to 3:1 the hydrogel mechanical property decreased and it became the lowest stiffness among three samples. They explained that, since pure collagen gel was considered as highly interconnected fibrous network where

additional chitosan to the pure collagen gel (chitosan-collagen ratio increased from 1:3 to 1:1) brought together collagen fibers along a chitosan backbone that formed thicker struts resulted in increasing on mechanical integrity. Further increasing the fraction of chitosan (chitosan-collagen ratio increased from 1:1 to 3:1) in the collagen hydrogel interfered with the original resultant fibrous network by further sequestering fibers and formed thicker 'struts', but largely reduced the degree of connectivity between resultant collagen fibers thus inducing the decrease of the hydrogel mechanical strengths. Thus, in this study, it is suggested the further increasing of chitosan fraction (up to RHC:CHI 20:80) decreased the number of the covalent bonds (cross-linking points) and resulted the decreasing the mechanical property. A sketch illustrates the cross-linking points and formed networks between RHC-RHC and RHC-chitosan molecules at different RHC to chitosan ratios are shown in Figure 5-2.

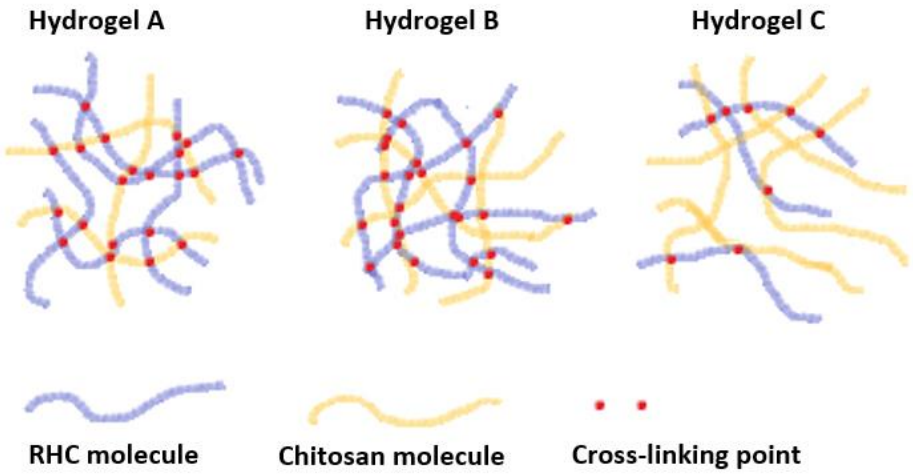

Figure 5-2. Covalent bonds (cross-linking points) and formed networks of hydrogel A, B and C.

Degraded hydrogel samples were also subjected to the mechanical test in this study, it shows the compressive modulus of each samples decreased gradually as increasing the degradation time (Figure 4-41). What's more, at each time point, the stiffness of each type of hydrogel sample was similar to the trends on stiffness variations found in un-degraded hydrogels (stiffness found in day 1). Similarly, Parlato *et al.* [293] found that the compressive modulus of some of their fabricated poly (ethylene glycol) hydrogels decreased significantly at degradation day 4 and 7 as compared to day 1. Another approach to improve the hydrogel stiffness in this study was achieved by increasing its concentration of the blend. It shows the modulus of hydrogel 3A (3.0% w/v) was 2.73 and 8.51-fold of hydrogel 2A and A, respectively (Figure 4-42), and such finding shows similarity to the findings that discovered in the RHC based porous scaffolds where compressive modulus of the scaffolds were found increased as increasing the RHC concentration (see in Table 5-1). The mechanical test on the different hydrogels in current study also shows that the mechanical strength of hydrogel could be tailored to a variety of stiffness and the mechanical properties of fabricated soft hydrogels were similar to some of the human soft tissues. It had been found the compressive modulus of the thyroid measured *in vivo* was around 9 kPa [294] whereas that of liver was around 0.6 kPa [295], and the premalignant breast was found around 2.2 kPa [296].

5.7 Cytocompatibility

5.7.1 Cytotoxicity test

Gelatin based porous scaffolds

Results of cytotoxicity test (Figure 4-43) indicated PA as a natural cross-linker show no potential toxicity to the cells at selected concentrations as compared to GA solution. This result agrees with previous studies which also concluded PA cross-linked scaffold were biocompatible as no inhibition on cell proliferation activities were detected [205, 297]. What's more, it had been reported that the cytotoxicity is only observed when concentration of PA reached 200 μg/ml [100].

RHC based porous scaffolds

The metabolic activity levels of seeded fibroblasts grew in all the extraction medium (Figure 4-44 and 45) indicated the cross-linked RHC scaffolds and RHC-CHI scaffolds had no potential toxicity to the cells. The results also indicated that the cell metabolic activities were not affected by increasing the use of EDC in cross-linking RHC-CHI scaffolds as the results were close to the control group. Water soluble EDC is generally considered an efficient cross-linker that not only has the ability to enhance the mechanical strength of the scaffolds but also shows low toxicity to the cells since it is not incorporated directly into cross-linked scaffolds but changes into water soluble urea derivatives that can be easily removed by rinsing [251, 298]. Lin *et al.* [268] found that mouse fibroblasts could proliferated well on EDC cross-linked collagen-hyaluronan-chitosan matrix where

cells maintained their unique fibrous morphology was also discovered at culturing day 14.

RHC based hydrogel scaffolds

The same method that was used to determine the cytotoxicity of the porous scaffolds was applied to the hydrogels. The relative fluorescent units obtained from each test group clearly indicated all fabricated RHC based hydrogels had no toxicity to the 3T3 fibroblasts as compared to the control group (Figure 4-46). Similarly, previous studies had also evidenced the using of EDC as cross-linker show no harmful to the cells. Rafat *et al.* [85] cross-linked recombinant type III collagen and chitosan blend using EDC as cross-linker and found the fabricated hydrogel were biocompatible to the cells. Ahn *et al.* [104] used EDC to cross-link recombinant human collagen solution and managed to produce a cornea like hydrogel on to which surface the human corneal epithelial cells well adhered and proliferated. What's more, cells not only proliferated well on EDC cross-linked hydrogel surfaces, but were also found to have survived after embedding in hydrogel system. McBane *et al.* [164] have shown circulating angiogenic cells successfully grown in the EDC cross-linked collagen or collagen-chitosan hydrogel with their great viability. Thus, previous results further proved that using EDC to cross-link the RHC-CHI hydrogel scaffolds did not bring toxicity to the hydrogel products.

By comparing the results obtained from the cytotoxicity tests (see Figure 5-3), it can be clearly seen that PA cross-linked gelatin-chitosan and EDC cross-linked

RHC based porous scaffolds and hydrogels had negligible toxicity. As can be seen, all test samples were above the 70% threshold of the cellular viability that determined from control group. Therefore, it confirming that it is safe to use these two cross-linkers.

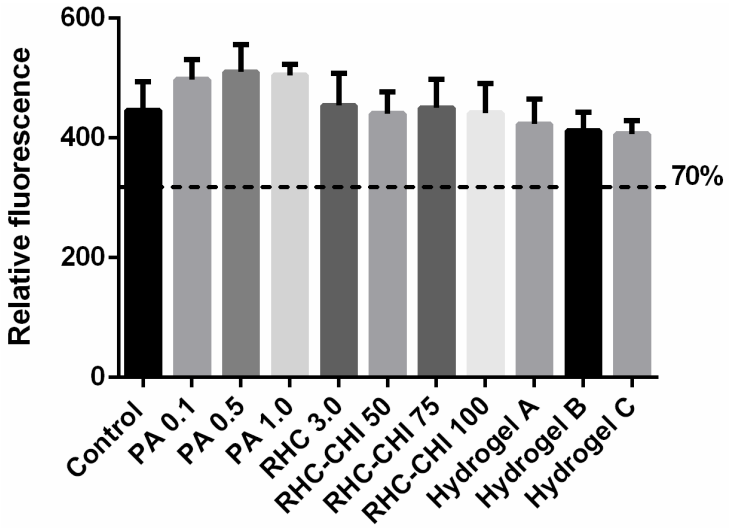

Figure 5-3. Cytotoxicity results obtained from scaffolds fabricated in this study.

5.7.2 Metabolic activities, proliferations and morphologies

Gelatin based porous scaffolds

The fibroblasts proliferation results were determined by using Hoechst DNA assay, and it was found the PA treated scaffold owns the highest cell proliferation activities among all three type of scaffolds (Figure 4-50). Meanwhile, as confirmed in cytotoxicity test that GA treated scaffolds show toxicity to the cells, the proliferation rate was also found with no significant increasing along with the most culturing period on cell seeded GA scaffold. Those findings on proliferation results were further proved with the fluorescent images that taken during the *in vitro*

culturing. The fluorescent images of cell seeded scaffolds show that, at early culturing stage, in both PA treated and uncross-linked scaffolds, cells firmly attached on porous structures to achieve homogenous distributions after seeding (Figure 4-55 A1 and B1). Meanwhile, cells in PA cross-linked scaffold showed the highest proliferation rate among all the samples which resulted in the highest cell density observed at the final culturing date (Figure 4-55 A3, B3 and C3). And such finding is in agreement with the proliferation results that determined in current study as PA treated scaffold shows the highest DNA content among all. Such results indicated PA cross-linked scaffold had the ability to promote cells attachment at the early stage after seeding. Meanwhile, it also increased cell proliferation rate compared to the GA and uncross-linked scaffolds. The result in our study shows agreement with previous finding that PA cross-linked scaffolds were found biocompatible, supporting the proliferation of seeded cells [205, 299]. What's more, it has been reported that PA related polyphenols could stimulate the proliferation of normal skin fibroblasts and increase the synthesis of ECM, and PA cross-linked collagenous materials could enhance the cell's ability to deposit collagen where collagen is widely known to play important role in cell adhesion and ECM formation [100, 300, 301]

Major differences on cell morphologies between uncross-linked and PA cross-linked scaffold were observed in this study. The proliferated 3T3 cells formed a connected but sheet-like structure on the porous structures of uncross-linked

scaffold, rather than firmly attaching onto the wall structure as shown in PA cross-linked scaffold (Figure 4-58 A1, B1). With the build-up of this sheet-like cell layer, the oxygen and nutrients might potentially have difficulty diffusing into the uncross-linked scaffold. What's more, it is suggested that the formed cell layer might further prevent the proliferated cells migrating to the inner of the scaffold, and as shown in Figure 4-55 A3, B3 and Figure 4-58 A2, B2, numbers of cells found in central part of PA treated scaffold were higher than uncross-linked scaffold. Thus, the fibroblasts proliferation might largely influenced, and as shown in Figure 4-50, the DNA concentration result of uncross-linked scaffold was found significantly lower compared to PA treated scaffold that further confirmed the phenomenon observed in cell morphology and fluorescent images. A possible explanation of this phenomenon is the PA treated scaffold has a higher stiffness on its porous wall structures, which induces the fibroblasts to attach and provides sufficient mechanical support for their proliferation and migration. Other studies have also reported that the affinity of the cell attachment to materials surface is not only related to the material itself but is also influenced by substrate stiffness, where materials with higher stiffness might benefit the attachments and proliferations on certain type of cells [192] and [302]. What's more, specific studies also indicated sensitivity of cell interaction to matrix (substrate) stiffness that cells prefer cell to cell interactions on compliant substrates and self-assemble into connected networks [303, 304]. On the contrary, cells were found prefer cell-substrate interactions as growing on stiffer substrates [191], and the SEM images of proliferated fibroblasts

found in current study were in agreement with these findings. Both images of attachments and proliferations of 3T3 cells within scaffolds indicated that the PA cross-linked scaffold had excellent cytocompatibility to sustain the proliferation and migration of seeded 3T3 cells and can be considered as a potential candidate for soft tissue engineering.

RHC based porous scaffolds

Alamar Blue dye is a sensitive and nontoxic assay that widely used to determine the cytotoxicity or cytocompatibility of the materials, and the assay showed reliable correlation with other cellular metabolic assays such as MTT and XTT assay [305, 306]. Since Alamar Blue has been found reliable and efficient in most cell works, it is also frequently applied to assess the viability of the seeded cells in solid collagen or chitosan scaffolds where tested scaffolds were usually incubated in the assay for varied durations [307-310]. Another approach to evaluate the cell status within the seeded scaffolds is to determine the proliferation by using DNA assay. CyQuant, PicoGreen and Hoechst 33258 are three DNA assays that frequently been used to determine DNA content in biomaterials [288, 311-313]. Specifically, Hoechst 33258 assay was used in this study to determine the DNA concentrations in scaffold as it labels the double strained DNA fluorescently.

To assess the viabilities and proliferation activities of the fibroblasts grew in porous scaffolds at different time points, Alamar Blue assay and Hoechst DNA assay was applied to determine the cellular metabolic levels and DNA content, respectively.

As previous study has emphasized that misusing metabolic assays to determine the proliferative activities will lead to an inaccurate results due to non-linear and miscorrelating changes in cell number and activity over time in culture [314], in concerns of accuracy, the cell metabolic levels determined by Alamar blue assay were normalised by DNA concentrations to demonstrate the cell viabilities at specific time points. The normalised metabolic levels (Figure 4-47 and 48) of the fibroblasts proliferated in the RHC and RHC-CHI porous scaffolds indicated the cell viabilities were not affected by the RHC concentration or EDC concentration that used in fabrication, and the results show agreement with the results obtained in cytotoxic tests that confirms all fabricate RHC and RHC-CHI scaffolds have no potential toxicity to the seeded cells. Meanwhile, as shown in Figure 4-51 and 52, the quantified DNA concentrations increased as increasing the culture time, and it suggested the RHC and RHC-CHI porous scaffolds are biocompatible which supported the proliferation of the seeded fibroblasts. Other researchers studied on cell-material interactions had noticed that the cell proliferation could be influenced by the scaffolds' stiffness. In a previous study, porous scaffolds with mean pore size of 84 μm were fabricated from porcine type I collagen and stiffness of the scaffolds were tuned by changing the collagen slurry concentration, the Young's modulus of the stiff scaffold was 8.5 kPa and the soft scaffold was 1.2 kPa [315], human dermal fibroblasts were then seeded into each type of scaffolds, and proliferated cell numbers were counted by DAPI staining at designated time point. At culturing day 14, it found the cell numbers increased 1.6-fold in scaffold with lower stiffness

while a 2.5-fold increasing was found in stiff scaffold. What's more, analysis of glucose consumption indicated stiff scaffold had relatively higher glucose consumption compared to soft scaffolds at day 7 which confirmed stiffer scaffold had a higher cell number. Not only the fibroblasts, Keogh *et al.* [288] also found osteoblasts favored stiffer 3-D scaffolds where both EDC and GA cross-linked porous collagen–glycosaminoglycan scaffolds with identified compressive modulus (EDC cross-linked scaffold 1.17 kPa, GA cross-linked scaffold 1.37 kPa) were used to host osteoblasts. At the selected culture time points (2, 4, and 6 week), the cell numbers determined by Hoechst 33258 assay showed higher number of cells were found in stiffer scaffolds. Meanwhile, viability results that carried out by Alamar Blue assay also indicated the scaffolds with higher stiffness resulted higher cell viabilities. Yeung *et al.* [316] found that the 3T3 fibroblasts achieve maximal spreading at type I collagen coated substrate with stiffness of 10 kPa compared to substrate with lower stiffness that fabricated with same material. Similar to 3T3 fibroblasts, the human lung fibroblasts are also found mechanically depended on substrate stiffness. Liu *et al.* [193] found fibroblast density increased as gel stiffness increasing when seeded in a stiffness gradient gel with modulus ranged from 0.5 to 50 kPa, which reflected increasing the stiffness of soft substrate could promote the proliferation of the fibroblasts in the selected mechanical stiffness. The stiffening of the ECM could also lead to the increasing of cell proliferation and migration, where a previous study indicated that the proliferation of epithelial cells were directly induced by increasing the matrix stiffness [317]. What's more, it has been

found the 3T3 fibroblasts owned the ability to migrate toward stiffer substrates that suggested the fibroblasts prefer substrate with higher stiffness [318]. Polyacrylamide matrix with different stiffness had been fabricated in a study and was coated with type I collagen, 3T3 cells were then seeded to the matrixes and they found the proliferation rate of the 3T3 cells was proportional to the matrix stiffness [319]. These findings are in agreement with the results that found in current study as it is suggested the cell proliferations were influenced by the stiffness of the porous scaffolds where higher DNA quantifications were found in porous scaffolds with higher stiffness (mechanical property).

Other than stiffness, cell proliferation can also be influenced by the stability of the porous scaffolds during *in vitro* culturing. In this case, another explanation to the differences of the proliferation results found on RHC-CHI porous scaffolds are suggested. Specifically, as shown in Figure 4-52, at culturing day 14, the determined DNA content of the RHC-CHI-100 were significantly higher compared to the RHC-CHI-50 and RHC-CHI-75, and a possible explanation to this phenomenon is the RHC-CHI-100 had significant lower degradation degree specifically found in degradation day 10 and 14 compared to the rest of RHC-CHI scaffolds (Figure 4-17). A slower degradation process of 3-D porous biomaterials might lead to a desirable microstructural stability with less collapses occur in the porous construction, as it has been discovered that porous structures collapsed due to the fast degradation on scaffold led to the defective microstructures which directly

influenced the diffusion of the nutrients and oxygen, cell proliferation as well as migration was also found been limited due to the changings on porous structures where cells attached [320, 321]. Keogh *et al.* [288] had also pointed out a stable microporous structure could provide sufficient surface area that support cell proliferation and migration, thus cells retained in a proliferative status. Similarly, a generally higher proliferation rate that found in PA cross-linked gelatin-chitosan scaffolds might also attributed by its slower degradation process as compared to uncross-linked scaffolds (shown in Figure 4-15).

From the obtained fluorescent images that shown in Figure 4-56 and 57, similar results are found in all RHC and RHC-CHI scaffolds at culturing day 7 and 14 as proliferated fibroblasts distributed homogenously within the porous structures that presented in the field of view. Meanwhile, it can be observed the cell densities increased along with culturing time where accumulation could be observed at day 14. These findings are in agreement with the data obtained from DNA content test, and they confirmed fibroblasts had an accelerated spreading and proliferation in fabricated RHC and RHC-CHI scaffolds during *in vitro* culturing. The morphology of the proliferated fibroblasts carried out by SEM (Figure 4-59 and 60) indicated cells reached to a spread status as fibroblasts were well connected to each other and firmly attached to the wall structures at the internal part of the scaffolds. At the same time, there were no significant differences on cell morphology that could be observed among the different RHC and RHC-CHI scaffolds as most pore wall

structures had been covered with connected fibroblasts at their elongated shapes. What's more, the morphologies of the proliferated fibroblasts found in porous RHC and RHC-CHI scaffolds were comparable to those grew in PA cross-linked gelatin-chitosan porous scaffold (shown in Figure 4-58). In general, it has been discovered that the stiffer substrate could increase the focal adhesion and cytoskeletal organization, specifically, fibroblasts were found in round shapes as grown on soft substrate while became extendable and spread morphology when grown on stiff substrate [316, 322]. Wang *et al.* [323] also indicated that by using soft substrate to culture the fibroblasts could reduce the synthesis of the focal adhesion complex proteins, which lead to the decreasing on actin stress fibers generation where actin stress fibers were known that regulate cell morphology. In current study, the SEM images of the fibroblasts grown in porous structures indicated all fabricated porous scaffolds supported the migration and the proliferation of the seeded fibroblasts, and further proved cell/substrate interaction has been achieved throughout the *in vitro* culturing period.

Interestingly, by comparing the results of DNA content throughout the entire culturing period among all fabricated porous samples (gelatin-chitosan, RHC and RHC-CHI porous scaffolds), it clearly shows the RHC scaffolds had generally higher readings compared to gelatin-chitosan as well as RHC-CHI porous scaffolds (see Figure 5-4). A hypothesis should then be given to explain the finding is the compositions of the porous scaffolds influenced the cellular activities as skeleton

of fabricated scaffolds contained RHC, which is considered a structural collagen that can be easily recognized by cellular integrins to enhance the cell-material interaction, thus induced the adhesion activities. Similarly, a study by Tierney *et al.* [244] also found that increased the collagen concentration in fabricated collagen-GAG scaffolds could enhance both cell viabilities and proliferation, and significant higher metabolic activities as well as proliferation rate were determined at culturing day 7. Thus, it is suggested that the containing of RHC in porous scaffolds might influence the cellular proliferation. Further confirmation of RHC prompt cell attachment and proliferation will be given in discussion part of RHC based hydrogels.

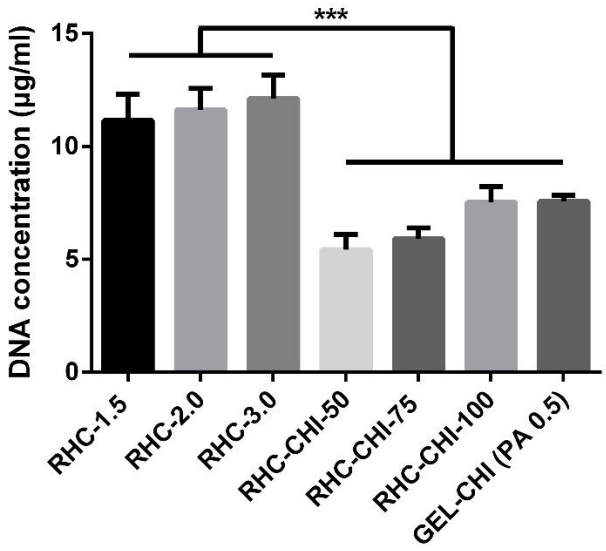

Figure 5-4. DNA concentration determined from different porous scaffolds at culturing day 14

qRT-PCR

The deposition of the ECM related proteins (integrin, collagen I and collagen III) within RHC based porous scaffolds were quantified by RT-PCR. As shown in Figure 4-65, it was found the expression of the integrin increased along with the

culturing period except RHC-CHI scaffold showed a slight decreasing at day 14. Since integrin is considered as a protein that directly associate with the cell adhesion to materials [191], the induction on integrin expression indicated that the fabricated RHC and RHC-CHI scaffold can prompt the adhesion and migration of the fibroblasts after seeding to the substrates. The increment on collagen I and III expressions were also found after 3 days, and gene expressions of these proteins significantly increased up to day 14. The expression trends on these three selected ECM relevant proteins are in agreement with the results found by Wang *et al.* [324], where integrin, collagen IV and VII were investigated from proliferated dermal fibroblasts that seeded in gelatin-chondroitin 6 sulphate-hyaluronic acid based scaffold. It was mentioned in their study that the mRNA of the ECM related proteins would highly expressed for 1 - 2 weeks as the seeded fibroblasts formed the base membrane and the reduction of the gene expressions were noticed thereafter and such phenomenon was also mentioned in other studies where epidermis, dermis and fibroblasts were studied [325, 326]. The results obtained in current study show expression of the collagen I increased significantly at day 7 and 14 in both RHC and RHC-CHI by comparing to the early stage of the culturing, and it is in agreement with the previous studies as the expression on collagen I increased from the 72 h which was found contributed by the proliferation of fibroblasts [327, 328], and it is well known that the collagen III is only predominate at the early stage of the wound healing and later replaced by stronger collagen I [19, 21],

The relatively low gene expression level on collagen III was also found at day 1 and 3 as compared to collagen I in all scaffolds, and such results was differ from the theoretical phenomenon as it is mentioned on above that the type III collagen is dominated at early stage within the wound tissue or seeded fibroblasts compare to type I collagen, a possible assumption to explain this finding is because both types of porous scaffolds (RHC and RHC-CHI porous scaffolds) had large amount of the recombinant type III collagen that can be provided as an ECM structural protein once they are released into the microenvironment. As a result, fibroblasts did not need to synthetize much of their own type III collagen in the first 3 days (at the early stage).

RHC based hydrogels

Substrate stiffness, ligand density are considered as the two factors that influence the cell focal adhesion and cell morphology through cell-material interaction [67, 323, 329-331]. In this study, no significant differences on cell morphologies were found among hydrogel samples with different stiffness (Figure 4-62), and fully confluence was observed on three samples where all of their morphologies became indistinguishable as cells formed monolayer on all hydrogels. Similar phenomenon was also mention by Yeung *et al.* [316], where they found cells lose morphologic difference once cell-cell contact occurs and cell density became less independent to the hydrogel stiffness as monolayer formed.

However, as comparing the cell morphology that found on hydrogel with fabrication in different RHC fractions (Figure 4-61), it clearly showed that the single cell area, spread area as well as cell-cell contact were increased as increasing the RHC fraction in the hydrogel system. Similarly, Gaudet *et al.* [332] had discovered that, the fibroblasts spread area was strongly influenced by varying the ligand densities where collagen I was coated on polyacrylamide gel surface which Young's modulus was determined around 5 kPa. Specifically, it was found the cell spread area is initially an increasing function of adhesive ligand density where type I collagen solutions at plating concentrations were adjusted from 0.00075 to 0.025 mg/mL. They also mentioned in their study that at lower density of collagen I coated gel, the number of ligand molecules which available for binding were far lower than the integrin receptors as Akiyama *et al.* [333] declared that there were approximate 5×10^5 integrin expressed by fibroblast. Although Di Lullo *et al.* [334] found that each collagen molecule can provide three integrin binding sites, but still, at low ligand density, the total number of the ligand molecules are far behind from number of integrin. Consequently, it suggested that the fibroblasts exerted enormous force through a small number of available linkages which led to the rounded morphology since cell spreading with flatten morphology require more force generated by binding sites. Like fibroblast cells, such phenomenon was also found in other mammal cells. Engler *et al.* [67] had found the spread of smooth muscle cells as well as cell area can be strongly modulated by the ligand density where varied amount of collagen I was used as ligand to coat the polyacrylamide gel surfaces.

Specifically, they found the cell spreading and projected cell area were significantly increased as the increasing on collagen I density (at a selected density range from 1 to 1000 ng/cm^2) on both soft (1 kPa) and stiff (8 kPa) gel substrates. The explanation to such finding given by the group was that, at low ligand density, cell could not form adequate adhesive sites to pull itself spread while by increasing the ligand density, more binding sites between ligand (collagen I) and cellular membrane through integrin were formed and such finding was also mentioned by Lauffenburger *et al.* [335]. Besides that, study also showed that endothelial cell adhesion was improved by increasing the density of RGD-contained peptides which coated on hydrogel surface [336]. Thus, it can be summarized from the current results, cell morphology, cell spreading and cell area are largely dependent to the RHC fraction of the fabricated RHC-CHI hydrogels, but less influenced by the hydrogel stiffness.

By comparing the optical microscopy images obtained in current study (Figure 4-61 and 62), not only the variations on cell morphologies were found on fabricated hydrogels, but it also showed that the cell densities (number of cells) were varied significantly, and these observations are in agreement with the results determined from cell proliferation study (see in Figure 4-53 and 54). Importantly, it showed the cell proliferation were associated with the cell morphologies, as higher proliferation activates were found on hydrogels with cells at their spread morphologies (Figure 4-53 and 61). Similar to these findings, Chen *et al.* [337] had also found that cell

proliferation was prompted by the increasing on cell spreading. Importantly, Ingber *et al.* [338] and Gaudet *et al.* [332] had discovered that integrin-dependent adhesive activities in focal adhesions regulate the cell growth and proliferation, where intergrin-mediated signaling pathway in focal adhesion activities had also been mentioned in another study [339]. And such engagements of integrin-ECM interactions (focal adhesions) had been found promote the clustering of integrin receptors resulting in phosphorylation of FAK (Focal adhesion kinase) as initiation of the signaling pathway to induce subsequent cell proliferation [66, 340-342]. In addition, studies of inhibition on FAK further confirmed the activation of FAK stimulates the signaling pathway that promote the cell proliferation [343-345]. Thus, it confirmed the findings determined in current cell-hydrogel study as cell spread morphology and their proliferation rate are closely related. In conclusion, the current results suggested the increase of RHC fraction in hydrogel system lead to an increasing on the number of available ligands on substrate, as a result, more focal adhesion binding sites are formed. And increasing the number of such bindings lead to a spread morphology of the fibroblasts with larger projected area on hydrogel surface. Consequently, the clustering of those integrins further increased the number of activated FAK that contribute as signal pathways to induce the cell proliferation.

Chapter 6 Summary

Gelatin based porous scaffolds

Highly porous (>90% porosity) GEL-CHI three dimensional scaffolds with homogenous pore distribution were cross-linked with GA and PA solution in different concentrations. All cross-linked scaffolds showed less swelling capability compared to untreated scaffolds. Results from mechanical tests indicated both cross-linkers have the ability to reinforce the original scaffold, but PA treated scaffold exhibited properties that more closely resembled that of soft tissue due to its viscoelastic behaviours and excellent recoverability. What's more, it was found that the mechanical properties of the porous scaffolds can be tuned by adjusting the PA concentration. Cytotoxicity tests, as well as cell culturing, indicated PA as a natural cross-linker had nontoxicity to 3T3 fibroblasts compared to GA groups which showed slight toxicity to cells at the concentrations used. Morphologies of the proliferated cells on different scaffolds illustrated the affinity of cells attachment to PA treated scaffold was much higher than uncross-linked scaffold. Therefore, the PA cross-linked GEL-CHI scaffolds can be potentially used in soft tissue engineering. Further study will investigate the cell proliferation and distribution within PA cross-linked scaffolds which subjected into dynamic culture condition.

RHC based porous scaffolds

RHC and RHC-CHI porous scaffolds with high porosity, pore size and interconnectivity has been fabricated through the freeze-drying method. To increase the scaffolds' stiffness as well as improve the resistance to degradation, the porous scaffolds were chemical cross-linked by various amount of EDC.

The FT-IR spectrums and cross-linking degree revealed that the RHC scaffold was fully cross-linked at selected EDC concentration. Iso-peptides were formed by introducing chitosan into the RHC-CHI scaffolds, the determined cross-linking degree also indicated the selected EDC was sufficient to secure the RHC with both chitosan and RHC molecules through covalent bondings and FT-IR results suggested the increasing EDC led to the formation of new bonds between amino and carboxylic groups which provided by RHC and chitosan molecules.

Swelling ability of the porous scaffolds was found influenced by composition of scaffolds and used EDC concentrations. It suggested the decreasing number of hydrophilic groups due to cross-linking could reduce the swelling ability.

The degradation rate of RHC scaffolds with different fabricated concentrations showed no significant difference. Meanwhile, degradation rate decreased as the increasing of EDC content in cross-linking the RHC-CHI scaffolds that proved the formation of additional covalent bonds were formed by increasing EDC. And in

general, both RHC and RHC-CHI scaffolds were found in good integrities during the 28 days degradation process.

The results of mechanical test found out the mechanical properties of the RHC and RHC-CHI porous scaffolds can be improved by increasing RHC concentration or increasing EDC concentration respectively. What's more, by varying the chitosan to RHC ratio in the scaffolds proved that it is possible to further adjust the mechanical properties. Importantly, by comparing the literatures with the results obtained in this study, the fabricated RHC and RHC-CHI scaffolds have certain mechanical features that were found closed to several biological tissues from human body.

The results determined from cytotoxic tests showed that all fabricated RHC and RHC-CHI porous scaffolds were biocompatible as no toxicity to the fibroblasts was detected, and the results were also comparable to the results determined from PA cross-linked GEL-CHI porous scaffolds. The results also evidenced not only the materials but also the fabricating methods can be trusted to reproduce reliable porous scaffolds that no harmful residues were left in the final products.

All RHC and RHC-CHI porous scaffolds showed great cytocompatibilities during *in vitro* culturing as fibroblasts proliferated within the porous structures. Fluorescent images indicated the proliferated fibroblasts firmly attached to the pore

wall structures and homogenous distribution were also achieved within the porous structures. The SEM images showed wall structures of all porous scaffolds were well covered by the proliferated fibroblasts at their spread morphology at culturing day 14. The Alamar Blue assay determined the metabolic activities of the fibroblasts in the scaffolds at different time points, and the proliferation of the fibroblasts were confirmed by the DNA quantifications in all fabricated porous scaffolds. Confirmed the gene expression levels of β-intergin, collagen I and collagen III from molecular aspect by qRT-PCR. From the current results, it also noticed that the cellular activities were influenced by the stiffness, integrity and RHC concentration of the porous scaffolds. Specifically, we had found cellular activities increased as increasing RHC fraction, a similar phenomenon had also been discovered on RHC based hydrogel scaffolds.

RHC based hydrogel scaffolds

A series of soft hydrogels with different RHC to chitosan ratios as well as varied blend concentrations have been fabricated in the current study. The appearance of all hydrogels was colourless and transparent soft gel like objects where the flattened and smooth surface of hydrogel were observed by ESEM.

The time taken for onset of gelation was found influenced by blend concentration, RHC fraction and temperature. The increase on gelation time was found related to increase the chitosan fraction in solution, while increased the solution concentration show a reduction of the onset gelation time. What's more, the hydrogel forming was also found can be manipulated by varying the solution temperatures as onset of gelation took much less time when solution incubated at 37^{o}C compared to solutions at 24^{o}C and 4^{o}C.

Compression tests discovered that the fabricated hydrogels show different mechanical properties, and their stiffness can be tuned by either adjusting the RHC fraction or blend concentration. It has been found the mechanical property of RHC-CHI 80:20 hydrogel was improved by increasing chitosan fraction to 50:50, while further increased the chitosan fraction to 20:80 led to a decrease on its stiffness. And this phenomenon was suggested as cross-linked RHC-CHI network interfered by additional chitosan molecules. Meanwhile, by increasing the blend concentration without changing the ratio of composition, it was found that hydrogel 3A had

highest stiffness among all fabricated hydrogels and the determined compressive modulus was found 2.73 and 8.51-fold of hydrogel 2A and A respectively.

The *in vitro* degradation rate of the fabricated hydrogels showed that, at early stage of the degradation, all hydrogels tended to have similar degradation rates. From day 14, the degradation rate was found to be stiffness dependent as hydrogel with highest chitosan fraction had a significant higher weight loss, and such phenomenon indicated an accelerated breakdown occurred in chitosan rich hydrogel compared to hydrogel with RHC to chitosan ratio of 80:20 and 50:50. It was then suggested the additional chitosan molecules not only brought extra amino groups need for cross-linking but also sequestered the cross-linked RHC-RHC and RHC-chitosan networks that subsequently weaken the structural integrity of hydrogel.

Cytotoxicity of the hydrogel samples had also been examined using the medium extraction cytotoxic test and the results were found comparable to the results obtained from porous scaffolds that further proved EDC cross-linked hydrogels had nontoxicity to the fibroblasts.

The morphology study of the proliferated fibroblasts suggested that, RHC can prompt the spreading of the fibroblasts on hydrogel surfaces as number of spread cells was found increased by increasing the RHC fraction in hydrogel blends. Importantly, DNA content determined by Hoechst 33258 DNA assay showed that

the fibroblasts proliferation activities were largely influenced by RHC fraction although all types of RHC hydrogels showed supporting the fibroblasts. These findings were in agreement with the results that discovered in porous RHC and RHC-CHI scaffolds as RHC fraction influenced the proliferation of the seeded fibroblasts. Thus, it is suggested that RHC as biomaterial can supports and prompts the adhesion and proliferation of the seeded fibroblasts.

Chapter 7 Project conclusions

To avoid the drawbacks and risks that animal derived collagens based biomaterials bring to soft tissue engineering applications, the recombinant type III human collagen-polypeptide is used as a safe biopolymer in this study. By using freeze-drying technique, 3-D porous scaffolds had been successfully fabricated which were based on gelatin-chitosan, RHC and RHC-CHI, respectively. Soft hydrogel scaffolds based on RHC had also been constructed in this study. Various characterisations have been carried out on the fabricated porous scaffolds and hydrogel scaffolds to test their feasibilities as potential candidates for applications in soft tissue engineering.

Results showed that the fabricated porous gelatin-chitosan, RHC and RHC-CHI porous scaffolds had high porosity with interconnected porous structures as well as acceptable pore size. The stiffness of the porous scaffolds could be tailored by either increasing the biopolymer (RHC) or cross-linker (PA and EDC) concentration and their biodegradation degrees were found to be cross-linking dependent. Moreover, by introducing chitosan into RHC scaffolds, the stiffness were further improved. Importantly, the stiffness of the porous scaffolds were also found comparable to some of the human native soft or connective tissues. The investigation of the cytocompatibility proved the fabricated 3-D porous scaffolds had no toxicity to the

seeded fibroblasts and they could prompt cell migration and proliferation. And qRT-PCR further confirmed the gene expression levels of β-intergin, collagen I and collagen III was enhanced from molecular aspect.

Soft RHC based hydrogels show that their stiffness can be varied, either by adjusting the blend concentration or changing the RHC fraction. Both mechanical test and *in vitro* biodegradation test illustrate the hydrogels scaffolds have acceptable biostability and comparable to some of the soft tissues. All hydrogel scaffolds showed good cytocompatibility as the seeded fibroblasts attached and proliferated on their surfaces. Meanwhile, results showed that proliferation and cell morphologies were highly dependent to the hydrogel compositions as RHC fraction influenced the cellular behaviors significantly.

By comparing the stiffness as well as cellular activities on 3-D porous scaffolds and hydrogel scaffolds, it found that cellular activities were both stiffness and RHC fraction dependent. However RHC fraction dominated the cellular activity response. These findings suggested that, the RHC as a bioactive polymer has the ability to prompt the adhesion, spreading and proliferation of the seeded fibroblasts through focal adhesion activities between RHC molecules and integrin.

This study demonstrated repeatable fabrication methods to produce porous 3-D porous scaffolds and soft hydrogel scaffolds, and the fabricated biodegradable

scaffolds showed feasibilities to mimic the native soft tissue as they were found biocompatible and their mechanical stiffness were comparable to some of the native tissues. Thus, the RHC based porous scaffolds as well as hydrogels can be suggested as potential candidates for tissue regeneration and wound healing in soft tissue engineering.

Chapter 8 Future work

In this study, PA cross-linked gelatin based porous scaffolds and EDC cross-linked RHC based porous scaffolds as well as RHC based hydrogels show tunable mechanical properties close to that of some of the human soft tissues and acceptable cytocompatibilities that support seeded cells attachment and proliferation. Given the opportunities these materials thus offer, some suggestions for improving the current study and future work are given below.

The static cell culturing was used in this study, for better understanding how fibroblasts respond to the mechanical stimulations. It would be worthwhile to change the *in vitro* culturing condition from static to dynamic by applying a unidirectional perfusion bioreactor system to host the porous scaffolds. A unidirectional perfusion bioreactor system could be designed to host the cell seeded RHC or RHC-CHI scaffolds and study the cellular behaviors by mechanical stimulation and try to find out the optimal fluid speed to support cell attachment and proliferation. Finally, it will be meaningful to complete the *in vivo* implantation within animal models where use either optimized cell-free scaffold or cell-seeded scaffold. In addition, as it has been proved that the modulus of the fabricated porous scaffolds matched to a variety of human soft tissues, thus, different cell lines other

than fibroblasts could be chosen to investigate feasibilities of porous scaffolds for other potential applications.

Fibroblasts growth on the hydrogel surface was achieved in the current study. Cell encapsulation using injectable hydrogels to replace defect soft tissue is one for which there is highly demand. Therefore, it would be possible to work on developing a cell embedded injectable hydrogel system to further extend its applications. In addition, a potential application for the current developed hydrogel would be used as a coating material to improve the cell adhesion and proliferation. Thus, another approach other than encapsulation should focus on coating technique and cellular response on combined substrates.

References

[1] Williams D. Benefit and risk in tissue engineering. Materials Today. 2004;7:24-9.
[2] Kramschuster A, Turng L-S. 17 - Fabrication of Tissue Engineering Scaffolds. In: Ebnesajjad S, editor. Handbook of Biopolymers and Biodegradable Plastics. Boston: William Andrew Publishing; 2013. p. 427-46.
[3] Place ES, George JH, Williams CK, Stevens MM. Synthetic polymer scaffolds for tissue engineering. Chemical Society Reviews. 2009;38:1139-51.
[4] Yang C, Hillas PJ, Baez JA, Nokelainen M, Balan J, Tang J, et al. The application of recombinant human collagen in tissue engineering. BioDrugs. 2004;18:103-19.
[5] Olsen D, Yang C, Bodo M, Chang R, Leigh S, Baez J, et al. Recombinant collagen and gelatin for drug delivery. Advanced Drug Delivery Reviews. 2003;55:1547-67.
[6] Werten MW, Wisselink WH, Jansen-van den Bosch TJ, de Bruin EC, de Wolf FA. Secreted production of a custom-designed, highly hydrophilic gelatin in Pichia pastoris. Protein engineering. 2001;14:447-54.
[7] Ikada Y. Challenges in tissue engineering. Journal of the Royal Society Interface. 2006;3:589-601.
[8] E.Bishop LDKA. Introduce to tissue engineering. USA: Woodhead publishing Limited; 2005.
[9] Mase VJ, Hsu JR, Wolf SE, Wenke JC, Baer DG, Owens J, et al. Clinical application of an acellular biologic scaffold for surgical repair of a large, traumatic quadriceps femoris muscle defect. Orthopedics. 2010;33.
[10] Kasbekar S, Kaye SB, Williams RL, Stewart RMK, Leow-Dyke S, Rooney P. Development of decellularised conjunctiva as a substrate for the ex-vivo expansion of conjunctival epithelium. Journal of Tissue Engineering and Regenerative Medicine. 2017:n/a-n/a.
[11] Parenteau-Bareil R, Gauvin R, Berthod F. Collagen-based biomaterials for tissue engineering applications. Materials. 2010;3:1863-87.
[12] Pawelec KM, Best SM, Cameron RE. Collagen: a network for regenerative medicine. Journal of Materials Chemistry B, Materials for Biology and Medicine. 2016;4:6484-96.
[13] Friess W. Collagen – biomaterial for drug delivery. European Journal of Pharmaceutics and Biopharmaceutics. 1998;45:113-36.
[14] Moura LIF, Dias AMA, Carvalho E, de Sousa HC. Recent advances on the development of wound dressings for diabetic foot ulcer treatment—A review. Acta biomaterialia. 2013;9:7093-114.
[15] Wolfram D, Tzankov A, Pülzl P, PIZA‐KATZER H. Hypertrophic scars and keloids—a review of their pathophysiology, risk factors, and therapeutic management. Dermatologic Surgery. 2009;35:171-81.
[16] Shoulders MD, Raines RT. Collagen structure and stability. Annual review of biochemistry. 2009;78:929-58.
[17] Buehler MJ. Nanomechanics of collagen fibrils under varying cross-link densities: atomistic and continuum studies. Journal of the mechanical behavior of biomedical materials. 2008;1:59-67.
[18] Robson MC, Steed DL, Franz MG. Wound healing: Biologic features and approaches to maximize healing trajectories. Current Problems in Surgery. 2001;38:A1-140.
[19] Clore JN, Cohen IK, Diegelmann RF. Quantitation of collagen type-I and type-III during wound-healing in rat skin. Proceedings of the Society for Experimental Biology and Medicine. 1979;161:337-40.
[20] Hayakawa T, Hashimoto Y, Myokei Y, Aoyama H, Izawa Y. Changes in type of collagen during the development of human post-burn hypertrophic scars. Clinica Chimica Acta. 1979;93:119-25.
[21] Velnar T, Bailey T, Smrkolj V. The wound healing process: an overview of the cellular and molecular mechanisms. Journal of International Medical Research. 2009;37:1528-42.
[22] Brown JC, Timpl R. The collagen superfamily. International archives of allergy and immunology. 1995;107:484-90.
[23] Kadler KE, Baldock C, Bella J, Boot-Handford RP. Collagens at a glance. Journal of cell science. 2007;120:1955-8.
[24] Asher DM. The transmissible spongiform encephalopathy agents: concerns and responses of

United States regulatory agencies in maintaining the safety of biologics. Developments in biological standardization. 1999;100.
[25] Brown P, Will RG, Bradley R, Asher DM, Detwiler L. Bovine spongiform encephalopathy and variant Creutzfeldt-Jakob disease: background, evolution, and current concerns. Emerging Infectious Diseases. 2001;7:6-16.
[26] Bonnet C, Charriere G, Vaquier J, Bertin P, Vergne P, Treves R. Bovine collagen induced systemic symptoms: antibody formation against bovine and human collagen. The Journal of rheumatology. 1996;23:545-7.
[27] Charriere G, Bejot M, Schnitzler L, Ville G, Hartmann DJ. Reactions to a bovine collagen implant: Clinical and immunologic study in 705 patients. Journal of the American Academy of Dermatology. 1989;21:1203-8.
[28] Meade KR, Silver FH. Immunogenicity of collagenous implants. Biomaterials. 1990;11:176-80.
[29] Patino MG, Neiders ME, Andreana S, Noble B, Cohen RE. Cellular inflammatory response to porcine collagen membranes. Journal of periodontal research. 2003;38:458-64.
[30] Apel-Sarid L, Cochrane DD, Steinbok P, Byrne AT, Dunham C. Microfibrillar collagen hemostat–induced necrotizing granulomatous inflammation developing after craniotomy: a pediatric case series: Report of 3 cases. Journal of Neurosurgery: Pediatrics. 2010;6:385-92.
[31] Cooperman L, Michaeli D. The immunogenicity of injectable collagen. I. A 1-year prospective study. Journal of the American Academy of Dermatology. 1984;10:638-46.
[32] Cooperman L, Michaeli D. The immunogenicity of injectable collagen. II. A retrospective review of seventy-two tested and treated patients. Journal of the American Academy of Dermatology. 1984;10:647-51.
[33] Gómez-Guillén MC, Pérez-Mateos M, Gómez-Estaca J, López-Caballero E, Giménez B, Montero P. Fish gelatin: a renewable material for developing active biodegradable films. Trends in Food Science & Technology. 2009;20:3-16.
[34] Vanja Kokol SG. Collagen- vs. Gelatine-Based Biomaterials and Their Biocompatibility: Review and Perspectives Biomaterials Applications for Nanomedicine. 2011.
[35] Prakashan KCN. Pharmaceutical microbiology-principles and applications. 2008;ISBN NO.978-81-85790-61-2.
[36] Jiankang H, Dichen L, Yaxiong L, Bo Y, Hanxiang Z, Qin L, et al. Preparation of chitosan–gelatin hybrid scaffolds with well-organized microstructures for hepatic tissue engineering. Acta biomaterialia. 2009;5:453-61.
[37] Tucci MG, Ricotti G, Mattioli-Belmonte M, Gabbanelli F, Lucarini G, Orlando F, et al. Chitosan and Gelatin as Engineered Dressing for Wound Repair. Journal of Bioactive and Compatible Polymers. 2001;16:145-57.
[38] Chiono V, Pulieri E, Vozzi G, Ciardelli G, Ahluwalia A, Giusti P. Genipin-crosslinked chitosan/gelatin blends for biomedical applications. Journal of Materials Science: Materials in Medicine. 2008;19:889-98.
[39] Ikada Y. Biological Materials, In: Integrated Biomaterials Science, Barbucci,R Kluwer Academic /Plenium Publishers, ISBN: 978-0-306-46678-6, New York, USA.
[40] Vuorela A, Myllyharju J, Nissi R, Pihlajaniemi T, Kivirikko KI. Assembly of human prolyl 4-hydroxylase and type III collagen in the yeast pichia pastoris: formation of a stable enzyme tetramer requires coexpression with collagen and assembly of a stable collagen requires coexpression with prolyl 4-hydroxylase. The EMBO Journal. 1997;16:6702-12.
[41] Alakokko L, Hyland J, Smith C, Kivirikko KI, Jimenez SA, Prockop DJ. Expression of a human cartilage procollagen gene (COL2A1) in mouse 3T3 cells. Journal of Biological Chemistry. 1991;266:14175-8.
[42] Geddis AE, Prockop DJ. Expression of Human COL1A1 Gene in Stably Transfected HT1080 Cells: The Production of a Thermostable Homotrimer of Type I Collagen in a Recombinant System. Matrix. 1993;13:399-405.
[43] Nokelainen M, Helaakoski T, Myllyharju J, Notbohm H, Pihlajaniemi T, Fietzek PP, et al. Expression and characterization of recombinant human type II collagens with low and high contents of hydroxylysine and its glycosylated forms. Matrix Biology. 1998;16:329-38.
[44] Myllyharju J, Lamberg A, Notbohm H, Fietzek PP, Pihlajaniemi T, Kivirikko KI. Expression of wild-type and modified pro alpha chains of human type I procollagen in insect cells leads to the formation of stable alpha 1(I) (2)alpha 2(I) collagen heterotrimers and alpha 1(I) (3) homotrimers but not alpha 2(I) (3) homotrimers. Journal of Biological Chemistry. 1997;272:21824-30.

[45] Helaakoski T, Annunen P, Vuori K, MacNeil IA, Pihlajaniemi T, Kivirikko KI. Cloning, baculovirus expression, and characterization of a second mouse prolyl 4-hydroxylase alpha-subunit isoform: formation of an alpha 2 beta 2 tetramer with the protein disulfide-isomerase/beta subunit. Proceedings of the National Academy of Sciences of the United States of America. 1995;92:4427-31.
[46] Pakkanen O, Pirskanen A, Myllyharju J. Selective expression of nonsecreted triple-helical and secreted single-chain recombinant collagen fragments in the yeast Pichia pastoris. Journal of Biotechnology. 2006;123:248-56.
[47] Myllyharju J, Nokelainen M, Vuorela A, Kivirikko KI. Expression of recombinant human type I-III collagens in the yeast Pichia pastoris. Biochemical Society Transactions. 2000;28:353-7.
[48] Liu B, Lei Y, Zhang J, Hu L, Yang S. Expression, Purification and Characterization of recombinant human gelatin in Pichia pastoris. In: Cao Z, He YH, Sun L, Cao XQ, editors. Application of Chemical Engineering, Pts 1-32011. p. 2905-12.
[49] Cereghino GPL, Cereghino JL, Ilgen C, Cregg JM. Production of recombinant proteins in fermenter cultures of the yeast Pichia pastoris. Current opinion in biotechnology. 2002;13:329-32.
[50] Nokelainen M, Tu H, Vuorela A, Notbohm H, Kivirikko KI, Myllyharju J. High‐level production of human type I collagen in the yeast Pichia pastoris. Yeast. 2001;18:797-806.
[51] Peng YY, Stoichevska V, Madsen S, Howell L, Dumsday GJ, Werkmeister JA, et al. A simple cost effective methodology for large scale purification of recombinant non-animal collagens. Applied microbiology and biotechnology. 2014;98:1807-15.
[52] John DC, Watson R, Kind AJ, Scott AR, Kadler KE, Bulleid NJ. Expression of an engineered form of recombinant procollagen in mouse milk. Nature biotechnology. 1999;17:385-9.
[53] Toman PD, Pieper F, Sakai N, Karatzas C, Platenburg E, de Wit I, et al. Production of recombinant human type I procollagen homotrimer in the mammary gland of transgenic mice. Transgenic research. 1999;8:415-27.
[54] Tomita M, Munetsuna H, Sato T, Adachi T, Hino R, Hayashi M, et al. Transgenic silkworms produce recombinant human type III procollagen in cocoons. Nature biotechnology. 2003;21:52-6.
[55] Shoseyov O, Posen Y, Grynspan F. Human recombinant type I collagen produced in plants. Tissue Engineering Part A. 2013;19:1527-33.
[56] Merle C, Perret S, Lacour T, Jonval V, Hudaverdian S, Garrone R, et al. Hydroxylated human homotrimeric collagen I in Agrobacterium tumefaciens-mediated transient expression and in transgenic tobacco plant. FEBS Letters. 2002;515:114-8.
[57] Ruggiero F, Exposito J-Y, Bournat P, Gruber V, Perret S, Comte J, et al. Triple helix assembly and processing of human collagen produced in transgenic tobacco plants. FEBs Letters. 2000;469:132-6.
[58] Liu B, Y. T. Lei,S. L. Yang Structure Analysis of a Highly Hydrophilic Recombinant Human-Source Gelatin. Chem Sci Trans. 2012;1:347- 54
[59] Bulleid N, John D, Kadler K. Recombinant expression systems for the production of collagen. Portland Press Limited; 2000.
[60] Schrieber R, Seybold U. Gelatine production, the six steps to maximum safety. Developments in biological standardization. 1992;80:195-8.
[61] Miekka S, Forng RY, Rohwer R, MacAuley C, Stafford R, Flack S, et al. Inactivation of viral and prion pathogens by γ‐irradiation under conditions that maintain the integrity of human albumin. Vox sanguinis. 2003;84:36-44.
[62] Tuderman L, Prockop DJ. Procollagen N-proteinase-properties of the enzyme purified from chick-embryo tendons. European Journal of Biochemistry. 1982;125:545-9.
[63] Kenyon K, Modi WS, Contente S, Friedman R. A novel human cDNA with a predicted protein similar to lysyl oxidase maps to chromosome 15q24-q25. Journal of Biological Chemistry. 1993;268:18435-7.
[64] DE WOLF FA. High-yield secretion of recombinant gelatins by Pichia pastoris. Yeast. 1999;15:1087-96.
[65] Ramshaw JAM, Werkmeister JA. Recombinant Proteins as Emerging Biomaterials. Reference Module in Materials Science and Materials Engineering: Elsevier; 2017.
[66] Clark EA, Brugge JS. Integrins and signal-transduction pathways-the road taken. Science. 1995;268:233-9.
[67] Engler A, Bacakova L, Newman C, Hategan A, Griffin M, Discher D. Substrate Compliance versus Ligand Density in Cell on Gel Responses. Biophysical Journal. 2004;86:617-28.
[68] Multhaupt HAB, Leitinger B, Gullberg D, Couchman JR. Extracellular matrix component

signaling in cancer. Advanced Drug Delivery Reviews. 2016;97:28-40.
[69] Rappaport L, Oliviero P, Samuel JL. Cytoskeleton and mitochondrial morphology and function. Molecular and Cellular Biochemistry. 1998;184:101-5.
[70] Hynes RO. Integrins: bidirectional, allosteric signaling machines. Cell. 2002;110:673-87.
[71] Barczyk M, Carracedo S, Gullberg D. Integrins. Cell and Tissue Research. 2010;339:269-80.
[72] Emsley J, Knight CG, Farndale RW, Barnes MJ, Liddington RC. Structural Basis of Collagen Recognition by Integrin α2β1. Cell. 2000;101:47-56.
[73] Tuckwell D, Calderwood DA, Green LJ, Humphries MJ. Integrin alpha 2 I-domain is a binding site for collagens. Journal of Cell Science. 1995;108:1629-37.
[74] Lutolf M, Hubbell J. Synthetic biomaterials as instructive extracellular microenvironments for morphogenesis in tissue engineering. Nature biotechnology. 2005;23:47-55.
[75] Rinaudo M. Chitin and chitosan: Properties and applications. Progress in Polymer Science. 2006;31:603-32.
[76] Zargar V, Asghari M, Dashti A. A Review on Chitin and Chitosan Polymers: Structure, Chemistry, Solubility, Derivatives, and Applications. ChemBioEng Reviews. 2015;2:204-26.
[77] Dutta PK, Dutta J, Tripathi VS. Chitin and chitosan: Chemistry, properties and applications. Journal of Scientific & Industrial Research. 2004;63:20-31.
[78] Jayakumar R, Menon D, Manzoor K, Nair SV, Tamura H. Biomedical applications of chitin and chitosan based nanomaterials-A short review. Carbohydrate Polymers. 2010;82:227-32.
[79] He X, Li K, Xing R, Liu S, Hu L, Li P. The production of fully deacetylated chitosan by compression method. The Egyptian Journal of Aquatic Research. 2016;42:75-81.
[80] Chang KLB, Tsai G, Lee J, Fu W-R. Heterogeneous N-deacetylation of chitin in alkaline solution. Carbohydrate Research. 1997;303:327-32.
[81] Martinou A, Kafetzopoulos D, Bouriotis V. Chitin deacetylation by enzymatic means: monitoring of deacetylation processes. Carbohydrate Research. 1995;273:235-42.
[82] Zhao Y, Park R-D, Muzzarelli RAA. Chitin Deacetylases: Properties and Applications. Marine Drugs. 2010;8:24-46.
[83] Dornish M, Kaplan D, Skaugrud O. Standards and guidelines for biopolymers in tissue-engineered medical products - ASTM alginate and chitosan standard guides. In: Hunkeler D, Cherrington A, Prokop A, Rajotte R, editors. Bioartificial Organs Iii: Tissue Sourcing, Immunoisolation, and Clinical Trials. New York: New York Acad Sciences; 2001. p. 388-97.
[84] Zeeman R, Dijkstra PJ, van Wachem PB, van Luyn MJA, Hendriks M, Cahalan PT, et al. Successive epoxy and carbodiimide cross-linking of dermal sheep collagen. Biomaterials. 1999;20:921-31.
[85] Rafat M, Li F, Fagerholm P, Lagali NS, Watsky MA, Munger R, et al. PEG-stabilized carbodiimide crosslinked collagen-chitosan hydrogels for corneal tissue engineering. Biomaterials. 2008;29:3960-72.
[86] Vrana N, Builles N, Kocak H, Gulay P, Justin V, Malbouyres M, et al. EDC/NHS cross-linked collagen foams as scaffolds for artificial corneal stroma. Journal of Biomaterials Science, Polymer Edition. 2007;18:1527-45.
[87] Grover CN, Gwynne JH, Pugh N, Hamaia S, Farndale RW, Best SM, et al. Crosslinking and composition influence the surface properties, mechanical stiffness and cell reactivity of collagen-based films. Acta biomaterialia. 2012;8:3080-90.
[88] Liu W, Merrett K, Griffith M, Fagerholm P, Dravida S, Heyne B, et al. Recombinant human collagen for tissue engineered corneal substitutes. Biomaterials. 2008;29:1147-58.
[89] Powell HM, Boyce ST. EDC cross-linking improves skin substitute strength and stability. Biomaterials. 2006;27:5821-7.
[90] Gratzer PF, Lee JM. Control of pH alters the type of cross-linking produced by 1-ethyl-3-(3-dimethylaminopropyl)-carbodiimide (EDC) treatment of acellular matrix vascular grafts. Journal of Biomedical Materials Research. 2001;58:172-9.
[91] Damink LO, Dijkstra P, Van Luyn M, Van Wachem P, Nieuwenhuis P, Feijen J. Glutaraldehyde as a crosslinking agent for collagen-based biomaterials. Journal of materials science: materials in medicine. 1995;6:460-72.
[92] Jayakrishnan A, Jameela SR. Glutaraldehyde as a fixative in bioprostheses and drug delivery matrices. Biomaterials. 1996;17:471-84.
[93] Huanglee LLH, Cheung DT, Nimni ME. Biochemical-changes and cytotoxicity associated with the degradation of polymeric glutaraldehyde derived cross-links Journal of Biomedical Materials Research. 1990;24:1185-201.

[94] Petite H, Duval LL, Frei V, Abdulmalak N, Sigotluizard MF, Herbage D. Cytocompatibility of calf pericardium treated by glutaraldehyde and by the acyl azide methods in an organotypic culture model Biomaterials. 1995;16:1003-8.
[95] Huang‐Lee LL, Cheung DT, Nimni ME. Biochemical changes and cytotoxicity associated with the degradation of polymeric glutaraldehyde derived crosslinks. Journal of biomedical materials research. 1990;24:1185-201.
[96] Davidenko N, Bax DV, Schuster CF, Farndale RW, Hamaia SW, Best SM, et al. Optimisation of UV irradiation as a binding site conserving method for crosslinking collagen-based scaffolds. Journal of Materials Science Materials in Medicine. 2016;27:14.
[97] Sung HW, Liang IL, Chen CN, Huang RN, Liang HF. Stability of a biological tissue fixed with a naturally occurring crosslinking agent (genipin). Journal of Biomedical Materials Research. 2001;55:538-46.
[98] He L, Mu C, Shi J, Zhang Q, Shi B, Lin W. Modification of collagen with a natural cross-linker, procyanidin. International Journal of Biological Macromolecules. 2011;48:354-9.
[99] Fine AM. Oligomeric proanthocyanidin complexes: history, structure, and phytopharmaceutical applications. Alternative medicine review : a journal of clinical therapeutic. 2000;5:144-51.
[100] Han B, Jaurequi J, Tang BW, Nimni ME. Proanthocyanidin: A natural crosslinking reagent for stabilizing collagen matrices. Journal of Biomedical Materials Research Part A. 2003;65A:118-24.
[101] Choi Y, Kim H-J, Min K-S. Effects of proanthocyanidin, a crosslinking agent, on physical and biological properties of collagen hydrogel scaffold. Restorative Dentistry & Endodontics. 2016;41:296-303.
[102] Kim S, Nimni ME, Yang Z, Han B. Chitosan/gelatin-based films crosslinked by proanthocyanidin. Journal of Biomedical Materials Research Part B-Applied Biomaterials. 2005;75B:442-50.
[103] Rothamel D, Schwarz F, Sager M, Herten M, Sculean A, Becker J. Biodegradation of differently cross-linked collagen membranes: an experimental study in the rat. Clinical Oral Implants Research. 2005;16:369-78.
[104] Ahn J-I, Kuffova L, Merrett K, Mitra D, Forrester JV, Li F, et al. Crosslinked collagen hydrogels as corneal implants: Effects of sterically bulky vs. non-bulky carbodiimides as crosslinkers. Acta biomaterialia. 2013;9:7796-805.
[105] Nair LS, Laurencin CT. Biodegradable polymers as biomaterials. Progress in Polymer Science. 2007;32:762-98.
[106] Lee CH, Singla A, Lee Y. Biomedical applications of collagen. International journal of pharmaceutics. 2001;221:1-22.
[107] Ma L, Gao C, Mao Z, Zhou J, Shen J. Enhanced biological stability of collagen porous scaffolds by using amino acids as novel cross-linking bridges. Biomaterials. 2004;25:2997-3004.
[108] Rho KS, Jeong L, Lee G, Seo B-M, Park YJ, Hong S-D, et al. Electrospinning of collagen nanofibers: Effects on the behavior of normal human keratinocytes and early-stage wound healing. Biomaterials. 2006;27:1452-61.
[109] Cao H, Chen M-M, Liu Y, Liu Y-Y, Huang Y-Q, Wang J-H, et al. Fish collagen-based scaffold containing PLGA microspheres for controlled growth factor delivery in skin tissue engineering. Colloids and Surfaces B: Biointerfaces. 2015;136:1098-106.
[110] Pensalfini M, Ehret AE, Stüdeli S, Marino D, Kaech A, Reichmann E, et al. Factors affecting the mechanical behavior of collagen hydrogels for skin tissue engineering. Journal of the Mechanical Behavior of Biomedical Materials. 2017;69:85-97.
[111] Hu K, Shi H, Zhu J, Deng D, Zhou G, Zhang W, et al. Compressed collagen gel as the scaffold for skin engineering. Biomedical Microdevices. 2010;12:627-35.
[112] Braziulis E, Diezi M, Biedermann T, Pontiggia L, Schmucki M, Hartmann-Fritsch F, et al. Modified plastic compression of collagen hydrogels provides an ideal matrix for clinically applicable skin substitutes. Tissue Engineering Part C: Methods. 2012;18:464-74.
[113] Awad HA, Boivin GP, Dressler MR, Smith FN, Young RG, Butler DL. Repair of patellar tendon injuries using a cell–collagen composite. Journal of Orthopaedic Research. 2003;21:420-31.
[114] Juncosa-Melvin N, Boivin GP, Gooch C, Galloway MT, West JR, Dunn MG, et al. The effect of autologous mesenchymal stem cells on the biomechanics and histology of gel-collagen sponge constructs used for rabbit patellar tendon repair. Tissue engineering. 2006;12:369-79.
[115] Boccafoschi F, Habermehl J, Vesentini S, Mantovani D. Biological performances of collagen-based scaffolds for vascular tissue engineering. Biomaterials. 2005;26:7410-7.
[116] Murray MM, Spindler KP, Ballard P, Welch TP, Zurakowski D, Nanney LB. Enhanced

histologic repair in a central wound in the anterior cruciate ligament with a collagen – platelet - rich plasma scaffold. Journal of Orthopaedic Research. 2007;25:1007-17.
[117] Xu Y, Gurusiddappa S, Rich RL, Owens RT, Keene DR, Mayne R, et al. Multiple binding sites in collagen type I for the integrins α1β1 and α2β1. Journal of Biological Chemistry. 2000;275:38981-9.
[118] Smith KH, Haycock JW. 14 - Modifying biomaterial surfaces to control stem cell growth and differentiation A2 - Williams, Rachel. Surface Modification of Biomaterials: Woodhead Publishing; 2011. p. 344-64.
[119] Gough J. 12 - Modifying biomaterial surfaces to optimise interactions with soft tissues A2 - Williams, Rachel. Surface Modification of Biomaterials: Woodhead Publishing; 2011. p. 309-25.
[120] Chen X, Qi Y-Y, Wang L-L, Yin Z, Yin G-L, Zou X-H, et al. Ligament regeneration using a knitted silk scaffold combined with collagen matrix. Biomaterials. 2008;29:3683-92.
[121] Hauser J, Zietlow J, Köller M, Esenwein S, Halfmann H, Awakowicz P, et al. Enhanced cell adhesion to silicone implant material through plasma surface modification. Journal of Materials Science: Materials in Medicine. 2009;20:2541-8.
[122] Olivero DK, Furcht LT. Type-IV collagen, laminin, and fibronectin promote the adhesion and migration of rabbit lens epithelial-cells in-vitro Investigative Ophthalmology & Visual Science. 1993;34:2825-34.
[123] Cooke MJ, Phillips SR, Shah DS, Athey D, Lakey JH, Przyborski SA. Enhanced cell attachment using a novel cell culture surface presenting functional domains from extracellular matrix proteins. Cytotechnology. 2008;56:71-9.
[124] Madihally SV, Matthew HWT. Porous chitosan scaffolds for tissue engineering. Biomaterials. 1999;20:1133-42.
[125] Sashiwa H, Aiba S-i. Chemically modified chitin and chitosan as biomaterials. Progress in Polymer Science. 2004;29:887-908.
[126] Nordtveit RJ, Vårum KM, Smidsrød O. Degradation of partially N-acetylated chitosans with hen egg white and human lysozyme. Carbohydrate Polymers. 1996;29:163-7.
[127] Shi C, Zhu Y, Ran X, Wang M, Su Y, Cheng T. Therapeutic Potential of Chitosan and Its Derivatives in Regenerative Medicine. Journal of Surgical Research. 2006;133:185-92.
[128] Madhumathi K, Shalumon KT, Rani VVD, Tamura H, Furuike T, Selvamurugan N, et al. Wet chemical synthesis of chitosan hydrogel–hydroxyapatite composite membranes for tissue engineering applications. International Journal of Biological Macromolecules. 2009;45:12-5.
[129] Jayakumar R, Prabaharan M, Sudheesh Kumar PT, Nair SV, Tamura H. Biomaterials based on chitin and chitosan in wound dressing applications. Biotechnology advances. 2011;29:322-37.
[130] Pillai CKS, Paul W, Sharma CP. Chitin and chitosan polymers: Chemistry, solubility and fiber formation. Progress in Polymer Science. 2009;34:641-78.
[131] Wang T, Zhu X-K, Xue X-T, Wu D-Y. Hydrogel sheets of chitosan, honey and gelatin as burn wound dressings. Carbohydrate Polymers. 2012;88:75-83.
[132] Oprenyeszk F, Chausson M, Maquet V, Dubuc JE, Henrotin Y. Protective effect of a new biomaterial against the development of experimental osteoarthritis lesions in rabbit: a pilot study evaluating the intra-articular injection of alginate-chitosan beads dispersed in an hydrogel. Osteoarthritis and Cartilage. 2013;21:1099-107.
[133] Luo Y, Teng Z, Wang X, Wang Q. Development of carboxymethyl chitosan hydrogel beads in alcohol-aqueous binary solvent for nutrient delivery applications. Food Hydrocolloids. 2013;31:332-9.
[134] Ding C-M, Zhou Y, He Y-N, Tan W-S. Perfusion seeding of collagen–chitosan sponges for dermal tissue engineering. Process Biochemistry. 2008;43:287-96.
[135] Cho Y-W, Cho Y-N, Chung S-H, Yoo G, Ko S-W. Water-soluble chitin as a wound healing accelerator. Biomaterials. 1999;20:2139-45.
[136] Ma J, Wang H, He B, Chen J. A preliminary in vitro study on the fabrication and tissue engineering applications of a novel chitosan bilayer material as a scaffold of human neofetal dermal fibroblasts. Biomaterials. 2001;22:331-6.
[137] Okamoto Y, Shibazaki K, Minami S, Matsuhashi A, Tanioka S-i, Shigemasa Y. Evaluation of chitin and chitosan on open wound healing in dogs. Journal of Veterinary Medical Science. 1995;57:851-4.
[138] Kojima K, Okamoto Y, Kojima K, Miyatake K, Fujise H, Shigemasa Y, et al. Effects of chitin and chitosan on collagen synthesis in wound healing. Journal of Veterinary Medical Science. 2004;66:1595-8.

[139] Kojima K, Okamoto Y, Miyatake K, Kitamura Y, Minami S. Collagen typing of granulation tissue induced by chitin and chitosan. Carbohydrate Polymers. 1998;37:109-13.
[140] Ueno H, Nakamura F, Murakami M, Okumura M, Kadosawa T, Fujinaga T. Evaluation effects of chitosan for the extracellular matrix production by fibroblasts and the growth factors production by macrophages. Biomaterials. 2001;22:2125-30.
[141] Shao HJ, Chen CS, Lee YT, Wang JH, Young TH. The phenotypic responses of human anterior cruciate ligament cells cultured on poly(epsilon-caprolactone) and chitosan. Journal of Biomedical Materials Research Part A. 2010;93A:1297-305.
[142] Funakoshi T, Majima T, Iwasaki N, Suenaga N, Sawaguchi N, Shimode K, et al. Application of tissue engineering techniques for rotator cuff regeneration using a chitosan-based hyaluronan hybrid fiber scaffold. American Journal of Sports Medicine. 2005;33:1193-201.
[143] VandeVord PJ, Matthew HWT, DeSilva SP, Mayton L, Wu B, Wooley PH. Evaluation of the biocompatibility of a chitosan scaffold in mice. Journal of Biomedical Materials Research. 2002;59:585-90.
[144] Chen WL, Huang CH, Chiou LL, Chen TH, Huang YY, Jiang CC, et al. Multiphoton Imaging and Quantitative Analysis of Collagen Production by Chondrogenic Human Mesenchymal Stem Cells Cultured in Chitosan Scaffold. Tissue Engineering Part C-Methods. 2010;16:913-20.
[145] Hollister SJ. Porous scaffold design for tissue engineering. Nat Mater. 2005;4:518-24.
[146] Lovett M, Lee K, Edwards A, Kaplan DL. Vascularization Strategies for Tissue Engineering. Tissue Engineering Part B, Reviews. 2009;15:353-70.
[147] Ko YG, Kawazoe N, Tateishi T, Chen GP. Preparation of chitosan scaffolds with a hierarchical porous structure. Journal of Biomedical Materials Research Part B-Applied Biomaterials. 2010;93B:341-50.
[148] Ma L, Gao CY, Mao ZW, Zhou J, Shen JC, Hu XQ, et al. Collagen/chitosan porous scaffolds with improved biostability for skin tissue engineering. Biomaterials. 2003;24:4833-41.
[149] El-Sherbiny IM, Yacoub MH. Hydrogel scaffolds for tissue engineering: Progress and challenges. Global Cardiology Science & Practice. 2013;2013:316-42.
[150] Rodriguez-Vazquez M, Vega-Ruiz B, Ramos-Zuniga R, Saldana-Koppel DA, Quinones-Olvera LF. Chitosan and Its Potential Use as a Scaffold for Tissue Engineering in Regenerative Medicine. Biomed Research International. 2015.
[151] Wu ZM, Zhang XG, Zheng C, Li CX, Zhang SM, Dong RN, et al. Disulfide-crosslinked chitosan hydrogel for cell viability and controlled protein release. European Journal of Pharmaceutical Sciences. 2009;37:198-206.
[152] Obara K, Ishihara M, Ishizuka T, Fujita M, Ozeki Y, Maehara T, et al. Photocrosslinkable chitosan hydrogel containing fibroblast growth factor-2 stimulates wound healing in healing-impaired db/db mice. Biomaterials. 2003;24:3437-44.
[153] Crompton KE, Goud JD, Bellamkonda RV, Gengenbach TR, Finkelstein DI, Horne MK, et al. Polylysine-functionalised thermoresponsive chitosan hydrogel for neural tissue engineering. Biomaterials. 2007;28:441-9.
[154] Yan L-P, Wang Y-J, Ren L, Wu G, Caridade SG, Fan J-B, et al. Genipin-cross-linked collagen/chitosan biomimetic scaffolds for articular cartilage tissue engineering applications. Journal of Biomedical Materials Research Part A. 2010;95A:465-75.
[155] Rafat M, Li F, Fagerholm P, Lagali NS, Watsky MA, Munger R, et al. PEG-stabilized carbodiimide crosslinked collagen–chitosan hydrogels for corneal tissue engineering. Biomaterials. 2008;29:3960-72.
[156] Dong C, Lv Y. Application of Collagen Scaffold in Tissue Engineering: Recent Advances and New Perspectives. Polymers. 2016;8:42.
[157] Han C-m, Zhang L-p, Sun J-z, Shi H-f, Zhou J, Gao C-y. Application of collagen-chitosan/fibrin glue asymmetric scaffolds in skin tissue engineering. Journal of Zhejiang University SCIENCE B. 2010;11:524-30.
[158] Mart ńez A, Blanco MD, Davidenko N, Cameron RE. Tailoring chitosan/collagen scaffolds for tissue engineering: Effect of composition and different crosslinking agents on scaffold properties. Carbohydrate Polymers. 2015;132:606-19.
[159] Gingras M, Paradis I, Berthod F. Nerve regeneration in a collagen–chitosan tissue-engineered skin transplanted on nude mice. Biomaterials. 2003;24:1653-61.
[160] Hamidi M, Azadi A, Rafiei P. Hydrogel nanoparticles in drug delivery. Advanced drug delivery reviews. 2008;60:1638-49.
[161] Wichterle O, Lim D. Hydrophilic gels for biological use. Nature. 1960;185:117-8.

[162] Hoffman AS. Hydrogels for biomedical applications. Advanced drug delivery reviews. 2012;64:18-23.
[163] Deng C, Zhang PC, Vulesevic B, Kuraitis D, Li FF, Yang AF, et al. A Collagen-Chitosan Hydrogel for Endothelial Differentiation and Angiogenesis. Tissue Engineering Part A. 2010;16:3099-109.
[164] McBane JE, Vulesevic B, Padavan DT, McEwan KA, Korbutt GS, Suuronen EJ. Evaluation of a Collagen-Chitosan Hydrogel for Potential Use as a Pro-Angiogenic Site for Islet Transplantation. Plos One. 2013;8.
[165] Fiejdasz S, Szczubiałka K, Lewandowska-Łańcucka J, Osyczka AM, Nowakowska M. Biopolymer-based hydrogels as injectable materials for tissue repair scaffolds. Biomedical Materials. 2013;8:035013.
[166] Shanmugasundaram N, Ravichandran P, Neelakanta Reddy P, Ramamurty N, Pal S, Panduranga Rao K. Collagen–chitosan polymeric scaffolds for the in vitro culture of human epidermoid carcinoma cells. Biomaterials. 2001;22:1943-51.
[167] Zhu C, Fan D, Wang Y. Human-like collagen/hyaluronic acid 3D scaffolds for vascular tissue engineering. Materials Science and Engineering: C. 2014;34:393-401.
[168] Hu K, Cui F, Lv Q, Ma J, Feng Q, Xu L, et al. Preparation of fibroin/recombinant human‐like collagen scaffold to promote fibroblasts compatibility. Journal of Biomedical Materials Research Part A. 2008;84:483-90.
[169] Yaari A, Schilt Y, Tamburu C, Raviv U, Shoseyov O. Wet Spinning and Drawing of Human Recombinant Collagen. ACS Biomaterials Science & Engineering. 2016;2:349-60.
[170] Hu K, Cui F, Lv Q, Ma J, Feng Q, Xu L, et al. Preparation of fibroin/recombinant human-like collagen scaffold to promote fibroblasts compatibility. Journal of Biomedical Materials Research Part A. 2008;84A:483-90.
[171] Jia L, Duan Z, Fan D, Mi Y, Hui J, Chang L. Human-like collagen/nano-hydroxyapatite scaffolds for the culture of chondrocytes. Materials Science and Engineering: C. 2013;33:727-34.
[172] State Food and Drug Administration Device (Approved) No. 2007 No. 3460510.
[173] Wang X, Ghasri P, Amir M, Hwang B, Hou Y, Khilili M, et al. Topical Application of Recombinant Type VII Collagen Incorporates Into the Dermal–Epidermal Junction and Promotes Wound Closure. Molecular Therapy. 2013;21:1335-44.
[174] Zhu C, Chen Y, Deng J, Xue W, Ma X, Hui J, et al. Preparation, characterization, and bioavailability of a phosphorylated human-like collagen calcium complex. Polymers for Advanced Technologies. 2015;26:1217-25.
[175] Merrett K, Fagerholm P, McLaughlin CR, Dravida S, Lagali N, Shinozaki N, et al. Tissue-engineered recombinant human collagen-based corneal substitutes for implantation: performance of type I versus type III collagen. Investigative ophthalmology & visual science. 2008;49:3887-94.
[176] Zhao L, Li X, Zhao J, Ma S, Ma X, Fan D, et al. A novel smart injectable hydrogel prepared by microbial transglutaminase and human-like collagen: Its characterization and biocompatibility. Materials Science and Engineering: C. 2016;68:317-26.
[177] Pramanik K, Ieee. Biomaterials for Tissue Engineered Scaffolds. 2010 Advanced Technologies for Enhancing Quality of Life (at-Equal). 2010:93-9.
[178] Whang K, Thomas CH, Healy KE, Nuber G. A novel method to fabricate bioabsorbable scaffolds Polymer. 1995;36:837-42.
[179] Pan Z, Ding J. Poly(lactide-co-glycolide) porous scaffolds for tissue engineering and regenerative medicine. Interface Focus. 2012;2:366-77.
[180] Mikos AG, Temenoff JS. Formation of highly porous biodegradable scaffolds for tissue engineering. EJB Electronic Journal of Biotechnology. 2000;3:1-12.
[181] Sieminski AL, Gooch KJ. Biomaterial–microvasculature interactions. Biomaterials. 2000;21:2233-41.
[182] Yin H-M, Li X, Xu J-Z, Zhao B, Li J-H, Li Z-M. Highly aligned and interconnected porous poly(ε-caprolactone) scaffolds derived from co-continuous polymer blends. Materials & Design. 2017;128:112-8.
[183] Brauker JH, Carr‐Brendel VE, Martinson LA, Crudele J, Johnston WD, Johnson RC. Neovascularization of synthetic membranes directed by membrane microarchitecture. Journal of Biomedical Materials Research Part A. 1995;29:1517-24.
[184] Mandal BB, Kundu SC. Cell proliferation and migration in silk fibroin 3D scaffolds. Biomaterials. 2009;30:2956-65.
[185] Yannas IV, Lee E, Orgill DP, Skrabut EM, Murphy GF. Synthesis and characterization of a

model extracellular-matrix that induces partial regeneration of adult mammalian skin. Proceedings of the National Academy of Sciences of the United States of America. 1989;86:933-7.
[186] Lien S-M, Ko L-Y, Huang T-J. Effect of pore size on ECM secretion and cell growth in gelatin scaffold for articular cartilage tissue engineering. Acta biomaterialia. 2009;5:670-9.
[187] Doillon CJ, Whyne CF, Brandwein S, Silver FH. Collagen-based wound dressing - control of the pores structure and morphology. Journal of Biomedical Materials Research. 1986;20:1219-28.
[188] Leong KF, Cheah CM, Chua CK. Solid freeform fabrication of three-dimensional scaffolds for engineering replacement tissues and organs. Biomaterials. 2003;24:2363-78.
[189] Leong KF, Chua CK, Sudarmadji N, Yeong WY. Engineering functionally graded tissue engineering scaffolds. Journal of the Mechanical Behavior of Biomedical Materials. 2008;1:140-52.
[190] Schrader J, Gordon-Walker TT, Aucott RL, van Deemter M, Quaas A, Walsh S, et al. Matrix Stiffness Modulates Proliferation, Chemotherapeutic Response and Dormancy in Hepatocellular Carcinoma Cells. Hepatology (Baltimore, Md). 2011;53:1192-205.
[191] Mason BN, Califano JP, Reinhart-King CA. Matrix Stiffness: A Regulator of Cellular Behavior and Tissue Formation. In: Bhatia SK, editor. Engineering Biomaterials for Regenerative Medicine: Novel Technologies for Clinical Applications. New York, NY: Springer New York; 2012. p. 19-37.
[192] Haugh MG, Murphy CM, McKiernan RC, Altenbuchner C, O'Brien FJ. Crosslinking and Mechanical Properties Significantly Influence Cell Attachment, Proliferation, and Migration Within Collagen Glycosaminoglycan Scaffolds. Tissue Engineering Part A. 2011;17:1201-8.
[193] Liu F, Mih JD, Shea BS, Kho AT, Sharif AS, Tager AM, et al. Feedback amplification of fibrosis through matrix stiffening and COX-2 suppression. The Journal of Cell Biology. 2010;190:693.
[194] Banerjee A, Arha M, Choudhary S, Ashton RS, Bhatia SR, Schaffer DV, et al. The Influence of Hydrogel Modulus on the Proliferation and Differentiation of Encapsulated Neural Stem Cells. Biomaterials. 2009;30:4695-9.
[195] O'Brien FJ. Biomaterials & scaffolds for tissue engineering. Materials Today. 2011;14:88-95.
[196] Keane TJ, Badylak SF. Biomaterials for tissue engineering applications. Seminars in Pediatric Surgery. 2014;23:112-8.
[197] Lu L, Peter SJ, D. Lyman M, Lai H-L, Leite SM, Tamada JA, et al. In vitro and in vivo degradation of porous poly(dl-lactic-co-glycolic acid) foams. Biomaterials. 2000;21:1837-45.
[198] Sung H-J, Meredith C, Johnson C, Galis ZS. The effect of scaffold degradation rate on three-dimensional cell growth and angiogenesis. Biomaterials. 2004;25:5735-42.
[199] Liu YW, Gan LH, Carlsson DJ, Fagerholm P, Lagali N, Watsky MA, et al. A simple, cross-linked collagen tissue substitute for corneal implantation. Investigative Ophthalmology & Visual Science. 2006;47:1869-75.
[200] Ma L, Gao CY, Mao ZW, Shen JC, Hu XQ, Han CM. Thermal dehydration treatment and glutaraldehyde cross-linking to increase the biostability of collagen-chitosan porous scaffolds used as dermal equivalent. Journal of Biomaterials Science-Polymer Edition. 2003;14:861-74.
[201] Kawase M, Michibayashi N, Nakashima Y, Kurikawa N, MIZOGUCHI T. Application of glutaraldehyde-crosslinked chitosan as a scaffold for hepatocyte attachment. Biological and Pharmaceutical Bulletin. 1997;20:708-10.
[202] Mirzaei B E, Ramazani S. A A, Shafiee M, Danaei M. Studies on Glutaraldehyde Crosslinked Chitosan Hydrogel Properties for Drug Delivery Systems. International Journal of Polymeric Materials and Polymeric Biomaterials. 2013;62:605-11.
[203] Sisson K, Zhang C, Farach-Carson MC, Chase DB, Rabolt JF. Evaluation of Cross-Linking Methods for Electrospun Gelatin on Cell Growth and Viability. Biomacromolecules. 2009;10:1675-80.
[204] Sung HW, Huang RN, Huang LLH, Tsai CC. In vitro evaluation of cytotoxicity of a naturally occurring cross-linking reagent for biological tissue fixation. Journal of Biomaterials Science-Polymer Edition. 1999;10:63-78.
[205] Wang X, Zhai W, Wu C, Ma B, Zhang J, Zhang H, et al. Procyanidins-crosslinked aortic elastin scaffolds with distinctive anti-calcification and biological properties. Acta biomaterialia. 2015;16:81-93.
[206] Tan H, Marra KG. Injectable, biodegradable hydrogels for tissue engineering applications. Materials. 2010;3:1746-67.
[207] Varghese S, Elisseeff JH. Hydrogels for musculoskeletal tissue engineering. Polymers for regenerative medicine: Springer; 2006. p. 95-144.

[208] Zhu J, Marchant RE. Design properties of hydrogel tissue-engineering scaffolds. Expert review of medical devices. 2011;8:607-26.
[209] Zhu J, Tang C, Kottke-Marchant K, Marchant RE. Design and synthesis of biomimetic hydrogel scaffolds with controlled organization of cyclic RGD peptides. Bioconjugate chemistry. 2009;20:333.
[210] Park CH, Hong YJ, Park K, Han DK. Peptide-grafted lactide-based poly (ethylene glycol) porous scaffolds for specific cell adhesion. Macromolecular research. 2010;18:526-32.
[211] Yun Y-R, Won JE, Jeon E, Lee S, Kang W, Jo H, et al. Fibroblast Growth Factors: Biology, Function, and Application for Tissue Regeneration. Journal of Tissue Engineering. 2010;2010:218142.
[212] Veilleux N, Spector M. Effects of FGF-2 and IGF-1 on adult canine articular chondrocytes in type II collagen–glycosaminoglycan scaffolds in vitro. Osteoarthritis and Cartilage. 2005;13:278-86.
[213] In Jeong S, Kim SY, Cho SK, Chong MS, Kim KS, Kim H, et al. Tissue-engineered vascular grafts composed of marine collagen and PLGA fibers using pulsatile perfusion bioreactors. Biomaterials. 2007;28:1115-22.
[214] Guo R, Xu S, Ma L, Huang A, Gao C. The healing of full-thickness burns treated by using plasmid DNA encoding VEGF-165 activated collagen-chitosan dermal equivalents. Biomaterials. 2011;32:1019-31.
[215] Doillon CJ, Silver FH. Collagen-based wound dressing - effects of hyaluronic - acid and fibronectin on wound-healing. Biomaterials. 1986;7:3-8.
[216] Babensee JE, Anderson JM, McIntire LV, Mikos AG. Host response to tissue engineered devices. Advanced drug delivery reviews. 1998;33:111-39.
[217] Kumbar SG, Nukavarapu SP, James R, Nair LS, Laurencin CT. Electrospun poly(lactic acid-co-glycolic acid) scaffolds for skin tissue engineering. Biomaterials. 2008;29:4100-7.
[218] Li WJ, Laurencin CT, Caterson EJ, Tuan RS, Ko FK. Electrospun nanofibrous structure: A novel scaffold for tissue engineering. Journal of Biomedical Materials Research. 2002;60:613-21.
[219] Pham QP, Sharma U, Mikos AG. Electrospinning of polymeric nanofibers for tissue engineering applications: a review. Tissue engineering. 2006;12:1197-211.
[220] Matthews JA, Wnek GE, Simpson DG, Bowlin GL. Electrospinning of collagen nanofibers. Biomacromolecules. 2002;3:232-8.
[221] Duan B, Wu L, Li X, Yuan X, Li X, Zhang Y, et al. Degradation of electrospun PLGA-chitosan/PVA membranes and their cytocompatibility in vitro. Journal of Biomaterials Science, Polymer Edition. 2007;18:95-115.
[222] Li C, Vepari C, Jin H-J, Kim HJ, Kaplan DL. Electrospun silk-BMP-2 scaffolds for bone tissue engineering. Biomaterials. 2006;27:3115-24.
[223] Heydarkhan-Hagvall S, Schenke-Layland K, Dhanasopon AP, Rofail F, Smith H, Wu BM, et al. Three-dimensional electrospun ECM-based hybrid scaffolds for cardiovascular tissue engineering. Biomaterials. 2008;29:2907-14.
[224] Sakai R, John B, Okamoto M, Seppälä JV, Vaithilingam J, Hussein H, et al. Fabrication of Polylactide‐Based Biodegradable Thermoset Scaffolds for Tissue Engineering Applications. Macromolecular Materials and Engineering. 2013;298:45-52.
[225] Annabi N, Nichol JW, Zhong X, Ji C, Koshy S, Khademhosseini A, et al. Controlling the Porosity and Microarchitecture of Hydrogels for Tissue Engineering. Tissue Engineering Part B, Reviews. 2010;16:371-83.
[226] Ma PX. Scaffolds for tissue fabrication. Materials Today. 2004;7:30-40.
[227] O'Brien FJ, Harley BA, Yannas IV, Gibson L. Influence of freezing rate on pore structure in freeze-dried collagen-GAG scaffolds. Biomaterials. 2004;25:1077-86.
[228] Schoof H, Apel J, Heschel I, Rau G. Control of pore structure and size in freeze-dried collagen sponges. Journal of Biomedical Materials Research. 2001;58:352-7.
[229] Davidenko N, Gibb T, Schuster C, Best SM, Campbell JJ, Watson CJ, et al. Biomimetic collagen scaffolds with anisotropic pore architecture. Acta biomaterialia. 2012;8:667-76.
[230] O'Brien FJ, Harley BA, Yannas IV, Gibson LJ. The effect of pore size on cell adhesion in collagen-GAG scaffolds. Biomaterials. 2005;26:433-41.
[231] Nam YS, Park TG. Porous biodegradable polymeric scaffolds prepared by thermally induced phase separation. Journal of Biomedical Materials Research. 1999;47:8-17.
[232] Nam YS, Yoon JJ, Park TG. A novel fabrication method of macroporous biodegradable polymer scaffolds using gas foaming salt as a porogen additive. Journal of Biomedical Materials

Research. 2000;53:1-7.
[233] Mooney DJ, Baldwin DF, Suh NP, Vacanti LP, Langer R. Novel approach to fabricate porous sponges of poly(D,L-lactic-co-glycolic acid) without the use of organic solvents. Biomaterials. 1996;17:1417-22.
[234] Das S, Hollister SJ, Flanagan C, Adewunmi A, Bark K, Chen C, et al. Freeform fabrication of Nylon-6 tissue engineering scaffolds. Rapid Prototyping Journal. 2003;9:43-9.
[235] Wilson WC, Boland T. Cell and organ printing 1: Protein and cell printers. Anatomical Record Part a-Discoveries in Molecular Cellular and Evolutionary Biology. 2003;272A:491-6.
[236] Landers R, Pfister A, Hübner U, John H, Schmelzeisen R, Mülhaupt R. Fabrication of soft tissue engineering scaffolds by means of rapid prototyping techniques. Journal of materials science. 2002;37:3107-16.
[237] Nicodemus GD, Bryant SJ. Cell Encapsulation in Biodegradable Hydrogels for Tissue Engineering Applications. Tissue Engineering Part B, Reviews. 2008;14:149-65.
[238] Johnson FA, Craig DQM, Mercer AD. Characterization of the block structure and molecular weight of sodium alginates. Journal of Pharmacy and Pharmacology. 1997;49:639-43.
[239] Smidsrød O, Skja˚k-Br1k G. Alginate as immobilization matrix for cells. Trends in Biotechnology. 1990;8:71-8.
[240] Damink LHHO, Dijkstra PJ, van Luyn MJA, van Wachem PB, Nieuwenhuis P, Feijen J. In vitro degradation of dermal sheep collagen cross-linked using a water-soluble carbodiimide. Biomaterials. 1996;17:679-84.
[241] Ji C, Annabi N, Khademhosseini A, Dehghani F. Fabrication of porous chitosan scaffolds for soft tissue engineering using dense gas CO2. Acta biomaterialia. 2011;7:1653-64.
[242] Ma L. Collagen/chitosan porous scaffolds with improved biostability for skin tissue engineering. Biomaterials. 2003;24:4833-41.
[243] Perez-Puyana V, Romero A, Guerrero A. Influence of collagen concentration and glutaraldehyde on collagen-based scaffold properties. Journal of Biomedical Materials Research Part A. 2016;104:1462-8.
[244] Tierney CM, Haugh MG, Liedl J, Mulcahy F, Hayes B, O'Brien FJ. The effects of collagen concentration and crosslink density on the biological, structural and mechanical properties of collagen-GAG scaffolds for bone tissue engineering. Journal of the Mechanical Behavior of Biomedical Materials. 2009;2:202-9.
[245] Offeddu GS, Ashworth JC, Cameron RE, Oyen ML. Multi-scale mechanical response of freeze-dried collagen scaffolds for tissue engineering applications. Journal of the Mechanical Behavior of Biomedical Materials. 2015;42:19-25.
[246] Searles JA, Carpenter JF, Randolph TW. Annealing to optimize the primary drying rate, reduce freezing-induced drying rate heterogeneity, and determine T-g ' in pharmaceutical lyophilization. Journal of Pharmaceutical Sciences. 2001;90:872-87.
[247] Freed LE, Vunjaknovakovic G, Biron RJ, Eagles DB, Lesnoy DC, Barlow SK, et al. Biodegradable polymer scaffolds for tissue engineering. Bio-Technology. 1994;12:689-93.
[248] Reis LA, Chiu LLY, Liang Y, Hyunh K, Momen A, Radisic M. A peptide-modified chitosan–collagen hydrogel for cardiac cell culture and delivery. Acta biomaterialia. 2012;8:1022-36.
[249] Chiu LLY, Radisic M. Controlled release of thymosin beta 4 using collagen-chitosan composite hydrogels promotes epicardial cell migration and angiogenesis. Journal of Controlled Release. 2011;155:376-85.
[250] Sionkowska A, Skopinska-Wisniewska J, Gawron M, Kozlowska J, Planecka A. Chemical and thermal cross-linking of collagen and elastin hydrolysates. International Journal of Biological Macromolecules. 2010;47:570-7.
[251] Wang XH, Li DP, Wang WJ, Feng QL, Cui FZ, Xu YX, et al. Crosslinked collagen/chitosan matrix for artificial livers. Biomaterials. 2003;24:3213-20.
[252] Garcia Y, Collighan R, Griffin M, Pandit A. Assessment of cell viability in a three-dimensional enzymatically cross-linked collagen scaffold. Journal of Materials Science: Materials in Medicine. 2007;18:1991-2001.
[253] Staroszczyk H, Sztuka K, Wolska J, Wojtasz-Pająk A, Kołodziejska I. Interactions of fish gelatin and chitosan in uncrosslinked and crosslinked with EDC films: FT-IR study. Spectrochimica Acta Part A: Molecular and Biomolecular Spectroscopy. 2014;117:707-12.
[254] Kuijpers AJ, Engbers GHM, Krijgsveld J, Zaat SAJ, Dankert J, Feijen J. Cross-linking and characterisation of gelatin matrices for biomedical applications. Journal of Biomaterials Science, Polymer Edition. 2000;11:225-43.

[255] McEwan K, Padavan DT, Ellis C, McBane JE, Vulesevic B, Korbutt GS, et al. Collagen-chitosan-laminin hydrogels for the delivery of insulin-producing tissue. Journal of Tissue Engineering and Regenerative Medicine. 2016;10:E397-E408.
[256] Wang L, Stegemann JP. Thermogelling chitosan and collagen composite hydrogels initiated with β-glycerophosphate for bone tissue engineering. Biomaterials. 2010;31:3976-85.
[257] Chen T, Embree HD, Brown EM, Taylor MM, Payne GF. Enzyme-catalyzed gel formation of gelatin and chitosan: potential for in situ applications. Biomaterials. 2003;24:2831-41.
[258] Shung AK, Behravesh E, Jo S, Mikos AG. Crosslinking characteristics of and cell adhesion to an injectable poly(propylene fumarate-co-ethylene glycol) hydrogel using a water-soluble crosslinking system. Tissue Engineering. 2003;9:243-54.
[259] Yang Y-l, Motte S, Kaufman LJ. Pore size variable type I collagen gels and their interaction with glioma cells. Biomaterials. 2010;31:5678-88.
[260] Wood GC, Keech MK. The formation of fibrils from collagen solutions 1. The effect of experimental conditions: kinetic and electron-microscope studies. Biochemical Journal. 1960;75:588-98.
[261] Bigi A, Cojazzi G, Panzavolta S, Rubini K, Roveri N. Mechanical and thermal properties of gelatin films at different degrees of glutaraldehyde crosslinking. Biomaterials. 2001;22:763-8.
[262] Gupta KC, Jabrail FH. Glutaraldehyde and glyoxal cross-linked chitosan microspheres for controlled delivery of centchroman. Carbohydrate Research. 2006;341:744-56.
[263] Trifkovic K, Milasinovic N, Djordjevic V, Zdunic G, Krusic MK, Knezevic-Jugovic Z, et al. Chitosan crosslinked microparticles with encapsulated polyphenols: Water sorption and release properties. Journal of Biomaterials Applications. 2015;30:618-31.
[264] Rehakova M, Bakos D, Vizarova K, Soldan M, Jurickova M. Properties of collagen and hyaluronic acid composite materials and their modification by chemical crosslinking. Journal of Biomedical Materials Research. 1996;30:369-72.
[265] Kim U-J, Park J, Joo Kim H, Wada M, Kaplan DL. Three-dimensional aqueous-derived biomaterial scaffolds from silk fibroin. Biomaterials. 2005;26:2775-85.
[266] Zhai WY, Chang J, Lin KL, Wang JY, Zhao Q, Sun XN. Crosslinking of decellularized porcine heart valve matrix by procyanidins. Biomaterials. 2006;27:3684-90.
[267] Yahyouche A, Zhidao X, Czernuszka JT, Clover AJP. Macrophage-mediated degradation of crosslinked collagen scaffolds. Acta biomaterialia. 2011;7:278-86.
[268] Lin Y-C, Tan F-j, Marra KG, Jan S-S, Liu D-C. Synthesis and characterization of collagen/hyaluronan/chitosan composite sponges for potential biomedical applications. Acta biomaterialia. 2009;5:2591-600.
[269] Tan W, Krishnaraj R, Desai TA. Evaluation of nanostructured composite collagen-chitosan matrices for tissue engineering. Tissue Engineering. 2001;7:203-10.
[270] Schiffman JD, Schauer CL. Cross-linking chitosan nanofibers. Biomacromolecules. 2007;8:594-601.
[271] Foda NH, El-laithy HM, Tadros MI. Optimization of biodegradable sponges as controlled release drug matrices. I. Effect of moisture level on chitosan sponge mechanical properties. Drug Development and Industrial Pharmacy. 2004;30:369-79.
[272] Mitra T, Sailakshmi G, Gnanamani A, Mandal AB. Studies on Cross-linking of Succinic Acid with Chitosan/Collagen. Materials Research-Ibero-American Journal of Materials. 2013;16:755-65.
[273] Fung YC. Elasticity of soft tissues in simple elongation. American journal of physiology. 1967;213:1532-44.
[274] Li C, Wang L, Yang Z, Kim G, Chen H, Ge Z. A Viscoelastic Chitosan-Modified Three-Dimensional Porous Poly(L-Lactide-co-epsilon-Caprolactone) Scaffold for Cartilage Tissue Engineering. Journal of Biomaterials Science-Polymer Edition. 2012;23:405-24.
[275] Van Loocke M, Lyons CG, Simms CK. Viscoelastic properties of passive skeletal muscle in compression: Stress-relaxation behaviour and constitutive modelling. Journal of Biomechanics. 2008;41:1555-66.
[276] Ratakonda S, Sridhar UM, Rhinehart RR, Madihally SV. Assessing viscoelastic properties of chitosan scaffolds and validation with cyclical tests. Acta biomaterialia. 2012;8:1566-75.
[277] Liang WH, Kienitz BL, Penick KJ, Welter JF, Zawodzinski TA, Baskaran H. Concentrated collagen-chondroitin sulfate scaffolds for tissue engineering applications. Journal of Biomedical Materials Research Part A. 2010;94A:1050-60.
[278] Harley BA, Leung JH, Silva ECCM, Gibson LJ. Mechanical characterization of collagen–glycosaminoglycan scaffolds. Acta biomaterialia. 2007;3:463-74.

[279] Deville S, Saiz E, Tomsia AP. Freeze casting of hydroxyapatite scaffolds for bone tissue engineering. Biomaterials. 2006;27:5480-9.
[280] Raftery RM, Woods B, Marques ALP, Moreira-Silva J, Silva TH, Cryan S-A, et al. Multifunctional biomaterials from the sea: Assessing the effects of chitosan incorporation into collagen scaffolds on mechanical and biological functionality. Acta biomaterialia. 2016;43:160-9.
[281] Kalra A LA, Al-Jumaily AM. Mechanical Behaviour of Skin: A Review. Journal of Material Science & Engineering. 2016;5:254.
[282] Ahima RS, Flier JS. Adipose tissue as an endocrine organ. Trends in Endocrinology and Metabolism. 2000;11:327-32.
[283] Samani A, Plewes D. A method to measure the hyperelastic parameters of ex vivo breast tissue samples. Physics in Medicine and Biology. 2004;49:4395-405.
[284] Patel PN, Smith CK, Patrick CW. Rheological and recovery properties of poly(ethylene glycol) diacrylate hydrogels and human adipose tissue. Journal of Biomedical Materials Research Part A. 2005;73A:313-9.
[285] Miller K, Chinzei K. Constitutive modelling of brain tissue: Experiment and theory. Journal of Biomechanics. 1997;30:1115-21.
[286] Kumaresan S, Radhakrishnan S. Importance of partitioning membranes of the brain and the influence of the neck in head injury modelling. Medical & Biological Engineering & Computing. 1996;34:27-32.
[287] Sarron J-C, Blondeau C, Guillaume A, Osmont D. Identification of linear viscoelastic constitutive models. Journal of Biomechanics. 2000;33:685-93.
[288] Keogh MB, O'Brien FJ, Daly JS. Substrate stiffness and contractile behaviour modulate the functional maturation of osteoblasts on a collagen–GAG scaffold. Acta biomaterialia. 2010;6:4305-13.
[289] Holzapfel GA. Biomechanics of soft tissue. The handbook of materials behavior models. 2001;3:1049-63.
[290] Chen CS, Yannas IV, Spector M. Pore strain behaviour of collagen-glycosaminoglycan analogues of extracellular matrix. Biomaterials. 1995;16:777-83.
[291] Robi K, Jakob N, Matevz K, Matjaz V. The physiology of sports injuries and repair processes. Current issues in sports and exercise medicine. 2013:43-86.
[292] Lin YC, Tan FJ, Marra KG, Jan SS, Liu DC. Synthesis and characterization of collagen/hyaluronan/chitosan composite sponges for potential biomedical applications. Acta biomaterialia. 2009;5:2591-600.
[293] Parlato M, Reichert S, Barney N, Murphy WL. Poly(ethylene glycol) Hydrogels with Adaptable Mechanical and Degradation Properties for Use in Biomedical Applications(). Macromolecular bioscience. 2014;14:687-98.
[294] Lyshchik A, Higashi T, Asato R, Tanaka S, Ito J, Hiraoka M, et al. Elastic moduli of thyroid tissues under compression. Ultrasonic Imaging. 2005;27:101-10.
[295] Yeh WC, Li PC, Jeng YM, Hsu HC, Kuo PL, Li ML, et al. Elastic modulus measurements of human liver and correlation with pathology. Ultrasound in Medicine and Biology. 2002;28:467-74.
[296] Levental I, Georges PC, Janmey PA. Soft biological materials and their impact on cell function. Soft Matter. 2007;3:299-306.
[297] Zhang J, Zhou A, Deng A, Yang Y, Gao L, Zhong Z, et al. Pore architecture and cell viability on freeze dried 3D recombinant human collagen-peptide (RHC)–chitosan scaffolds. Materials Science and Engineering: C. 2015;49:174-82.
[298] Tomihata K, Burczak K, Shiraki K, Ikada Y. Cross-linking and biodegradation of native and denatured collagen. In: Shalaby SW, Ikada Y, Langer R, Williams J, editors. Polymers of Biological and Biomedical Significance1994. p. 275-86.
[299] Zhai W, Chang J, Lue X, Wang Z. Procyanidins-Crosslinked Heart Valve Matrix: Anticalcification Effect. Journal of Biomedical Materials Research Part B-Applied Biomaterials. 2009;90B:913-21.
[300] Huang C-H, Chi C-Y, Chen Y-S, Chen K-Y, Chen P-L, Yao C-H. Evaluation of proanthocyanidin-crosslinked electrospun gelatin nanofibers for drug delivering system. Materials Science and Engineering: C. 2012;32:2476-83.
[301] Khanna S, Venojarvi M, Roy S, Sharma N, Trikha P, Bagchi D, et al. Dermal wound healing properties of redox-active grape seed proanthocyanidins. Free Radical Biology and Medicine. 2002;33:1089-96.
[302] Tierney CM, Haugh MG, Liedl J, Mulcahy F, Hayes B, O'Brien FJ. The effects of collagen

concentration and crosslink density on the biological, structural and mechanical properties of collagen-GAG scaffolds for bone tissue engineering. Journal of the Mechanical Behavior of Biomedical Materials. 2009;2:202-9.
[303] Reinhart-King CA, Dembo M, Hammer DA. Cell-Cell Mechanical Communication through Compliant Substrates. Biophysical Journal. 2008;95:6044-51.
[304] Califano JP, Reinhart-King CA. A Balance of Substrate Mechanics and Matrix Chemistry Regulates Endothelial Cell Network Assembly. Cellular and Molecular Bioengineering. 2008;1:122.
[305] Back SA, Khan R, Gan X, Rosenberg PA, Volpe JJ. A new Alamar Blue viability assay to rapidly quantify oligodendrocyte death. Journal of Neuroscience Methods. 1999;91:47-54.
[306] Page B, Page M, Noel C. A new fluorometric assay for cytotoxicity measurements in-vitro. International Journal of Oncology. 1993;3:473-6.
[307] Kievit FM, Florczyk SJ, Leung M, Veiseh O, Park JO, Disis ML, et al. Chitosan-alginate 3D scaffolds as a mimic of the glioma tumor microenvironment. Biomaterials. 2010;31:5903-10.
[308] Adhikari U, Rijal NP, Khanal S, Pai D, Sankar J, Bhattarai N. Magnesium incorporated chitosan based scaffolds for tissue engineering applications. Bioactive Materials. 2016;1:132-9.
[309] Ucar S, Ermis M, Hasirci N. Modified chitosan scaffolds: Proliferative, cytotoxic, apoptotic, and necrotic effects on Saos-2 cells and antimicrobial effect on Escherichia coli. Journal of Bioactive and Compatible Polymers. 2016;31:304-19.
[310] Baktur R, Yoon SH, Kwon S. Effects of Multiwalled Carbon Nanotube Reinforced Collagen Scaffolds on the Osteogenic Differentiation of Mesenchymal Stem Cells. Journal of Nanomaterials. 2013.
[311] Unsworth JM, Rose F, Wright E, Scotchford CA, Shakesheff KM. Seeding cells into needled felt scaffolds for tissue engineering applications. Journal of Biomedical Materials Research Part A. 2003;66A:425-31.
[312] Jones LJ, Gray M, Yue ST, Haugland RP, Singer VL. Sensitive determination of cell number using the CyQUANT® cell proliferation assay. Journal of Immunological Methods. 2001;254:85-98.
[313] Blaheta RA, Kronenberger B, Woitaschek D, Weber S, Scholz M, Schuldes H, et al. Development of an ultrasensitive in vitro assay to monitor growth of primary cell cultures with reduced mitotic activity. Journal of Immunological Methods. 1998;211:159-69.
[314] Quent VMC, Loessner D, Friis T, Reichert JC, Hutmacher DW. Discrepancies between metabolic activity and DNA content as tool to assess cell proliferation in cancer research. Journal of Cellular and Molecular Medicine. 2010;14:1003-13.
[315] Petersen A, Joly P, Bergmann C, Korus G, Duda GN. The Impact of Substrate Stiffness and Mechanical Loading on Fibroblast-Induced Scaffold Remodeling. Tissue Engineering Part A. 2012;18:1804-17.
[316] Yeung T, Georges PC, Flanagan LA, Marg B, Ortiz M, Funaki M, et al. Effects of substrate stiffness on cell morphology, cytoskeletal structure, and adhesion. Cell Motility and the Cytoskeleton. 2005;60:24-34.
[317] Paszek MJ, Zahir N, Johnson KR, Lakins JN, Rozenberg GI, Gefen A, et al. Tensional homeostasis and the malignant phenotype. Cancer Cell. 2005;8:241-54.
[318] Lo CM, Wang HB, Dembo M, Wang YL. Cell movement is guided by the rigidity of the substrate. Biophysical Journal. 2000;79:144-52.
[319] Wang HB, Dembo M, Wang YL. Substrate flexibility regulates growth and apoptosis of normal but not transformed cells. American Journal of Physiology-Cell Physiology. 2000;279:C1345-C50.
[320] Patnaik SS, Wang B, Weed B, Wertheim JA, Liao J. Decellularized Scaffolds: Concepts, Methodologies, and Applications in Cardiac Tissue Engineering and Whole-Organ Regeneration. Tissue Regeneration Where Nano-Structure Meets Biology: World Scientific Publication Company; 2014. p. 77-124.
[321] Khosro A, Shadi Y, Solmaz Maleki D. Pharmaceutical and Medical Applications of Nanofibers. In: Raj KK, Anil KS, Rajesh Kumar K, editors. Novel Approaches for Drug Delivery. Hershey, PA, USA: IGI Global; 2017. p. 338-63.
[322] Georges PC, Janmey PA. Cell type-specific response to growth on soft materials. Journal of Applied Physiology. 2005;98:1547-53.
[323] Wang YK, Wang YH, Wang CZ, Sung JM, Chiu WT, Lin SH, et al. Rigidity of collagen fibrils controls collagen gel-induced down-regulation of focal adhesion complex proteins mediated by alpha(2)beta(1) integrin. Journal of Biological Chemistry. 2003;278:21886-92.

[324] Wang T-W, Sun J-S, Huang Y-C, Wu H-C, Chen L-T, Lin F-H. Skin basement membrane and extracellular matrix proteins characterization and quantification by real time RT-PCR. Biomaterials. 2006;27:5059-68.
[325] Ralston DR, Layton C, Dalley AJ, Boyce SG, Freedlander E, Mac Neil S. The requirement for basement membrane antigens in the production of human epidermal/dermal composites in vitro. British Journal of Dermatology. 1999;140:605-15.
[326] Amano S, Akutsu N, Matsunaga Y, Kadoya K, Nishiyama T, Champliaud M-F, et al. Importance of Balance between Extracellular Matrix Synthesis and Degradation in Basement Membrane Formation. Experimental Cell Research. 2001;271:249-62.
[327] Xue M, Jackson CJ. Extracellular Matrix Reorganization During Wound Healing and Its Impact on Abnormal Scarring. Advances in Wound Care. 2015;4:119-36.
[328] Gay S, Vijanto J, Raekallio J, Penttinen R. Collagen types in early phases of wound healing in children. Acta chirurgica Scandinavica. 1977;144:205-11.
[329] Cukierman E, Pankov R, Stevens DR, Yamada KM. Taking cell-matrix adhesions to the third dimension. Science. 2001;294:1708-12.
[330] Mooney D, Hansen L, Vacanti J, Langer R, Farmer S, Ingber D. Switching from differentiation to growth in hepatocytes - control by extracellular-matrix. Journal of Cellular Physiology. 1992;151:497-505.
[331] Hansen LK, Mooney DJ, Vacanti JP, Ingber DE. Integrin binding and cell spreading on extracellular matrix act at different points in the cell cycle to promote hepatocyte growth. Molecular Biology of the Cell. 1994;5:967-75.
[332] Gaudet C, Marganski WA, Kim S, Brown CT, Gunderia V, Dembo M, et al. Influence of Type I Collagen Surface Density on Fibroblast Spreading, Motility, and Contractility. Biophysical Journal. 2003;85:3329-35.
[333] Akiyama SK, Yamada KM. The interaction of plasma fibronectin with fibroblastic cells in suspension. Journal of Biological Chemistry. 1985;260:4492-500.
[334] Di Lullo GA, Sweeney SM, Korkko J, Ala-Kokko L, San Antonio JD. Mapping the ligand-binding sites and disease-associated mutations on the most abundant protein in the human, type I collagen. Journal of Biological Chemistry. 2002;277:4223-31.
[335] Lauffenburger DA, Linderman J. Receptors: models for binding, trafficking, and signaling: Oxford University Press; 1993.
[336] Lin HB, Sun W, Mosher DF, Garciaecheverria C, Schaufelberger K, Lelkes PI, et al. Synthesis, surface, and cell-adhesion properties of polyurethanes containing covalently grafted RGD-peptides. Journal of Biomedical Materials Research. 1994;28:329-42.
[337] Chen CS, Mrksich M, Huang S, Whitesides GM, Ingber DE. Geometric control of cell life and death. Science. 1997;276:1425-8.
[338] Ingber DE, Prusty D, Frangioni JV, Cragoe EJ, Lechene C, Schwartz MA. Control of intracellular pH and growth by fibronectin in capillary endothelial-cells. Journal of Cell Biology. 1990;110:1803-11.
[339] Howe A, Aplin AE, Alahari SK, Juliano RL. Integrin signaling and cell growth control. Current Opinion in Cell Biology. 1998;10:220-31.
[340] Sieg DJ, Hauck CR, Ilic D, Klingbeil CK, Schaefer E, Damsky CH, et al. FAK integrates growth-factor and integrin signals to promote cell migration. Nature Cell Biology. 2000;2:249-56.
[341] Giancotti FG, Ruoslahti E. Integrin signaling. Science. 1999;285:1028-33.
[342] Cox BD, Natarajan M, Stettner MR, Gladson CL. New concepts regarding focal promotion of cell migration adhesion kinase and proliferation. Journal of Cellular Biochemistry. 2006;99:36-52.
[343] Taylor JM, Mack CP, Nolan K, Regan CP, Owens GK, Parsons JT. Selective Expression of an Endogenous Inhibitor of FAK Regulates Proliferation and Migration of Vascular Smooth Muscle Cells. Molecular and Cellular Biology. 2001;21:1565-72.
[344] Ren XD, Kiosses WB, Schwartz MA. Regulation of the small GTP-binding protein Rho by cell adhesion and the cytoskeleton. The EMBO Journal. 1999;18:578-85.
[345] Gilmore AP, Romer LH. Inhibition of focal adhesion kinase (FAK) signaling in focal adhesions decreases cell motility and proliferation. Molecular Biology of the Cell. 1996;7:1209-24.

Appendix

Partial mRNA sequence of the RHC polypeptide (GenBank Access Number: EF376007)

```
gactggttcc aattgacaag cttttgattt taacgacttt taacgacaac ttgagaagat     60
caaaaaacaa ctaattattc gaaggatcca aacgatgaga tttccttcaa tttttactgc    120
agttttattc gcagcatcct ccgcattagc tgctccagtc aacactacaa cagaagatga    180
aacggcacaa attccggctg aagctgtcat cggttactca gatttagaag gggatttcga    240
tgttgctgtt ttgccatttt ccaacagcac aaataacggg ttattgttta taaatactac    300
tattgccagc attgctgcta aagaagaagg ggtatctctc gagaaaagag aggctgaagc    360
ttacgtagaa ttcctcgaga aaagaggtcc acccggtgag ccaggtaacc caggttctcc    420
aggaaaccaa ggtcaacctg gaaacaaggg ttctcctgga aacccaggtc aacctggtaa    480
cgagggacaa ccaggtcaac ctggtcaaaa cggtcaacca ggtgagcctg gatctaacgg    540
tcctcaaggt tcccaaggta acccaggtaa gaacggtcaa ccaggttctc caggttccca    600
aggttctcct ggaaaccaag gttctccagg tcaaccaggt aacccaggtc aacctggaga    660
gcaaggtaag ccaggtaacc aaggtccagc cggtgagcca ggtaacccag gttctccagg    720
aaaccaaggt caacctggaa acaagggttc tcctggaaac ccaggtcaac ctggtaacga    780
gggacaacca ggtcaacctg gtcaaaacgg tcaaccaggt gagcctggat ctaacggtcc    840
tcaaggttcc caaggtaacc caggtaagaa cggtcaacca ggttctccag gttcccaagg    900
ttctcctgga aaccaaggtt ctccaggtca accaggtaac ccaggtcaac ctggagagca    960
```

Partial amino sequence of the RHC polypeptide (Patent Cooperation Treaty: PCT/CN2016/102430, 102435 and GenBank Access Number: EF376007)

```
atg aga ttt cct tca att ttt act gca gtt tta ttc gca gca tcc tcc      48
Met Arg Phe Pro Ser Ile Phe Thr Ala Val Leu Phe Ala Ala Ser Ser
1               5                  10                  15
gca tta gct gct cca gtc aac act aca aca gaa gat gaa acg gca caa      96
Ala Leu Ala Ala Pro Val Asn Thr Thr Thr Glu Asp Glu Thr Ala Gln
            20                  25                  30
att ccg gct gaa gct gtc atc ggt tac tca gat tta gaa ggg gat ttc     144
Ile Pro Ala Glu Ala Val Ile Gly Tyr Ser Asp Leu Glu Gly Asp Phe
        35                  40                  45
gat gtt gct gtt ttg cca ttt tcc aac agc aca aat aac ggg tta ttg     192
Asp Val Ala Val Leu Pro Phe Ser Asn Ser Thr Asn Asn Gly Leu Leu
    50                  55                  60
ttt ata aat act act att gcc agc att gct gct aaa gaa gaa ggg gta     240
Phe Ile Asn Thr Thr Ile Ala Ser Ile Ala Ala Lys Glu Glu Gly Val
65                  70                  75                  80
tct ctc gag aaa aga gag gct gaa gct tac gta gaa ttc ctc gag aaa     288
Ser Leu Glu Lys Arg Glu Ala Glu Ala Tyr Val Glu Phe Leu Glu Lys
                85  ①              90                  95
aga ggt cca ccc ggt gag cca ggt aac cca ggt tct cca gga aac caa     336
Arg Gly Pro Pro Gly Glu Pro Gly Asn Pro Gly Ser Pro Gly Asn Gln
  ②         100                 105                 110
ggt caa cct gga aac aag ggt tct cct gga aac cca ggt caa cct ggt     384
Gly Gln Pro Gly Asn Lys Gly Ser Pro Gly Asn Pro Gly Gln Pro Gly
        115                 120                 125
aac gag gga caa cca ggt caa cct ggt caa aac ggt caa cca ggt gag     432
Asn Glu Gly Gln Pro Gly Gln Pro Gly Gln Asn Gly Gln Pro Gly Glu
    130                 135                 140
cct gga tct aac ggt cct caa ggt tcc caa ggt aac cca ggt aag aac     480
Pro Gly Ser Asn Gly Pro Gln Gly Ser Gln Gly Asn Pro Gly Lys Asn
145                 150                 155                 160
ggt caa cca ggt tct cca ggt tcc caa ggt tct cct gga aac caa ggt     528
Gly Gln Pro Gly Ser Pro Gly Ser Gln Gly Ser Pro Gly Asn Gln Gly
                165                 170                 175
tct cca ggt caa cca ggt aac cca ggt caa cct gga gag caa ggt aag     576
Ser Pro Gly Gln Pro Gly Asn Pro Gly Gln Pro Gly Glu Gln Gly Lys
            180                 185                 190
cca ggt aac caa ggt cca gcc ggt gag cca ggt aac cca ggt tct cca     624
Pro Gly Asn Gln Gly Pro Ala Gly Glu Pro Gly Asn Pro Gly Ser Pro
        195                 200                 205
```